Coagulation candidates and metastasis in renal cell carcinoma: mechanisms and therapeutic applications

Iván Prieto Durán

UNIVERSITAT DE BARCELONA

FACULTAT MEDICINA Y CIENCIAS DE LA SALUD

PROGRAMA DE DOCTORADO EN BIOMEDICINA

COAGULATION CANDIDATES AND METASTASIS IN RENAL CELL CARCINOMA: MECHANISMS AND THERAPEUTIC APPLICATIONS

IVÁN PRIETO DURÁN

2022

UNIVERSITAT DE BARCELONA

FACULTAD DE MEDICINA Y CIENCIAS DE LA SALUD

PROGRAMA DE DOCTORADO EN BIOMEDICINA

COAGULATION CANDIDATES AND METASTASIS IN RENAL CELL CARCINOMA: MECHANISMS AND THERAPEUTIC APPLICATIONS

IVÁN PRIETO DURÁN

2022

Memoria presentada por Iván Prieto Durán para optar al grado de Doctor por la Universitat de Barcelona

Dr. Oriol Casanovas Casanovas
Director

Dr. Francesc Viñals Canals
Tutor

Iván Prieto Durán
Autor

TABLE OF CONTENTS

LIST OF ABBREVIATIONS

%	Percentage
∞	Infinity
Δ	Delta
°C	Centigrade degrees
µg	Microgram
µl	Microliter
µm	Micrometer
µM	Micromolar
aa	Aminoacid
AAALAC	Association for Assessment and Accreditation of Laboratory Animal Care
AJCC	American Joint Committee on Cancer
APS	Ammonium persulfate
BCA	Bicinchoninic acid
BM	Basement membrane
BSA	Bovine serum albumin
Ca_2^+	Calcium
ccRCC	Clear cell renal cell carcinoma
cDNA	Complementary DNA
CEIC	Centre Ètic d'Investigació Clínica
chr	Chromosome
Chi^2	Chi square
cm	Centimeter
CNAG	Centro Nacional de Análisis Genómico
CO_2	Carbon dioxide
Cpm	Counts per million
CSIC	Consell Superior d'Investigacions Científiques
Ct	Threshold cycle
CTC	Circulating tumor cell
CRC	Colorectal cancer
DAB	3,3'-Diaminobenzidine
DAPI	4',6-Diamidino-2-phenylindole dihydrochloride
dH_2O	Distilled water

ddH$_2$O	Bi-distilled water
ddNTP	2',3' dideoxynucleotides
DMEM	Dulbecco's Modified Eagle's Medium
DMSO	Dimethyl sulfoxide
DNA	Deoxyribonucleic acid
DOAC	Direct oral anticoagulants
DOX	Doxycycline
DPX	Distyrene, plasticiser and xylene
DTC	Disseminated Tumor Cell
ECM	Extracellular matrix
EDTA	Ethylenediaminetetraacetic acid
EMT	Epithelial-mesenchymal transition
F2R	Coagulation Factor 2 Thrombin Receptor
FXIII/F13	Blood Coagulation Factor XIII/13
FAK	Focal Adhesion Kinase
FBS	Fetal bovine serum
FC	Fold change
FDA	Food and Drug Administration
FDR	False discovery rate
G	Gauge
g	Gram
GDP	Guanosine diphosphate
GEMSA	Guanidinoethylmercaptosuccinic acid
GEO	Gene Expression Omnibus
GTP	Guanosine triphosphate
GPCR	G-protein coupled receptor
GSEA	Gene set enrichment analysis
h	Hour
H&E	Hematoxylin and eosin
H$_2$O$_2$	Hydrogen peroxide
HCC	Hepatocellular carcinoma
HCl	Chloridric acid
HEPES	4-(2-hydroxyethyl)-1-piperazineethanesulfonic acid

HIF	Hypoxia-Inducible Factor
HRP	Horseradish peroxidase
ICGC	International Cancer Genome Consortium
ICO	Institut Català d'Oncologia
IDIBELL	Institut d'Investigació Biomèdica de Bellvitge
IgG	Immunoglobulin G
IGV	Integrative Genomics Viewer
Ind	Inducible
IRB	Institut de Recerca Biomèdica
ISUP	International Society of Urological Pathology
ITGA3	Integrin Subunit Alpha 3
ITGA5	Integrin Subunit Alpha 5
ITGB1	Integrin Subunit Beta 1
IV	Intravenous
Kan	Kanamycin
Kb	Kilobase
KDa	Kilodalton
Kg	Kilogram
KH_2PO_4	Potassium phosphate monobasic
KIRC	Kidney renal clear cell carcinoma
KIRP	Kidney renal papillary cell carcinoma
Km	Michaelis constant
L	Litre
LB	Lysogeny broth
KMWH	Low-Molecular-Weight Heparin
lnRNA	Long-non-coding ribonucleic acid
LOH	Loss of heterozygosis
Met	Metastatic
MET	Mesenchymal-epithelial transition
mg	Milligram
min	Minute
ml	Milliliter
mm	Millimeter

mm²	Square millimeter
mm³	Cubic millimeter
mM	Millimolar
MMP	Matrix metalloprotease
mRNA	Messenger ribonucleic acid
miRNA	Micro ribonucleic acid
MSigDB	Molecular Signatures DataBase
NaCl	Sodium chloride
Na₂HPO₄	Monosodium phosphate
NCDB	National Cancer Data Base
NEDD9	Neural Precursor Cell Expressed, Developmentally Down-Regulated 9
NEAA	Non-essential amino acids
NIS	National Inpatient Sample
ng	Nanogram
NK	Natural killer
nm	Nanometer
Non-met	Non-metastatic
O/N	Over night
OCT	Optimum cutting temperature compound
OT	Orthotopic
PAGE	Polyacrylamide gel electrophoresis
PAR	Protease-Activator Receptor
PEBC	Programa d'Epigenètica i Biologia del Càncer
PBS	Phosphate buffered saline
PCR	Polymerase chain reaction
PDX	Patient-derived xenograft
PDOX	Patient-derived orthoxenograft
PEI	Polyethylenimine
PES	Polyethersulfone
PFA	Paraformaldehyide
pg	Picogram
PHEO	Pheochromocytoma
prºCURE	Programa Contra la Resistència Terapèutica del Càncer

Puro	Puromycin
RCC	Renal cell carcinoma
RER	Rough endoplasmic reticulum
RIPA	Radioimmunoprecipitation assay buffer
RNA	Ribonucleic acid
RNAseq	Ribonucleic acid sequencing
rpm	Revolutions per minute
RPMI	Roswell Park Memorial Institute
RSEM	Reservoir Sampling based Ensemble Method
RFP	Red Fluorescent Protein
RSP	Regulated secretory pathway
RT	Room temperature
RT-qPCR	Real-time quantitative PCR
s	Second
SciPY	Python Scipy library
SD	Standard deviation
SDS	Sodium dodecyl sulfate
SERPINE1	Serpin Family E Member 1
SOC	Super optimal broth with catabolic repression
SPF	Specific pathogen free
Src	SRC Proto-Oncogene, Non-Receptor Tyrosine Kinase
TAE	Tris-acetate-EDTA
TBS	Tris-buffered saline
TCA	Trichloroacetic acid
TCGA	The Cancer Genome Atlas
TEM	Transendothelial migration
TEMED	Tetramethylethylenediamine
TFPI	Tissue Factor Pathway Inhibitor
TGN	Transgolgi
TNM	Tumor-node-metastasis
Tris	Tris(hydroxymethyl)aminomethane
TPBS	Triton-phosphate buffered saline
TTBS	Tween-tris-buffered saline

UV	Ultraviolet
V	Volt
VEGF	Vascular Endothelial Growth Factor
VHIO	Vall d'Hebrón Institut d'Oncologia
VHL	Von Hippel-Lindau
VTE	Venous thromboembolism
WHO	World Health Organization

Amino acids

F Phe, phenylalanine	**S** Ser, serine	**Y** Tyr, tyrosine	**K** Lys, lysine	**W** Trp tryptophan
L Leu, leucine	**P** Pro, proline	**H** His, histidine	**D** Asp, aspartic acid	**R** Arg, arginine
I Ile, isoleucine	**T** Thr, threonine	**Q** Gln, glutamine	**E** Glu, glutamic acid	**G** Gly, glycine
M Met, methionine	**A** Ala, alanine	**N** Asn, asparagine	**C** Cys, cysteine	**V** Val, valine

LIST OF FIGURES

LIST OF TABLES

SUMMARY

Nowadays, cancer is the second cause of human mortality and most deaths are caused by metastasis. While several hypotheses have been postulated to explain its progression, solid mechanisms and valid targets have not been found yet. Clear Cell Renal Cell Carcinoma (RCC) is the most frequent RCC and represents on average over 90% of all kidney malignancies in adults of both sexes.

In this study, we tackle this problem with a xenograft murine model (PDOX) developed from a human biopsy of a patient who had a clear cell RCC (ccRCC) with a ganglionar metastasis. The first implanted mouse spontaneously generated metastasis in the lung. Perpetuation of both the metastatic and the primary tumors in different mice leads to the generation of two tumor mouse models with strong differences in their metastatic potential. Previous work from our group had sequenced the high and low metastatic variants of this PDOX model, both at DNA and RNA levels to find markers and therapeutic targets related to metastasis. One of the most promising candidates was Coagulation Factor II Thrombin Receptor (F2R), a receptor involved in the coagulation pathway which is highly overexpressed in the metastatic tumors of this model. Through *in vitro* and *in vivo* validations, the aim of this thesis is to find the relationship between F2R and metastatic potential.

We have validated the possible implication of F2R in the aggressiveness of the primary tumor without affecting its growth (proliferation). Besides, an interesting interaction between F2R and integrins has been evaluated. Furthermore, we described a possible role of F2R in the later steps of the metastatic cascade. Despite having overexpression of many genes of the coagulation pathway, none alteration of blood hemostasis was founded in our models, suggesting that the coagulation factors are implicated in tumor malignization. Clinical validation demonstrated that overexpression of coagulation-related genes and F2R-interactors are related to a poor prognosis of ccRCC patients.

To sum up, this study opens new insights of the pathways involved in metastasis, and together with the mechanisms of invasion and resistance to current therapies, we could allow establishing new therapies for treating metastasis.

RESUMEN

Hoy en día, el cáncer es la segunda causa de mortalidad en el ser humano y la mayoría de las muertes son producidas por la metástasis. Aunque se han postulado varias hipótesis para explicar su progresión, aún no se han encontrado mecanismos sólidos ni dianas válidas. El carcinoma renal de célula clara (CRcc) es el más frecuente de los carcinomas renales ya que representa más del 90% de todas las neoplasias renales en adultos de ambos sexos.

En este estudio, abordamos este problema con un modelo murino de xenoinjerto (Ren-PDOX) desarrollado a partir de una biopsia humana de un paciente que desarrolló un CRcc con una metástasis ganglionar. El primer ratón implantado generó espontáneamente una metástasis en el pulmón. La perpetuación de los tumores metastásicos y primarios en diferentes ratones nos llevó a la generación de dos modelos de ratón con tumores con diferencias en su potencial metastásico. Estudios previos de nuestro grupo secuenciaron las variantes de con bajo y alto nivel metastático de este modelo PDOX, tanto a nivel de ADN como de ARN para encontrar marcadores y dianas terapéuticas relacionadas con la metástasis. Uno de los candidatos más prometedores fue el Receptor de la Trombina (F2R), un receptor implicado en la vía de la coagulación que está altamente sobreexpresado en los tumores metastásicos de este modelo. Mediante validaciones *in vitro* y *in vivo*, el objetivo de esta tesis es encontrar la relación entre el F2R y el potencial metastásico.

Hemos validado la posible implicación de F2R en la agresividad del tumor primario sin afectar a su crecimiento (proliferación). Además, se ha evaluado una interesante interacción entre F2R y diferentes integrinas. Por otro lado, hemos descrito un posible papel de F2R en los últimos pasos de la cascada metastásica. A pesar de tener una sobreexpresión de muchos genes de la vía de la coagulación, no se encontró ninguna alteración de la homeostasis sanguínea en nuestros modelos, lo que sugiere que los factores de coagulación están implicados en la malignización tumoral sin afectacion de la coagulacion sanguínea. Por otro lado, la validación clínica demostró que la sobreexpresión de los genes relacionados con la coagulación y los interactores F2R están relacionados con un mal pronóstico de los pacientes con CRcc.

En resumen, este estudio abre nuevas perspectivas sobre las vías implicadas en la metástasis, y junto con los mecanismos de invasión y resistencia a las terapias actuales podría permitir establecer nuevas terapias para tratar la metastasis.

INTRODUCTION

1. CANCER

Cancer consists of a neoplasm, which is an alteration of cell proliferation and very often also of cell differentiation that is expressed by an abnormal mass of tissue named tumor. Every year, 14 million new cases of cancer are detected globally and 9.6 million people die from the disease. In Europe, more than 3.7 million new cases of cancer are diagnosed annually and it is responsible for 1.9 million deaths. Cancer is the second leading cause of death and morbidity after cardiovascular diseases("World Cancer Organization, 2022). Given these adverse statistics, it has never been more important to understand and fight cancer.

In the year 2000, Douglas Hanahan proposed six hallmarks of cancer that comprise six biological capabilities acquired during the multistep development of human tumors. The hallmarks constitute an organizing principle for rationalizing the complexities of neoplastic diseases. They include sustaining proliferative signaling, evading growth suppressors, resisting cell death, enabling replicative immortality, inducing angiogenesis, and activating invasion and metastasis (Hanahan & Weinberg, 2000).

In 2011 two new emerging hallmarks (Deregulating cellular energetics and avoiding immune destruction) and two enabling characteristics (Genome instability and mutation and Tumor-promoting inflammation) were added (Hanahan & Weinberg, 2011b). Finally, in 2022 it was proposed to include new emerging hallmarks and enabling characteristics that include unlocking phenotypic plasticity, nonmutational epigenetic reprogramming, polymorphic microbiomes, and senescent cells (Figure 1) (Hanahan, 2022).
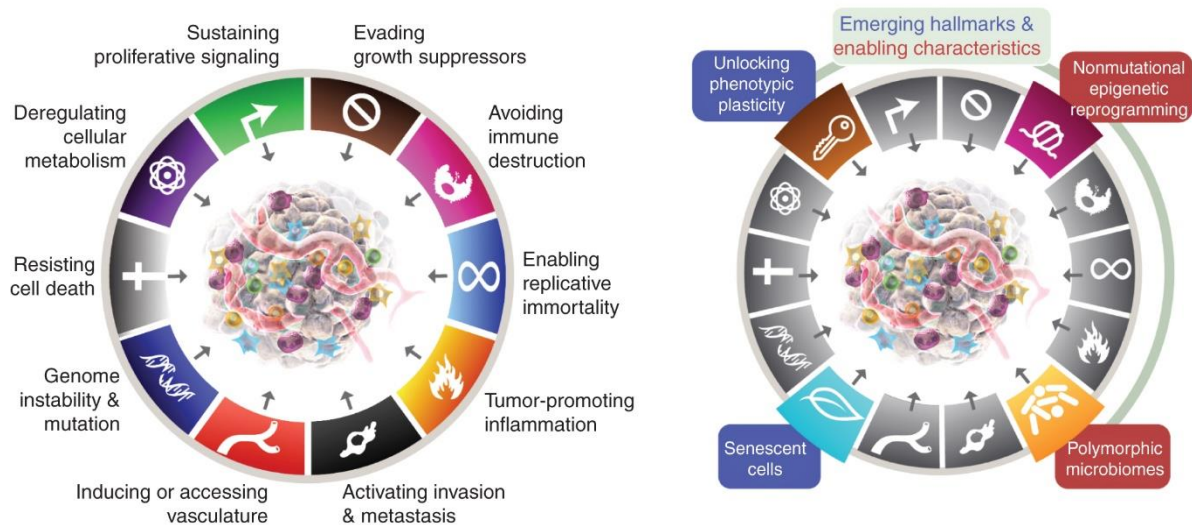
Figure 1. Hallmarks of cancer. Left, Hallmarks of cancer and enable capabilities until 2011. Right, new additional proposed emerging hallmarks in 2022. Image has been obtained from (Hanahan, 2022).

Taking all these hallmarks into account, the metastatic spread of cancer cells to distant parts of the body represents the major cause of cancer-related deaths, being one of the most life-threatening pathologic events. Concretely, it is estimated that more than 90% of deaths are a consequence of metastases and not due to the primary tumor (Chaffer & Weinberg, 2011b).

2. METASTASIS

Metastasis is the process of spreading to a nearby or distant secondary site and the establishment of macroscopic secondary foci. The metastatic cascade is a series of stochastic events that collectively lead to the formation of overt metastases in a distant organ. It involves different steps: invasion, intravasation, dissemination in the circulation and survival, extravasation, and finally, colonization (Figure 2) (Fares et al., 2020; Obenauf & Massagué, 2015)
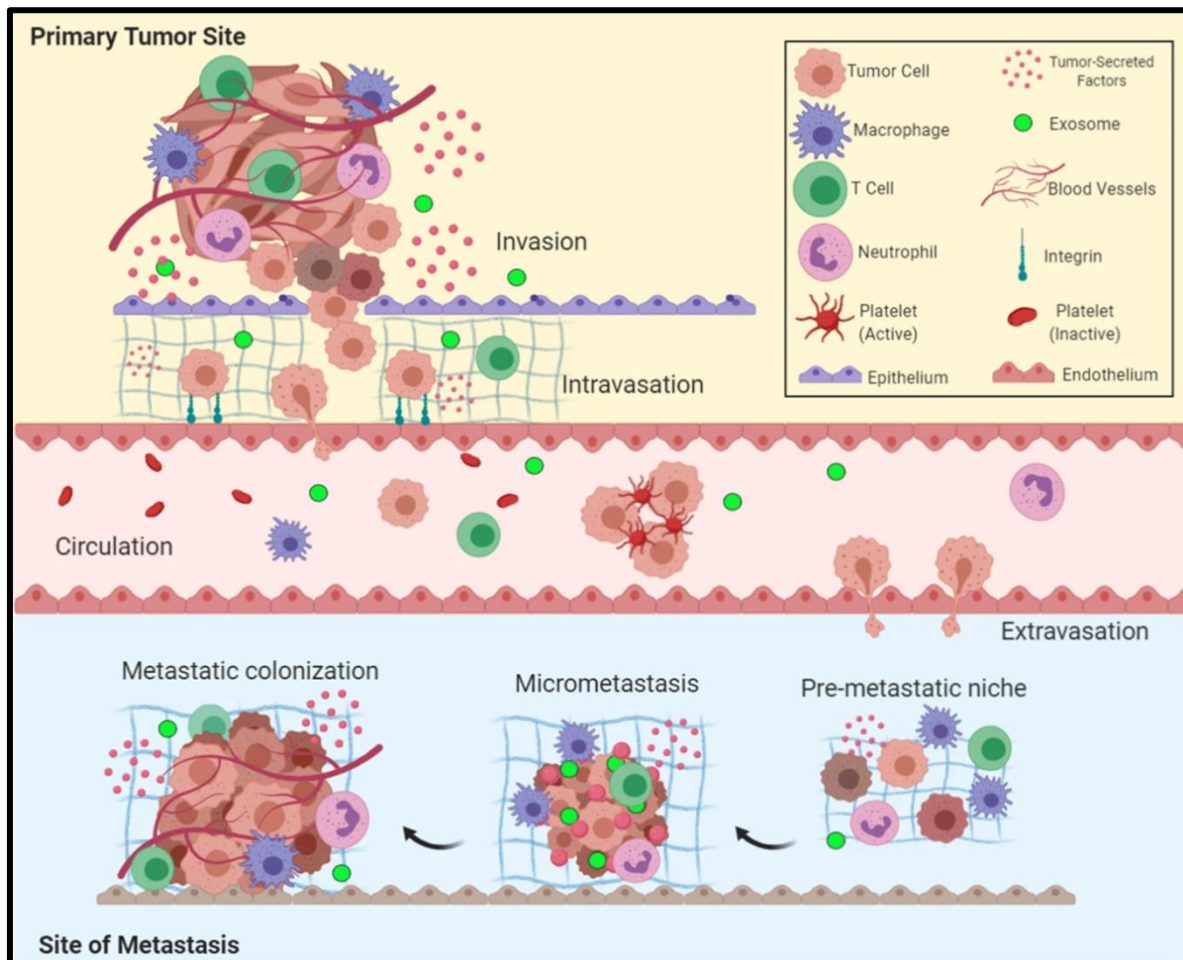
Figure 2. Metastatic cascade. The five key steps of the metastatic cascade include primary tumor invasion, intravasation, survival in circulation, extravasation, and colonization. Image has been obtained from (Fares et al., 2020).

2.1 Local invasion

Metastasis originates in the primary tumor invasive front, where cancer cells migrate into the surrounding tumor-associated stroma and, later, into the normal tissue parenchyma. For most solid tumors, the metastatic cascade begins with cancer cells breaching the underlying basement membrane (BM). To achieve this movement, cellular motility is altered by cytoskeleton reorganization and the secretion of extracellular matrix (ECM) remodelers, mainly proteases (Gupta & Massagué, 2006; Kessenbrock et al., 2010). This process which requires proteolytic activity is driven/supported by integrins that upregulate the expression of matrix metalloproteinases and thereby facilitate protease activation at the ECM interface (Munshi & Stack, 2006) (Figure 3).

Integrins are a family of 24 transmembrane heterodimers generated from a combination of 18α integrin and 8β integrin subunits. As the principal receptors for ECM molecules, integrins are critical in regulating cell motility in normal physiological processes, such as development and wound healing, and during cancer dissemination. While some integrins bind to only specific ECM ligands (for example, α5β1 integrin to fibronectin), others exhibit a broader ligand-binding repertoire overlapping with other integrin heterodimers (for example, αvβ3 integrin binds to fibronectin, vitronectin, fibrinogen, and thrombospondin, etc... (Humphries et al., 2006).

Integrin-controlled cell migration is largely mediated by signalling pathways involving members of the focal adhesion kinase (FAK)-SRC family kinase(M. Li et al., 2021). In addition, integrin ligation can also activate other signalling pathways such as the activation of mitogen-activated protein kinase (MAPK)/extracellular regulated kinase (ERK) pathway, phosphatidylinositol 3-kinase (PI3K)/protein kinase B (AKT) pathway, and stress-activated MAP kinases (SAPKs) or nuclear factor-kB (NF-kB) signalling, amongst others (Spoerri et al., 2020)

During cell invasion and migration, cells project lamellipodia that attach to the ECM, allowing them to pull themselves forward. Extension of lamellipodia is induced by actin polymerization and reorganization and is facilitated by a localized decrease in membrane tension. (Raucher & Sheetz, 2000)

During the entire process of cancer invasion, cancer cells are in close contact with other tumor-associated stroma that includes endothelial cells, pericytes, immune cells, and Cancer-associated Fibroblasts (CAFs). CAFs can contribute to cancer progression via several integrin-linked mechanisms and trigger invasiveness by generating pro-migratory tracks through the stromal ECM, by depositing fibronectin, by regulating fibronectin alignment, or by physically pulling cancer cells out of the primary tumor (Attieh & Vignjevic, 2016; Erdogan et al., 2017).
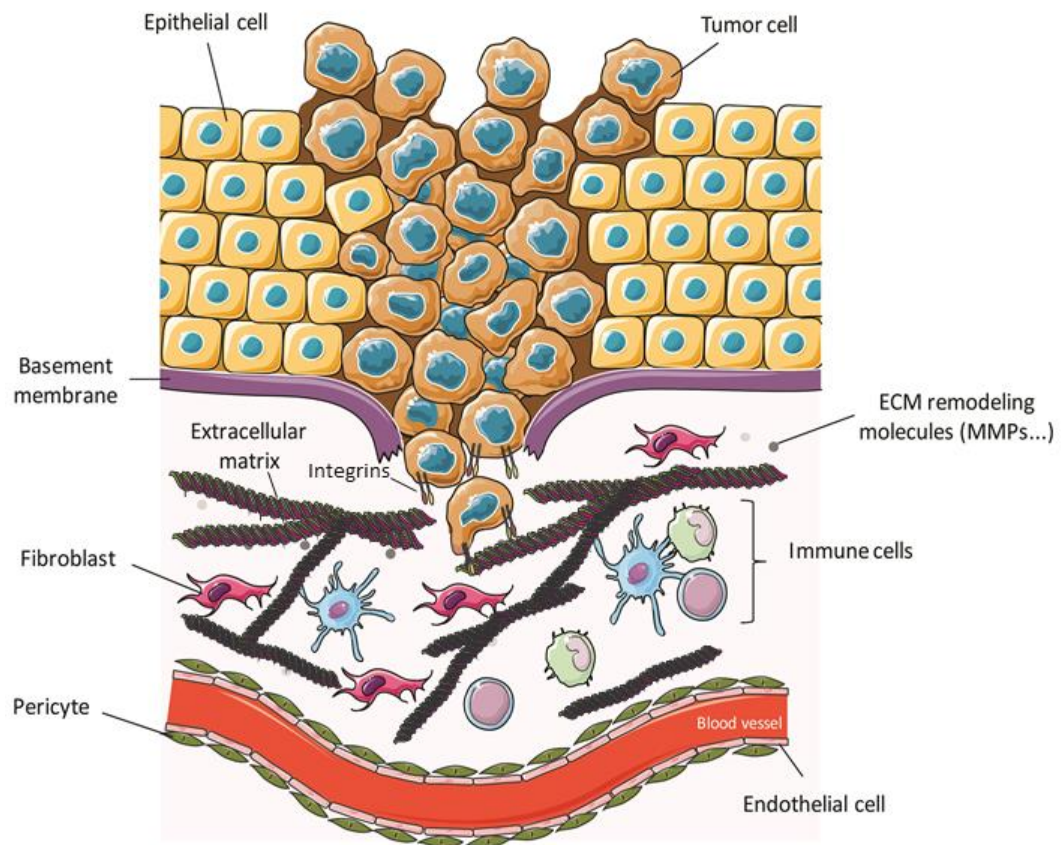
Figure 3. Schematic representation of local invasion by the tumor. Local invasion of the primary tumor into the surrounding parenchyma is driven by integrins and proteases and starts with the degradation of the BM and the subsequent invasion of normal stroma which is composed of ECM and a variety of cells, such as Fibroblasts, immune cells, pericytes or endothelial cells.

2.2 Intravasation

Intravasation is a key step in cancer metastasis during which tumor cells penetrate the vessel wall and enter the circulation, thereby becoming circulating tumor cells (CTCs) and potential metastatic seeds. Intravasation of tumor cells is an essential step in metastasis. Some of these cells can form metastatic tumors, depending on the number CTCs (Zavyalova et al., 2019)

To intravasate, metastatic cells undergo an epithelial-to-mesenchymal transition (EMT). The loss of epithelial features, like adhesion or polarization, followed by a gain of invasiveness greatly contributes to metastasis. In this regard, the downregulation of epithelial protein E-cadherin is a well-established prognostic marker for metastasis (Beavon, 2000).

In addition, this process is backed by the formation of new vessels created from pre-existing ones; a process called angiogenesis. Angiogenesis not only supports tumor growth by providing nutrients and oxygen, but it also contributes to the dissemination of tumor cells (Ronca et al., 2017; Sherwood et al., 2010). One of the major factors involved in the formation of new vessels is the Vascular Endothelial Growth Factor (VEGF). The tumor vasculature is a physical barrier for cancer cells and to facilitate its penetration, they can secrete several factors that increase vascular permeability, thereby allowing their entry into the circulation (Figure 4) (Carmeliet, 2005; Moserle & Casanovas, 2013).
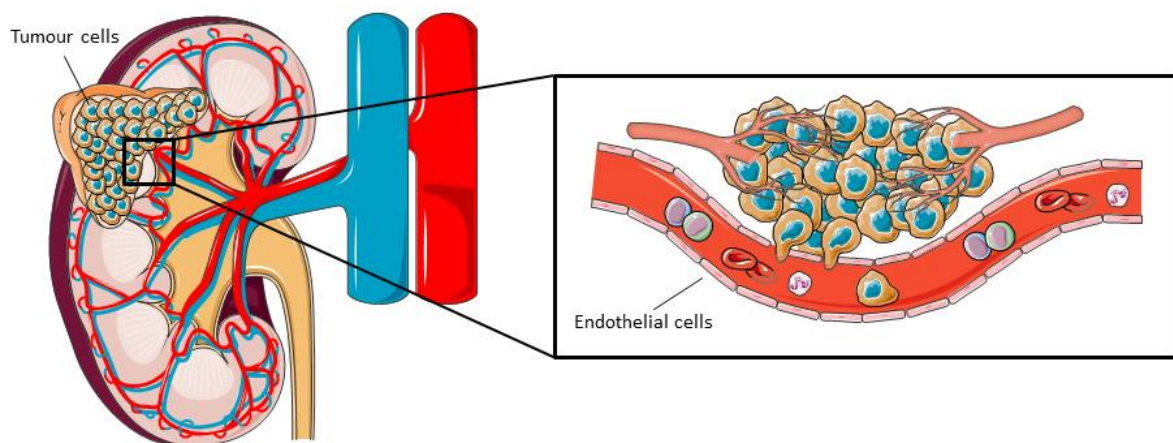
Figure 4. Schematic representation of intravasation. During tumor growth, new capillaries sprout from the pre-existing vessels, forming a new capillary network. This process is known as angiogenesis. The creation of these new leaky vessels together with the factors secreted by cancer cells increases the vascular permeability and facilitates the entrance of cancer invasive cells into the bloodstream.

2.3 Dissemination and survival in the circulation

Once CTCs enter the bloodstream or lymphatic system, they find themselves in a hostile environment, which results in massive cell death during the transition through vessels.

On the one hand, CTCs encounter mechanical and environmental stress, such as shear stress. Because cell adhesion to ECM transmits cell survival signals, upon detachment, normal cells promote anoikis, a particular apoptotic death due to loss or inappropriate cell adhesion (Frisch & Francis, 1994). Integrins can regulate cell viability through their

interaction with the ECM, sensing mechanical forces arising from contacts and converting them into intracellular signals (Giancotti, 2000).

On the other hand, they can be attacked by natural killer cells of the immune system. CTCs can circulate as single cells or clusters of cells, with clusters appearing to have increased metastatic potential and a shorter half-life in the circulation (6–10 min for clusters vs. 25–30 min for single cells). Those clusters of cells can contain stromal cells and immune components from the original microenvironment that increase survival (Aceto et al., 2014; M. Yu et al., 2013). Neutrophils participate in cluster formation and suppress leukocyte activation, which increases the chances of CTC survival (Leach et al., 2019).

Furthermore, it has been described that also platelets are a key component of these clusters. In homeostasis, platelets are activated during thrombus formation. This activation is mainly caused by thrombin, a protease that binds to the G protein-linked protease-activated receptors (PARs family) present on their surface. Its activation triggers a reorganization of the platelet cytoskeleton with a subsequent increase of adhesion molecules – such as integrins- distributed on their surface. Consequently, platelets can form a coating shield around cancer cells, together with fibrinogen and fibrin molecules that prevent CTCs clearance from Natural Killer cells (Strilic & Offermanns, 2017), but also provide the structure needed to bear the physical stresses of circulation (Figure 5) (L. J. Gay & Felding-Habermann, 2011).

It is stunning how CTCs overcome these perils, by taking advantage of components of blood coagulation. Many authors have demonstrated a significant correlation between the incidence of thromboembolic events and a worse prognosis of neoplastic disease, supporting the idea that the activation of the blood coagulation system contributes to tumor aggressiveness and vice versa.

It is worth noting that the lower survival rate observed in cancer patients displaying a thrombophilic profile is not necessarily related to the thrombotic event itself, but probably to tumors with more aggressive behavior, suggesting a possible implication of

the hemostatic system on fundamental aspects of cancer pathogenesis such as angiogenesis, metastasis, and the modulation of innate immune responses (Degen & Palumbo, 2012; Lima & Monteiro, 2013).
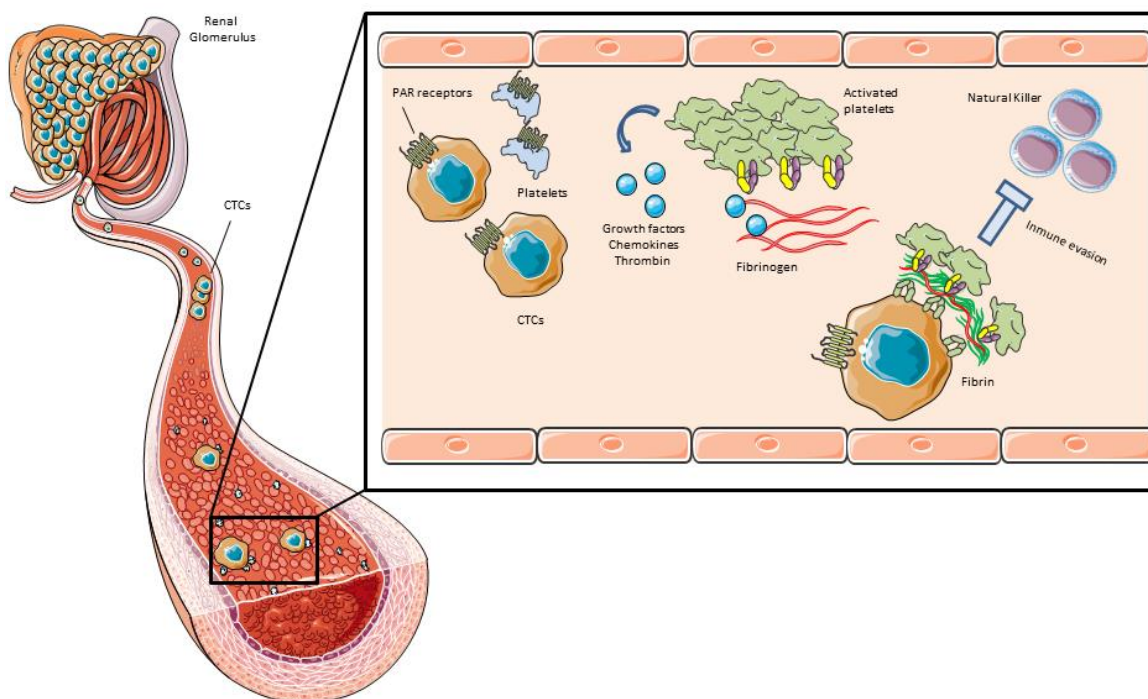
Figure 5. Schematic representation of tumor cell survival in the circulation. Many factors of the coagulation pathway are affecting CTCs survival. Platelets, once they are activated, form heteroaggregates with tumor cells, shielding them against the immune system. Platelet activation also triggers PARs activation in tumor cells, leading to thrombin activation, which then binds PARs on their surface and reactivates the pathway in a feedback loop. Integrins are also involved in these interactions. This figure has been adapted from (L. J. Gay & Felding-Habermann, 2011)

2.4 Arrest at a distant organ site and extravasation

After reaching the secondary site, metastatic cells are arrested in the microvasculature of the host organ prior to extravasation. To overcome this critical step, multiple factors must occur. Adhesion and interaction between CTCs and the host stroma facilitate microvasculature trapping. For example, the permeability and integrity of the vascular endothelium determine the rate of extravasation in many organs. Bone or liver extravasation is facilitated by the intrinsic permeability of its capillaries. In other organs like lungs, cancer cells must acquire new features to cross the vessel wall (composed of

endothelial cells, basement membrane, and tissue-specific cells) and enter the parenchyma. Several mechanisms involving platelet-released ATP, inflammatory mediators, and cancer cell-secreted growth factors and proteases have been implicated in the regulation of capillary wall permeability (Lambert et al., 2017).

Moreover, Integrins are implicated in extravasation as well. These cell–ECM contacts combined with protein tyrosine kinase-induced signalling are important regulators of vessel integrity(Holash et al., 1999). One mechanism involved in this process is α3β1 integrin-mediated cancer cell adhesion to subendothelial laminin, which is crucial for transendothelial migration. β1 integrin is also a prerequisite for tumor cells to fully clear the endothelial layer and invade the basement membrane.

The presence of fibronectin patches on endothelial cells promotes cancer cell adhesion to the vessel wall in a talin 1-dependent manner. Furthermore, as it was commented in the previous section, features of the blood clotting cascade can promote integrin-mediated cancer cell invasive protrusion and extravasation, such as local recruitment of plasma fibronectin to trigger αvβ3 integrin activation (Figure 6) (Hamidi & Ivaska, 2018).
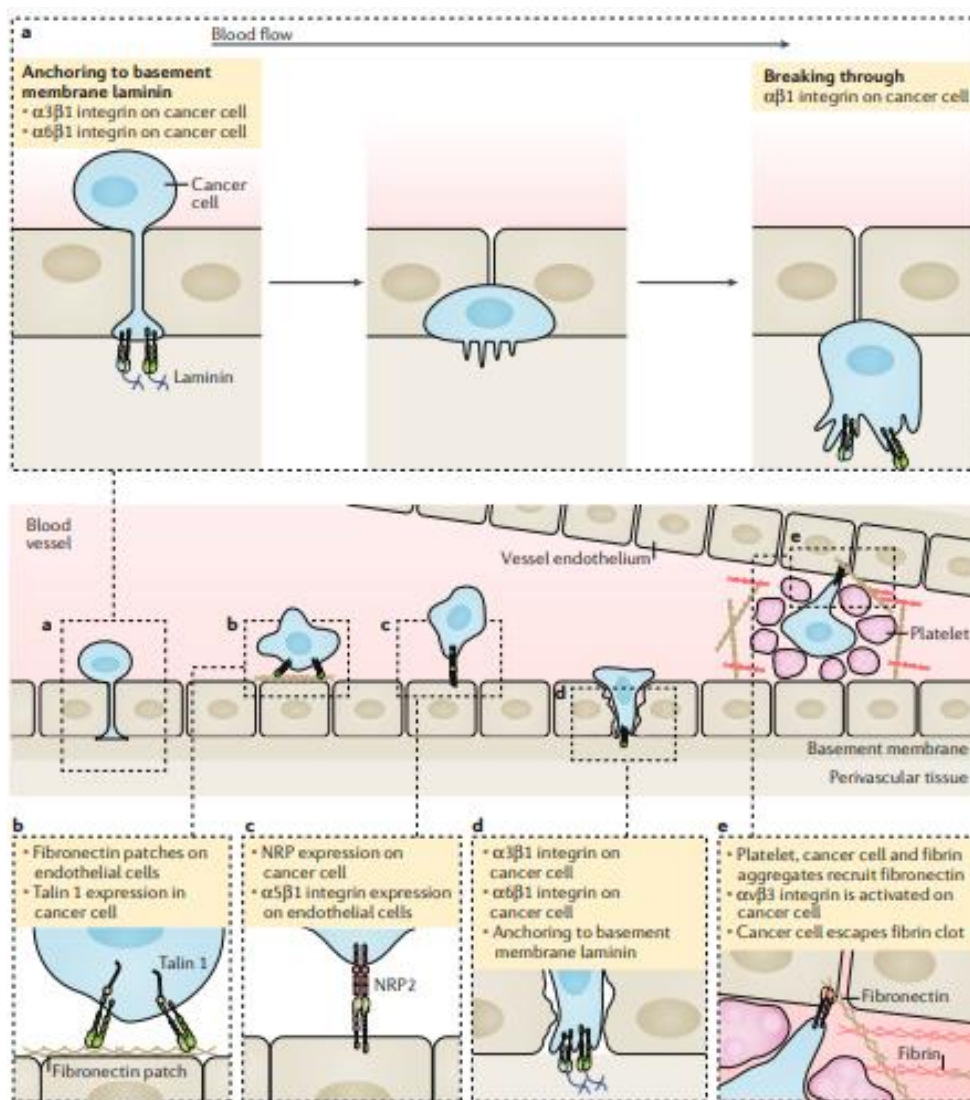
Figure 6. Mechanism of arrest at a distant organ site and extravasation. Multiple integrins and coagulation-related factors are implicated in the process of arrest at a distant organ site and extravasation. The image has been adapted from (Hamidi & Ivaska, 2018).

2.5   Initial survival and micrometastasis formation

Once metastatic cells extravasate and settle into the secondary site as Disseminated Tumor Cells (DTCs), they must adapt to the new foreign tissue. Organ-specific extrinsic factors, including ECM, stroma, cytokines, and growth factors, compromise the survival and growth of DTCs (Peinado et al., 2017). Several secreted tumor-derived factors from the primary tumor and bone marrow-derived cells signal the formation of the Pre-Metastatic Niche (PMN), in which the tumor cells colonize and grow (Peinado et al., 2011). Mature monocytes and macrophages can secrete factors such as matrix-

degrading enzymes that induce a more permissive local microenvironment allowing the growth of DTCs (Hiratsuka et al., 2006). Besides, exosomes have been described to play a vital role in forming the PMN as well (Peinado et al., 2012).

Metastasis is known to be an extremely inefficient process and only a few cells escaping from the primary tumor successfully form secondary tumors. Interestingly, *in vivo* video microscopy and cell-fate analysis have shown that early steps in the metastatic cascade are completed very efficiently. By contrast, later steps in the process are inefficient (Chambers et al., 2002a). Therefore, it is important to understand what is happening to cancer cells between their entry into the circulation and the formation of metastasis. As mentioned in Section 2.3, some cells die in the circulation due to hemodynamic forces or due to the action of the immune system, however, some authors also described that more than 80% of melanoma cells injected through the tail vein can survive initial arrest in the microcirculation and extravasate (Luzzi et al., 1998). For that reason, they suggested that metastatic inefficiency is caused by the events that occurred after the extravasation.

To overcome these obstacles, metastatic cells use cell-autonomous traits that facilitate homing and survival by altering the SRC-AKT tyrosine kinase signalling pathway (X. H. F. Zhang et al., 2009). Furthermore, DTCs can enter a state of dormancy, which occurs in metastatic cancer clusters when the rate of cellular proliferation within the cluster is equal to the rate of apoptosis. In this state, the tumor cluster does not expand into micrometastasis. This balance is achieved through suppressive gene signalling, restricted angiogenesis, and/or an active immune microenvironment (Gomis & Gawrzak, 2017). A major problem is that these dormant cancer cells can be present even after radical removal of the primary tumor and are thought to be responsible for late relapses (Giancotti, 2013)

2.6 Metastatic colonization

The last step in the metastatic cascade is the overgrowth of micromestastases into full-grown symptomatic lesions that are clinically detectable.

Once metastatic cells reach new foreign tissue, they require signals to further grow. Signalling pathways that have been identified to be implicated in metastatic colonization are the PI3K/AKT, MAPK, and HIF signalling pathways. Metastatic cells may achieve stimulation of these pathways by expressing autocrine pathway activators or recruiting stromal cells that secrete them (Massagué & Obenauf, 2016). Furthermore, cancer cells could get vital support through contact with stromal cells. For instance, breast cancer cells that infiltrate the lungs express the membrane protein VCAM-1, which then contacts α4-integrins on stromal monocytes and macrophages and consequently activates PI3K/AKT signalling (Lu et al., 2011). Another way how cancer cells can increase the activity of pro-metastatic pathways is by increasing epigenetic alterations that expand the range of a pathway's gene responses. For example, VHL-mutant renal cell carcinoma cells gain metastatic activity in multiple organs by modifying DNA methylation and histone acetylation that expand the range of HIF (hypoxia-inducible factor) target genes, the dominant oncogenic pathway in these cells (Vanharanta et al., 2012)

Additionally, to stimulate the growth of micrometastasis into macrometastais, an angiogenesis switch is necessary. Some authors provide evidence for the presence of pre-angiogenic micrometastasis which shows a balance between proliferation and division. When these pre-angiogenic micrometastases acquire the ability to become vascularized, the dormant state ceases and tumor growth is initiated (Chambers et al., 2002b).

Besides, as mentioned in Section 2.2, EMT contributes to the early steps of the metastatic cascade. A reversion of EMT occurs in DTCs into a more epithelial-like phenotype through a process called mesenchymal-to-epithelial transition (MET), crucial for the formation of macrometastases. This process explains why carcinoma-derived

metastases show epithelial characteristics and resemble, to a certain extent, the primary tumor (Brabletz, 2012).

2.7 Metastatic treatment

The increasing knowledge about the biology of metastasis provides opportunities to improve the clinical outcomes of cancer patients. Evaluating the biological differences between micro- and macrometastases, targeting the vulnerabilities of metastatic cancer cells, and exploiting the properties of metastatic tumor microenvironments provide a basis for present and future treatments of metastasis (Ganesh & Massagué, 2021)

What treatment is administered is decided depending on the stage of the disease. More precisely, there are advanced stages, where metastasis may be clinically manageable by systemic therapy, but is typically incurable. On the other hand, there are early-stage patients where no metastasis is apparent but micrometastasis is assumed to be present. Therapy might be administered either before surgery (neoadjuvant therapy) or after surgery (adjuvant therapy) and is applied to high-risk early-stage cancer, in which a visible tumor is localized at the originating organ and can be completely surgically removed. In most cancers, adjuvant and/or neoadjuvant therapy substantially reduces recurrence and prolongs overall survival for subsets of patients with stage II or stage III cancer, demonstrating the feasibility of eliminating disseminated tumor cells or their metastasis-initiating capacity (Ganesh & Massagué, 2021).

There are many strategies to follow up treatment by either targeting metastatic cancer cells, the metastatic microenvironment, or by treating specific organ metastasis.

Metastatic cancer cells of both, micrometastatic and macrometastatic diseases are currently treated with three broad systemic approaches: chemotherapy, targeted therapy, and immunotherapy. Targeting the metastatic microenvironment on the other hand became feasible only recently due to advances in immunotherapy (Binnewies et al., 2018). One example worth mentioning is the antibody Bevacizumab, which aims at inhibiting the tumor's neovasculature by targeting the vascular endothelial growth factor (VEGF) (Sherwood et al., 1971). However, even though this therapy has shown some

efficacy in metastatic cancers, it failed to show substantial results in RCC, as dormant micrometastasis does not require angiogenesis for proliferation (Iheanacho & Vaishampayan, 2020).

Finally, another interesting therapy that has been shown to improve survival is regional therapy, which focuses on organ-specific treatment and is mostly used in those cancers that only metastasize at a single organ (Ganesh & Massagué, 2021).

Future directions to treat metastatic cancers are needed to decrease the mortality of cancer patients. Targeting the plasticity of metastatic cells, and the mechanisms that regulate the induction of dormancy or targeting the microbiome environment could be promising targets and deserve further study.

3. COAGULATION PATHWAY

The coagulation pathway is a cascade of events that leads to hemostasis, preventing bleeding or hemorrhage. It is composed of two paths; the intrinsic and extrinsic pathways that originated separately but finally converged at a specific point, leading to fibrin activation that ultimately stabilizes the platelet plug with a fibrin mesh. The intrinsic pathway consists of factors I, II, IX, X, XI, and XII. The extrinsic pathway on the other hand consists of factors I, II, VII, and X. Finally, the common pathway consists of factors I, II, V, VIII, X (Figure 7). Many of these factors are activated into serine proteases that act as a catalyst by cleaving other downstream factors of the coagulation pathway leading to even more serine proteases that ultimately activate fibrinogen (Chaudhry et al., 2021).
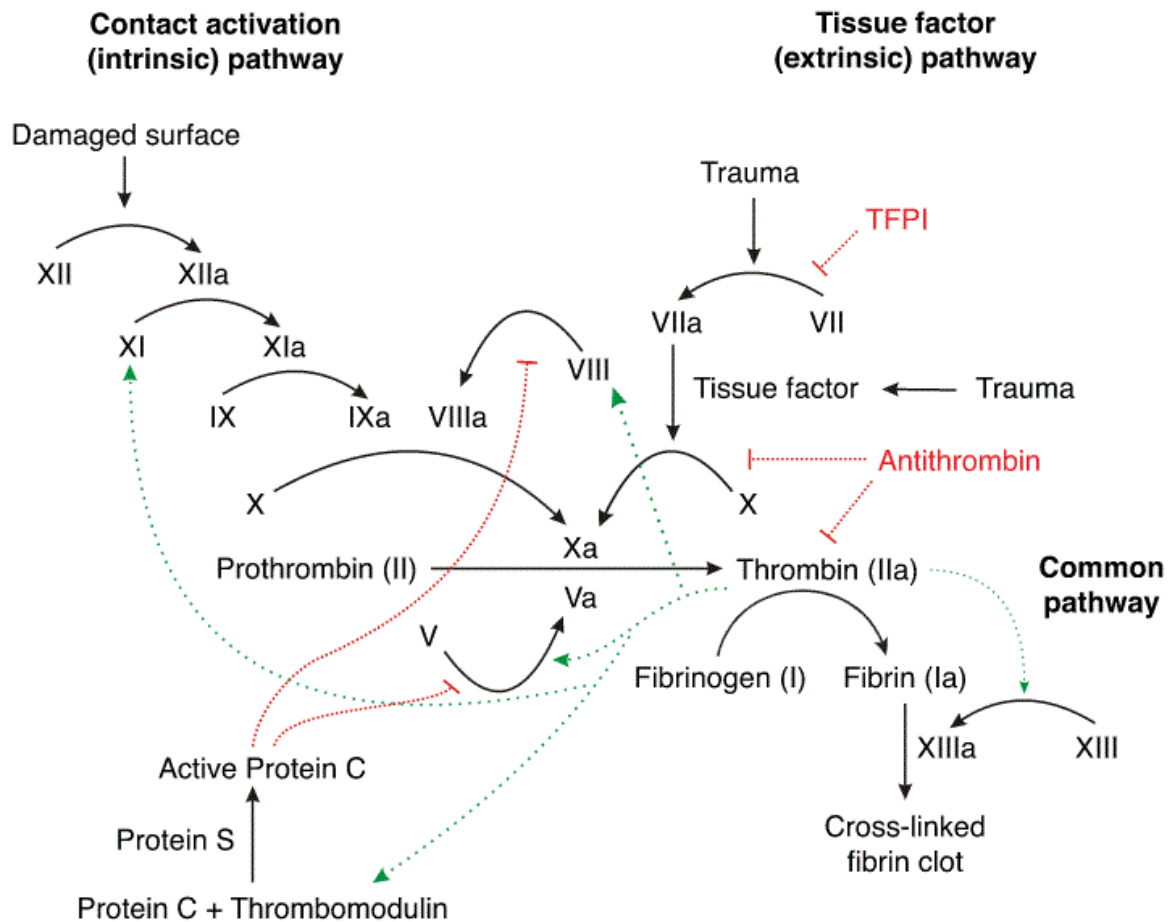
Figure 7. Coagulation cascade representation. Intrinsic and extrinsic pathway factors convert into the common pathway that cross-links fibrin clots. As a result, platelets are formed. The image has been obtained from Wikipedia.

3.1 Coagulation pathway and cancer

Cancer represents a highly prothrombotic state. Thrombosis is one of the most common comorbidities associated with cancer. Indeed, cancer-associated thromboembolism is the second leading cause of death for cancer patients, second only to cancer itself. Moreover, it has been discovered that there is a bidirectional relationship between the activity of coagulation-related factors and cancer, whereby the activation of the pathological hemostatic system associated with cancer not only promote thromboembolism but also drives the progression of the malignancy (Sharma et al., 2019).

Tissue Factor (TF) - the primary initiator of the hemostatic cascade- has been described to participate in the very early steps of oncogenesis in many different cancer types.

Several studies describe how the expression of TF in newly transformed cells can result in oncogenic mutations in different cancer types such as gliomas, colorectal carcinoma, breast cancer, or Pancreatic ductal adenocarcinoma (J. L. Yu et al., 2004).

TF initiates the extrinsic pathway by binding activated factor VIIa that in turn activates factor Xa. The complex TF/fVIIa/fXa can activate the Proteinase-Activated-Receptor family (PARs). The activation of PAR-2 has been linked to tumor cell proliferation and EMT (L. Sun et al., 2018).

Another major factor of the coagulation cascade is thrombin due to its central role as a hemostatic protease. Thrombin has over a dozen of substrates, the PAR-1 receptor being one of them. PAR-1 activation has been linked to a mechanistic interplay between thrombin and tumorigenesis and tumor growth (Adams et al., 2015).

3.2 Coagulation pathway and metastasis

During the last years, multiple lines of evidence emerged that point to a substantial role of the hemostatic system in favouring metastasis.

Regarding the early steps of the metastatic cascade, TF -apart from favouring tumorigenesis- has been suggested to promote metastasis by supporting the expression of adhesions molecules and promoting cell motility through PAR-1 activation (Shi et al., 2004b). Furthermore, TF is triggering signalling through non-proteolytic interaction with $\alpha6\beta1$ and $\alpha v\beta3$ integrins, which results in the activation of PI3K/Akt, MAPK, and FAK signalling pathways that ultimately support tumor angiogenesis (van den Berg et al., 2009). Besides, the activation of PAR-1 and PAR-2 induces the activation of PI3K/AKT signalling pathways to establish $\alpha5\beta1$integrin-mediated adhesion(Spoerri et al., 2020). All these interplays with integrins are promoting the escape of cancer cells from the primary tumor.

Considering the pivotal role of platelets in facilitating metastasis as described in the previous section 2.3, it also seems that platelets can modulate functions of the immune system, such as inhibiting the anti-tumor immunity (Jenne & Kubes, 2015). Furthermore,

Platelet-derived growth factors have also been proposed to upregulate endothelial expression of adhesion molecules and alter endothelial permeability, thereby facilitating the adhesion and extravasation of metastatic tumor cells (Chiang et al., 2016; Labelle et al., 2011). Besides, thrombus formation is thought to support tumor cell extravasation by recruiting fibronectin and thereby facilitating the attachment of CTCs to blood vessels (Malik et al., 2010)

In addition, procoagulant thrombin has been described to target Factor XIII and fibrin(ogen), which are implicated in metastasis. Distinct functions such as thrombus stabilization have been proposed for FXIII and fibrin(ogen). FXII has also been described to play a role in directing macrophages. Given the importance of macrophages in metastasis, FXII could impact the metastatic potential (Muszbek et al., 2011). Fibrin(ogen) can also interact with immune cells such as macrophages and neutrophils that are associated with the formation of metastatic foci (Griesmann et al., 2017; Quail & Joyce, 2013; Spiegel et al., 2016).

4. RENAL CELL CARCINOMA (RCC)

According to the American Cancer Society, RCC cancer is among the 10 most common cancers in both sexes (Key Statistics About Kidney Cancer, 2022). Every year, nearly 430,000 new cases are diagnosed, and more than 150,000 deaths are reported. Approximately 1.8 percent of men and women will be diagnosed with kidney and renal pelvis cancer at some point during their lifetime.

Most RCC patients are already affected by the metastatic disease at the time of diagnosis. Specifically, data from one of the most important studies of metastasis distribution in RCC from the National Inpatient Sample (NIS) reported that the most common sites of metastasis are the lungs (45%), followed by bones (30%), lymph nodes (22%) and liver (20%). In a low incidence, adrenal and brain metastases were also found (9% each) (Bianchi et al., 2012).

RCC consists of more than 10 subtypes of Renal Cancers: Clear cell RCC, Papillary RCC, Chromophobe RCC, Multilocular cystic renal neoplasm of low malignant potential,

Collecting duct carcinoma, Renal medullary carcinoma, amongst others… the three first being the most common subtypes accounting for 85% of all renal malignancies. Each subtype of RCC varies widely in its genetic, pathologic, and clinical characteristics (Dudani et al., 2021).

4.1 Clear cell Renal Cell Carcinoma (ccRCC)

83% of RCC cases are represented by ccRCC, the most common subtype of this disease. It is believed that cells responsible for ccRCC originate from renal proximal epithelial cells, but the exact origin and differentiation process are still unknown (Tun et al., 2010). Histologically, ccRCC is characterized by showing clear cell morphology due to the accumulation of lipid and glycogen inside the cytoplasm, as shown in Figure 8 (Tun et al., 2010).
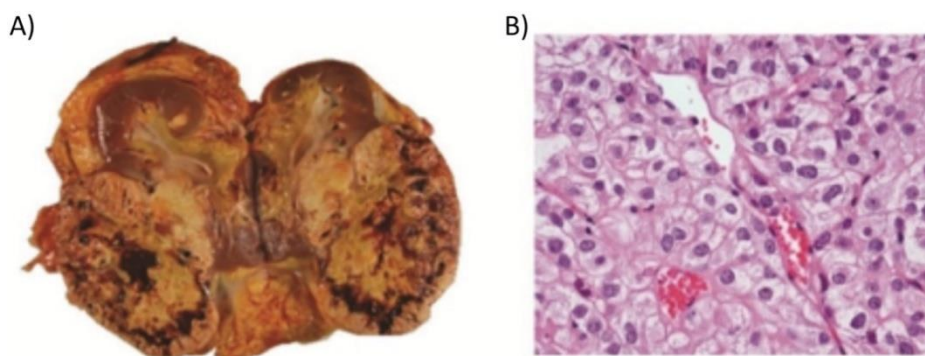
Figure 8. RCC tumor. A) Kidney with a tumor of a human patient. B) H&E staining of a ccRCC tumor (20X). Tumor cells present a clear phenotype, and the tumor has a delicate vascular network.

One of the most important genetic events in the development of ccRCC is the inactivation of the tumor suppressor gene von Hippel-Lindau (VHL). The VHL gene expresses a ubiquitin-ligase protein involved in the degradation of Hypoxia-Inducible Factor 1α (HIF1-α) and HIF2-α through oxygen and iron sensing mechanisms. Notably, tumors associated with the inactivation of this gene often present a high level of vascularization and an overproduction of mRNAs responsive to hypoxia and different angiogenic factors (Linehan et al., 2010).

4.2 Histopathological classification of RCC

Over the years, many different systems have been proposed to classify RCC. The most used one was the Fuhrman Grading System (FGS) proposed in 1982, classifying tumors depending on the nuclear size, shape, and nucleolar prominence of their cells. This classification uses four grades and correlates them with patient prognosis. The higher the grade the worse the prognosis (Fuhrman et al., 1982). However, this grading method did not include chromophobe RCC and the new subtypes of RC. In 2016, the WHO following the International Society of Urological Pathology (ISUP) proposed another grading system valid for most RCC subtypes (Table 1). However, it has not yet been validated for tumors with only a few reported cases (Moch et al., 2016).

WHO/ISUP grading system for RCC	
Grade	**Description**
Grade 1	Nucleoli absent or inconspicuous and basophilic at 40X
Grade 2	Nucleoli are not prominent at 10X but visible and eosinophilic at 40X
Grade 3	Nucleoli conspicuous and eosinophilic at 10X
Grade 4	Extreme nuclear pleomorphism, multinucleated cells, rhabdoid or sarcomatoid differentiation

Table 1. Nuclear grade classification of RCC. Table adapted from (Moch et al., 2016)**.**

4.3   Clinical classification of RCC

To describe the anatomic extension of RCC and the progression of the disease, it is classified into stages using the tumor-node-metastasis (TNM) system (Table 2). Initiated by the American Joint Committee on Cancer (AJCC), TNM is now the most common staging system to classify solid tumors and is based on three principal tumor features:

T	N	M
The size and extent of the main tumor	The extension to adjacent lymph nodes	The extension to distant organs

Table 2. Tumor-node-metastasis staging system

Another evaluation system divides RCC progression into four stages (Table 3) (Amin et al., 2017). One unresolved problem of RCC is that there are no screening methods to detect renal cancer in the early stages. For that reason, most patients tend to progress to metastatic disease at the time of diagnosis, and one-third of patients who undergo surgical resection will have a recurrence (Cairns, 2011). When the tumor is localized in the kidney the 5-year relative survival rate of patients is about 93%. However, as the tumor progresses, the survival rate of patients is drastically reduced to 14% when the cancer has metastasized ("National Cancer Institute," 2022). This critical data poses metastasis as one of the most relevant processes to study in RCC, to find possible therapies or predictive biomarkers.
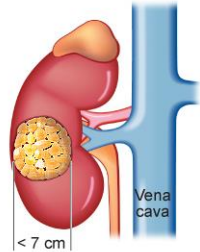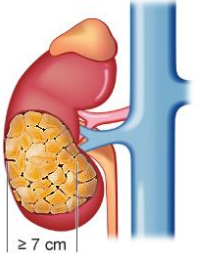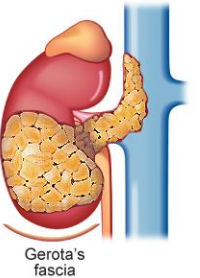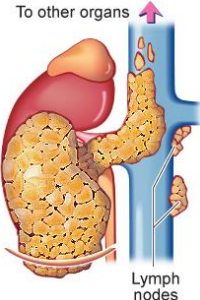
STAGE	DESCRIPTION	SCHEMATIC REPRESENTATION	5-YEAR SURVIVAL RATE
Stage I	Tumor is only in the kidney and it is smaller than 7cm.		**93%**
Stage II	Tumor is still limited to the kidney but is larger than 7cm.		**71%**
Stage III	Tumor has spread from the kidney to the surrounding tissue or nearby lymph nodes		**53%**
Stage IV	It is the last and the most advanced stage of the disease. The tumor has invaded the Gerota's fascia and cancer has spread to the lymph system or distant organs.		**14%**

Table 1. Stages of RCC. RCC is classified into stages I to IV depending on the progression and the extension of the disease. Images are extracted and adapted from("New Health Advisor", 2018). 5-year rate survival data has been extracted from the National Cancer Data Base (NCDB) (*American Cancer Society*, 2018)

4.4 RCC treatment

Surgery is the first treatment of choice in RCC, as only by re-sectioning the tumor mass it is possible to entirely cure the disease. The surgery is comprised of partial or radical nephrectomy (Hsieh et al., 2017b). As described previously in section 3.3, many patients experience recurrence or might already be affected by metastasis at diagnosis, requiring additional systemic treatment.

Anti-angiogenic therapies are commonly used in RCC patients with advanced stages of the disease. The previous section 4.1 describes how numerous RCC patients had an inactivated VHL gene that led to an upregulation of pro-angiogenic factors such as VEGF. For that reason, targeting VEGF receptor and its ligands is considered a potential therapeutic intervention for RCC patients (Rini, 2007). Several agents such as Bevacizumab, Sorafenib, Sunitinib, and Pazopanib are used in mRCC patients as a 1st line treatment (de Falco, 2014)

Another strategy to treat RCC patients is mTOR inhibitors. mTOR is a highly conserved serine/threonine kinase from the PI3K-related kinase family/AKT and plays a crucial role in the regulation of cell growth, proliferation, and metabolism. Temsirolimus is administered to RCC patients in an advanced stage of the disease and Everolimus is administered as a second-line treatment for RCC patients when sorafenib and/or sunitinib therapy fails (Pontes et al., 2022; Voss et al., 2011)

Finally, immunotherapy is another way to treat RCC patients. A new generation of immunotherapeutic drugs called T-cell immune-checkpoint inhibitors came out. Some examples are Avelumab and Atezolizumab, two antibodies against the cell death protein-1 ligand (PDL-1). Other antibodies target the programmed cell death protein-1 (PD-1) such as Nivolumab and Pembrolizumab (Hsieh et al., 2017b).

Figure 9 sums up approved treatments against metastatic RCC (mRCC) that appeared over time. Despite the enormous progress therapeutic strategies have seen, there is still

great variability in treatment response. This is due to the heterogeneity between tumors and even between different parts of the same tumor (Hsieh et al., 2018).
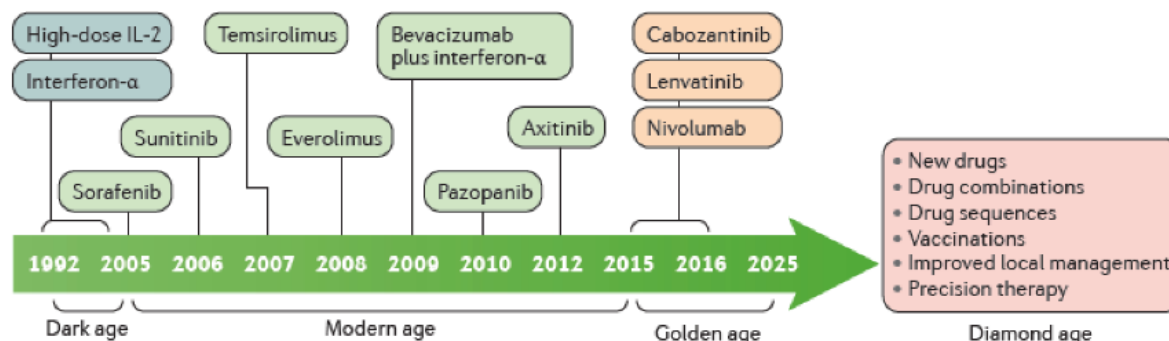
Figure 9. Treatment evolution of metastatic Renal Cell Carcinoma over time. First treatments were based on immunotherapy. Since 2005 new drugs appeared to enhance the treatment and the survival of patients. Finally, the golden age was characterized by the discovery of some monoclonal antibodies. Nevertheless, new drugs are being investigated to overcome the limitations of existing therapies. Figure extracted from (Hsieh et al., 2017).

5. PREVIOUS DATA

5.1 Spontaneous generation of two variants of a ccRCC patient-derived orthoxenograft mouse model

Previous work in the laboratory, performed by Mar Martínez-Lozano, consisted of developing a patient-derived orthoxenograft (PDOX) murine model based on a human biopsy, that originated from a patient who suffered from ccRCC and ganglionic metastasis at the time of diagnosis (pT3a pN1). The tumor had a Fuhrman 4-grade and was implanted into the kidney of an athymic mouse (orthotopic) (Figure 10A) and then further passaged, which led to an orthoxenograft line named Ren 50. Later on, the patient also developed lung metastasis, and consistent with this diagnosis we also found a spontaneous macrometastasis in the lungs of a euthanized orthotopic mouse (Figure 10B). This spontaneous macrometastasis was also implanted into another animal, generating a different line named Ren 50M. This procedure was repeated several times to generate two different orthoxenograft groups of tumors with shared mouse and patient origins (Figure 10C). However, Ren 50M line has been generated from a natural selection of cells with the capacity to metastasize *in vivo*.
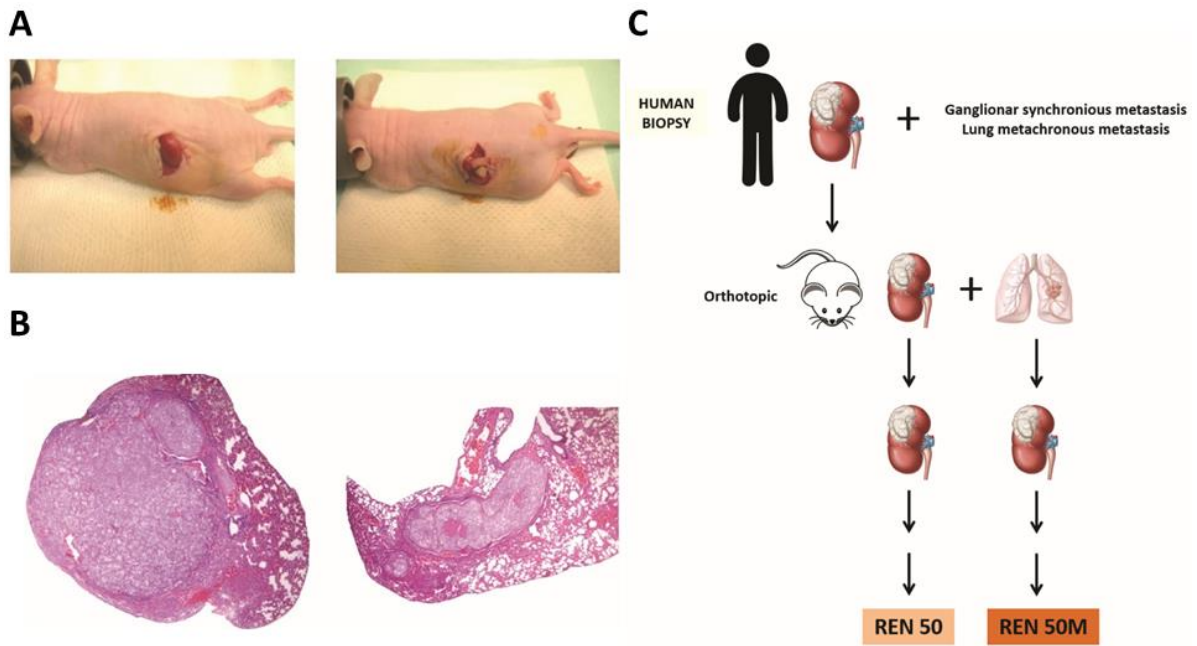
Figure 10. PDOX mouse model of ccRCC. Tumor implantation of a RCC piece of tumor into an athymic mouse. A, left) A skin incision was performed on the kidney's space and the organ was externally visible. A, right) The piece of tumor was implanted into the kidney of the orthotopic mouse. B) The orthotopic mouse presented both, micrometastases and macrometastases in the lung. Pictures of H&E staining (4X) of lung metastases from the orthotopic mouse. C) Graphic representation of Ren 50 and Ren 50M mouse orthoxenograft tumor line models. Figure has been adapted from Dra. Mariona Bartrolí thesis.

5.2 Metastatic potential of Ren 50 and Ren 50M tumors

After different rounds of tumor implantations of Ren 50 and Ren 50M lines, the metastatic capacity of both lines was evaluated. Ren 50 tumors presented a very low metastatic potential and the type of lesions identified were only micrometastasis. Ren 50M, on the other hand, developed ccRCC tumors and lung metastases at a higher frequency. Furthermore, we found both macro and micrometastasis lesions within the lungs (Figure 11). Altogether, these results demonstrated a clear difference in metastatic capacity between Ren 50 and Ren 50M tumors, even though both came from the same orthotopic animal and the same cancer patient.
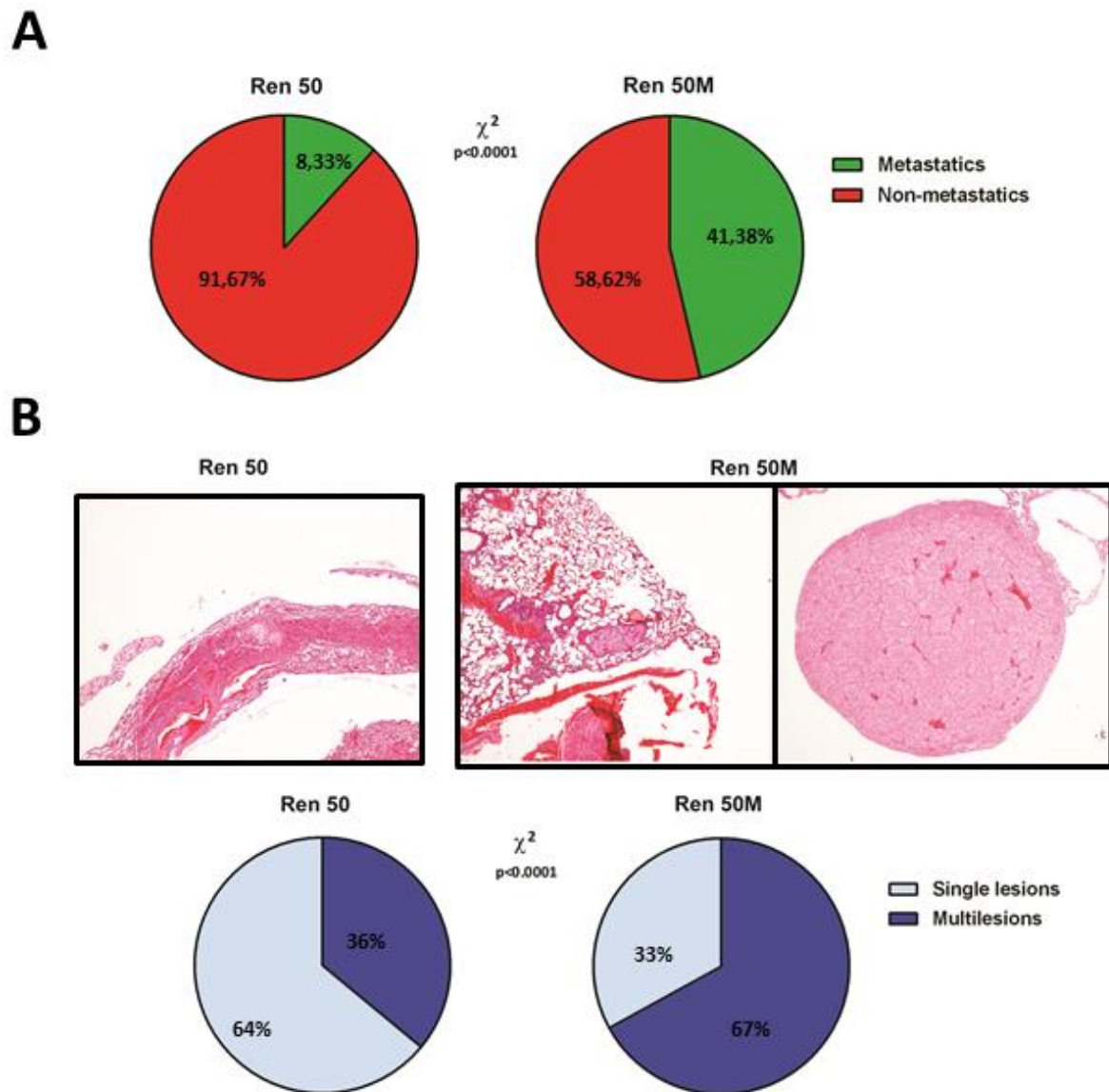
Figure 11. Ren 50M tumors presented higher metastatic incidences and multiple lesions compared to Ren 50 tumors. A) Schematic representation of the percentage of metastasis analyzed after 25-40 days. On the left, Ren 50 mice % of metastasis, and on the right, Ren 50M mice % of metastasis. Results show a statistically significant difference between both groups by Chi-square test. B) Pictures at 4x of H&E staining of a micrometastasis from a Ren 50 lung and micro and macrometastasis from a Ren 50M lung with the radial representation of the percentage of single lesions or multilesions present in the lungs. Results showed a statistically significant difference between both groups by Chi-square test. Figure has been adapted from Dra. Mariona Bartrolí thesis.

5.3 RNA sequencing and gene set enrichment analysis of Ren 50 and Ren 50M tumors

Whole RNA sequencing was performed to detect mRNA expression differences between groups. Four Ren 50 and four Ren 50M tumors were analyzed by this technique, resulting

in a long list of differentially expressed genes, presenting both downregulations and upregulations.

The expression profiles were subjected to a gene set enrichment analysis (GSEA) to analyze whether any gene signature was upregulated or downregulated in our samples.

GSEA is a computational method that determines which set of genes shows statistically significant differences in gene expression levels. Gene sets are available at Molecular Signatures Database (MSigDB) and GSEA was run according to default parameters: collapses each probe set into a single gene vector (identified by its HUGO gene symbol), permutation number= 1000, and permutation type= "gene-sets". Calculation of the FDR was used to correct for multiple comparisons and gene set sizes(Subramanian et al., 2005). RNA sequencing results were compared to all gene sets available (From C1 to C7). Remarkably, results from the GSEA showed an upregulation of genes related to hemostatic regulation within the signature "Regulation of body fluid levels" (from the C5-Biological Process data set) in the metastatic Ren 50M tumors compared to non-metastatic Ren 50 tumors (Figure 12).
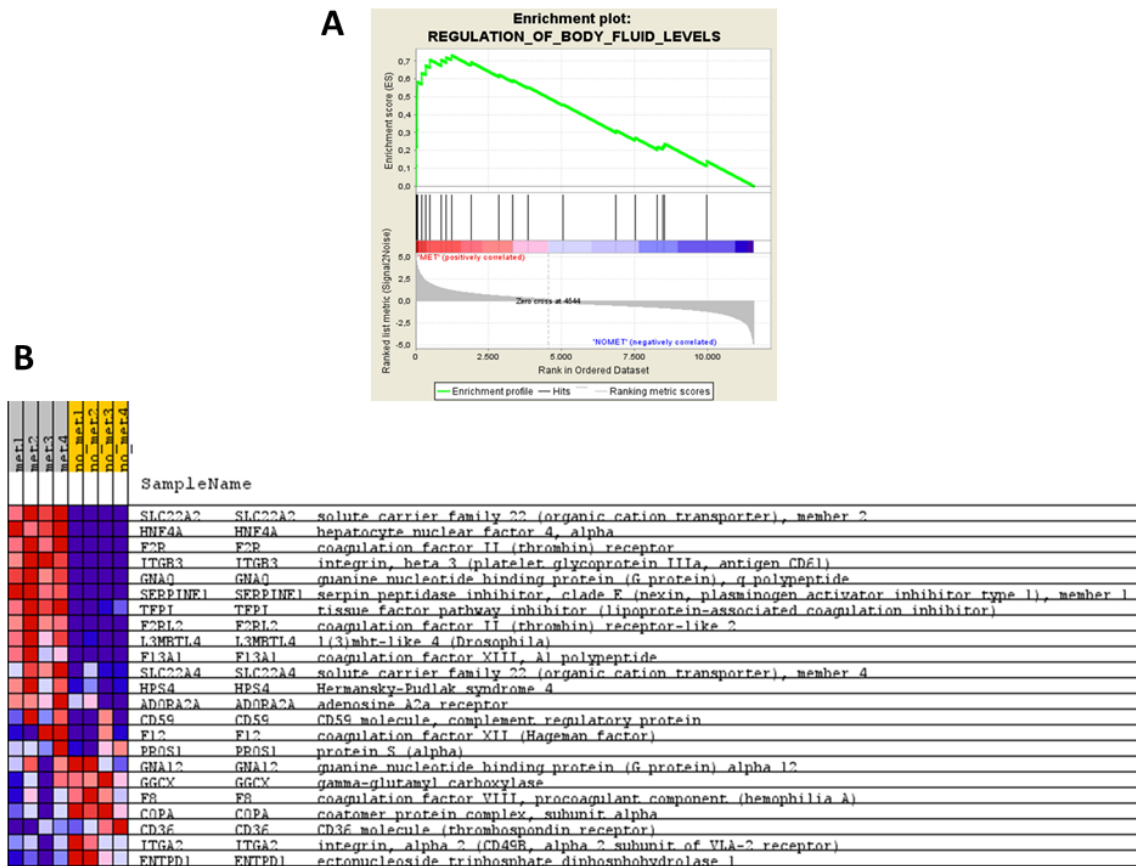
Figure 12. Results from GSEA revealed that Ren 50M samples highly correlated with the Regulation of body fluid levels signature. A) Regulation of blood fluid levels enrichment plots. In red: enriched genes in our four samples, which positively correlated with the signature. In blue: genes which expression was negatively correlated. B) Heat map of gene expression of genes from the Regulation of body fluid levels signature in Ren 50 and Ren 50M. "MET" samples corresponded to four tumors of Ren 50M and "NOMET" samples corresponded to four tumors of Ren 50. Figure has been extracted from Dra. Mariona Bartrolí thesis.

5.4 Coagulation pathway-related genes

Among all the genes of the Regulation of body fluid levels signature, twelve genes are implicated in the blood coagulation pathway (Figure 13).

GENE_Symbol	Description	GSEA Core Enrichment	Fold Change	P Value	FDR	Mean Ren 50	Mean Ren 50M
SLC22A2	Solute Carrier Family 22 (organic cation transporter), member 2	YES	1322.4672	9.39E-93	1.35E-89	0.0347	45.9164
F13A1	Coagulation factor XIII, A1 polypeptide	YES	639.2797	1.04E-40	2.21E-38	0.6037	385.9226
HNF4	Hepatocyte Nuclear Factor 4, alpha	YES	287.6259	2.29E-91	8.48E-46	0.0447	12.8683
F2R	Coagulation factor II Thrombin Receptor	YES	76.9164	5.91E-82	5.88E-79	1.9530	150.2202
GNAQ	Guanine Nucleotide Binding Protein (G protein), q polypeptide	YES	16.9633	8.43E-53	2.87E-50	3.4701	58.8640
ITGB3	Integrin, Beta 3 (platelet glycoprotein IIIa, antigen CD61)	YES	12.9162	2.49E-28	3.15E-26	1.0127	13.0808
SERPINE1	Serpin Peptidase Inhibitor, clade E (nexin, plasminogen activator inhibitor type 1), member 1= PAI1)	YES	8.7405	3.04E-49	9.92E-47	64.8592	566.9026
F2RL2	Coagulation Factor II (thrombin) Receptor-like 2	YES	8.4343	1.98E-10	5.92E-09	0.2238	1.8877
TFPI	Tissue Factor Pathway Inhibitor (lipoprotein-associated coagulation inhibitor)	YES	3.6902	1.11E-14	5.39E-13	28.4133	104.8516
L3MBTL4	l(3)mbt-like 4 (Drosophila)	YES	2.6331	1.07E-06	1.75E-05	2.8373	7.4710
SLC22A4	Solute Carrier Family 22 (organic cation transporter), member 4	YES	1.8178	0.0068	0.0384	1.5504	2.8183
HPS4	Hermansky-Pudlak Syndrome 4	YES	1.6589	0.0001	0.0016	342.4818	568.1597

Figure 13. Twelve genes from the Regulation of body fluid levels signature of GSEA were enriched in our data set. F2R was one of the genes with a high fold change and also high gene expression levels in Ren 50M tumors. Table of selected gene sets enriched in samples from Ren 50M (n=4) compared to Ren 50 (n=4) tumors. Fold Change was obtained by comparing their expression levels (cpm). p-value and FDR represent the value of a test for statistical significance. Figure has been extracted from Dra. Mariona Bartrolí thesis.

During the passages of the tumor, we observed that Ren 50M animals normally featured reddish skin. In contrast, no alteration in skin color was observed in mice from the Ren 50 line (Figure 14A). However, we did not find any difference in the hematocrit analysis that we performed using animals from both groups (data not shown). However, by performing a microscopic analysis of the H&E tumor staining, we found some differences in the vascular phenotype between both lines. We also performed IHC analyses using the endothelial marker CD31 and the results show that Ren 50 tumors have long and thin vessels, whereas Ren 50M normally are characterized by dilated vessels with big lumens (Figure 14B)

The alteration of blood vessel shape could be associated with the increase in metastasis. For that reason, we decided to perform more analysis to determine its possible

correlation. We decided to group the animals regardless of the Ren line, based on two parameters: the vascular and the metastatic phenotype. We classified the tumors with long and thin vessels as Phenotype 1 and the others with dilated vessels as Phenotype 2. Using this classification, we realized that Ren 50 tumors show both phenotypes, whereas almost all tumors from the Ren 50M line only show phenotype 2 (Figure 14C). Besides, phenotype 1 could be associated with the non-metastatic animals and almost all metastatic animals presented phenotype 2 (Figure 14D).
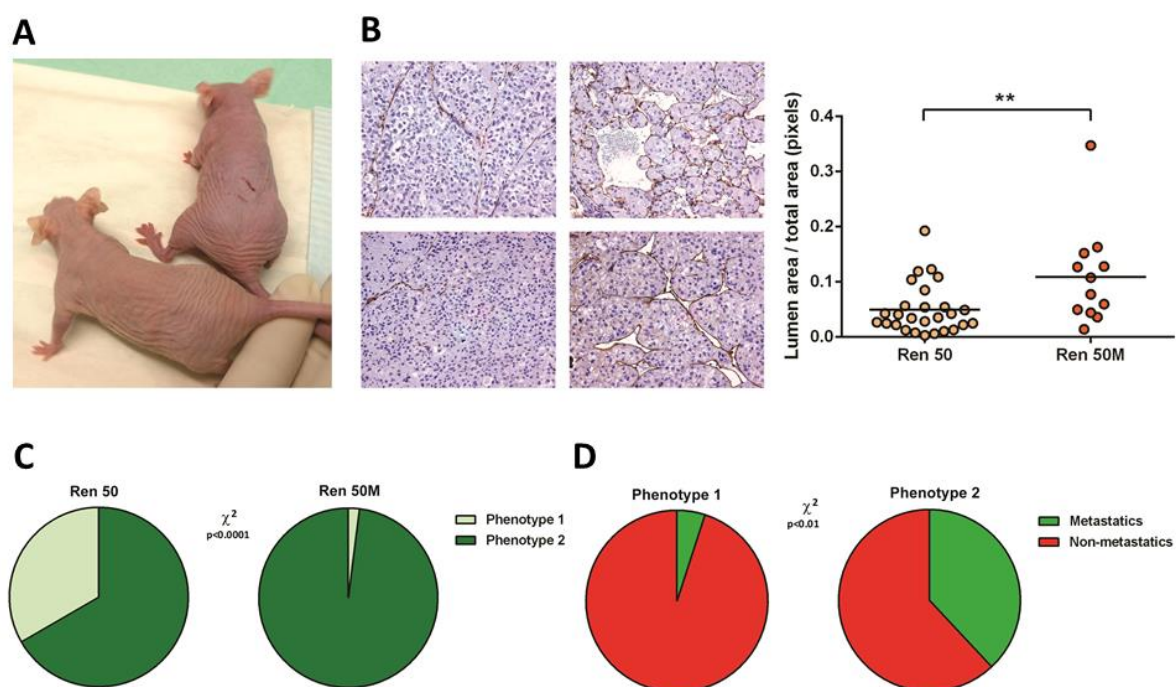
Figure 14. Ren 50M tumors presented reddish skin and differences in the tumor vasculature A) Picture of mice from Ren 50 (on the left) and Ren 50M (on the right). B) IHC against CD31 endothelial marker was performed. From left to right, two pictures of Ren 50 tumors and two of Ren 50M (20X) with their respective quantification of lumen vessels' area from 27 tumors of Ren 50 and 12 tumors of Ren 50M. Results were statistically significant by the Mann-Whitney test. C) Quantification of mice classification regarding their Ren line and vascular phenotype. Results were statistically significant by Chi-square test, ****p value <0.0001. D) Quantification of mice classification regarding their vascular and metastatic phenotype. Results were statistically significant by Chi-square test, **p value<0.01. Quantifications were performed considering 112 mice in total. Figure has been adapted from Dra. Mariona Bartrolí thesis.

5.5 Coagulation Factor II Thrombin Receptor (F2R)

After careful evaluation of the data, Dra. Susana Aguilar and Dra. Mariona Bartrolí decided to focus on one of the top-ranked genes that presented a clear overexpression in Ren 50M in comparison with Ren 50: Coagulation Factor 2 Thrombin Receptor (F2R or PAR1). Being a membrane receptor with known ligands and inhibitors, F2R represents an ideal candidate, whose activity can be easily modulated to study its implication in metastasis.

Protease-activated receptor 1 (PAR1), also named Coagulation Factor Thrombin Receptor 2 (F2R), is a member of the PAR family and is composed of a sequence of 425 amino acids and a molecular mass of 68-80 kDa with a reduction to a 36-40 kDa by deglycosylation (Soto et al., 2015; Soto & Trejo, 2010).

Homeostasis of blood coagulation is partially regulated by protease-activated receptor (PAR)-signaling (Isermann, 2017). Protease-activated receptors (PARs) are the largest family of signaling receptors expressed in mammalian cells. This family consists of seven-transmembrane G-protein coupled receptors (GPCRs) localized at cell surfaces that are activated uniquely by the cleavage of their extracellular N-terminus at a specific site, allowing the internal ligand to autoactivate (Alberelli & de Candia, 2014)

Four members of this family have been described: PAR1, PAR2, PAR3, and PAR4. Depending on the receptor, they can be activated by different serine proteases or matrix metalloproteases. Thrombin is the major activator of PAR 1/3/4, whereas PAR2 is activated by trypsin-like enzymes as well as coagulation factors VIIa and Xa (S. Coughlin, 2005; Flaumenhaft & de Ceunynck, 2017)

The activation of these receptors affects signaling events involved in different cellular processes, such as proliferation, migration, invasion, or the production of chemotactic and proangiogenic factors, regulating both, physiological and pathological processes in multiple organs (Han et al., 2011).

F2R is activated by thrombin, which cleaves its amino-terminal exodomain between residues Arg 41 and Ser 42 (LDPR41/42SFLLRN) irreversibly. Cleavage of the N-terminal segment reveals a tethered ligand that associates with a shallow binding site on the extracellular face of the receptor. Ligation of the binding site induces a conformation change in the receptor that is transmitted to cognate G-proteins which in turn initiate transmembrane signaling (Flaumenhaft & de Ceunynck, 2017). GPCRs interact with heterotrimeric G proteins composed of α, β, and γ subunits that are bound to GDP in the resting state. Agonist binding triggers a conformational change in the receptor, which catalyzes the dissociation of GDP from the α subunit followed by GTP-binding to Gα and the dissociation of Gα from Gβγ subunits. The Gβ and Gγ subunits function as a dimer to activate several signaling molecules, including phospholipases, ion channels, and lipid kinases (Dorsam & Gutkind, 2007) (Figure 15).
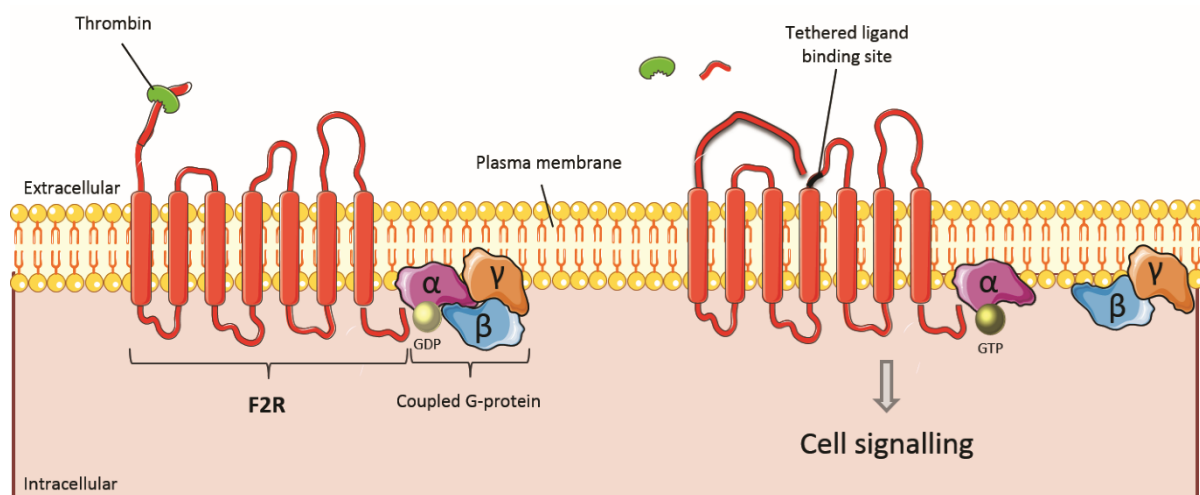
Figure 15. Schematic representation of thrombin-mediated F2R activation. After F2R cleavage by thrombin, a new amino-terminus domain binds to the body of PAR1 itself, triggering signaling G-proteins. The image has been adapted from (Alberelli & de Candia, 2014).

Apart from its role in homeostasis by controlling blood coagulation (Isermann, 2017), F2R is involved in cancer through different mechanisms (Wojtukiewicz et al., 2015a).

On the one hand, it is involved in the early steps of the metastatic cascade, since its interaction with integrins has been demonstrated to enhance the invasive phenotype of tumor cells (Cohen Even-Ram et al., 2001). On the other hand, it plays an interesting role in the systemic circulation of tumor cells. It acts on the surface of tumor cells and platelets by increasing procoagulant activity and by enabling their cohesion to form

heteroaggregates, thus helping tumor cell extravasation and preventing NK-mediated elimination (L. Gay & Felding-Habermann, 2011a; Palumbo, 2008).

Furthermore, PAR1 has been described to be overexpressed and plays different roles in breast cancer (Hernández et al., 2009), melanoma (Tellez & Bar-Eli, 2003) CRC (Darmoul et al., 2003), and HCC (Kaufmann et al., 2007). Considering that, together with the increased expression in Ren 50M tumors, we decided to focus on this receptor, trying to find new roles of F2R in metastasis.

5.6   Expression of F2R in Ren 50 and Ren 50M tumors

First of all, we decided to confirm the robust differences found in RNA sequencing by Taqman® assay (qRT-PCR) in tumors throughout different passages. The newly obtained results confirmed that RNA expression of our receptor in Ren 50 tumors is indeed very low. RNA levels in Ren 50M tumors are higher (Figure 16A). We could hence confirm that despite performing different passages, RNA expression is maintained in both, Ren 50 and Ren 50M tumors.

Next, we also validated these observations at the protein level. Results of western blot analysis (Figure 16B) and immunohistochemistry (Figure 16C) show almost no expression of F2R proteins in Ren 50 tumors and their metastasis. In contrast, Ren 50M tumors and metastasis -from different passages- show much higher protein expression levels.

We then hypothesized that the few and small metastases in Ren 50 mice were probably generated by mechanisms that involved other genes than the Ren 50M driving ones. As previously observed, the incidence and size of metastases between both groups differ considerably. Moreover, there is a strong association between the expression of our candidate and Ren 50M tumors and their metastases. Altogether, these results prompted us to further study F2R and its important role in the metastatic process.
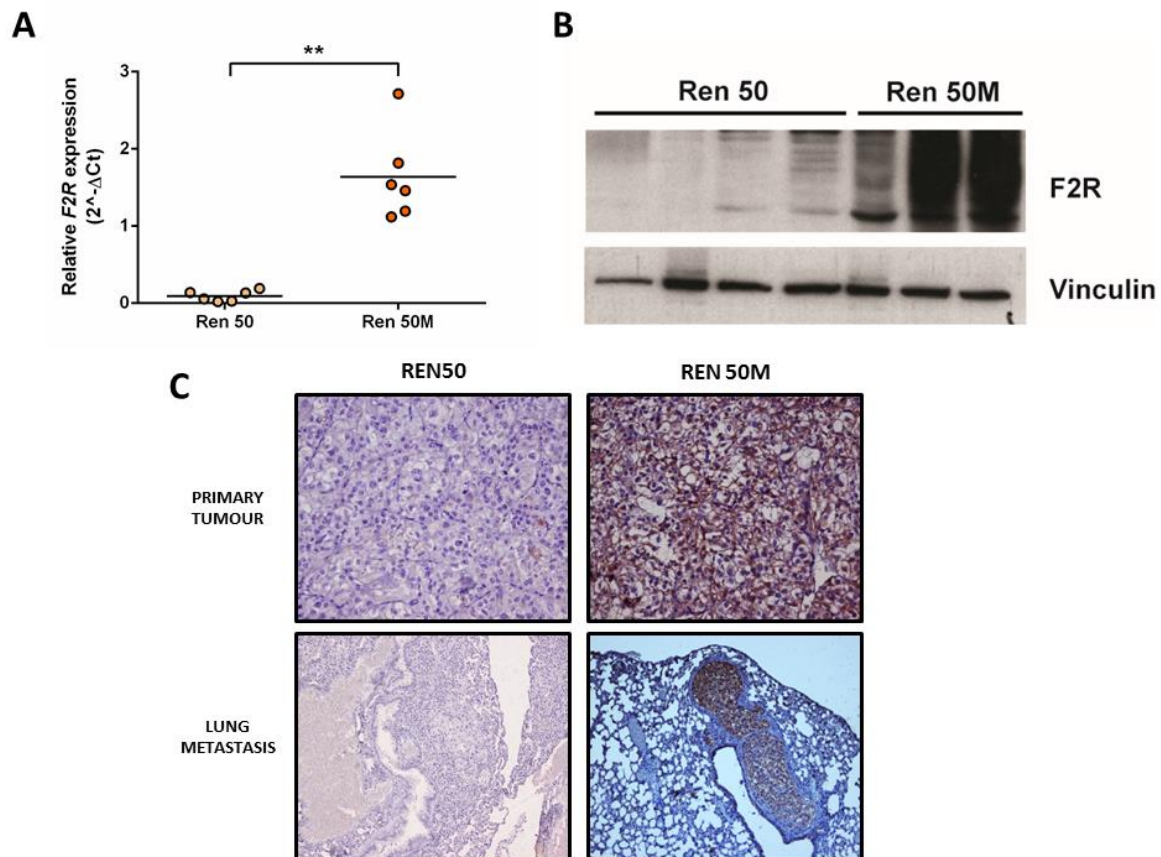
Figure 16. Ren 50M tumors and metastasis showed higher levels of F2R expression in comparison to Ren 50. A) Results were obtained from a Taqman® assay of six tumors of Ren 50 and Ren 50M. RNA quantification of F2R was normalized with HPRT1 and measured by $2^{-\Delta CT}$. B) Western Blot analysis of F2R protein expression in Ren 50 and Ren 50M tumors. C) F2R protein detection by IHC of Ren 50 and Ren 50M tumors. Images were taken at 20X. Figure has been adapted from Dra. Mariona Bartrolí thesis.

5.7 F2R expression in RCC cell lines and tumors

Previous work in the group was dedicated to the generation of a stable primary cell line derived from Ren 50M tumors, but without any success. For that reason, we decided to search for an *in vitro* model that could mimic the properties of Ren 50M tumor cells. We, therefore, analyzed F2R expression in different RCC cell lines by performing Taqman® assays and were able to detect some cell lines with a distinct F2R expression. The highest levels were expressed by RCC4- and SN12C cells (Figure 17A). Furthermore, F2R expression was evaluated in SN12C by Inmunocitofluorescence (Figure 17B). Besides, tumors were generated and F2R was analyzed by IHC (Figure 17C). Based on previous studies in our group that could observe a high aggressiveness and an elevated metastatic capacity *in vivo* (data not shown), SN12C cells were chosen to evaluate our candidate.
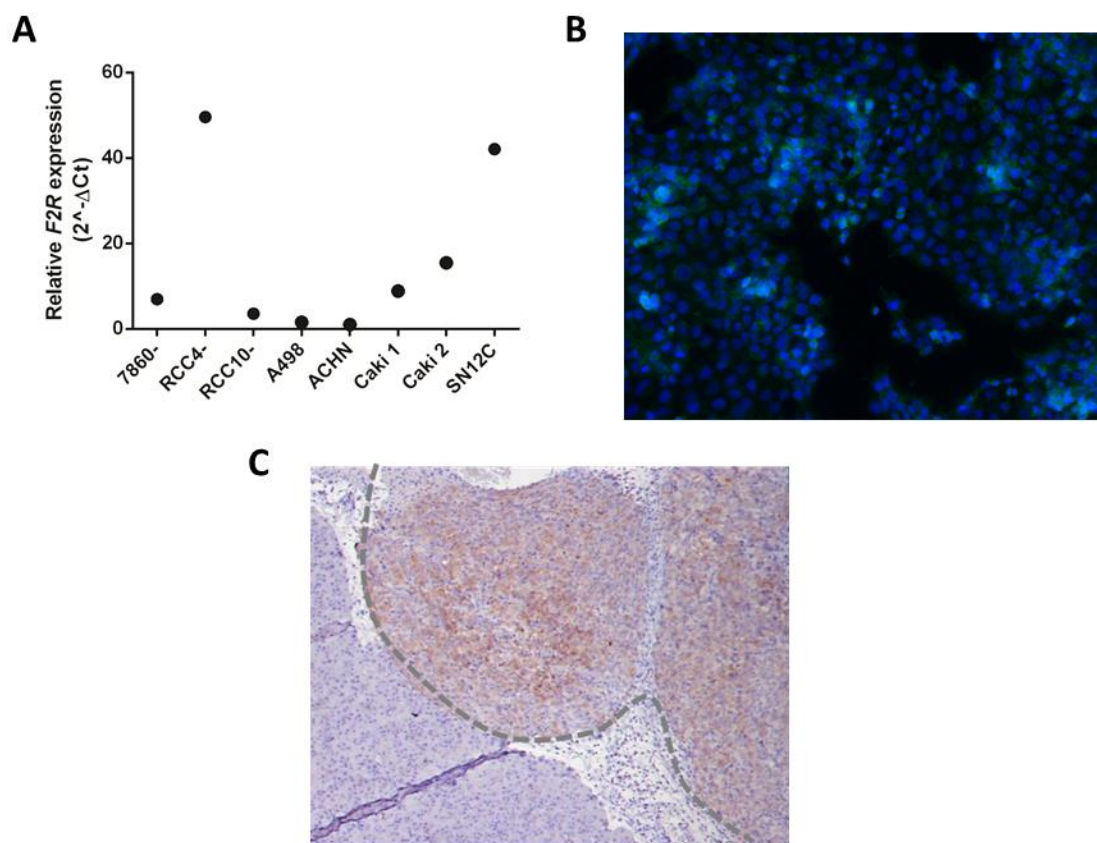
Figure 17. RCC4- and SN12C cell lines showed higher expression of F2R at RNA and protein levels. A) Results were obtained from a Taqman® assay of different RCC cell lines. RNA quantification of F2R was normalized with HPRT1 and measured by $2^{-\Delta CT}$. B) Immunocytofluorescence of F2R in SN12C cells. Representative pictures at 10X are shown. C) F2R IHC of SN12C tumors. Cells were injected into the kidney of mice and then tumors were perpetuated. Grey line represents the tumor-kidney contact. Picture was taken at 10X. Figure has been adapted from Dra. Mariona Bartrolí thesis.

5.8 Effects of F2R inhibition in *in vivo* models of SN12C

As many studies assign a role of PAR receptors in the different metastatic steps, we decided to study whether we could see any effect in metastasis when inhibiting F2R. For that reason, we inoculated SN12C cells through the tail vein, forcing the process of generating metastasis. Then, mice were orally treated with a control vehicle or vorapaxar, a competent selective F2R inhibitor already approved in patients for the antithrombotic treatment of coronary and peripheral vascular disease (Chackalamannil et al., 2008).

Results showed that F2R inhibition did not affect the number of affected lobes (Figure 18A). However, a clear decreasing tendency in the total metastatic area and density was observed in animals treated with vorapaxar (Figure 18B).
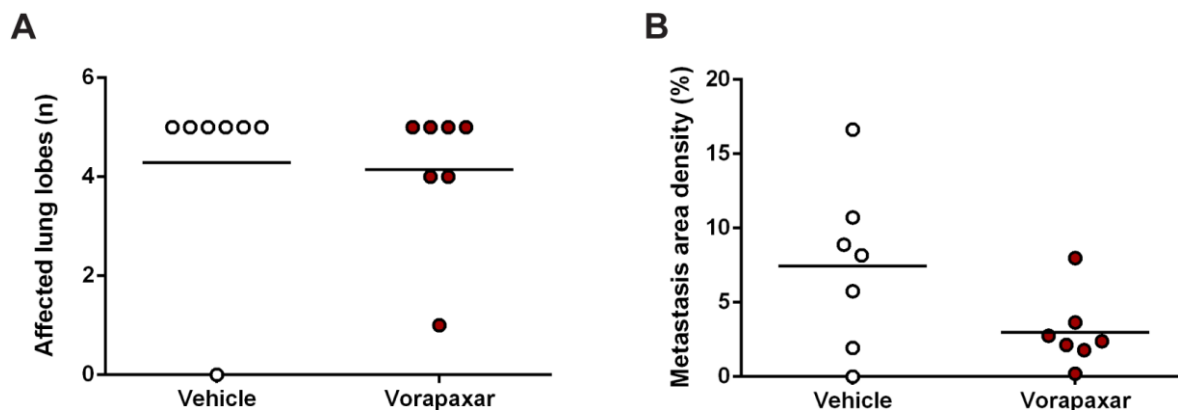
Figure 18. F2R inhibition did not affect the number of affected lung lobes but showed a reduction in the total metastasis area density. 10^6 SN12C cells were injected through the tail vein. Mice were divided into two groups and were orally treated with vehicle (n=7) or vorapaxar (n=7) at a dose of 20mg/kg/day since the day after injection. Analyses were performed using vimentin immunohistochemistry. A) Affected lung lobes were quantified depending on the presence of lesions. B) Quantification of the total metastasis area density. To quantify, the total metastasis area was normalized by the total lung area quantified for each animal per group. Figure has been extracted from Dra. Mariona Bartrolí thesis.

To confirm the possible implication of F2R in metastasis, we generated SN12C tumors in the kidney. After that, two groups were orally treated with vehicle or vorapaxar. First, to study if F2R was affecting tumor growth, tumor volume was monitored during the entire treatment by palpation. Results show that tumors have the same growth rate regardless of F2R inhibition (Figure 18).

Then, we decided to study whether F2R inhibition was affecting tumor invasiveness. For that reason, we qualitatively classified tumors regarding their invasive phenotype. We confirmed that vorapaxar treatment tends to reduce the invasive capacity of tumors compared to controls (Figure 19B). Then, we characterized tumor invasion by quantifying tumor invasive fronts (Figure 19C). Results did not show a clear and significant difference between both groups. However, the vorapaxar-treated group show a downward trend in tumor invasion compared to mice treated with vehicle (Figure 19D).
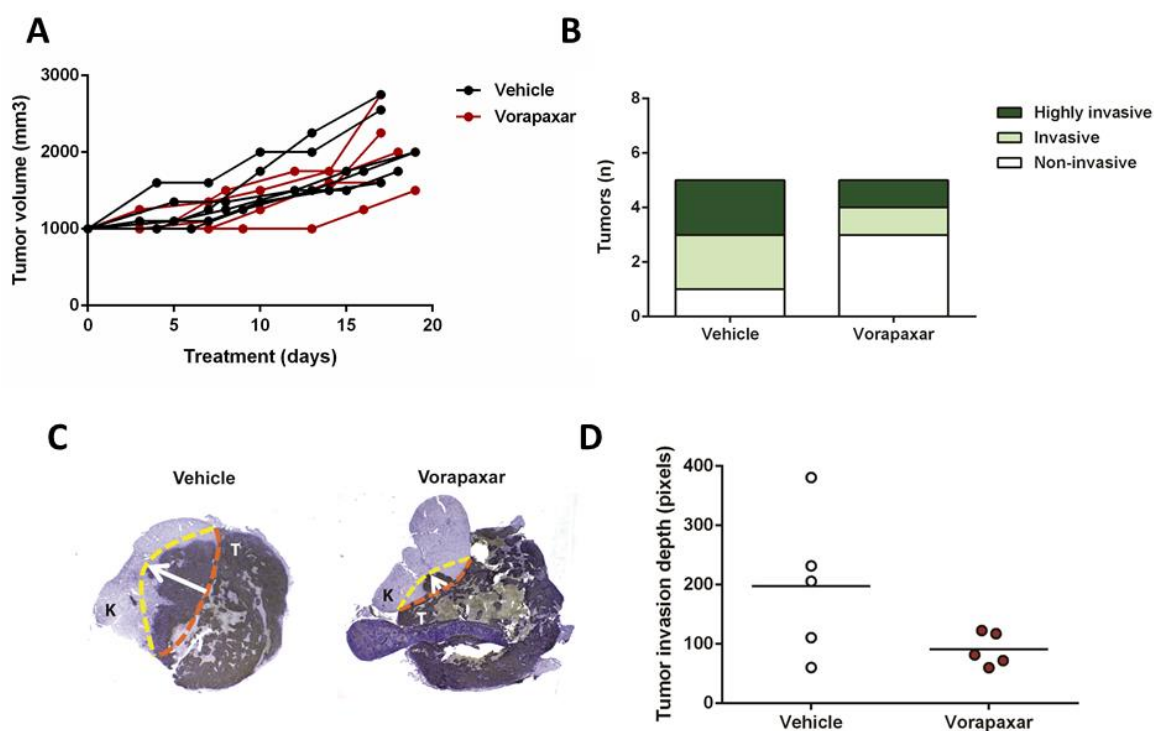
Figure 19. F2R inhibition did not affect tumor growth but is affecting the invasive capacity of tumors. A) Tumor volume was monitored by palpation and treatment started when tumors reached 1000mm^3. 6 mice were treated with vehicle and 5 mice with vorapaxar at a dose of 20mg/kg/day. Measurements were taken during 17-19 days. B) H&E staining was microscopically classified into three groups, regarding their invasive phenotype. 5 tumors from each group were analyzed C) Vimentin immunohistochemistry was performed to quantify invasive fronts of 5 control tumors and 5 vorapaxar-treated tumors. Pictures were taken at 0.57X and the invasive front was drawn and quantified. T: Tumor. K: Kidney. D) Tumor invasion depth quantification. Results were not statistically significant but a clear tendency on reduced invasion was observed. Figure has been adapted from Dra. Mariona Bartrolí thesis.

We next investigated if F2R inhibition has any effect on the metastatic capacity of SN12C tumors. For that reason, we performed a more thorough metastatic study analyzing lung metastases from treated and untreated mice.

We started analyzing the affected lung lobes, but no differences could be observed (Figure 20A). However, we realized that the lesions were more frequent and bigger in controls compared to vorapaxar-treated mice (Figure 20B and Figure 20C). This data confirms that F2R inhibition results in a clear reduction of total metastatic area and density (Figure 20D).
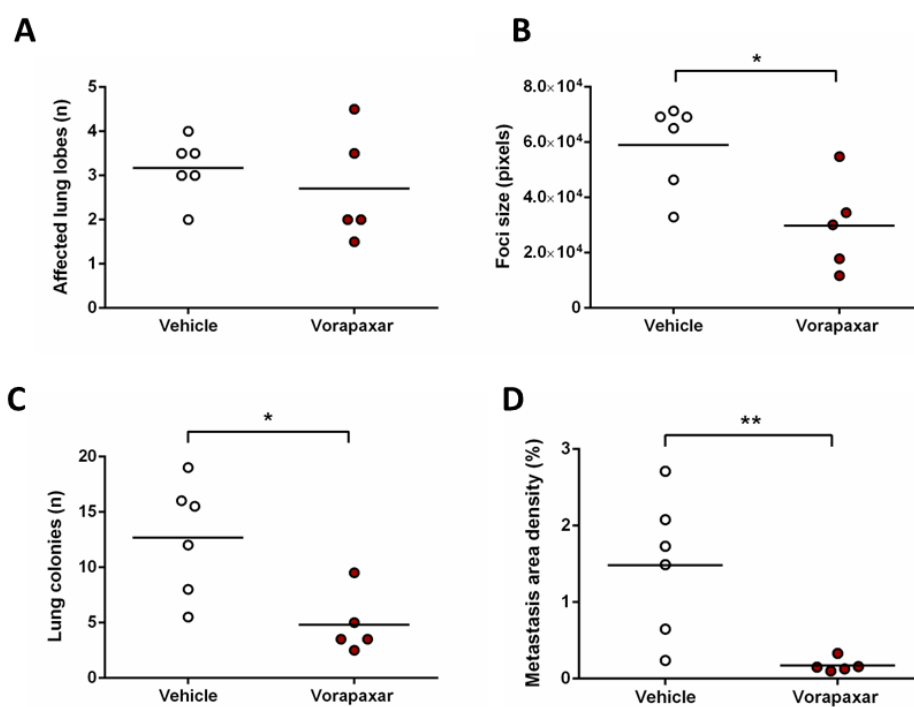
Figure 20. F2R inhibition leads to a reduction of the metastatic capacity of SN12C tumors. A) Tumor cells were detected and quantification of affected lung lobes was analyzed. B) Foci size was calculated by quantifying all metastatic areas normalized by the number of foci present in each lung C) Number of lung colonies in each lung was determined. D) Total metastatic area density was determined by quantifying the total metastatic area normalized by the total lung area of each lung. Pictures of metastases were taken at 10X pictures of the lungs at 0.57X. Figure has been adapted from Dra. Mariona Bartrolí thesis.

In summary, our results demonstrate that F2R inhibition causes a decrease in metastasis in SN12C tumors and a downward trend in tumor invasion, which represent two of the hallmarks of cancer (Hanahan & Weinberg, 2011). For that reason, we decided to put the focus of this thesis on the study of the mechanism through which F2R is contributing to tumor aggressiveness.

HYPOTHESIS

Taking the interesting interplay between the coagulation factors described in the literature, and taking into account that we found an overexpression of different coagulation-related genes in a metastatic RCC, we hypothesize **that Coagulation Factor II Thrombin Receptor (F2R) is contributing to tumor malignization and metastasis**. For that reason, we wanted to evaluate the implication of F2R on metastasis, to ultimately find prognostic factors and new therapeutic targets to block this insidious event in advanced RCC patients.

OBJECTIVES

To confirm the global hypothesis, we will start focusing on the mechanism of how F2R is contributing to metastasis by using PDOX animal models of RCC and *in vitro* cell culture systems for Loss-of-Function and Gain-of-Function. Finally, we will end up with a clinical validation of the obtained results. Therefore, the specific objectives are:

1. To validate our candidate F2R both *in vitro* and *in vivo* by Gain-of-Function and Loss-of-Function studies in cells and tumors.

2. To elucidate the molecular mechanism by which the coagulation factor F2R is contributing to tumor malignization and metastasis.

3. Clinical validation by a selection of markers that could be useful as prognostic factors to detect metastatic potential, and also identify therapeutic targets that could allow the inhibition of this process.

MATERIALS AND METHODS

1. IN VITRO

1.1 Cell culture

1.1.1 Cell line maintenance

Renal cell lines (RCC4, RenCa, and 786-O) were maintained with RPMI Medium 1640 (Gibco, #31870-025) and SN12C cells were maintained with Dulbecco's Modified Eagle Medium (DMEM) (Lonza, #BE12614F), both supplemented with 50U/ml of penicillin, 50µg/ml of streptomycin sulfate, 2mM of L-glutamine, 10mM of HEPES, 1% of Non-essential aminoacids and 10% of fetal bovine serum (FBS) (all from Gibco), which was previously inactivated by heating at 55$^{\circ C}$ for 30min. All cells were maintained at 37$^{\circ C}$ in humidified conditions with 5% CO_2.

1.1.2 Cell lines

All cell lines used in this thesis have human kidney tissue origin and are outlined in Table 4. pVHL-deficient 786O cell line was kindly provided by B. Jimenez (Instituto de Investigaciones Biomédicas CSIC-UAM, Madrid, Spain). The rest of them were kindly supplied by F. Setién from the cell culture facility of the Programa d'Epigenètica i Biologia del Càncer (PEBC).

Cell line	Disease	Medium
786O-	Renal Cell Adenocarcinoma	RPMI 1640
RCC4-	Clear Cell Carcinoma	RPMI 1640
SN12C	Renal Cell Carcinoma	DMEM
RenCa	Renal Adenocarcinoma	RPMI 1640

Table 4. List of cell lines derived from human tissue used

1.1.3   Mycoplasma test

All cell lines were routinely tested from mycoplasma contamination by PCR using the following oligonucleotides:

Oligonucleotide	Sequence
MICO-1	5'- GGCGAATGGGTGAGTAACACG - 3'
MICO-2	5'- CGGATAACGCTTGCGACTATG - 3'

Table 5. Oligonucleotides are used for the detection of mycoplasma contamination.

As a template for the PCR, media from cells incubated in overconfluence and absence of antibiotics for at least 5 days had been collected. All tests were negative.

1.1.4   Cell counting

Trypan blue (Sigma) dying exclusion test by manual counting method was used to determine cell concentrations.

Cells adhered to the plate were detached by incubation with pre-warmed trypsin-EDTA (Gibco) at 37ºC for 5min. Then, trypsin was inactivated using a fresh medium supplemented with FBS. Cells were centrifuged for 5min at 250G and resuspended with a fresh full medium.

For cell counting, cells were diluted 1:1 in trypan blue, and then, they were counted using a Neubauer chamber. To calculate the number of cells per ml, the following formula was used:

$$Concentration\ (cells/ml) = Mean\ viable\ cells\ per\ quadrant \times Dilution\ factor \times 10^4$$

1.1.5   Cell freezing and cryopreservation

Adherent cells were detached with trypsin-EDTA and centrifuge for 5 min at 250G. Then, cells were resuspended in a cold freezing medium (90%FBS and 10%DMSO from Sigma) in a ½ dilution of a p100 plate.

Cell suspension was distributed in cryotubes at 1ml/tube and placed in a cell freezing container at -80ºC for 24h minimum. Then, cryotubes were stored in a liquid nitrogen tank.

To defrost cells, cryotubes containing cells were quickly transported into dry ice to a warm bath at 37ºC. Then, cells were diluted in a pre-warmed medium (1/10) and trespassed into a Falcon tube. Cells were centrifuged and pellets were resuspended in a fresh medium. Finally, they were plated onto a p100 plate to have a high confluence and recover.

1.1.6 3D culture generation

3D cultures of tumoroids were derived from 2D primary cell cultures. Firstly, primary cells from a confluent p100 plate were detached manually with DMEM. Cells were passed through a cell strainer of 40 µm, and grouped cells were mixed with 50µl of Matrigel® (Corning), thawed O/N in ice, and immediately seeded as a drop. Matrigel® drops were incubated at 37ºC for 30min until Matrigel® solidification. Cells cultured inside the Matrigel® grew as groups of cells called tumoroids for approximately 4 days until to get the appropriate tumoroid size.

1.1.7 Cell line treatment

For nutrient deprivation, cells were incubated in media with 0,5% of FBS 24 hours previously to start the experiments. It was also maintained the nutrient deprivation during the whole experiment.

F2R expression was downregulated through doxycycline induction at 2,5 µg/ml (Sigma).

For evaluating F2R inhibition, SN12C cells were treated with different doses of SCH 79797 (Dihydrochloride) (Axon Medchem). This non-peptide is a selective F2R antagonist based on the natural alkaloid himbacine. Also, vorapaxar was used at different doses. vorapaxar -with its commercial name Zontivity – is a FDA-approved drug indicated for the reduction of atherothrombotic events in adult patients as it is a potent inhibitor of F2R.

For evaluating F2R activation, thrombin (Merck, T6884-100UN) was used at 1 U/mL. Also, TFLR-NH2 (Abcam) was used as F2R activator and acts as a PAR1 selective agonist.

For evaluating PI3K/AKT signaling pathway inhibition, we used the following inhibitors: Perifosine (AKT inhibitor) and Gallein (Gβγ inhibitor):

Inhibitor	Reference	Manufacturer	Concentration
Perifosine	KRX-0401	Selleckchem	5µM
Gallein	CAS2103642	MERCK	10µM

Table 6. Inhibitors used for PI3K/AKT signaling pathway inhibitors *in vitro* assays

1.2 Molecular analysis

1.2.1 RNA detection

1.2.1.1 RNA extraction from cells

Adherent cells were washed with PBS (0.15 M NaCl, 0.9 mM Na2HPO4, and 0.1mM KH2PO4), and then 1ml of PBS was added to the plate. Cells were detached carefully with a cell scrapper and cell suspension was transferred to 1.5ml Eppendorf. Cells were centrifuged for 5min at 250G and the pellet was directly stored at -80ºC until the day of RNA extraction. RNA was extracted using the RNeasy Plus Kit (Qiagen) following the manufacturer's instructions.

Once RNA was extracted it was quantified using the spectrophotometer NanoDrop TM1000 (Thermo Scientific). The quality of the RNA was validated by loading 500ng of RNA in a 1% agarose gel using 1kb Plus DNA ladder (Invitrogen) as a molecular weight marker.

1.2.1.2 Getting cDNA from RNA

Firstly, 2µg of RNA were diluted in sterile water to a total volume of 20µl and incubated for 10min at 65ºC. Then, it was used the High Capacity cDNA Reverse Transcription kit (Applied Biosystems) to prepare the retrotranscription mix: 1µl of RNAse inhibitor, 3µl

of RT buffer, 3µl of random primers, 1,2 µl of ddNTPs, 1µl of reverse transcriptase and 0,8µl of sterile water. 10µl of the mix was added to each sample previously warmed. Then, the reserve transcription was performed under the following conditions: 10min at 65ºC, 2h at 37ºC, 5 min at 85ºC, and ∞ at 4ºC. cDNA obtained was stored at -20ºC until use.

1.2.1.3 Real-time quantitative PCR

To detect RNA expression, Real-Time quantitative PCR (RT-qPCR) analyses were performed using Taqman® Technology (Applied Biosystems). First, 25ng of cDNA obtained from different cell lines were loaded into each well of the plate mixed with 5µl of TaqMan® Universal PCR Master Mix (Applied Biosystems), 0.5µl of the Taqman® Probe of interest (Table 7) and ddH20 to a final volume of 10µl. The 384-well plate was read at Lightcycler 480. Results were visualized and analyzed using software RQ Manager 1.2.1 and SDS 2.4 (Applied Biosystems).

Gene	Specie	Dye-Label	Reference
F2R	Human	FAM^{TM}-MGB	Hs0101692588
HPRT1	Human	FAM^{TM}-MGB	Hs02800695
GAPDH	Human	FAM^{TM}-MGB	Hs99999905

Table 7. Specific probes used in Taqman® analyses.

The cycle threshold (Ct) obtained for each gene was normalized against the same value of the housekeeping gene, GAPDH, or HPRT1. Then, RNA expression for each gene was calculated using the next formula:

$$2^{-\Delta Ct} = 2^{-(Ct\, gene\, A - Ct\, housekeeping\, gene)}$$

1.2.2 Protein detection

1.2.2.1 Preparation of protein lysates from cell culture

When cells seeded in a p100 plate reached 90-100% confluence were lysed. First, they were washed with PBS and then, 400µl of RIPA lysis buffer (0.1%SDS, 1%NP-40, 0.5%sodium deoxycholate, 50mM NeF, 5mM EDTA, 40mM β-glycerolphosphate, 200µM sodium orthovanadate, 100µM phenylmethylsulfonyl fluoride, 1µM pepstatin A, 1µg/ml leupeptin, 4µg/ml aprotinin in PBS, pH 7.4) were added to the plate. The plate was kept on ice for 5min. After this, cells were scraped using a cell scraper (Sarstedt) and the lysate was transferred into a 1.5ml Eppendorf. It was incubated on ice for 5min and incubated in rotation for 30-40min at 4ºC. Finally, the lysate was centrifuged at 14000rpm for 15min at 4ºC, and supernatants were stored at -20ºC to titer them.

1.2.2.2 Quantification of protein extracts

The colorimetric PierceTM BCA Protein Assay Kit (Thermo Scientific) was used for quantifying protein lysates.

First, it was performed a standard curve ranging from 0 to 2mg/ml diluting bovine serum albumin (BSA). Samples of interest were diluted too at 1:10 or 1:5.

Then, 10 µl of the standard curve and the samples of interest were loaded into a 96-well plate. 200µl of BCA Working Reagent (50:1, Reagent A:B) was added to each well and carefully mixed. The plate was incubated for 30min at 37ºC. The absorbance was measured at 560nm wavelength by spectrophotometry (Power Wave XS, BIO-TEK) using the KCJr Win Software. Protein concentration was calculated by extrapolation in the standard curve.

To prepare protein lysates for Western Blot, samples were prepared at 1µg/µl in loading buffer (Laemmli buffer: 300mM Tris-HCl pH 6,8, 600mM DTT, 12% SDS, 0,6% bromophenol blue, 60% glycerol) and boiled at 95ºC during 5min. Finally, they were stored until used at -20ºC.

1.2.2.3   Protein analysis by western blotting

To further evaluate and compare protein expression values, western blotting from cell samples was performed. To start, it was prepared sodium dodecyl sulfate-polyacrylamide gels (SDS-PAGE) for protein separation using 1,5mm glass plates (Bio-rad). They were composed of mixing dH2O, acrylamide-bisacrylamide, Tris-HCl 1,5M pH 6,8 or 8,8, APS, and TEMED. Gels had two parts: the stacking gel that had a fixed percentage of acrylamide and the resolving gel which the acrylamide percentage ranged from 7,5 to 12% depending on the molecular weight of the proteins of interest.

Once gels were prepared, 30 µg of protein lysates and a molecular weight marker (Page RulerTM prestained, Thermo Scientific) were loaded into the wells of SDS-PAGE gel. The gels were submerged into the running buffer (25mM Tris, 192mM glycine, 0.1% SDS) and proteins migrated at a constant voltage of 100V. Then, acrylamide gels were transferred to a PVDF membrane (Immobilon-P, Merck Millipore) at 100V and 4ºC for 120min. Membranes were blocked to prevent unspecific bindings of the antibody with 5% skimmed milk (Nestle®) or 5% BSA in TTBS (Tris 50mM, NaCl 150mM, Tween 20 0.1%) for 1h at room temperature (RT) in agitation. After, membranes were incubated with appropriate dilutions of primary antibodies (see Table 8) in TTBS 1% skimmed milk or TTBS 5% BSA overnight (O/N) at 4ºC.

The next day, membranes were washed in TTBS four times for 10min each and they were incubated with 1:3000 anti-rabbit IgG or 1:3000 anti-mouse IgG horseradish peroxidase (HRP) linked antibodies (GE Healthcare) in TTBS 1% skimmed milk for 1h at RT. Finally, blots were washed in TTBS four times for 10min each and developed with Amersham ECL SelectTM Western Blotting Detection Reagent (GE Healthcare Life Sciences) according to the manufacturer's instructions. Chemiluminescent signals on blots were detected with ChemiDoc Touch (Bio-Rad) and analyzed with Image Lab Software (Bio-Rad).

Antigen	Antibody	Specie	Dilution	Dilution Buffer	Manufacturer
Vimentin	180052, Clone V9	Mouse	1/1000	1% milk	Invitrogen
Actin	A5441	Mouse	1/2000	1% milk	Sigma-Aldrich
Vinculin	V9131, Clone hVIN-1	Mouse	1/2000	1% milk	Sigma-Aldrich
F2R	Ab32611	Rabbit	1/1500	1% milk	Abcam
Integrin $\beta 1$	9699	Rabbit	1/1000	1% milk	Cell Signaling
Integrin $\alpha 3$	SC-374242, Clone A-3	Mouse	1/500	1% milk	Santa Cruz
Integrin $\alpha 5$	Ab150361, [EPR7854]	Rabbit	1/1000	1% milk	Abcam
Fibronectin	Ab2413	Rabbit	1/1000	1% milk	Abcam
p-AKT	9271	Rabbit	1/1000	5% milk	Cell Signalling
Phospho-FAK (Tyr397)	44-625G, Clone 141-9	Rabbit	1/500	5% BSA	Thermo
Phospho-Src (Tyr416)	2101S	Rabbit	1/1000	1% milk	Cell Signaling
Phospho-Erk (Thr202/Tyr204)	9101S	Rabbit	1/1000	1% milk	Cell Signaling

Table 8. Primary antibodies used for Western Blot detections

1.2.2.4 Protein detection by immunofluorescence

Aiming to detect protein levels and localization through immunocytofluorescence, glass coverslips were sterilized and deposited onto 24-well plates. Then, cells were seeded in those wells and after a minimum of 48h, they were washed with PBS and fixed for 5min with 4% paraformaldehyde (PFA). The fixation process maintains cells in their current state and preserves the preparation by chemical reagents over an extended period.

After fixation, cells were washed twice with PBS and permeabilized for 15min with TPBS (PBS, Triton 0.1%). The permeabilization process allows antibodies to access intracellular structures to detect intracellular antigens.

Then, glass coverslips were transferred to a humidity chamber and blocked with 20% goat serum in PBS for 30min at RT to avoid unspecific bindings of primary antibodies.

Cells were incubated with primary antibodies with appropriate dilutions in 20% goat serum (see Table 9) for 1h at RT.

Afterward, coverslips were washed thrice with PBS and incubated with Alexa Fluor Secondary Antibodies diluted 1/200 and DAPI (Sigma) diluted 1/3000 for 1h at RT. Finally, they were mounted on slides using FluoromountTM Aqueous Mounting Medium (Sigma) to be suitable for microscopy. Cells were visualized with Zeiss Axio Observer Z1+ Apotome inverted fluorescent microscope and Confocal Leica SP5 microscope. Images were analyzed using Image J software.

Antigen	Antibody	Specie	Dilution	Manufacturer
F2R	Ab32611	Rabbit	1/200	Abcam
Integrin β1	RB9010-P0	Rabbit	1/500	Thermo
Integrin α3	HPA008572	Rabbit	1/100	Sigma
Integrin α5	Ab105361	Rabbit	1/100	Abcam

Table 9. Primary antibodies used for protein detection by immunocytofluorescence of 2D cultures.

1.2.2.5 Phalloidin staining

Phalloidin is a highly selective bicyclic peptide used for staining actin filaments (also known as F-actin). To perform phalloidin staining cells were washed with warmed PBS. Next, cells were fixed with 4% PFA in PBS and left for 10 minutes at room temperature. Then, cells were washed with PBS and we placed each coverslip with cells in a glass petri dish and dehydrated with a solution of acetone permeabilized with 0,1% TTBS for 5 minutes. After that, cells were washed twice with PBS and proceeded stained with phalloidin. Fluorescent Phalloidin-TRITC conjugate solution was diluted at 1:10 in PBS for 40 minutes at room temperature. Finally, cells were washed several times with PBS to remove unbound phalloidin conjugate and stained with DAPI (Sigma).

1.2.3 Doxycycline inducible shRNA system

To inducible downregulate F2R expression in cells, SMARTvector Inducible Lentiviral shF2R vector (V3SH7669-228480128, Horizon) was used (Figure 21).
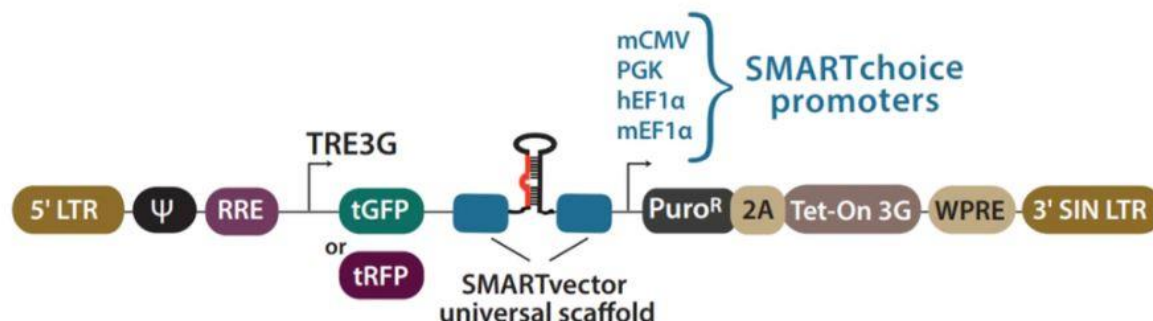
Figure 21. SMARTvector Inducible Lentiviral shRNA.

SMARTvector Inducible Lentiviral shRNA vectors utilize the Tet-On 3G bipartite induction system. This tightly regulated system consists of an inducible RNA polymerase II promoter, which has been optimized for both minimal basal expression and potent activation upon induction (Loew et al., 2010). In the presence of doxycycline, the TRE3G promoter is bound and activated by the constitutively expressed Tet-On 3G transactivator protein, which is also encoded within the Inducible shRNA vector. Together, the Tet-On 3G protein and TRE3G promoter permit tight regulation of the shRNA expression.

1.2.3.1 Lentiviral infections

Firstly, SN12C primary cells were seeded to reach 70-75% confluence at the time of infection. According to the supplier's instructions.

Cells were transduced at a low MOI of 0.3 TU/well in a 6 well-plate with Polybrene 8 µg/mL in DMEM 10% FBS medium. The following morning, the medium was replaced by a 10% FBS full medium. 48h after infection, 2µg/ml of puromycin (Sigma) were added to cell cultures to select effectively infected cells.

Finally, the inducible shRNA system was validated by 2,5 µg/ml doxycycline induction for 48h. Red fluorescent cells were checked using an inverted microscope Leica DMiL LED and shRNA efficiency was analyzed by western blot and RT-qPCR.

shRNA	Targeted sequence	Specie	CLONE
shF2R	AACCGGTCAATGCTTATGA	Human	V3SH7669-228480128

Table 10. Targeted sequence of F2R that has been used to perform shF2R

1.3   In vitro assays

1.3.1   Migration assays

1.3.1.1   Wound healing assay

Wound Healing assay was performed to determine the migration capacity of cells under different conditions. To generate a precise scratch, 2-well culture inserts (Ibdi®) with a cell-free gap in the middle were used. They were stacked into wells of a 12-well plate.

Cells were washed, detached with trypsin, centrifuged, and resuspended in 1ml of fresh medium. Then, they were counted as explained in Section 1.1.4. A determined number of cells (depending on their size) were plated inside both compartments of the insert in a final volume of 70µl. 500µl of the medium was added around the insert.

After 24h inserts were removed with sterile tweezers leaving a gap between both wells of the insert. Medium of cells was removed and replaced by a fresh medium. Pictures of the scratch were taken at 0, 3, 6, 9, 12, and 24 hours or 0, 12, 15, 18, 21, and 24 hours depending on the experiment. Two pictures of each well were taken using an inverted microscope (Leica DMi1). Opened area was automatically quantified using T-Scratch software.

Control and experimental groups were performed in parallel in triplicates.

1.3.1.2 Transwell migration assay

To assess directional migration, transwell migration assays were performed. Cells were placed in 6.5mm inserts with an 8μm polycarbonate membrane of the Costar Transwell® Permeable Supports (Corning). The number of cells and the containing factors of both media were determined for each experiment depending on which parameters were to be evaluated. The chamber was incubated for 24h at 37ºC in a humidified atmosphere with 5% CO_2. First of all, the membrane was wiped with a cotton swab to remove non-migrated cells on the upper part of the chamber and was fixed for 2 minutes with methanol. Then, it was washed with PBS and stained with hematoxylin (0.1% Hematoxylin, Merck Millipore, in ethanol 96%) for 90 seconds. Finally, it was removed from the insert using a blade and mounted with sterile water on a slide.

Pictures of 5/11 representative fields of all the membranes were visualized using the Nikon Eclipse 80i microscope and images were taken at 20X magnification with a Nikon DS-Ri1 digital camera using NIS-Elements BR 3.2 (64-bit) Software. Finally, they were analyzed with Image J Software.

All control and experimental groups were performed in parallel in duplicates or triplicates. Migrated stained cells were manually counted using Image J Software and are represented as the total number of migrated cells/field for each condition.

1.3.2 Invasion assays

1.3.2.1 Transwell invasion assays

To determine the invasive capacity of cells, a transwell Matrigel® invasion assay was performed. Inserts of the Corning® BiºCoat™ Matrigel® Invasion Chamber with an 8μm polycarbonate membrane were used for the experiment.

The protocol followed to develop the experiment and to take the images was the same as in the transwell migration assay. Control and experimental groups were performed in parallel in duplicates.

1.3.2.2   3D invasion assays

To quantify the invasion of SN12C tumoroids the invasive area was quantified concerning the central core nucleus of the tumoroid. A ratio between the size of the core nucleus from the tumoroid and the area from the invasive tumoroid is represented.

1.3.3   DeadEnd™ Colorimetric TUNEL System

The DeadEnd™ Colorimetric TUNEL System provides the reagents to perform terminal deoxynucleotidyl transferase-mediated dUTP nick-end labeling (TUNEL) of fragmented nuclear DNA to assess apoptosis in situ at the single-cell level in tissue sections or cultured cells. For making this stain slides were immersed in 4% paraformaldehyde for 25 minutes. Next, slides were immersed in 0.2% TPBS for 5 minutes. Then slides were washed twice in PBS, 5 minutes each time, and equilibrated with 100µl Equilibration Buffer for 15 minutes. After that, 100µl of TdT reaction mix was added to the cells on the slides for 60 minutes at 37°C in a humidified chamber. Afterward, plastic Coverslips were removed and the slides were immersed in 2X SSC for 15 minutes. Then, slides were washed three times in PBS, 5 minutes each time, and the next slides were immersed in 0.3% hydrogen peroxide for 14 minutes at room temperature. Then, slides were washed three times in PBS, 5 minutes each time and 100µl Streptavidin HRP (diluted 1:500 in PBS) were added for 30 minutes at room temperature. Then, slides were washed three times in PBS, 5 minutes each time, and 100µl DAB Solution (prepare immediately before use by adding 100µl DAB 10X Chromogen to 900µl DAB Substrate 1X Buffer) was added. We developed until a light brown background appeared. Finally, slides were immersed several times in deionized water and mounted slides with Floromount.

1.3.4   DNA synthesis-based cell proliferation assay (Click-it EdU)

In this assay, the modified thymidine analog EdU (5-ethynyl-2'-deoxyuridine, a nucleoside analog of thymidine) is efficiently incorporated into newly synthesized DNA. Firstly, we plated the cells on coverslips and incubate overnight. Then, 10 µL of 10 mM EdU stock solution were diluted in 5 mL of prewarmed tissue culture medium to make a 20 µM EdU labeling solution. After that, half of the medium was removed from the cells

and replaced with an equal volume of EdU labeling solution (final concentration of 10 µM). Cells were incubated under appropriate growth conditions and treatments for 2 hours and then proceeded to fix the cells with PFA4% for 10 minutes and permeabilized for 10 minutes with 0,5% TPBS. After that, a 1X Click-iT® EdU buffer additive was made by diluting the 10X solution created above 1:10 in deionized water. Then, the Click-iT® reaction cocktail was prepared according to the specifications of the kit and incubated for 30 minutes protected from light. After that, the reaction cocktail was removed and washed each well once with PBS and mounted with Floromount+DAPI. Images were taken with Zeiss Axio Observer Z1+Apotome inverted fluorescent microscope

1.3.5 Platelet Aggregation assays

Platelet aggregation assay was analyzed by multiplate® analyzer to detect if SN12C cell line can secrete factors that are stimulating the activation of platelets, and consequently, their aggregation. SN12C was seeded and maintained since it was over-confluence for 48 hours. After that, the supernatant was collected and centrifugated at 250G. Finally, these supernatants were incubated with whole human blood and with an agonist activator of F2R (TRAP) inside the Multiplate analyzer cuvette. Platelet aggregation was measured for 6 minutes.

Besides, it was performed in the same experiment but with the presence of SN12C cells in contact with platelets. Different amounts of SN12C cells (1250, 2500, 10000, and 20000 cells) were co-cultured with platelets to check the platelet aggregation capacity of cells.

2. IN VIVO

2.1 Animals and conditions

All animal studies were performed at the IDIBELL Animal Core Facility (AAALAC unit 1155) and approved by the Ethics Committee for Animal Experimentation from the Biomedical Research Institute of Bellvitge (IDIBELL) and the Generalitat de Catalunya. They were

performed following the European directives on ethical usage of rodents for animal research (approval DARP #4899).

All mice used in this thesis were male athymic nude mice (Harlan Laboratories) and were maintained in individually ventilated cages at constant temperature (20-25ºC) in SPF (Specific Pathogen Free) conditions and sterility. Animals were under an artificial circadian 12h light/dark cycle and received ad libitum standard diet and water. All experiments were performed inside a vertical laminar flow cabinet.

2.2 Patient-derived orthoxenograft mouse model from RCC human biopsy

To obtain our orthoxenograft mouse model, a small fresh piece of tissue from a biopsy of a patient who had ccRCC (chronologically named Ren 50) was obtained from the Bellvitge Hospital under the local ethics committee's approved protocols (CEIC approvals ref. PR322/11).

Primary tumor line was maintained throughout several passages by orthotopic implantation of a tumor piece into the kidney of another mouse. Mice were normally sacrificed when their survival was compromised.

2.3 Cell lines mouse models

Besides orthoxenograft mouse models, cell line tumor models were also used to perform *in vivo* experiments.

2.3.1 Kidney tumors

To establish SN12C human cancer cells as kidney tumors in athymic mice, 10^6 cells were directly injected into the right kidney of the animals using a 0.5ml needle (BD Micro-Fine). Once injected, tumor cells grew in the kidney, generating a palpable tumor in approximately 20-30 days. Then, tumors were perpetuated into successive passages and sacrificed as it was performed with the orthoxenograft model to obtain an experimental cohort.

2.3.2 Intravenous – Tail vein injection

To determine if F2R was involved in the last steps of the metastatic process, human cell lines were injected via the tail vein. 10^6 cells were resuspended in 100 µl of medium w/o FBS and other supplementary factors and were injected using a 1ml needle (Novico Medica) into the mice tail vein. Animals were sacrificed when symptoms of metastasis could be detected.

2.4 Tumor and organ collection

Tumors and other organs from sacrificed mice were collected to further analysis. Tumors, that grew attached to the kidney were divided into two parts. One part of the tumor was fixed using formaldehyde 4% O/N to be included in a cassette for paraffin embedding. The other piece of the tumor was included in OCT (Tissue-TEK® Sakura) and stored at -80ºC for further frozen tissue analyses. Some small pieces of the periphery and some pieces from the center of the tumor were frozen directly in cryotubes and maintained at -80ºC to extract protein or RNA. Lungs, spleen, liver, diaphragm, and contralateral kidney were also collected and fixed in formaldehyde 4% to be included in paraffin.

2.5 Blood collection and coagulation analysis

To collect the blood from mice for fibrinogen and blood coagulation parameters analysis, mice were previously anesthetized with Isofluran and by a heart tap the blood was collected and mixed in a blood collection tube with citrate diluted 1:10. Subsequently, the blood was centrifuged at 5000 rpm and plasma was carefully collected for fibrinogen analysis. This analysis was performed in Servei d'Hematologia Clinica Veterinaria from UAB.

2.6 Paraffin inclusion

Tissues were fixed in formaldehyde at 4% O/N and rinsed in PBS. Then, tissue samples were incubated through a battery of alcohols of crescent graduation (1h in ethanol 70%, 1h in 96% twice, and O/N in a new 96% and 1.5h in absolute ethanol thrice) and finally

submerged into xylene for 1.5h. Then, tissue cassettes were left in liquid paraffin at 65ºC O/N. Next day, tissues were embedded in paraffin inside a block sharp and dried at 37ºC.

2.7 Determination of tumor burden

Tumor size (mm2) was measured at the time of sacrifice using a caliper. Tumor weight (g) was determined with a balance.

2.8 Evaluation of tumor local invasiveness

Paraffin-embedded samples were stained with hematoxylin and eosin (H&E) and used for the invasion quantification because only formaldehyde-fixed and paraffin-embedded tissues preserve their morphology and allow studying the architecture of the tissue.

Paraffin-embedded blocks were cut into 3-5µm thick sections using a microtome and deposited into poly-L-lysine pretreated slides. Sections were deparaffinized by subjecting them to a battery of 4 xylenes (10min each), 3 absolute ethanols, 3 96% ethanols, 1 70% ethanols, and 1 50% ethanol (5min each). Finally, sections were rehydrated by submerging them in dH2O.

Then, they were stained with H&E. Slides were submerged for 10min in hematoxylin and rinsed in tap water to eliminate the excess liquid. Afterward, in some cases, they were submerged in HCl 1% until the tissue color shifted to red and then in ammonia water solution (200ml of dH2O with 1ml of ammonia 30%) until it turned back into blue. Sections were finally counterstained in eosin (2.5 g of eosin in 1L of ethanol 50%) for 10min.

Finally, slides were covered with coverslips and mounted using DPX (Merck). Tissues were visualized using the Zeiss Axio Observer Z1+ Apotome inverted fluorescent microscope and images were taken with a Nikon DS-Ri1 digital camera using NIS-Elements BR 3.2 (64-bit) Software. To quantify tumor invasion, it was evaluated the widest extension of tumor protrusions into the kidney parenchyma for each image (depth) by calculating the average for each tumor. Pictures were taken using the Fluo

Stereo Leica Macrofluo Lupa (0.57X magnification) and invasion was quantified using the Image J Software.

2.9 Metastasis determination

The presence of metastases in the lungs and the liver or diaphragm, as in other parts of the mice, was determined at the moment of sacrifice and was annotated as macrometastases.

Furthermore, aiming to detect micrometastases, H&E staining of slides from paraffin-included organ blocks was analyzed. Aiming to perform further analysis of 50mm deeper sections was also analyzed. Thanks to the automation of the Zeiss Axio Observer Z1+ Apotome inverted fluorescent microscope, a general picture (created by many different pictures at 10X) of the whole lung parenchyma was obtained in a few minutes.

Firstly, the incidence of metastasis was determined by scoring for presence or absence in each animal and counting the number of lesions. Also, the number of affected lobes was taken into account. In addition, all metastasis area density was calculated and normalized by total lung area using Image J software and expressed as a percentage.

2.10 Animal treatment

2.10.1 Vorapaxar treatment

The administration of vorapaxar (SCH 530348) (BOC Sciences) to inhibit F2R *in vivo* was started when tumor volume determined by palpation reached 1000mm^3.

First, mice were randomized into two groups. Control group was treated with a vehicle solution, composed of 0.9% Benzyl alcohol (Merck Millipore) diluted in NaCl 0.9% (Braun). The rest of the animals were treated with a vorapaxar dose of 20mg/kg/day diluted in the vehicle solution used in controls.

Vorapaxar is a synthetic tricyclic 3-phenylpyridine that orthosterically inhibits F2R. As the *in vitro* inhibitor SCH 79797, is based on the natural alkaloid himbacine. This drug has

been demonstrated to be well absorbed in rats at a dosage of 10mg/kg/day and in monkeys at 1mg/kg/day. In addition, it has been approved by FDA for human administration of 2.5mg/day (Chackalamannil et al., 2008; Flaumenhaft & de Ceunynck, 2017).

After taking into account the above-mentioned doses and applying conversion of different animal models using the following formula (Km values based on data from FDA Draft Guidelines), we decided to use a dose of 20mg/kg/day in the mouse.

Mouse dose (mg/kg) = Rat dose (mg/kg) * (rat Km/mouse Km) = 10mg/kg/day*(6/3) = 20mg/kg/day

Both groups were treated orally daily and tumor growth was followed by palpation twice a week. Animals were finally sacrificed 19 days after treatment and tumors and organs were collected, processed, and analyzed, as mentioned in the aforementioned sections.

2.10.2 Doxycycline administration

Animals were also treated with doxycycline (400mg/200mL of drinking water) to induce the shRNA system and downregulate F2R protein expression.

2.11 Molecular analysis

2.11.1 RNA detection

2.11.1.1 RNA extraction of tumor samples and cDNA obtention

RNA was obtained from tumor pieces stored at -80ºC at the time to sacrifice. Pieces were mechanically homogenized with RLT buffer from the RNeasy Plus Kit (Qiagen) in a glass homogenizer on ice. RNA extraction, quantification, and cDNA conversion were performed using the same procedure explained for cells (see section 1.2.1.1).

2.11.1.2 Real-time quantitative PCR

The analysis of RNA levels in tumors was performed by RT-qPCR using the TaqMan® system. The protocol used and the quantification procedure are described in section 1.2.1.1.

2.11.1.3 RNA-seq

Samples were sequenced at Centro Nacional de Análisis Genómico (CNAG-CRG, Barcelona, Spain). RNAseq reads were aligned to the human (GRCh38/hg38) and mouse (GRCm38/mm10) reference genomes using STAR (version 2.5.1b) and GSNAP (version 2015-06-23), respectively, with ENCODE parameters for long RNA (Dobin et al., 2013). Transcripts were quantified using RSEM (version 1.2.28) and read counts were used as input for DESeq2 (version 1.10.1) (Love et al., 2014). The cut-off for considering a gene significantly up-sampled or down-sampled was false discovery rate (FDR) < 5%.

2.11.2 Protein detection

2.11.2.1 Protein extraction of tumor samples and quantification.

Tumor pieces stored at -80ºC were used for protein extraction. Using RIPA buffer and a glass homogenizer small tumor pieces were mechanically disrupted on ice. RIPA buffer composition and the protocol used are explained in Section 1.2.2.1.

The colorimetric Pierce™ BCA Protein Assay Kit (Thermo Scientific) was used to quantify protein lysates obtained from tumor pieces as explained in Section 1.2.2.2.

2.11.2.2 Immunohistochemistry in paraffinized sections

To determine the expression and localization of proteins in tumors, paraffin-embedded blocks were cut into 3-5µm thick sections. They were deparaffinized by incubation in a battery of 4 xylenes (10min each), 3 absolute ethanol, 3 96% ethanol, 1 70% ethanol, and 1 50% ethanol (5min each). Then, sections were rehydrated through submersion in dH2O. After that, it was necessary to retrieve the antigens masked during the fixation process. To do that, slides were submerged in a sodium citrate solution (0,38mg/ml) at pH6 under heating conditions for 15min. Then, samples were cooled down inside the citrate solution for 20-30min and washed for 5min with dH_2O. Endogenous peroxidase activity was blocked by incubating tumor slides for 10min with 6% H_2O_2. This process

was repeated twice. Then, samples were washed with dH_2O for 5min. Next, they were submerged for 10min in PBS-T to permeabilize cell membranes. Afterward, unspecific bindings were blocked by incubating tumor samples with 20% goat serum in PBS for 1h at RT in a humidity chamber. Then, a primary antibody with appropriate dilution was added to slides O/N at 4ºC (see Table 11).

Antigen	Antibody	Specie	Dilution	Manufacturer
Vimentin	180052 Clone V9	Mouse	1/200	Invitrogen
Fibronectin	Ab2413	Rabbit	1/150	Abcam
F2R	Sc-13503 (ATAP2)	Mouse	1/200	Santa Cruz
Integrin β1	RB9010-P0	Rabbit	1/500	Thermo
Integrin α3	SC-374242, Clone A-3	Mouse	1/100	Santa Cruz
Integrin α5	Ab150361, [EPR7854]	Rabbit	1/100	Abcam
Ki67	RM-9106S1, SP6	Rabbit	1/200	Thermo

Table 11. Primary antibodies used for protein detection by immunohistochemistry

On the second day, tumor slides were tempered for 20-30min at RT and then washed with TPBS for 10min twice. Then, they were incubated with secondary anti-mouse or anti-rabbit Envision+-System-HRP antibodies (DAKO) for 1h at RT in the humidity chamber.

Tumor slides were firstly washed with TPBS 10min thrice and then developed with the chromogenic substrate DAB+ (EnVisionTM Kit, DAKO), from the 30s to 10min, depending on the antibody and tissue sample, until a brown precipitate appeared. Finally, the slides were rinsed in tap water to stop the reaction.

To observe the cells, sections were counterstained with hematoxylin and rinsed in tap water to eliminate the excess liquid. Then, they were dehydrated by submerging them in a battery of 1 70% ethanol, 3 96% ethanol, 3 absolute ethanol (5min), and 4 xylene (10min). Finally, slides were covered with coverslips and mounted using DPX (Merck).

Tissues were visualized using the Nikon Eclipse 80i microscope and images were taken with a Nikon DS-Ri1 digital camera using NIS-Elements BR 3.2 (64-bit) software. Then, they were analyzed with ImageJ software.

2.11.2.3 Hematoxylin-Eosin staining in paraffin sections

To visualize the phenotype and to quantify the invasive front of tumors, hematoxylin-eosin (HE) staining was performed in paraffin sections. Firstly, slides were deparaffinized and rehydrated as explained in section 2.11.2.2. Then, tumor sections were submerged in hematoxylin 0.1% (Merck) in ethanol 96% for 10 minutes and rinsed in tap water to remove the excess. Slides were later submerged in HCl 1% for a few seconds and ammonia water solution (200ml of dH2O and 1ml of ammonia 30%) until tissue turned blue. Finally, sections were counterstained with eosin (2.5g of eosin in 1L of ethanol 50%) for 2 minutes and mounted using DPX (Merck). Stained tumors were visualized in a Nikon eclipse 80i microscope and images were taken with a Nikon DS-Ri1 digital camera using NIS-Elements BR 3.2 (64-bit) software.

2.11.2.4 Martius Scarlet Blue staining (MSB)

This kit (Martius Scarlet Blue, RRSK2-100, Atom Scientific) is used to demonstrate Fibrin by selective staining of Red Cells, Fibrin, and collagen. Fibrin is stained in red, Collagen/ Elastic Fibres/Basement Membrane in blue, and finally, erythrocytes in yellow. Firstly, we prepared fresh Weigert hematoxylin by mixing equal volumes of solutions A & B as required. Next, we dewaxed sections, dehydrated them through alcohol, and rinsed them in tap water. Afterward, we stained nuclei with Weigerts Iron hematoxylin for 10 minutes and immediately washed them quickly in water, and differentiate them in 1% acid alcohol solution leaving the nuclei slightly overstained. Next, we proceeded to wash well in running tap water and then blue in Scotts tap water. Then, we rinsed in 95% alcohol and stained with Martius yellow solution for 5 minutes. Later, we washed quickly in running tap water and stained with a crystal scarlet solution for 5 minutes and we washed in tap water. After that, we were treated with a phosphotungstic acid solution for 10 minutes and washed in running tap water. Finally, we stained with aniline blue

solution for 5 minutes, washed in tap water, and proceeded to dehydrate, clear, and mounted with DPX. Stained tumors were visualized in Nikon eclipse 80i microscope and images were taken with a Nikon DS-Ri1 digital camera using NIS-Elements BR 3.2 (64-bit) software.

3. CLINICAL VALIDATION: IN SILICO ANALYSES

3.1 TCGA analyses

Clinical data were obtained from The Cancer Genome Atlas (TCGA) and analyses were performed in collaboration with Luis Palomero and Roderic Espin from PrºCURE (ICO-IDIBELL, Barcelona)

TCGA is a project that has generated multidimensional genomics data from multiple cancer types from which we selected samples from 18 solid tumors (Ma et al., 2018). We studied the expression of F2R in the TCGA from the main histological subtypes of RCC. Then, the analysis was focused on the TCGA from ccRCC patients (TCGA-KIRC) and the analysis of correlations between F2R expression levels and its interactors (data available in cBioPortal software)(Cerami et al., 2012)

4. STATISTICAL ANALYSIS

Graphs and statistic tests were performed using GraphPad Prism v6 software (GraphPad Software, Inc. USA).

Results are represented as mean ± SD. For most cases, due to the small sample size and the lack of normal distribution, a suitable non-parametric test was used. For continuous variables, the Mann-Whitney test or t-test was used for unpaired analyses. For contingency analyses, Chi-squared or Fisher's exact test was used to compare two categorical paired samples. For correlation analyses, Spearman's non-parametric correlation test was calculated. The statistical significance was defined as a p-value lower than 0.05 (*$p < 0.05$, **$p < 0.01$, ***$p < 0.001$).

5. FIGURE DESIGN

Graphics elements from Servier Medical Art or Biorendes according to a Creative Commons Attribution 3.0 Unporter License guidelines 3.0 were used in figures designed by the author of this thesis. Simplification and color changes were made to the original cartoons. https://creativecommons.org/licenses/by/3.0/ .

5. FIGURE DESIGN

RESULTS

1. ROLE OF F2R IN PRIMARY TUMOR CELLS

As it has been described in the previous results section, preliminary results suggest the possible implication of F2R on metastasis. For that reason, we decided to perform deep studies of this receptor.

1.1 Loss of function studies

To know how F2R is contributing to metastasis different tests with specific inhibitors of the receptor - vorapaxar and SCH79797 – were performed. Furthermore, we made a F2R knockdown of SN12C cell line to confirm the results from the inhibitors.

1.1.1 vorapaxar inhibitor is not affecting SN12C cells

As it was mentioned in the previous results section, promising results with vorapaxar inhibitor were obtained in *in vivo* experiments of SN12C-generated tumors. As we saw a clear decrease in metastasis after treating the tumors with vorapaxar, we wanted to test the effects of this drug *in vitro*. One of the hallmarks of malignancy is the acquisition of migrative or invading capacity of the cells, helping them to invade healthy tissue and to arrive at vessels to colonize the metastatic organ. For that reason, a transwell migration assay was performed at different doses of vorapaxar. No effects on cell migration were observed (Figure 22)

A

- VORAPAXAR   + VORAPAXAR 125 nM

+ VORAPAXAR 250 nM   + VORAPAXAR 500 nM

B
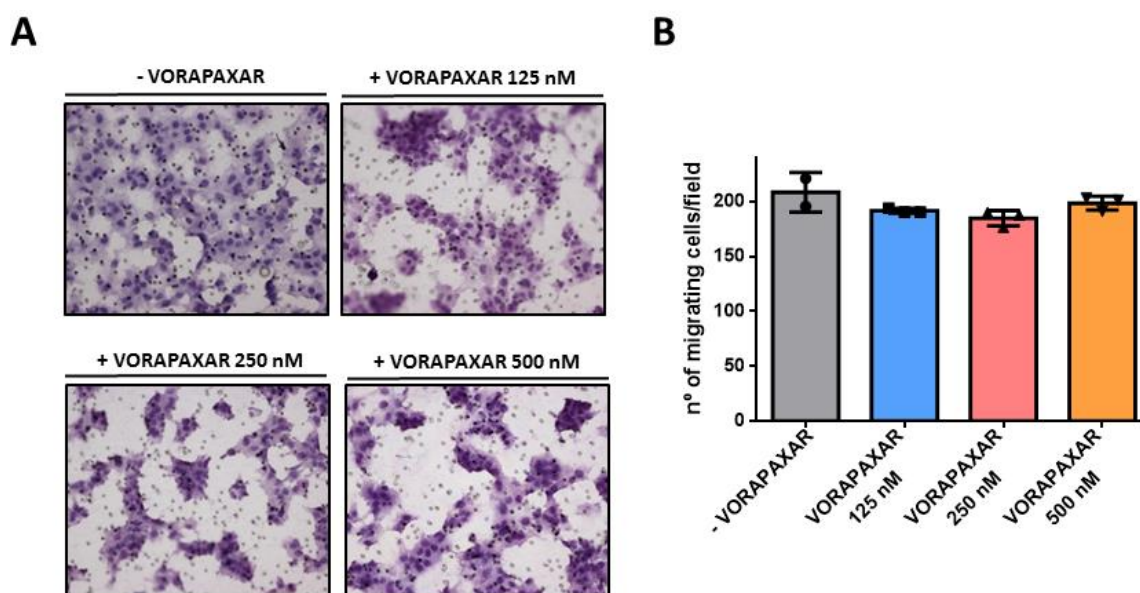
Figure 22. Vorapaxar did not show any effect on migration. The effects of cell migration after inhibiting F2R with vorapaxar at 125, 250, and 500 nM were studied through Transwell Migration assay®. A) Representative images (20X) of transwell membranes hematoxylin stained from cells treated with vehicle and vorapaxar. B) Quantification of migrating cells through Transwell migration membranes. Error bars represent S.D. 1 independent replicate. wells/condition n=3.

As we had a clear effect *in vivo* but no effects were observed *in vitro*, we moved to check if, after the administration of the drug, we had a decrease in the activation of AKT signaling pathway. As it is not a receptor that is activated by phosphorylation and its activation can be detected by western blot, we had to use the AKT pathway as a read-out for activation or inhibition of F2R. Results showed that no effect on the inhibition of p-AKT was observed (Figure 23).

CONTROL   VORAPAXAR 1uM

60 —   p-AKT

130 —   VINCULIN
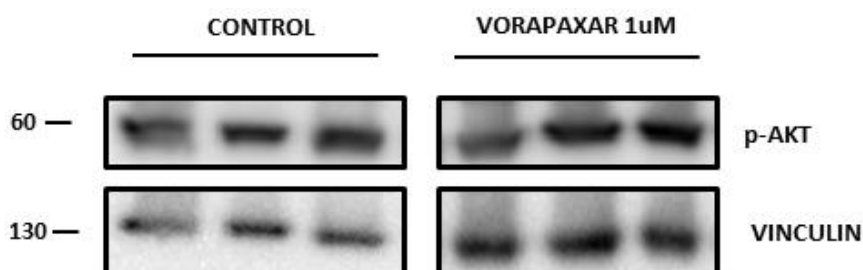
Figure 23. F2R inhibition with vorapaxar did not affect the PI3K/AKT signalling pathway. Western Blot for p-AKT in SN12C cell line after vorapaxar inhibitor at 1 µM

1.1.2 Vorapaxar inhibitor in Ren 50M tumors did not show any effect on metastasis

Once it was checked that vorapaxar was causing a reduction of total metastasis area in SN12C tumors and after solving the problems we had with the growth of Ren 50M tumors, we performed the experiment with vorapaxar and Ren 50M tumors. We had analyzed metastasis incidence (Figure 24A), total lung area (Figure 24B), affected lung lobes (Figure 24C), and total metastasis area density (Figure 24D). Results did not show any difference in the metastatic incidence, affected lobes, and total metastasis area.
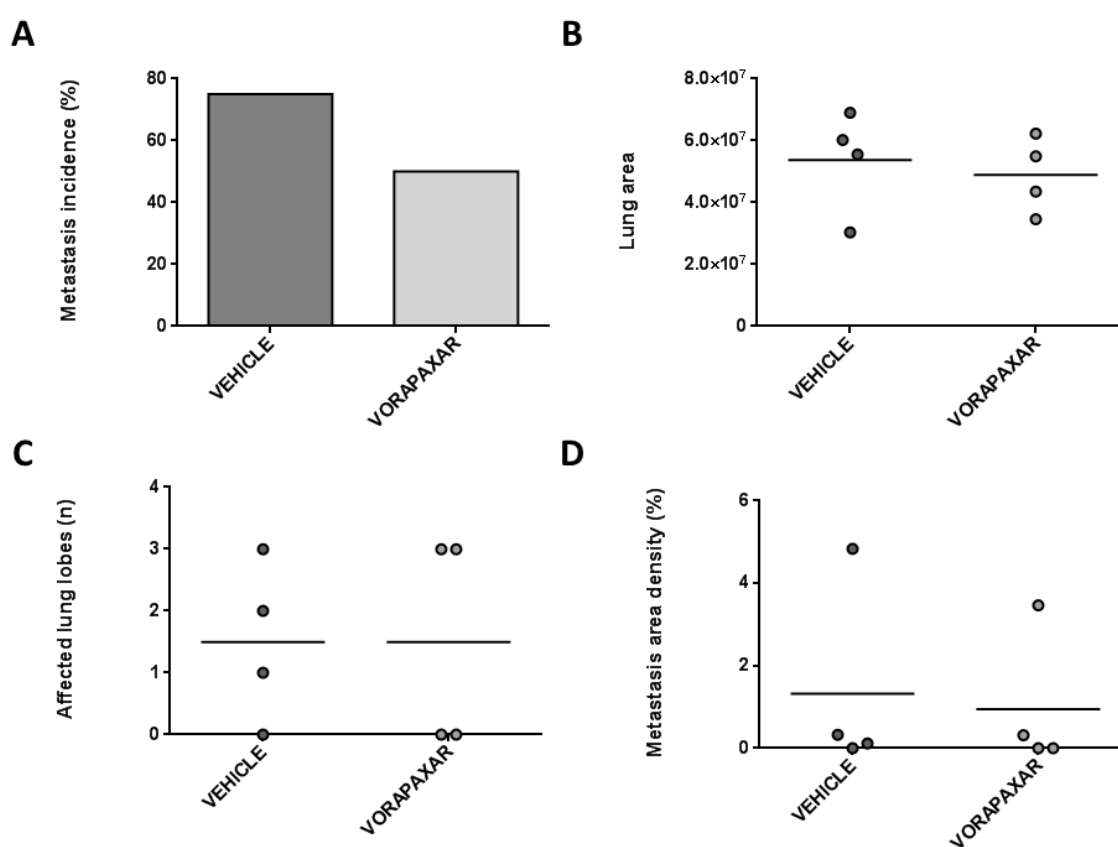
Figure 24. vorapaxar inhibition in Ren 50M tumors did not affect metastasis. Different parameters related to metastasis were analyzed in Vehicle mice (n=4) and vorapaxar-treated mice (n=4). A) Metastasis incidence was analyzed macroscopically once mice were euthanized. B) Total lung area was quantified to check that all areas analyzed were comparable. C) Number of lung lobes with lesions was quantified. D) Total metastasis area density was determined by quantifying the total metastatic area normalized by the total lung area of each lung. Images from lungs were taken with Zeiss Axio Observer Z1+ Apotome inverted microscope at 4X and a mosaic was created with all pictures.

To conclude, no effects of vorapaxar *in vitro* were found, together with the unexpected results from the Ren 50M tumors, we cannot reproduce the interesting findings from *in vivo* experiments of SN12C tumors.

Considering that, we wanted to check a different F2R inhibitors available in the market.

1.1.3 SCH 79797 inhibitor caused toxicity in RCC cell lines in an independent-F2R mechanism

We chose SCH 79797 because it is a selective non-peptide F2R antagonist used by other groups (di Serio et al., 2007). As it was described that this inhibitor could be causing toxicity at higher doses, we treated our SN12C cell line with different doses, and mortality was checked and quantified with Tunnel Assay. Results showed that at 400nM cells started to die (Figure 25).
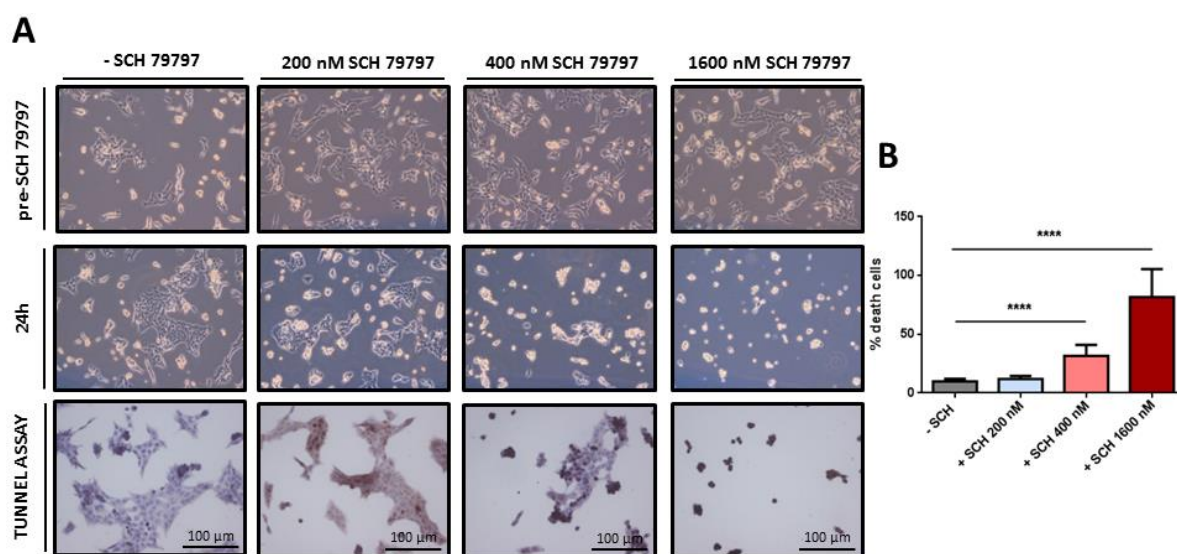
Figure 25. SCH79797 inhibitor caused toxicity in SN12C cell line at higher doses. Cell death was analyzed through Tunnel Assay® technology after doses of 200, 400, and 1600 nM. A) Representative images (10X) from SN12C cultured *in vitro* pre and post SCH 79797 administration. Furthermore, representative images after Tunnel Assay are shown. Brown cells were those cells that are dead. B) Total death cells were quantified and divided by total cells. Data is represented in %. Error bars represent S.D, wells/condition n=5. Mann Whitney test, p<0.005***)

To check if this mortality is dependent or not on F2R, different RCC with different F2R expression were analyzed. SN12C and RCC4 had higher F2R expression compared with 786o no F2R expression was detected. After treating with different doses of those cell

lines, we concluded that mortality was not due to F2R inhibition because all cell lines started to die after higher doses of SCH 79797 inhibitor (Figure 26).
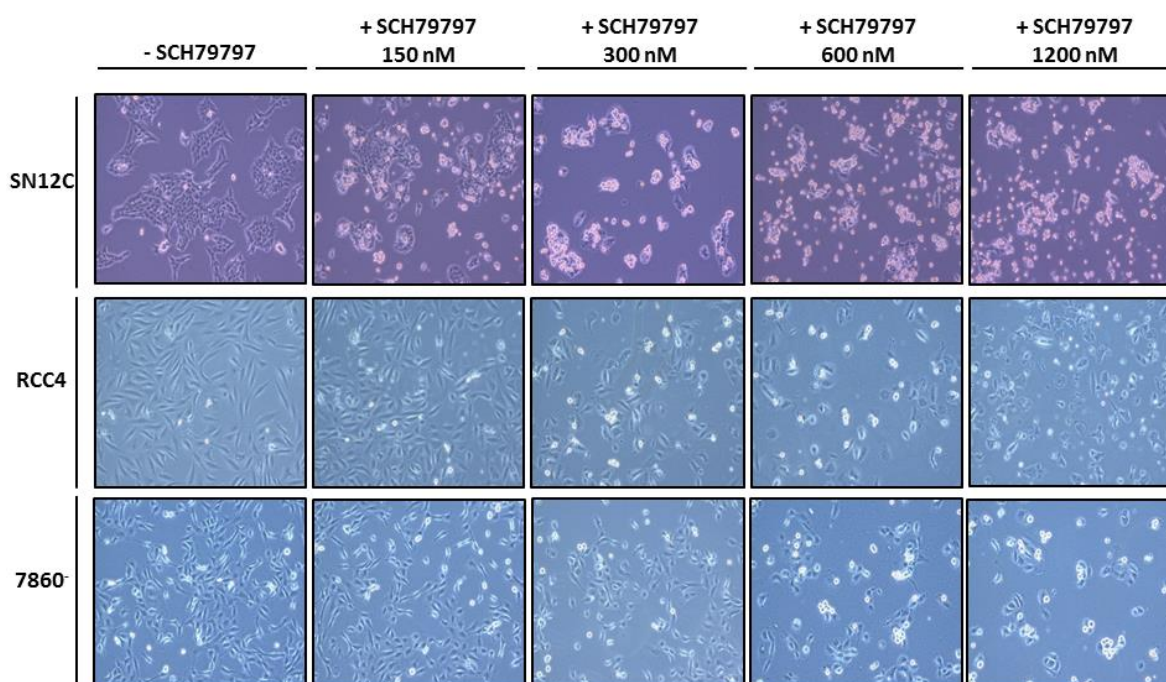
Figure 26. F2R inhibition with SCH79797 inhibitor caused toxicity in RCC cell lines. Cell death phenotype was analyzed in SN12C, RCC4, and 786o after 24 hours of SCH79797 incubation at 150, 300, 600, and 1200 nM.

1.1.4   SCH 79797 inhibitor is affecting migration and invasion of SN12C cell line

Then, as we had validated which doses did not cause toxicity, we moved to analyze the effect on migration and invasion after inhibiting F2R. For this purpose, we performed Transwell migration assays after lower doses of SCH 79797. Results showed a clear tendency to reduce cell migration after the inhibition of F2R (Figure 27)
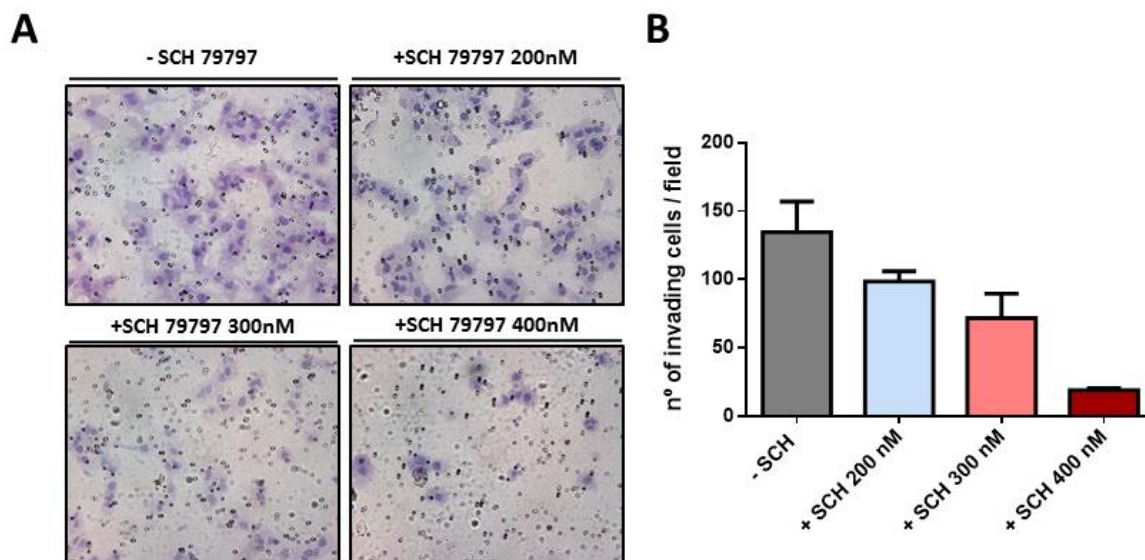
Figure 27. F2R inhibition with SHC79797 affected the cell migration capacity of SN12C cells. The effects of cell migration after inhibiting F2R with SCH79797 at 200, 300, and 400 nM were studied through Transwell migration assay®. A) Representative images (20X) of transwell membranes hematoxylin stained from cells treated with vehicle and SCH 79797. B) Quantification of migrating cells through Transwell migration membranes. Error bars represent S.D. 1 Independent replicate wells/condition n=3.

Furthermore, we generated spheroids from SN12C cell line and embedded them into Matrigel to analyze the invasiveness of these spheroids after SCH 79797 treatment. Results showed that there was a clear decrease in the invasiveness of SN12C spheroids after 48 and 72 hours of treatment (Figure 28).
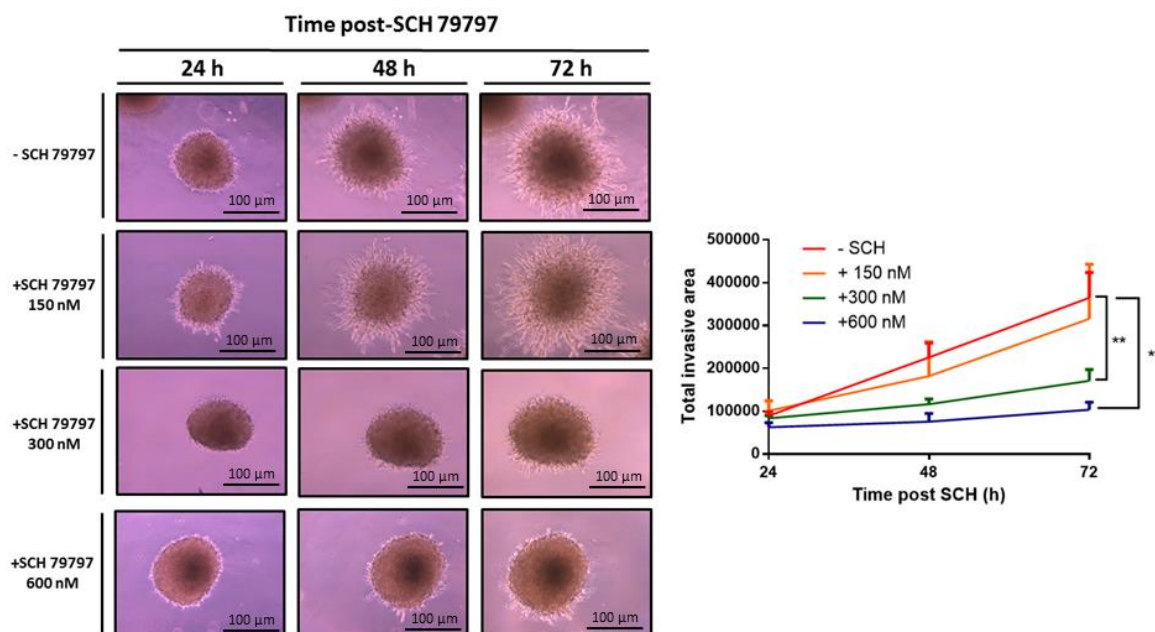
Figure 28. SCH79797 inhibitor showed a clear decrease in the invasive capacity of SN12C spheroids. SN12C cell line were seeded and embedded in Matrigel and after some days, spheroids were generated. Once they were generated, we administrate SCH 79797 inhibitor at different doses (150, 300, and 600 nM) and at different time points (24, 48, and 72 hours). A) Representative images of different spheroids after different doses and time points. B) Quantification of the invasive area of SN12C spheroids. Error bars represent S.D, Mann Whitney test, p<0.01**)

Considering the possible off-target effects of this drug despite using lower doses, we decided to generate a genetic knockdown of F2R. With that, we ensured that we were affecting only F2R and no other off-targets.

1.1.5 F2R decreased expression was confirmed in SN12C cell line

We decided to perform a F2R knockdown in SN12C cell lines as its cell line had a higher expression of F2R as was shown in the previous results section. The shRNA of F2R is expressed after doxycycline administration, having the highest decrease in protein and RNA levels after 48 hours of doxycycline (Figure 29). This knocked-down was checked by Western Blot (Figure 29A), RT-PCR (Figure 29B), and Inmunocitofluorescence (ICF) (Figure 29C).
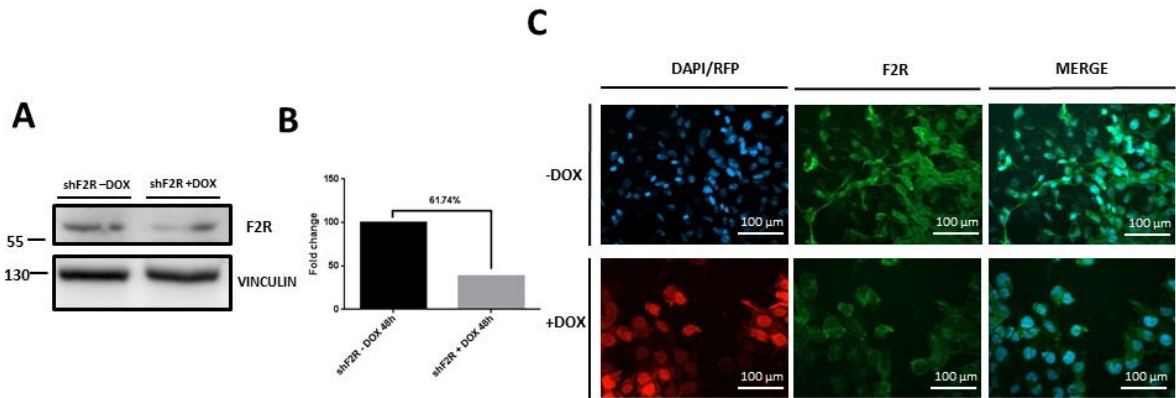
Figure 29. F2R knockdown was confirmed in SN12C cell line. doxycycline-inducible F2R knock-down was performed in SN12C cell line. A) Western Blot of F2R protein after 48 hours of Doxycycline administration. B) qRT-PCR was performed after 48 hours of doxycycline administration to check the decrease of F2R RNA levels. Fold change between -DOX cells and +DOX cells is represented. C) Inmunocitofluorescence of F2R in SN12C cell line after 48 hours of doxycycline administration. Cells after doxycycline became red.

1.1.6 PI3K/AKT signaling pathway was affected after F2R knocked down expression

As was previously mentioned, one of the signalling pathways implicated after the stimulation of F2R is PI3K/AKT. For that reason, we wanted to confirm if the decrease in the expression of F2R had any effect on the activation of PI3K/AKT signalling pathway. Results confirmed that there were no differences in shNS SN12C cell line (Figure 30A), but there was a clear decrease in AKT activation in those shF2R cells that were administrated with doxycycline (Figure 30B)
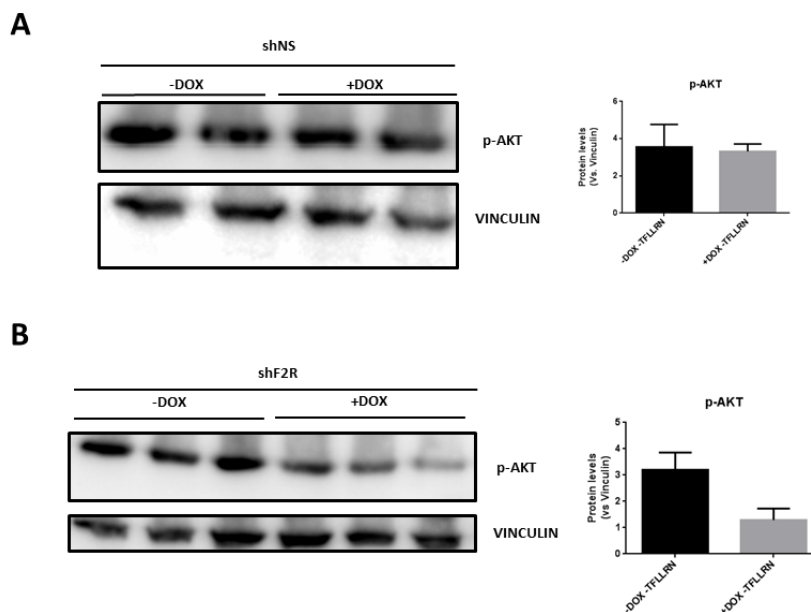
Figure 30. WB analysis revealed that there was a clear reduction in p-AKT level when F2R was decreased in SN12C shF2R cell line. PI3K/AKT signalling pathway was analyzed and quantified in SN12C shF2R and shNS cell line. A) p-AKT in shNS SN12C cell line analyzed by Western Blot. B) p-AKT in shF2R SN12C cell line through Western Blot.

1.1.7 SN12C F2R knocked down tumors presented a clear reduction of F2R

Once we have confirmed that there is a decrease in F2R in SN12C cell line, we proceeded to generate tumors to see the effect on metastasis due to a decrease in F2R expression. After tumor implantation, we waited until tumors arrived at a volume of 1000mm^3 before the administration of doxycycline to mice.

Firstly, we moved to check the decrease of the expression of F2R in these generated tumors. We confirmed this decrease by IHC (Figure 31A) and by qRT-PCR (Figure 31B).
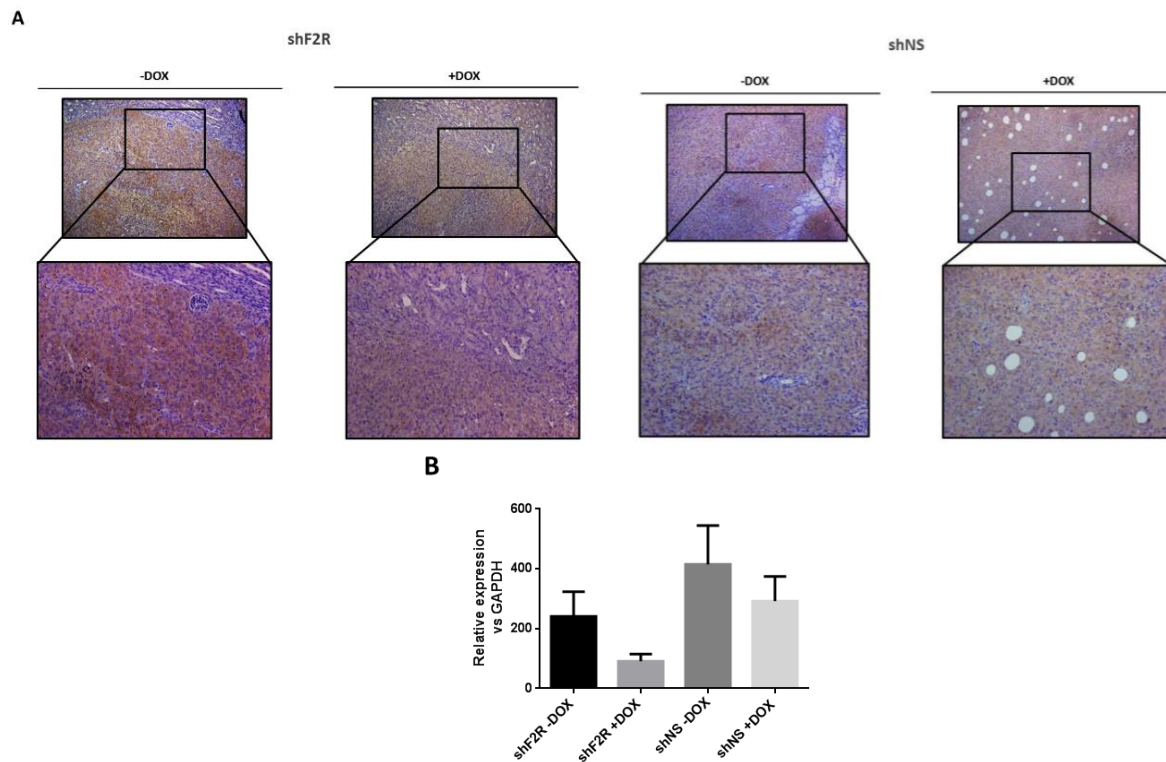
Figure 31. F2R protein and RNA levels were diminished in SN12C shF2R tumors. A) Inmunohistochemical analysis of shF2R and shNS tumors from mice administrated or not with doxycycline. B) F2R mRNA levels were analyzed by qRT-PCR in shF2R and shNS administrated or not with doxycycline. Error bars represent S.D, n=5 animals/group.

1.1.8 F2R decreased expression in primary tumors was not affecting the tumor growth

Primary tumors were monitored during the whole experiment (Figure 32A) and after mice sacrifice, tumor weight was quantified. We concluded that no effects on primary tumor growth were found (Figure 32B).
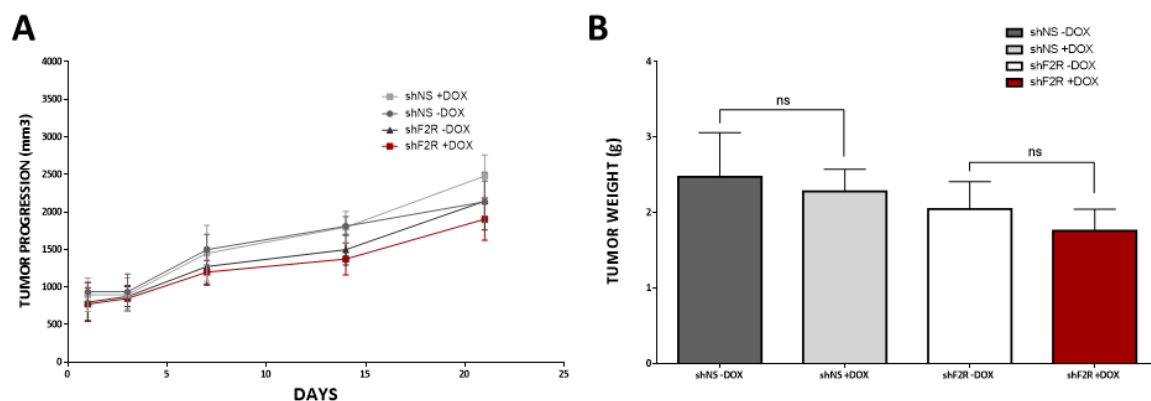
Figure 32. F2R knocked down did not affect tumor growth. A) Tumor volume was evaluated by palpation and doxycycline administration started when it measured 800mm3. Measurements were registered during the experiment (21 days). Tumor weight was also evaluated after mice were euthanized. Error bars represent S.D, n=10 animals/group. Mann Whitney test, p>0.05 ns)

Moreover, we confirmed also that SN12C shF2R cells did not affect cell proliferation *in vitro* after decreasing F2R expression (Figure 33).
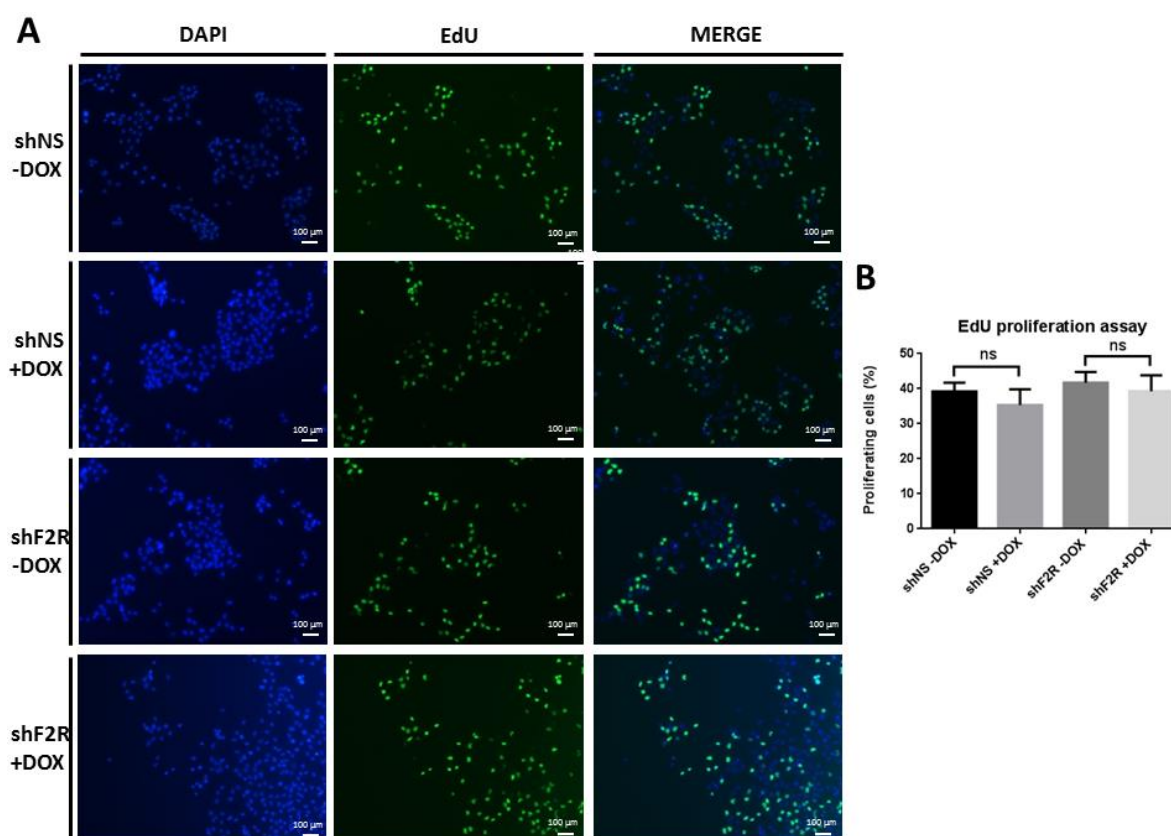
Figure 33. F2R decreased expression did not affect proliferation. EdU Staining Proliferation Kit was used to analyze cell proliferation. A) Representative images of SN12C shF2R and shNS administrated with or without doxycycline *in vitro.* Green nuclei are proliferative cells. B) Total proliferating cells were quantified and divided by total cells. Data is represented in %. Error bars represent S.D. 2 independent replicates. wells/condition n=5. Mann Whitney test, p>0.05 ns)

1.1.9 SN12C F2R knocked down primary tumor invasiveness was decreased

We next decided to test whether F2R inhibition was affecting tumor invasion (Figure 34A). We characterized tumor invasion by quantifying tumor invasive fronts. Results showed a clear decrease in tumor invasion in those animals who had the reduction of F2R protein levels (Figure 34B).
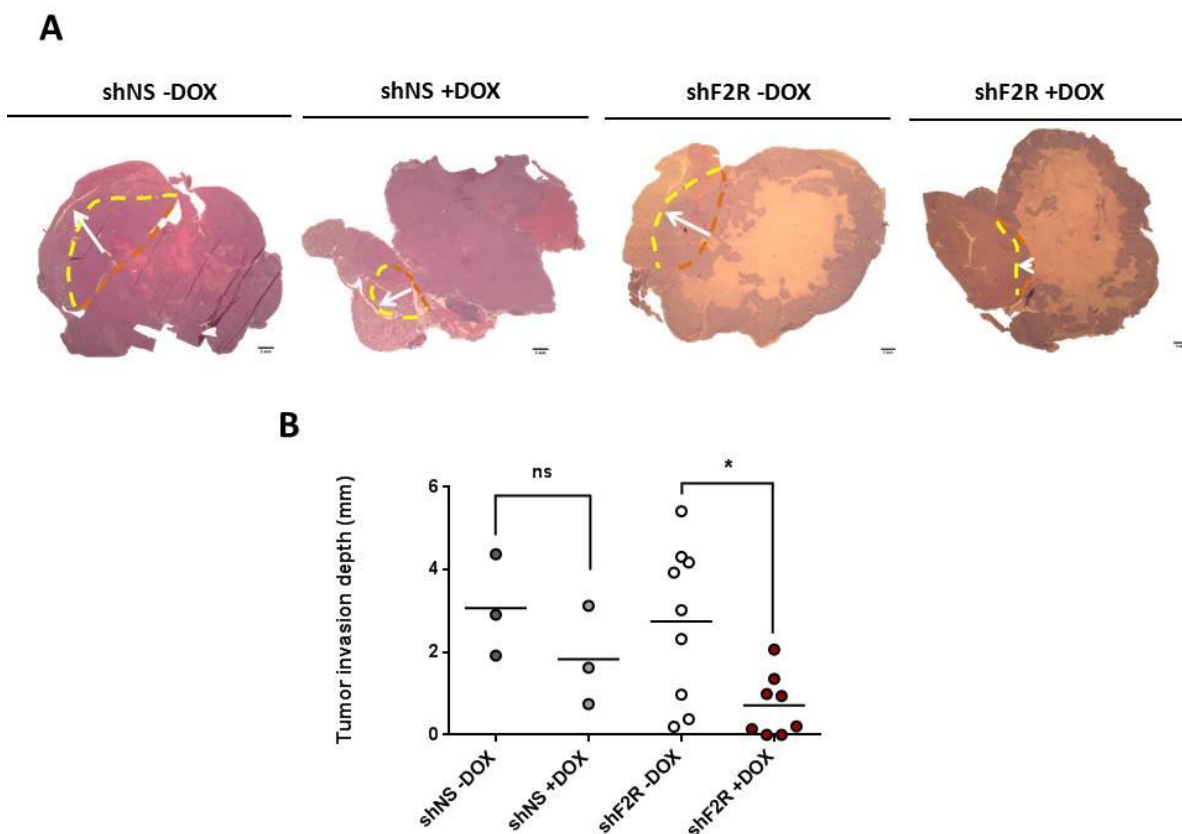
Figure 34. Tumor invasiveness quantification in SN12C shF2R tumors. To quantify tumor invasiveness, Hematoxylin/Eosin staining was performed to distinguish between Kidney and Tumor. A) Representative SN12C shNS and shF2R tumors with or without the administration of doxycycline. Pictures were taken at 0,57X and the invasive front was drawn and quantified. B) Tumor invasion depth quantification. Each group of animals n=3 in shNS and n=10 in shF2R. Mann Whitney test, $p < 0.05$ *)

Having this interesting result, we decided to perform migration assays with SN12C shF2R to check if we had the same effects of less invasiveness *in vitro*. We checked by Wound Healing assay (Figura 35A) and by Transwell migration technique (Figura 35B) and we had a clear decrease in migrative capacity of SN12C knocked down cells by wound healing. However, a slightly decreased tendency by transwell was observed after decreasing F2R expression.
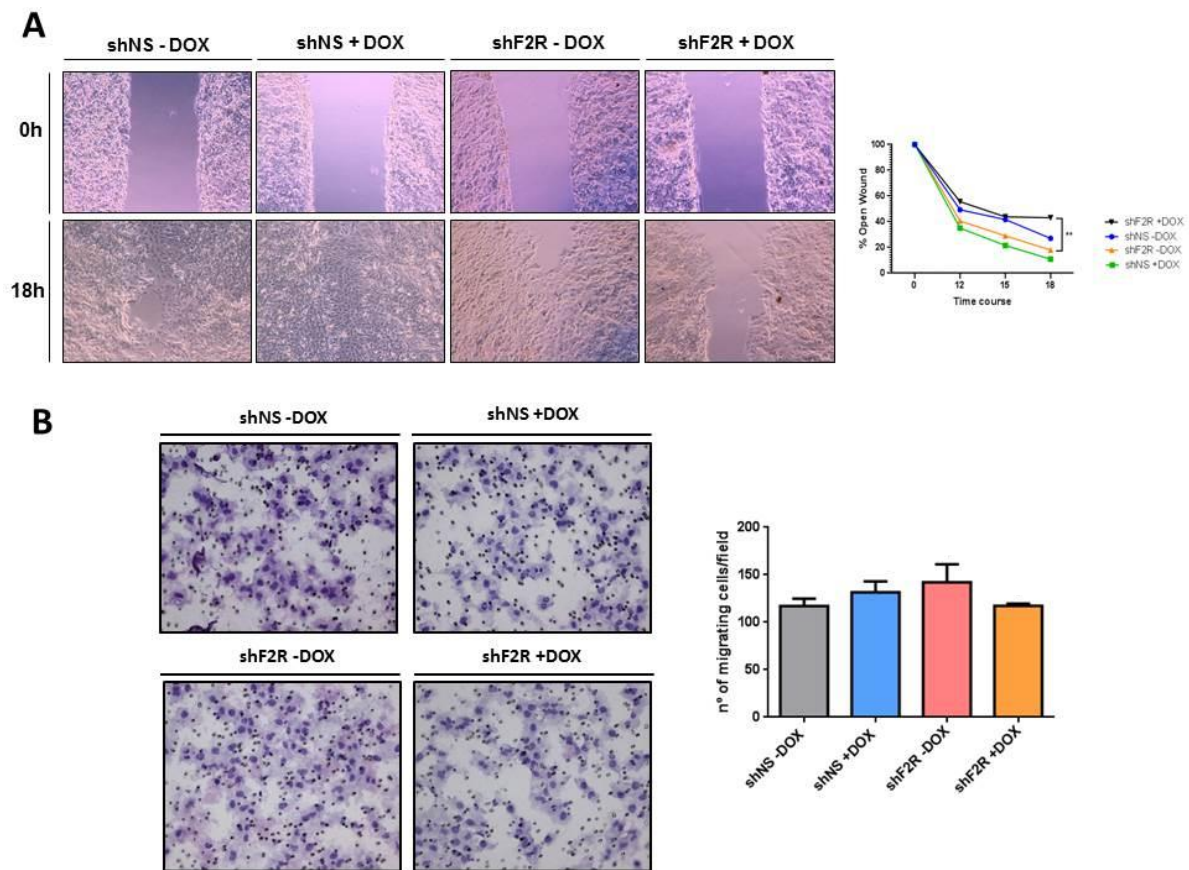
Figure 35. F2R knocked down SN12C cell line showed less migative capacity. A) Wound healing of SN12C shF2R cell line after 18 hours of assay. Cells were previously administrated with doxycycline for 24 hours. Error bars represent S.D. 3 independent replicates. Wells/condition n=3/4. Mann Whitney test, p<0.01 **, p<0.005*** B) Transwell migration assay of SN12C shF2R cell line after 24 hours of assay. Cells were previously administrated with doxycycline for 24 hours. Error bars represent S.D. 1 independent replicate. Wells/condition n=3.

Furthermore, we supposed that if we had a decrease in cell migration of SN12C cells, we should have actin cytoskeleton remodeling. For that reason, we performed with SN12C shF2R cells a phalloidin staining. Results confirmed that after decreasing F2R expression, we had less organized actin filaments in the invasive front of cells (Figure 36).
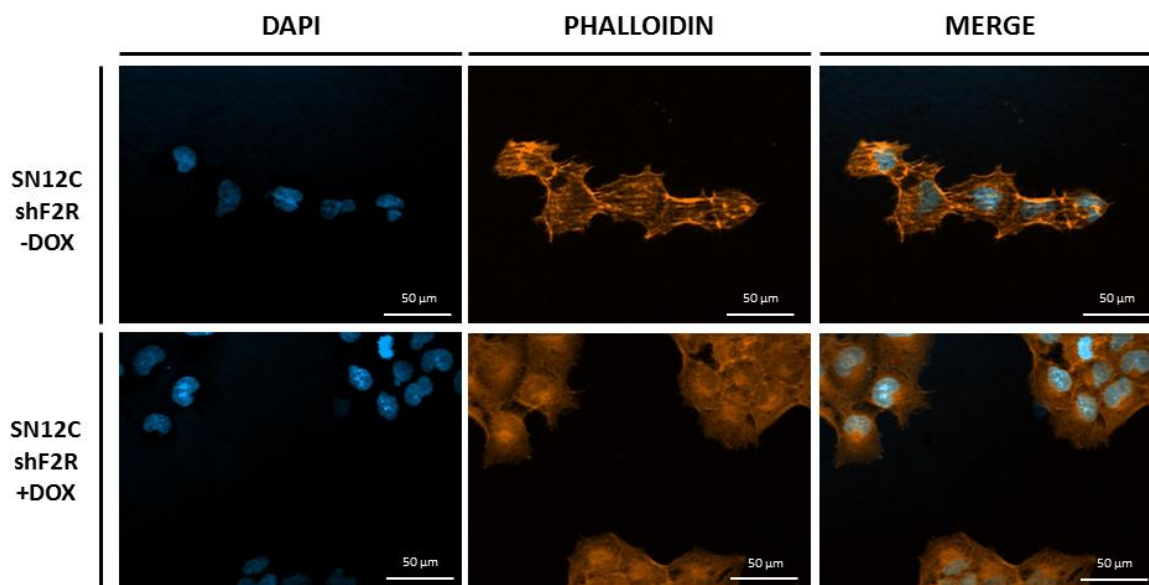
Figure 36. Actin cytoskeleton was remodeled after F2R decreased expression. Cells were 48 hours previously administrated with doxycycline and then phalloidin staining was performed. Representative pictures were taken from both groups at 40X.

1.1.10 F2R decreased expression in tumors was affecting metastasis

Considering all these results, we decided to study deeply whether F2R knockdown had any effect on the metastatic capacity of shF2R knocked down tumors. For this purpose, we performed a more thorough metastatic study analyzing lung metastasis from shNS and shF2R SN12C tumors induced or not with doxycycline.

For that reason, we analyzed the total area of the lungs (Figure 37A), number of affected lung lobes (Figure 37B), number of foci lesions (Figure 37C), and how bigger were the lesions (Figure 37D). No differences were found but in those shF2R tumors administrated with doxycycline, a tendency for reduction of the number of affected lobes was found.
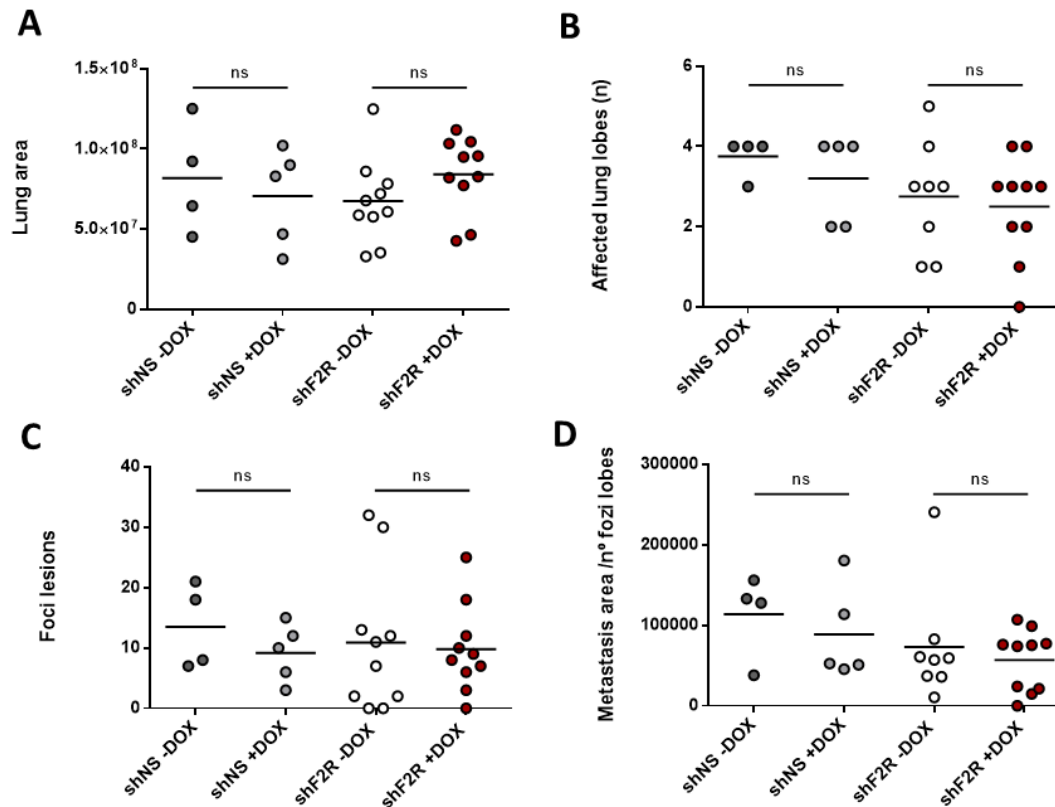
Figure 37. F2R knocked down did not show clear differences in metastatic parameters analyzed except for the affected lung lobes. Different parameters related to metastasis were analyzed in shNS (n=5) and shF2R (n=10) tumors. A) Total lung area was quantified to check that all areas analyzed were comparable. B) Number of lung lobes with lesions was quantified. C) Number of foci lesions quantified per mouse. D) The size of each lesion was quantified by dividing the total metastasis area by the number of foci lesions. Images from lungs were taken with Zeiss Axio Observer Z1+ Apotome inverted microscope at 4X and a mosaic was created with all pictures to quantify. Mann Whitney test, $p>0.05$ ns.

However, analyzing total metastasis area relativized by total lung area, results showed a tendency on reduction of total metastasis (Figure 38).
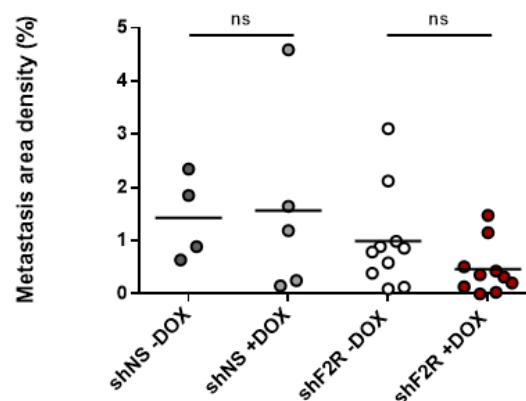
Figure 38. F2R knocked down in tumors showed a tendency on decreasing metastasis. Total metastasis area density was determined by quantifying the total metastatic area normalized by the total lung area of each lung. Images from lungs were taken with Zeiss Axio Observer Z1+ Apotome inverted microscope at 4X and a mosaic was created with all pictures to quantify. Mann Whitney test, $p>0.05$ ns.

Considering all these experiments, a possible implication of F2R in the migration/invasion of tumors and cells has been validated. This could be associated with the decreased tendency of reducing metastasis without affecting primary tumor growth.

1.2 Gain of function studies

Having those interesting results inhibiting F2R or decreasing its expression, we decided to analyze what would be happening if we activate that receptor. For that reason, we tested Thrombin as the main-gold activator of F2R (Heuberger & Schuepbach, 2019a) and the activating TFLLR-NH2 peptide (Gieseler et al., 2013).

1.2.1 Thrombin is increasing SN12C cell migration and invasion

We started using the main-gold activator of F2R to check if its activation we were having an increase in cell migration capacity of SN12C cells. To acquire this goal, we performed a transwell migration assay and wound healing assay. Results showed a slightly increased tendency on cell migration with both techniques after thrombin activation. However clear differences were observed in wound healing technique (Figure 39).
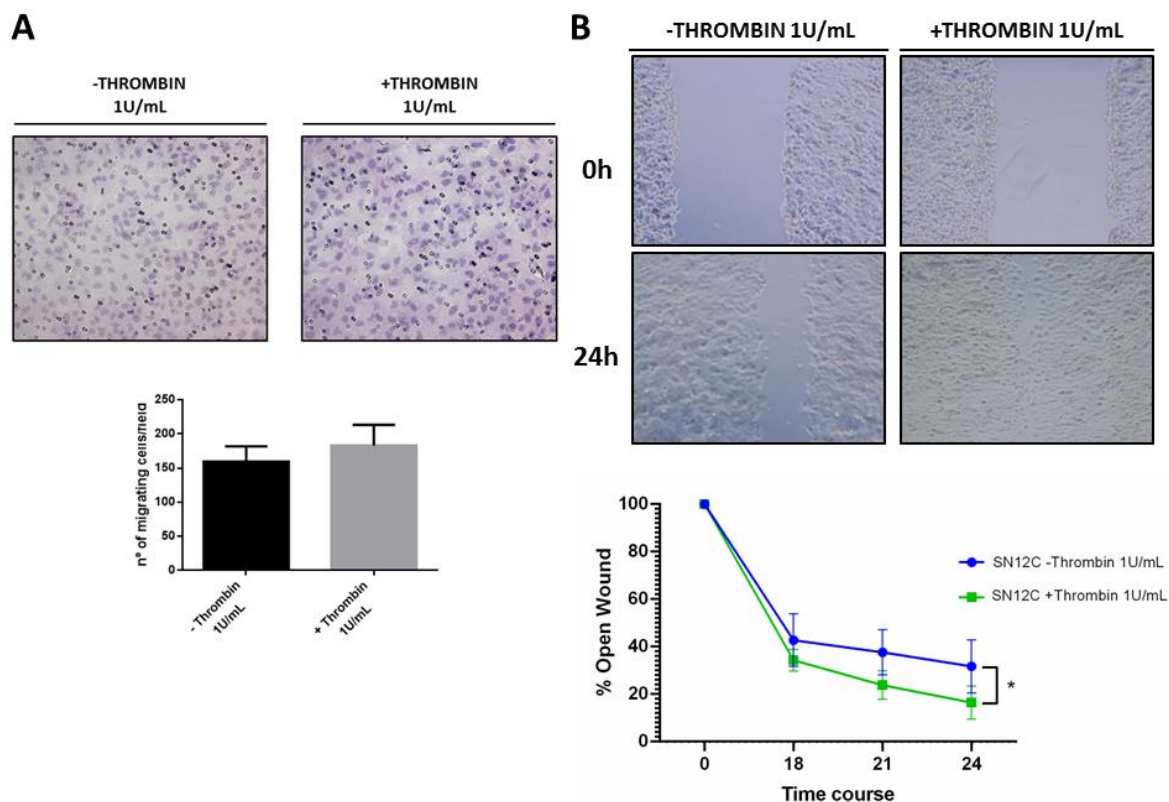
Figure 39. F2R activation through thrombin increased cell migration in SN12C cell line. A) The effects of cell migration at 10% FBS after activating F2R with Thrombin at 1U/mL were studied through Transwell Migration assay®. Up. Representative images (20X) of transwell membranes hematoxylin stained from cells treated with vehicle and Thrombin. Down. Quantification of migrating cells through Transwell migration membranes. Error bars represent S.D, 1 independent replicate. Each replication n=3 wells/condition. 10 pictures for each well/condition were quantified. Mann Whitney test, p>0.05, ns. B) The effects of cell migration at 0,5% FBS after activating F2R with Thrombin at 1U/mL were studied through a wound healing assay. Up. Representative images (10X) after the first time point and after 24 hours of assay. Down. Quantification of % of wound opened area. Error bars represent S.D. 2 independent replicate. Each replication n=3 wells/condition. Mann Whitney test, p<0.05*)

Furthermore, we also decided to perform a transwell invasion assay. Tranwell invasion assay is the same experiment as Transwell migration but with a coat of Matrigel that mimics the extracellular matrix present in tumors. In addition, as there were no higher differences in transwell migration assay, we decided to decrease the amount of FBS from 10% to 0,5% 24 hours before starting the experiment and during the next 24 hours of the transwell invasion experiment. Taking that into account, differences in cell migration should be a consequence of the activation of the receptor and not of the presence of a

higher number of factors in the FBS. Results clearly showed an increase in the cell invasion capacity of SN12C cells after F2R activation (Figure 40)
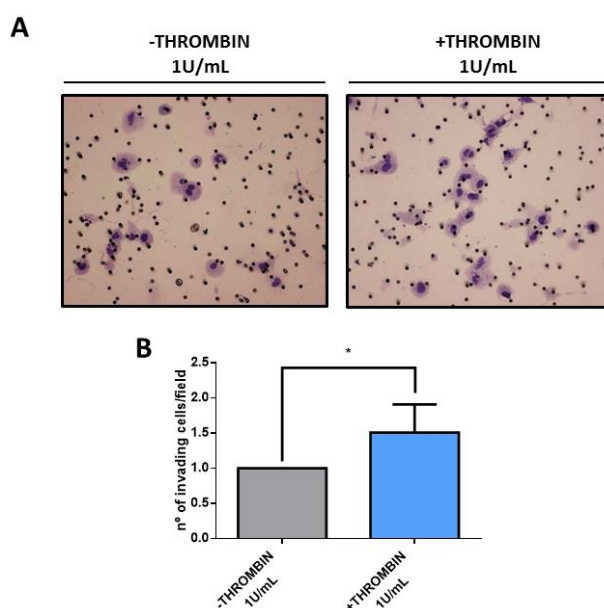
Figure 40. F2R activation through thrombin showed an increase in cell invasion capacity on SN12C cell line. The effects of cell invasion (at 0,5% FBS 24 hours before starting the assay) after activating F2R with thrombin were studied through Transwell Invasion assay®. A) Representative images (20X) of Transwell invasion membranes hematoxylin stained from cells treated with vehicle and thrombin. B) Quantification of invading cells through Transwell invasion membranes. Error bars represent S.D, 2 independent replicates. Each replication n=3 wells/condition. 5 pictures for each well/condition were quantified. t-test, p<0.05*)

Considering this interesting results, we also wanted to validate with a different activator of F2R available in the market.

1.2.2 TFLLRN-NH$_2$ peptide increased cell migration and invasion in SN12C cell line.

TFLLRN-NH2 synthetic peptide had the sequence that mimics the tethered ligand that can activate PAR signaling without the need for receptor proteolysis (Gieseler et al., 2013) We decided to use this specific peptide as it was one of the most used by many other groups, and it's activating only F2R receptor and no other PAR receptors.

We started checking if after the activation of F2R we had any effect on increasing cell migration. For this purpose, we performed a transwell migration assay technique.

Results confirmed that there is an increased tendency on cell migration after the activation with the peptide (Figure 41).
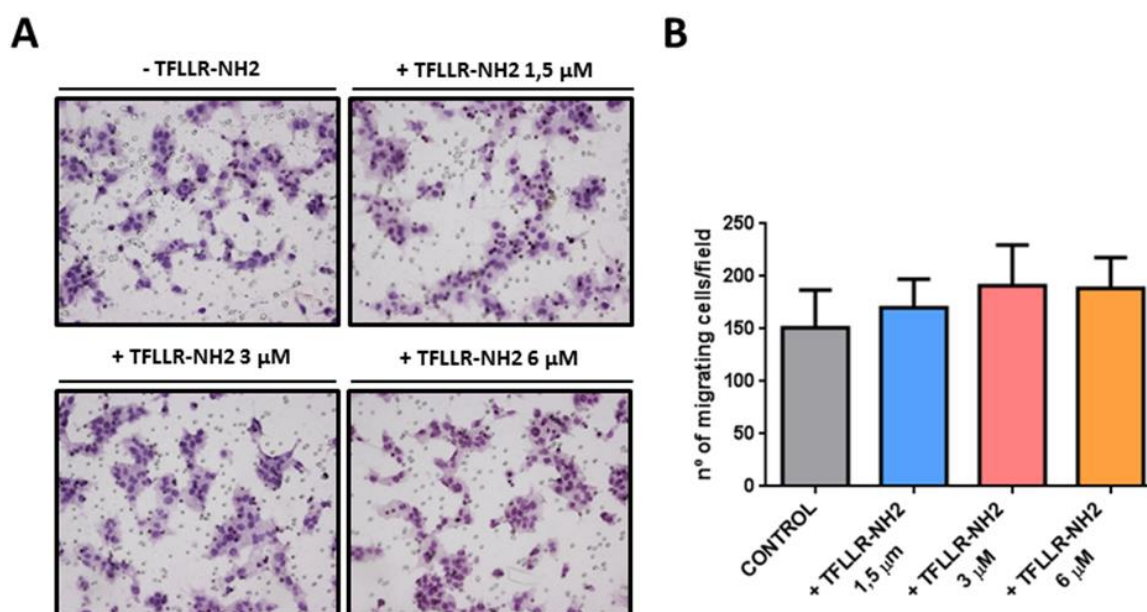
Figure 41. F2R activation through TFLLR-NH2 peptide showed a slightly increased tendency on cell migration capacity in SN12C cell line. The effects of cell migration at 10% FBS after activating F2R with TFLLR-NH2 at 1.5, 3, and 5 µM were studied through Transwell Migration assay®. A) Representative images (20X) of transwell membranes hematoxylin stained from cells treated with vehicle and TFLLR-NH2. B) Quantification of migrating cells through Transwell migration membranes. Error bars represent S.D. 1 independent replicate. Each replication n=3 wells/condition. 10 pictures were quantified per well/condition.

As there were not many differences, we decided to decrease the amount of FBS from 10% to 0,5% 24 hours before starting the experiment and during the next 24 hours of the transwell migration experiment. Taking that into account, and as we explained before, differences on cell migration should be a consequence of the activation of the receptor and not of the presence of higher number of factors in the FBS. Results clarify that there was an increase on the cell migration capacity of cells when we activated F2R (Figure 42).
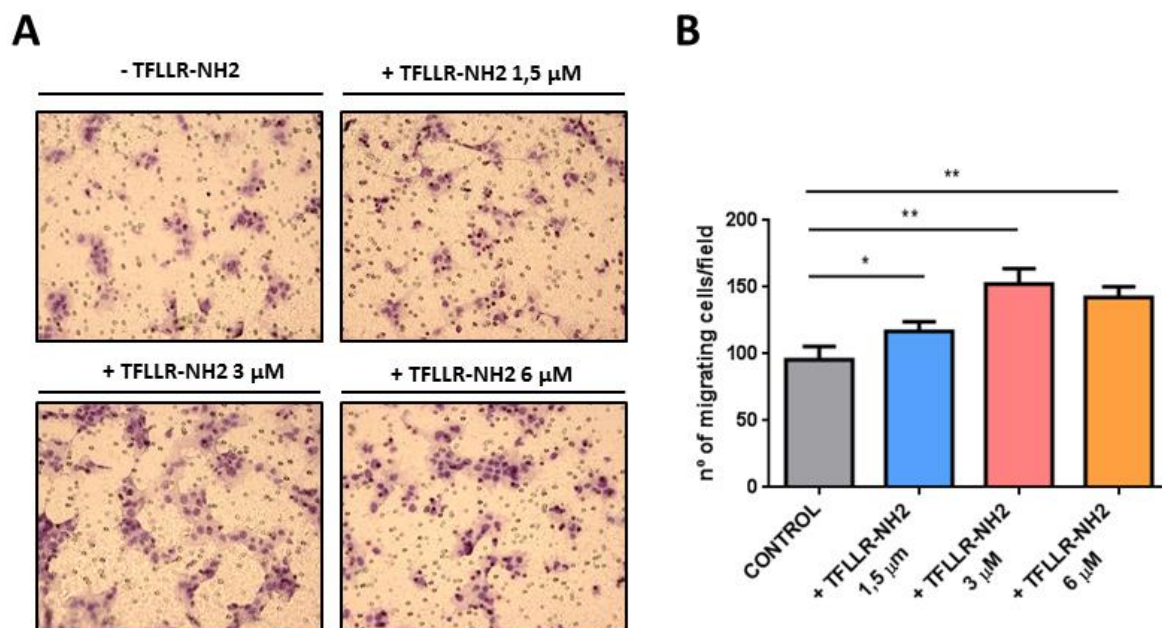
Figure 42. F2R activation through TFLLR-NH2 peptide showed an increase on cell migration capacity on SN12C cell line after pre-nutrient deprivation in Transwell migration technique. The effects of cell migration (at 0,5% FBS 24 hours before starting the assay) after activating F2R with TFLLR-NH2 at 1.5, 3, and 5 µM were studied through Transwell Migration assay®. A) Representative images (20X) of Transwell membranes hematoxylin stained from cells treated with vehicle and TFLLR-NH2. B) Quantification of migrating cells through Transwell migration membranes. Error bars represent S.D. 3 independent replicates. Each replication n=3 wells/condition. 10 pictures were quantified per well/condition. Mann Whitney test, $p < 0.05$ *, $p < 0.01$ **)

We also wanted to confirm this cell migration increase by other technique. For that reason, we performed a Wound Healing assay with the same conditions of decrease of FBS before starting the experiment and during the whole Wound Healing. We can confirm the same results as Transwell migration: cells migrated faster after the activation of F2R (Figure 43).
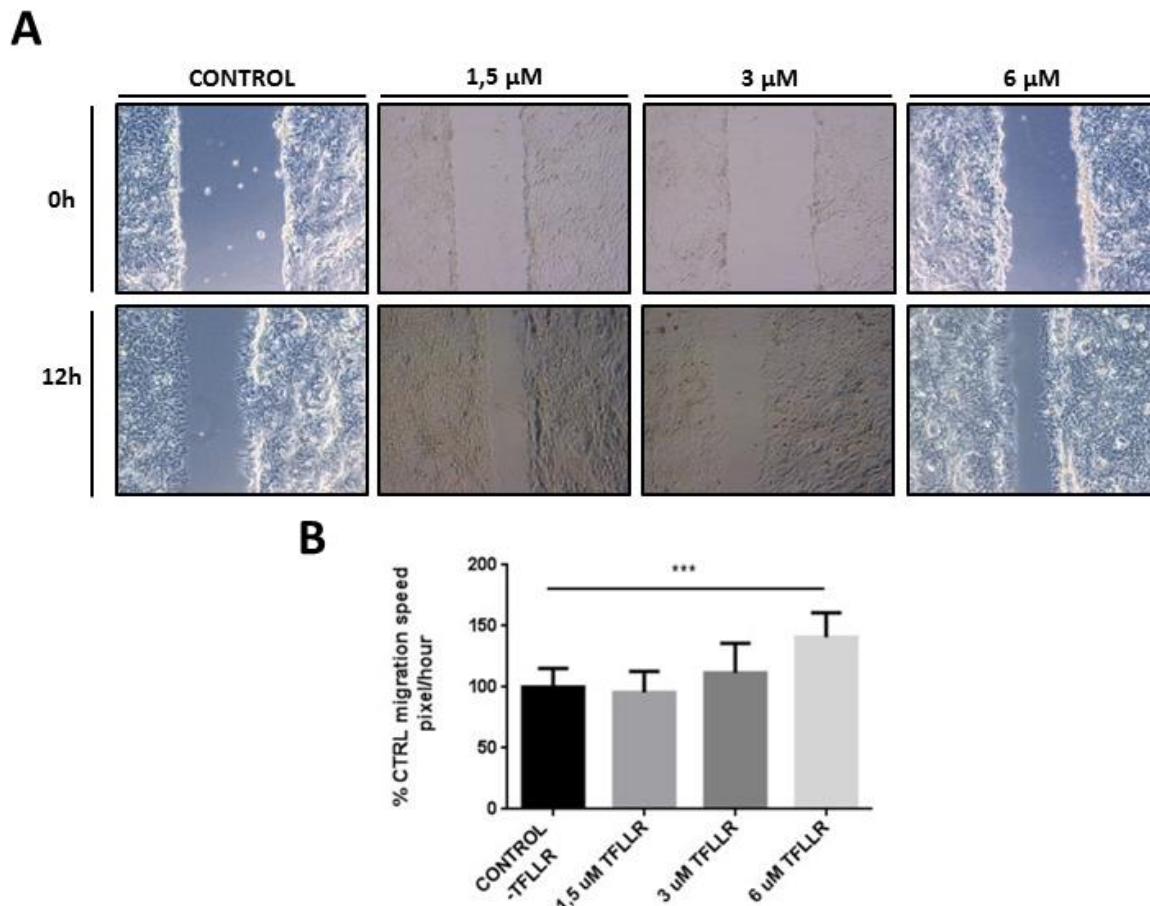
Figure 43. F2R activation through TFLLR-NH2 peptide showed an increase on cell migration capacity on SN12C cell line after pre-nutrient deprivation in Wound healing assay. The effects of cell migration (at 0,5% FBS 24 hours before starting the assay) after activating F2R with TFLLR-NH2 at 1.5, 3, and 6 µM were studied through Wound healing. A) Representative images after the first time point and after 12 hours of assay. B) Quantification of migration speed. Error bars represent S.D, 3 independent replicates. Each replication n=2 wells/condition. Mann Whitney test, p<0,005***)

After confirming the implication of F2R on cell migration, we wondered to check if we were affecting cell invasion capacity of SN12C cell line. We performed a Transwell invasion. The maximum differences on migration assays were shown at 6 µM, so we selected this dose to perform the invasion analysis. Results confirmed that after the activation of F2R, we had a clear increase in the invasiveness of SN12C cells (Figure 44)
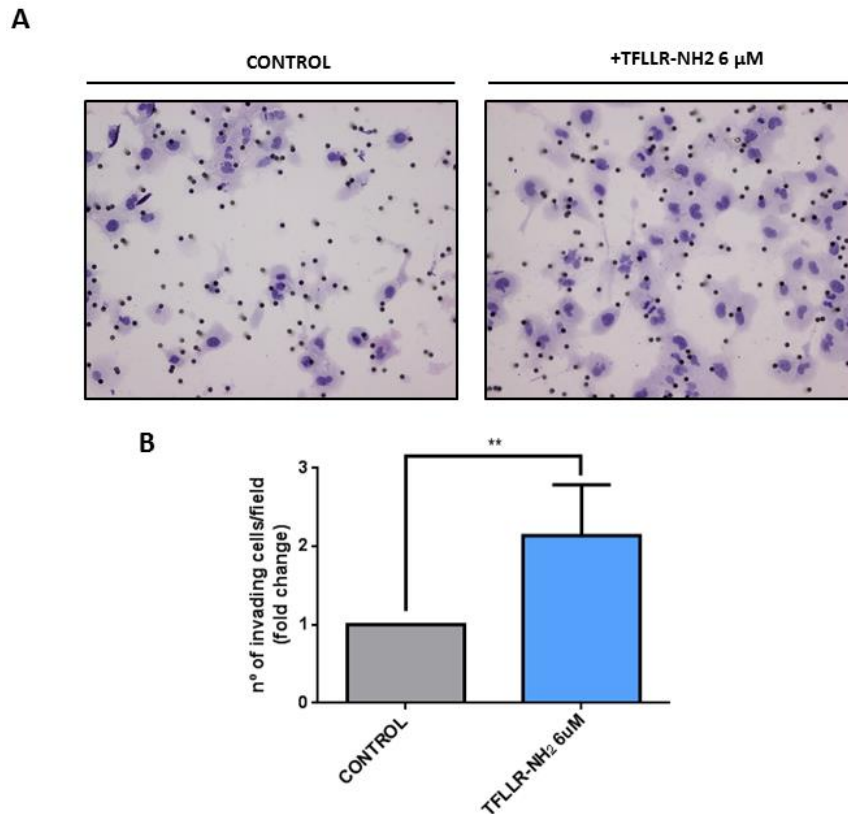
Figure 44. F2R activation through TFLLR-NH2 peptide showed an increase on cell invasive capacity on SN12C cell line. The effects of cell invasion (at 0,5% FBS 24 hours before starting the assay) after activating F2R with TFLLR-NH2 at 6 µM were studied through Transwell Invasion assay®. A) Representative images (20X) of Transwell invasion membranes hematoxylin stained from cells treated with vehicle and TFLLR-NH2. B) Quantification of invading cells through Transwell invasion membranes. Error bars represent S.D, 2 independent replicates. Each replication n=3 wells/condition. 5 pictures for each well/condition were quantified. Mann Whitney test p<0.05**)

Furthermore, this increase on cell migration and invasion should be associated with actin cytoskeleton remodeling. For that reason, we performed a phalloidin staining and we confirmed that after F2R activation, more invasive front and cytoskeleton remodeling occurred (Figure 45).
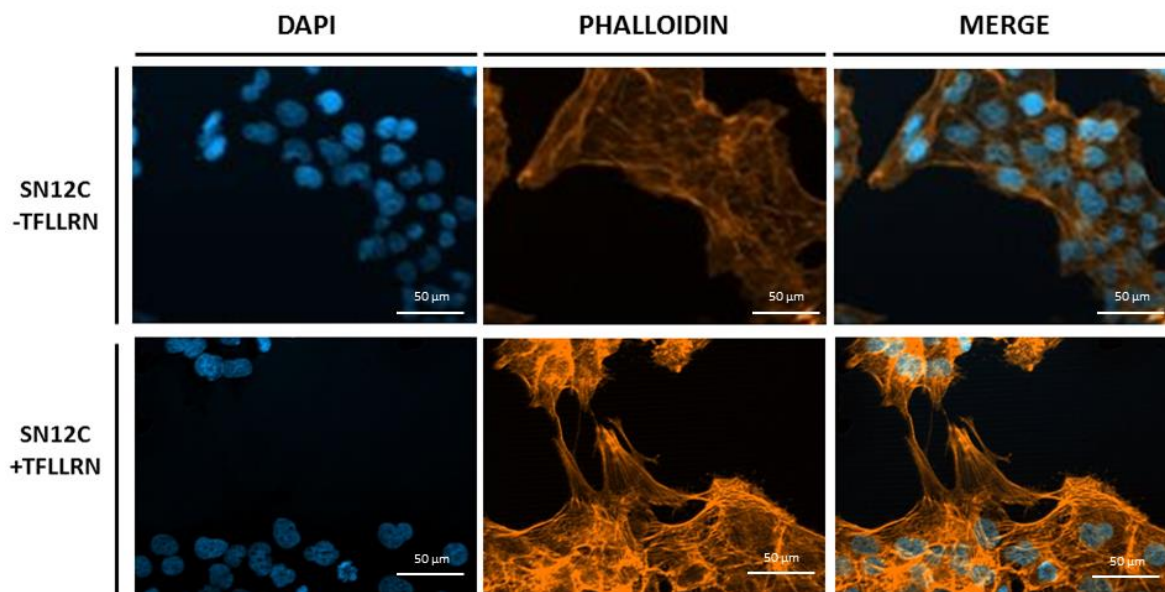
Figure 45. Actin cytoskeleton after F2R activation through TFLLRN-NH2 was remodeled. After 24 hours of TFLLR-NH2 administration, phalloidin staining was performed. Representative pictures were taken from both groups at 20X.

1.2.3 TFLLRN-NH₂ peptide increased cell migration in RCC4 and Renca cell lines

To further confirm that after F2R activation we had an increase on cell migration capacity, we wanted to validate it in different cell lines. First, we decided to test RCC4 cell line. As it was mentioned before, this cell line has higher levels of F2R. We performed a Transwell migration assay, and we confirmed that there was an increase in cell migration after administrating the activating peptide (Figure 46).
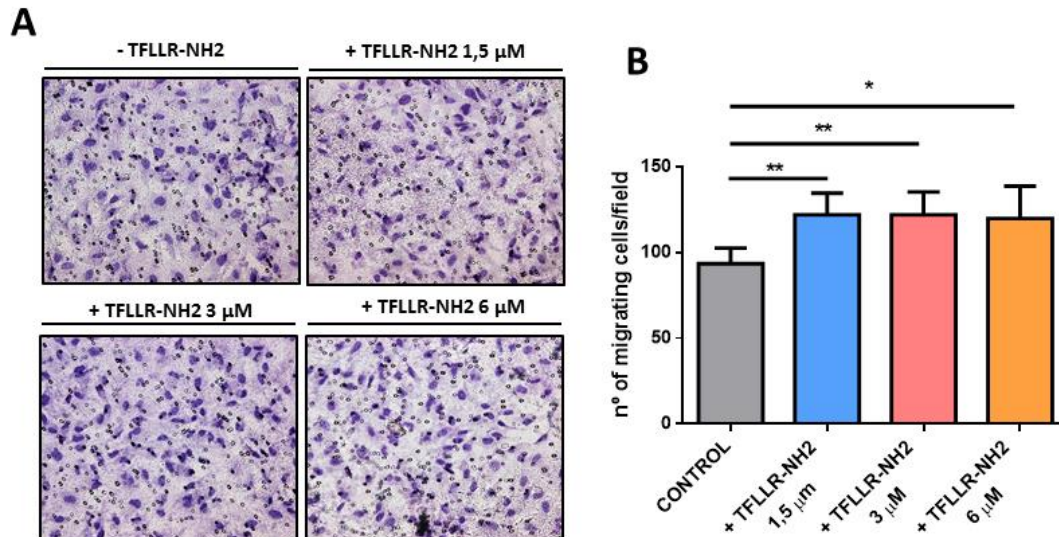
Figure 46. F2R activation through TFLLR-NH2 peptide showed an increase on cell migration in RCC4 cell line after pre-nutrient deprivation. The effects of cell migration (at 0,5% FBS 24 hours before starting the assay) after activating F2R with TFLLR-NH2 at 1.5, 3, and 5 µM were studied through Transwell Migration assay®. A) Representative images (20X) of Transwell membranes hematoxylin stained from cells treated with vehicle and TFLLR-NH2. B) Quantification of migrating cells through Transwell migration membranes. Error bars represent S.D, 2 independent replicates. Each replication n=3 wells/condition. 5 pictures for each well/condition were quantified. Mann Whitney test $p < 0.05$**)

We also confirmed this result with RenCa cell line. This cell line was derived from a tumor that arose spontaneously as a renal cortical adenocarcinoma in mice. Due to its higher aggressiveness in generating metastasis (data not shown), we decided to test TFLLR-NH2 peptide. Results showed a tendency to increase on cell migration after F2R activation (Figure 47).
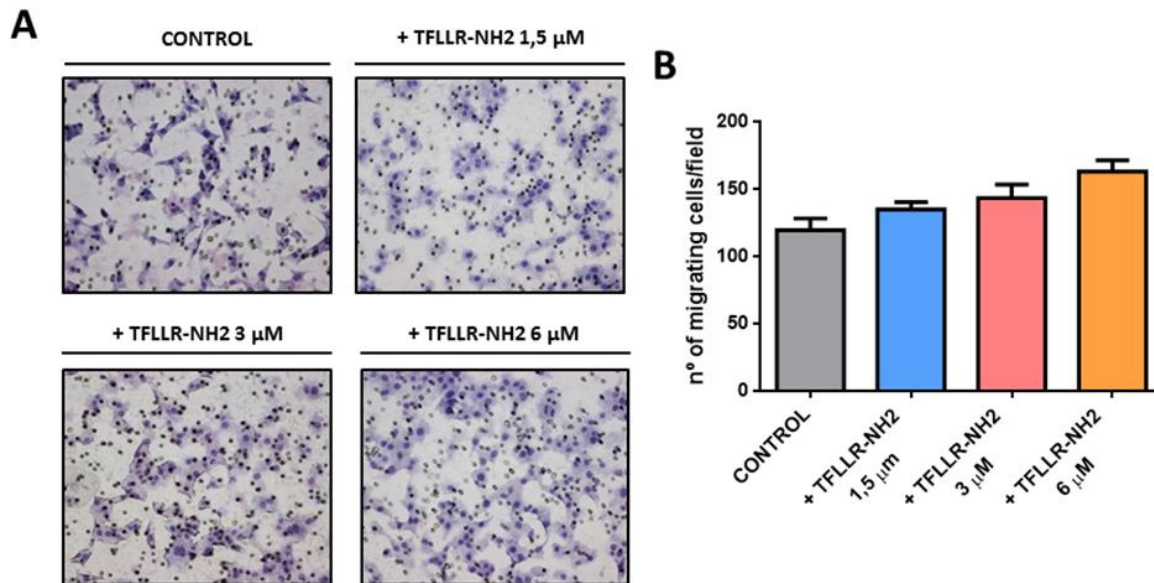
Figure 47. F2R activation through TFLLR-NH2 peptide showed a tendency to increase the migrative capacity of RenCa cell line after pre-nutrient deprivation. The effects of cell migration (at 0,5% FBS 24 hours before starting the assay) after activating F2R with TFLLR-NH2 at 1.5, 3, and 5 µM were studied through Transwell Migration assay®. A) Representative images (20X) of Transwell membranes hematoxylin stained from cells treated with vehicle and TFLLR-NH2. B) Quantification of migrating cells through Transwell migration membranes. Error bars represent S.D. 1 independent replicate. Each replication n=3 wells/condition. 10 pictures were quantified per well/condition.

Overall, we concluded that the activation of F2R is activating mechanism responsible for increasing migration and invasion of different RCC cell lines. Besides, all these results are in concordance with those presented in the loss of function studies: F2R seemed to be implicated in the acquisition of higher aggressive traits such as an increase in migration and invasion capacity of RCC cells.

1.2.4 PI3K/AKT and FAK signalling pathways were activated after F2R stimulation

Once it was confirmed the effect on cell migration and invasion that provokes the activation of F2R, we wanted to know the specific molecular mechanism by which its activates cell motility. For that reason, we tested different doses of activating peptide at different time points. Results showed a clear activation of p-AKT after 30 minutes of

activating peptide treatment. No more signalling pathways were activated after F2R
activation (Figure 48).
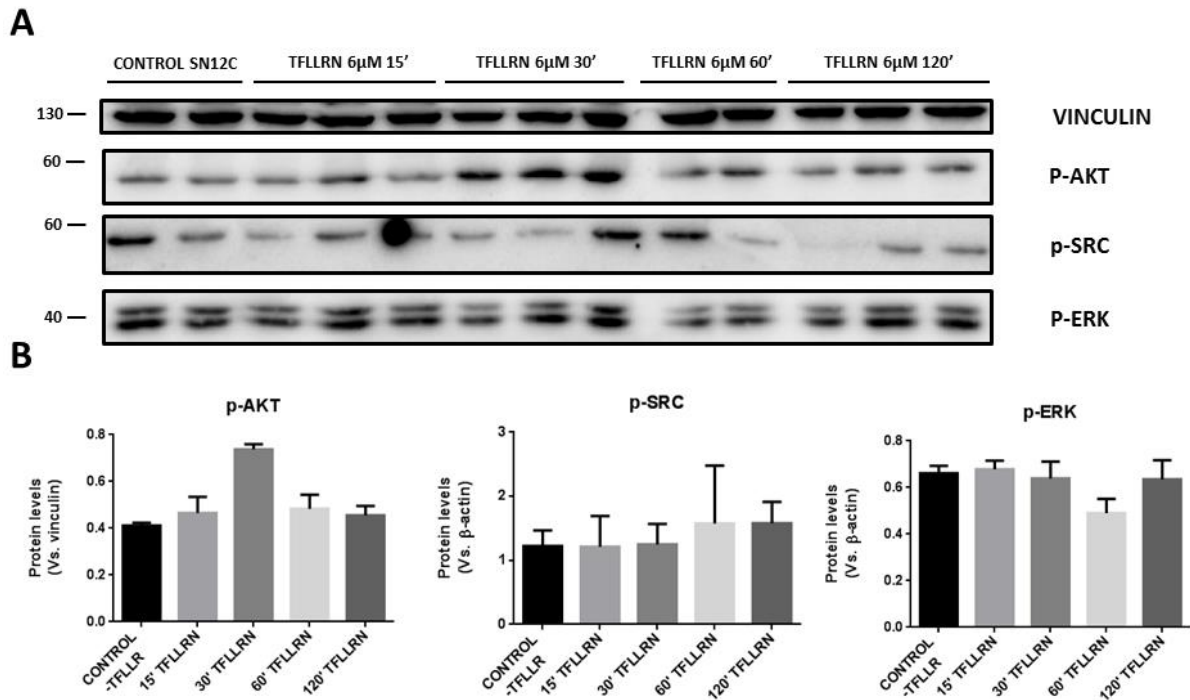
Figure 48. p-AKT signaling pathway was activated after TFLLR-NH2 peptide in SN12C cell line. Cells
were previously deprived of 24 hours with 0,5% FBS before administrating TFLLR-NH2 peptide. After
that, we incubated the peptide for 15, 30, 60, and 120 minutes at 6 µM. A) Westerns blot of p-AKT,
p-SRC, and p-ERK relativized by Vinculin. B) Quantification of the intensity of bands relativized by
Vinculin. Error bars represent S.D, wells/condition n=2/3.

Also, we wanted to test FAK signaling pathway because the regulation of cell migration
by integrin signaling through FAK is well established in many cell types which contribute
to the pathogenesis of cancer and other diseases (Zhao & Guan, 2011). For this purpose,
we analyzed the activation of FAK signalling pathway at different time points of F2R
activation with higher doses of TFLLRN-NH2 peptide (Figure 49A), but also, we analyzed
at long-term different doses of activating peptide (Figure 49B). Results showed that
there is a clear activation of FAK signalling pathway after F2R activation.
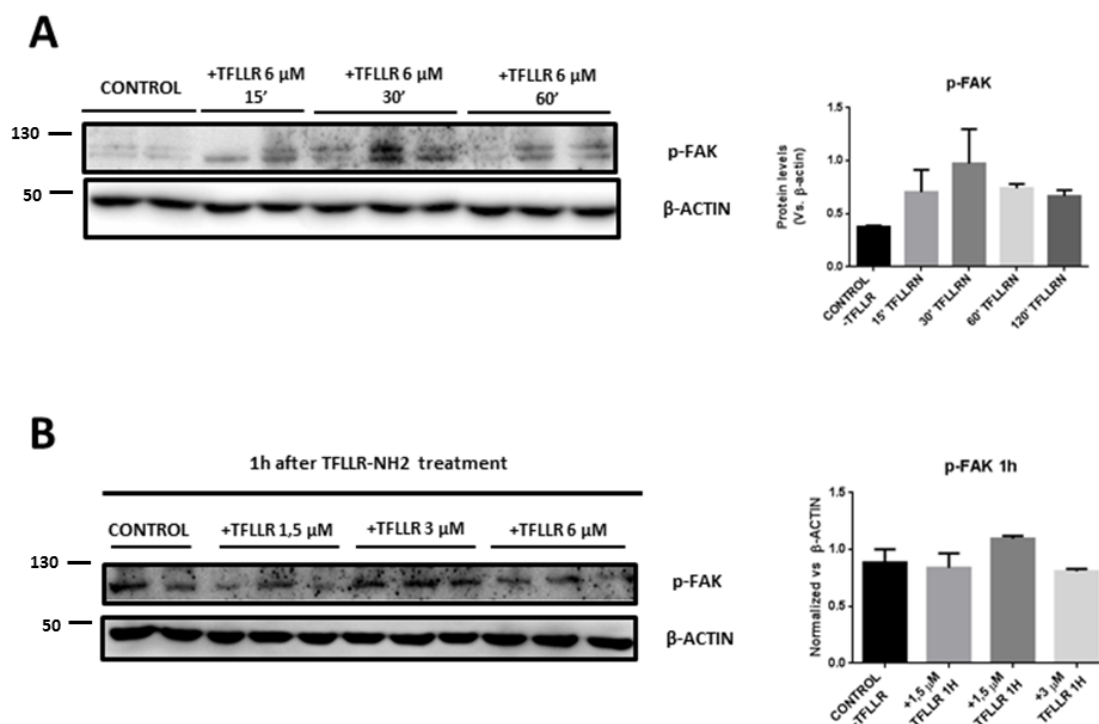
Figure 49. p-FAK signaling pathway was activated after TFLLR-NH2 peptide in SN12C cell line. A) Cells were previously deprived of 24 hours with 0,5% FBS before administrating TFLLR-NH2 peptide. After that, we incubated the peptide for 15, 30, 60, and 120 minutes at 6 µM. Westerns blot of p-FAK and its quantification relativized by Vinculin. B) Cells were previously deprived of 24 hours with 0,5% FBS before administrating TFLLR-NH2 peptide. After that, we incubated the peptide for 60 minutes at 1.5, 3, and 6 µM. Westerns blot of p-FAK and its quantification relativized by Vinculin. Error bars represent S.D, wells/condition n=2/3.

Furthermore, we checked p-FAK and PI3K/AKT signalling pathway after thrombin activation. Results confirmed the activation of both signaling pathways as it happened with the peptide (Figure 50).
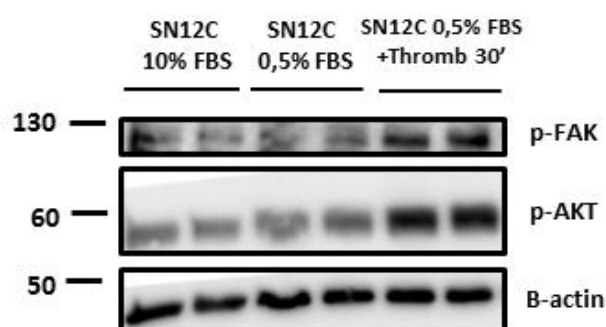
Figure 50. p-FAK and p-AKT were activated after thrombin treatment in SN12C cell line. Cells were previously deprived of 24 hours with 0,5% FBS before administrating thrombin. After that, we incubated the thrombin for 30 minutes at 1U/mL. Western blot of p-FAK and p-AKT with the housekeeping actin control is represented.

1.2.5 FAK signalling pathway was activated in Ren 50M

Considering the interesting pathways activated after F2R activation in SN12C cell line, we wondered to know if the same signalling pathways were activated in Ren 50M models in comparison with Ren 50. Despite the fact of not having higher differences in PI3K/AKT signaling pathway activation, clear differences were observed in FAK pathway (Figure 51).
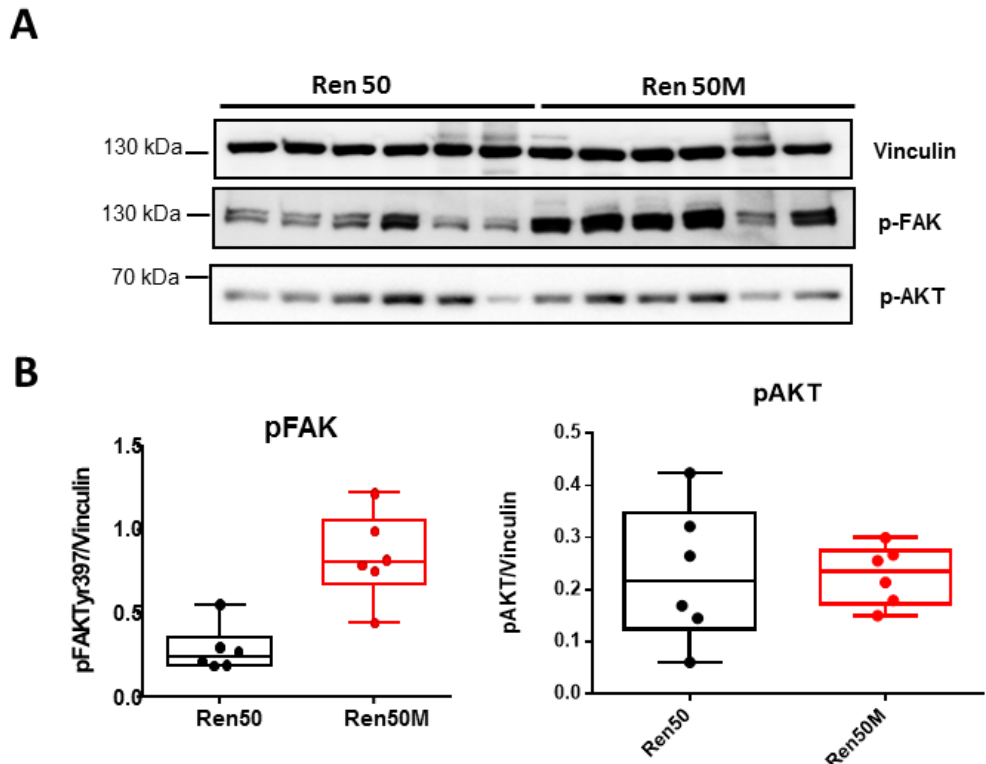
Figure 51. p-FAK and p-AKT were activated in Ren 50M tumors. Western blot of p-FAK and p-AKT with the housekeeping actin control is represented and quantified. Error bars represent S.D, wells/condition n=6

Considering all this data, we hypothesize that the activation of F2R through PI3K/AKT signaling pathway is implicated in the activation of integrins (FAK) that permits the remodeling of the actin cytoskeleton that is causing the increase of the cell migration and invasion of RCC cell lines and the higher aggressiveness of Ren 50M tumors (Figure 52).
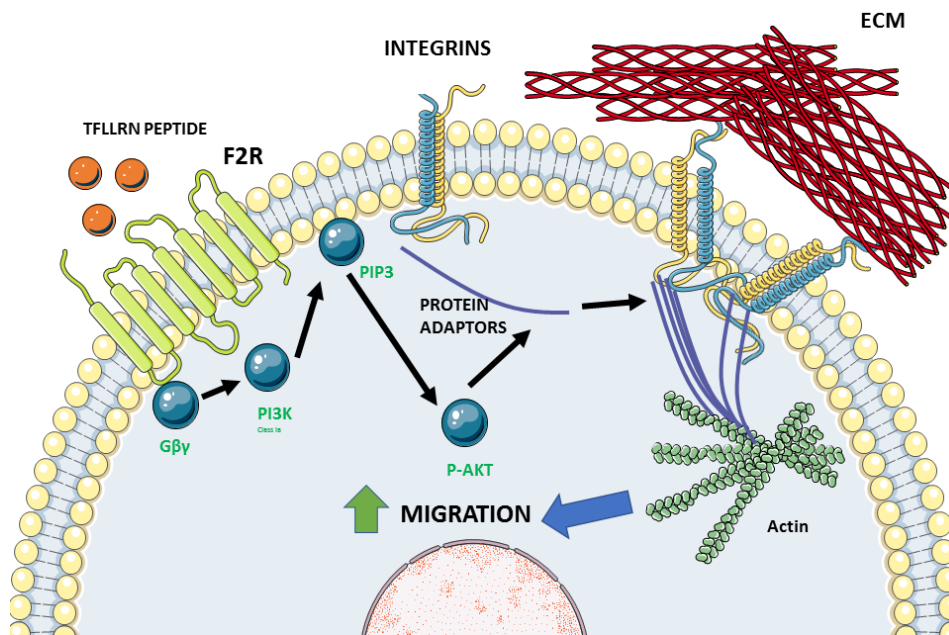
Figure 52. Hypothesis of the possible interplay between F2R and integrins. Schematic representation of how the activation of F2R is activating PI3K/AKT signalling pathway. This pathway seemed to be recruiting protein adaptors which could be affecting Integrin conformational changes of its structure that could be finally affecting cytoskeleton remodeling and activating migration on cells

1.2.6   AKT inhibition with perifosine is affecting SN12C cell migration

Once we had confirmed the possible implication of this signaling pathway on cell migration as it has been described in the literature, we wanted to test if the inhibition of this pathway implies a reduction in cell migration. To acquire this objective, we tested a specific AKT inhibitor -Perifosine – and we checked by Transwell migration the possible effects on cell migration. Results showed that after Perifosine treatment there was a decreasing tendency in cell migration compared with peptide treatment (Figure 53).
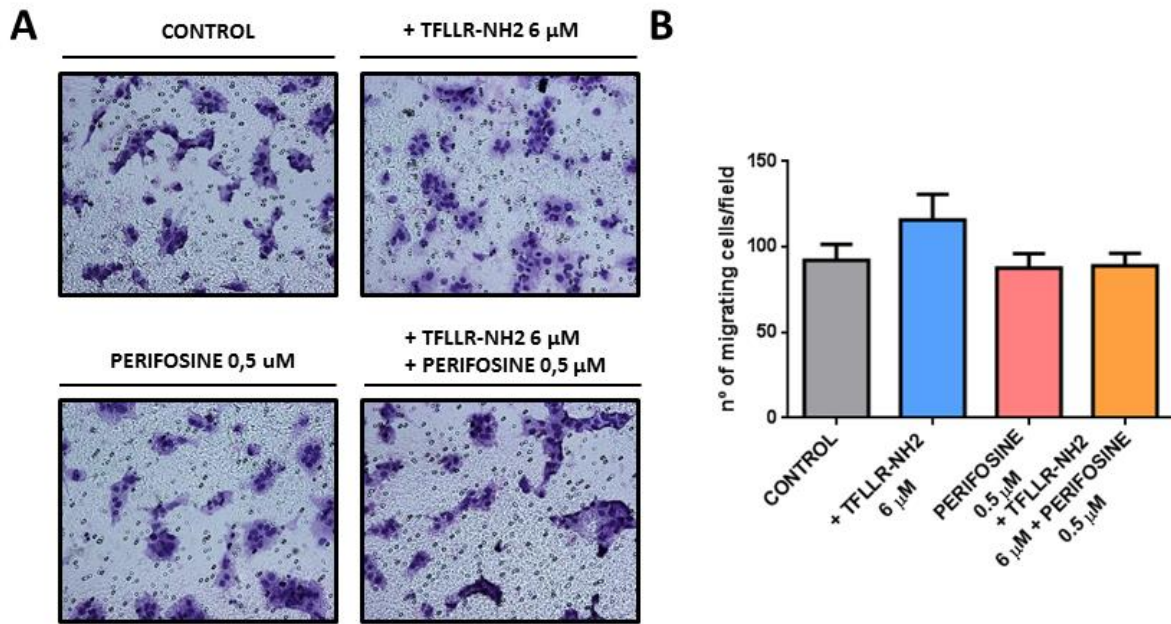
Figure 53. Effects of Perifosine on cell migration (Transwell Migration) in SN12C cell line. The effects of cell migration (at 0,5% FBS 24 hours before starting the assay) after inhibiting AKT with Perifosine, activation with TFLLR-NH2 peptide at 6 µM, and both treatments were studied through Transwell Migration assay®. A) Representative images (20X) of Transwell membranes hematoxylin stained from cells treated with vehicle, Perifosine, TFLLR-NH2, and both treatments. B) Quantification of migrating cells through Transwell migration membranes. Error bars represent S.D. 1 independent replicate. n=3 wells/condition. 10 pictures were quantified per well/condition.

Also, we wanted to validate with the same conditions but by Wound Healing technique. Results showed clear differences if we compared the TFLLR-NH2 condition with Perifosine treatment. But also, cells treated with the peptide and Perifosine had a clear decrease in cell migration capacity despite the activator treatment (Figure 54).
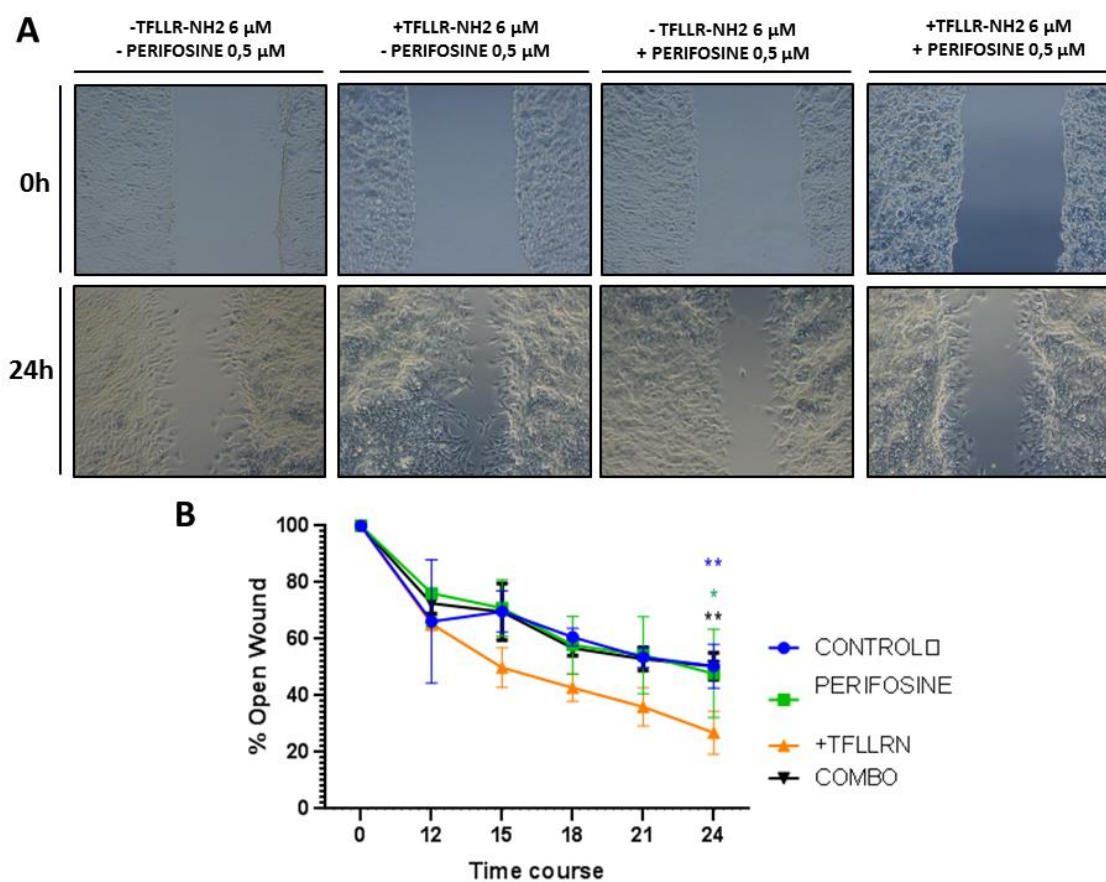
Figure 54. Effects of Perifosine on cell migration (Wound Healing) in SN12C cell line. The effects of cell migration (at 0,5% FBS 24 hours before starting the assay) after inhibiting AKT with Perifosine 5 μM, activation with TFLLR-NH2 peptide at 6 μM, and both treatments were studied through Wound Healing assay. A) Representative images after the first time point and after 24 hours of assay. B) Quantification of migration speed. Error bars represent S.D. 1 independent replicate. n=3 Wells/condition. Mann Whitney test, $p < 0.05$*, $p < 0.01$ **)

Finally, to validate that we had a clear inhibition of the phosphorylation of AKT, we checked by Western blot. Results confirmed a strong decrease in AKT phosphorylation after 30 minutes of Perifosine treatment. Also, we confirmed that in the combination treatment with Peptide and Perifosine, we also had a clear decrease in p-AKT (Figure 55).
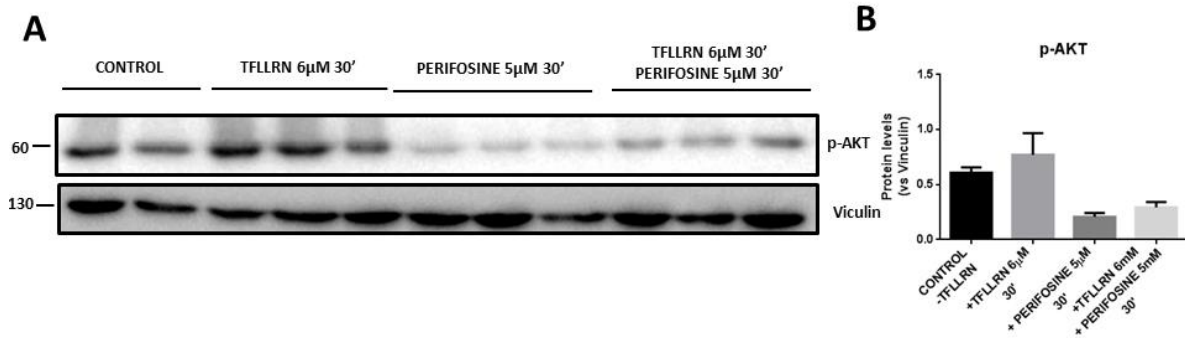
Figure 55. p-AKT protein level analysis after Perifosine inhibitor. Cells were previously nutrient-deprived at 0,5% FBS and cells were treated with Perifosine 5 µM, TFLLR-NH2 peptide 6 µM, and both treatments for 30 minutes. A) Western blot analysis of p-AKT and housekeeping Vinculin gene. B) Westerns blot of p-FAK and its quantification relativized by Vinculin. Error bars represent S.D, wells/condition n=2/3.

1.2.7 Gβγ inhibition with gallein is decreasing SN12C cell migration

To further confirm the implication of PI3K/AKT signaling pathway on cell migration, we also wanted to inhibit the Gβγ subunit of F2R. For that reason, we tested Gallein inhibitor as a potent selective Gβγ inhibitor.

To check the effects of Gallein on cell migration, we performed a Wound healing assay with different treatments of activating peptide, Gallein inhibitor, and a combination of both treatments. Results showed the same results of Perifosine inhibitor: there was a clear decrease in cell migration if we compare TFLLRN-NH2 treatment with Gallein inhibitor or both treatments (Figure 56).
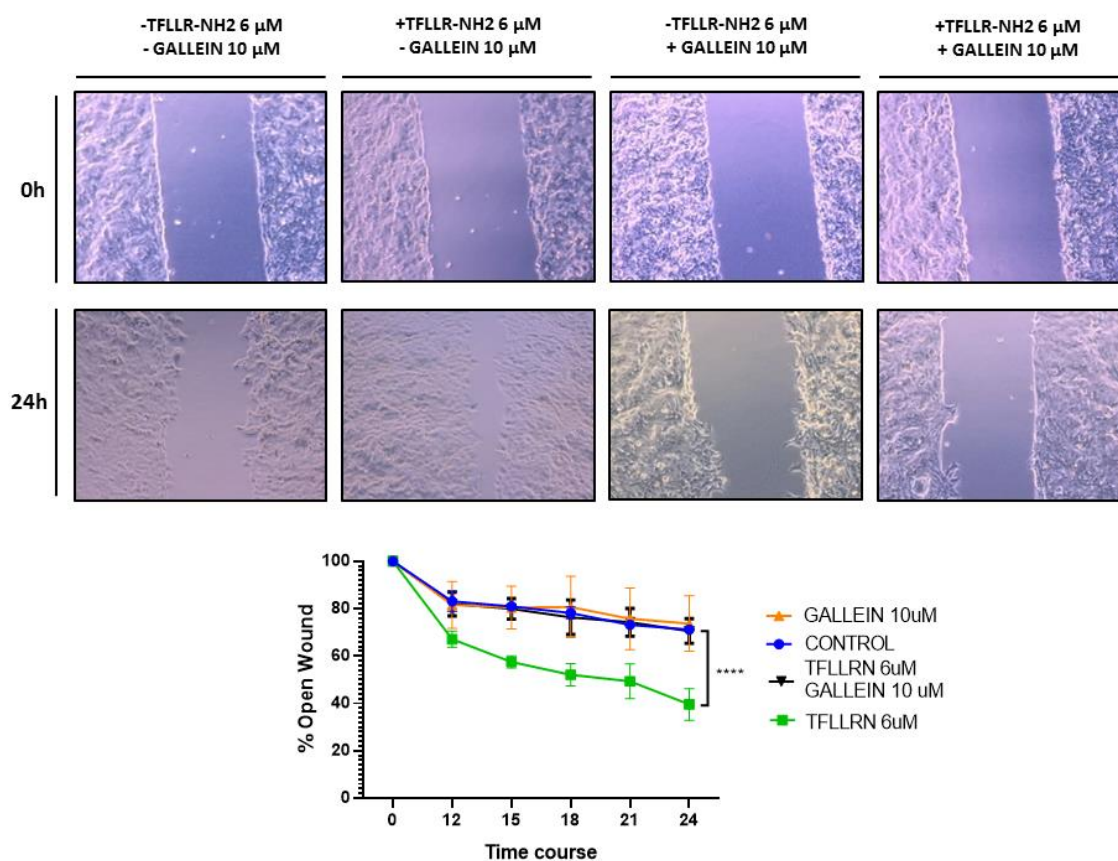
Figure 56. Effects of Gallein on cell migration (Wound Healing) in SN12C cell line. The effects of cell migration (at 0,5% FBS 24 hours before starting the assay) after inhibiting Gβγ subunit with Gallein 10 µM, activation with TFLLR-NH2 peptide at 6 µM, and both treatments were studied through Wound Healing assay. A) Representative images after the first time point and after 24 hours of assay. B) Quantification of % of the open wound. Error bars represent S.D. 1 independent replicate. n=3 Wells/condition. Mann Whitney test, $p < 0.005$ ***)

Finally, we also checked that after Gallein treatment, we had a reduction of AKT phosphorylation by Western Blot. Results showed a slight decrease of p-AKT after Gallein alone or in combination with TFLLR-NH2 in comparison with the clear phosphorylation of AKT after peptide treatment (Figure 57).
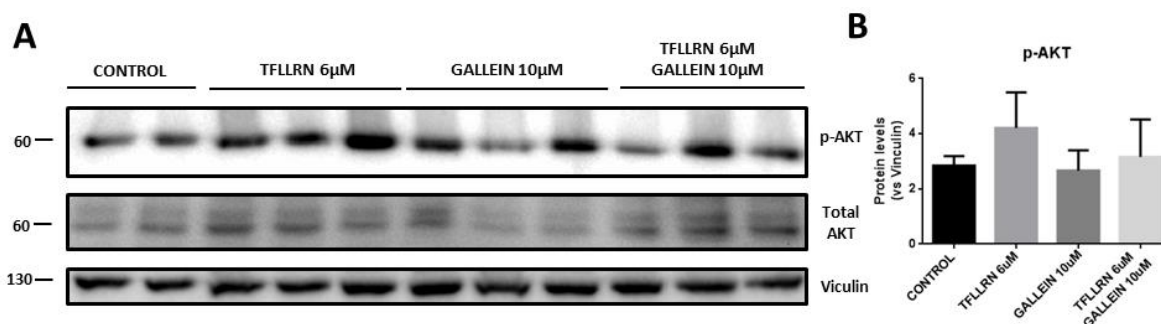
Figure 57. p-AKT protein level analysis after Gallein inhibitor. Cells were previously nutrient-deprived at 0,5% FBS and cells were treated with Gallein 10 μM, TFLLR-NH2 peptide 6 μM, and both treatments for 30 minutes. A) Western blot analysis of p-AKT and housekeeping Vinculin gene. B) Westerns blot of p-FAK and its quantification relativized by Vinculin. Error bars represent S.D, wells/condition n=2/3.

Overall, the inhibition of the different proteins of the PI3K/AKT signalling pathway affected the migration capacity of SN12C cells. Having analyzed and demonstrated the possible implication of F2R in the acquisition of higher migration and invasion capacity of SN12C cells we decided to study the possible interplay between F2R and integrins.

1.3 Integrins family analysis

One of the main players that facilitates cell migration is integrins. For that reason, we moved to our PDOX models to compare which integrins are overexpressed in metastatic tumors (Ren50M) in comparison with non-metastatic tumors (Ren50). We analyzed the expression levels of different integrins from the RNA sequencing. Criteria for selecting candidates were both the presence of a high fold change between Ren 50 and Ren 50M tumors and high expression levels in Ren 50M, ensuring detection of these genes at the protein level. Following these parameters, we chose Integrin α3 and Integrin α5 (Table 12A) which are making dimers with Integrin β1 (Table 12B).

α SUBUNIT INTEGRINS

Gene Symbol	Description	Fold Change	PValue	FDR	Mean Ren50	Mean Ren50M
ITGA4	Integrin α4	309,703015	2,969E-09	7,55E-08	0,19896407	61,6197726
ITGAX	Integrin αX	8,29420384	4,4285E-11	1,42E-09	0,27106963	2,24830677
ITGA11	Integrin α11	8,27874054	1,8898E-09	4,97E-08	0,23155778	1,91700681
ITGA3	Integrin α3	4,93947182	1,2961E-24	1,41396E-22	50,0114852	247,030322
ITGA5	Integrin α5	1,71427768	0,0004466	0,003898499	111,539817	191,210219
ITGA6	Integrin α6	1,16568871	0,37949555	0,591299125	202,306604	235,826525
ITGAV	Integrin Av	1,16512929	0,26507061	0,488113886	485,750227	565,961817
ITGAE	Integrin AE	1,0207957	0,89482528	0,940605162	23,1833623	23,6654765

β SUBUNIT INTEGRINS

Gene Symbol	Description	Fold Change	PValue	FDR	Mean Ren50	Mean Ren50M
ITGB2	Integrin β2	41,0790994	7,3884E-59	3,41E-56	3,78732496	155,579899
ITGB3	Integrin β3	12,9162191	2,485E-28	3,15E-26	1,01274256	13,0808048
ITGB4	Integrin β4	11,7900268	4,9237E-30	6,63E-28	2,53167606	29,8485286
ITGB5	Integrin β5	1,52585321	0,00291029	0,018932969	217,391252	331,70714
ITGB1	Integrin β1	1,34227748	0,02815583	0,116516829	567,257891	761,417494
ITGB8	Integrin β8	1,31786336	0,13628041	0,342003907	86,0544978	113,408069

Table 12. Selected integrins subunits α and β overexpressed in Ren 50M tumors. Table of selected genes regarding their fold change when comparing Ren 50 and Ren 50M tumors. Fold change (FC) was obtained by comparing their expression levels (cpm). P-value and FDR represent the value of a test for statistical significance. A) α subunit integrins analysis. B) β subunit integrins analysis.

1.3.1 Integrin α3 was expressed in patient biopsy

Once we had selected that these integrins could be helping cancer cells to escape from the primary tumor to colonize new organs, we wanted to analyze its expression in the biopsy from the patient to confirm that this integrin was expressed before PDOX generation. For that reason, we analyzed Integrin α3 by IHC. Results confirmed its expression in the patient (Figure 58).
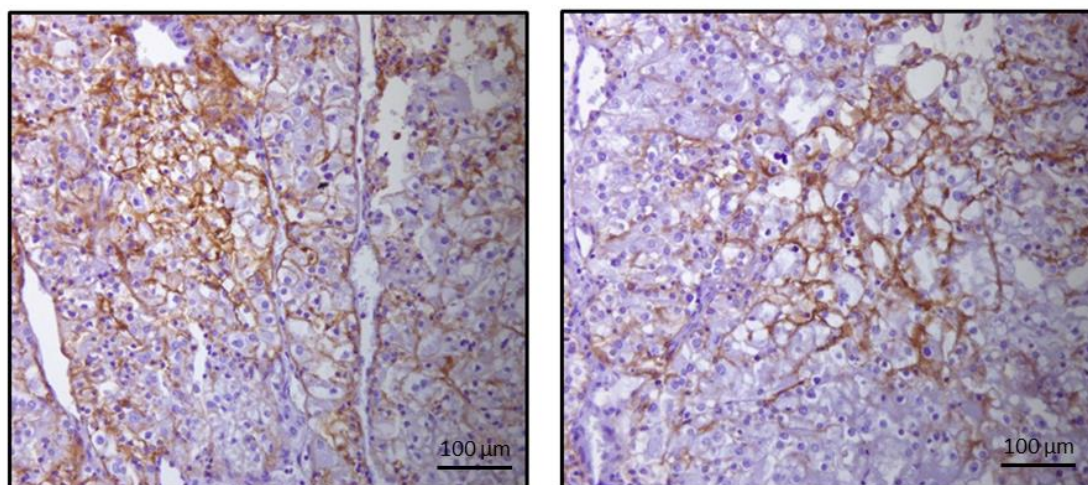
Figure 58. Patient biopsy presented higher levels of Integrin α3. Immunohistochemistry of Integrin α3 in the biopsy from the patient. Representative images (20X) are represented.

1.3.2   Integrin α5 was expressed in patient biopsy

Furthermore, it was analyzed the integrin α5 and as happened with the integrin α3, higher levels of integrin α5 were observed (Figure 59).
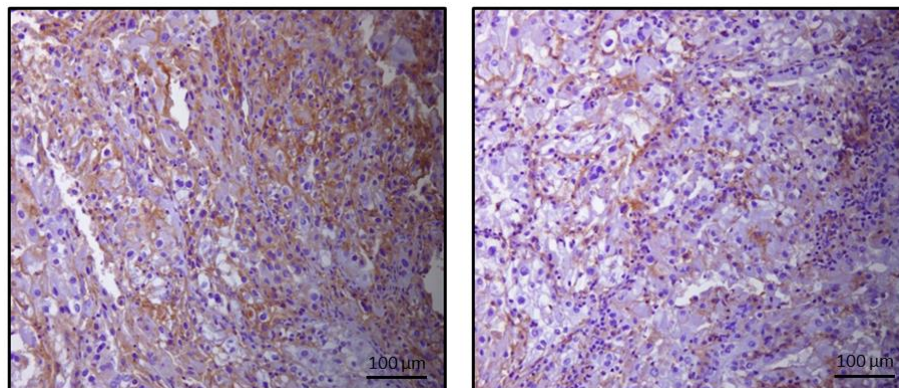
Figure 59. Patient biopsy presented higher levels of Integrin α5. Immunohistochemistry of Integrin α5 in the biopsy from the patient. Representative images (20X) are represented.

1.3.3   Integrin α3, α5, and β1 were overexpressed in Ren 50M tumors

Next, we analyzed integrin α3 in Ren 50 and Ren 50M tumors. Results showed an increased level of this integrin by WB (Figure 60A), IHC (Figure 60B), and by RNA-sequencing (Figure 60C).
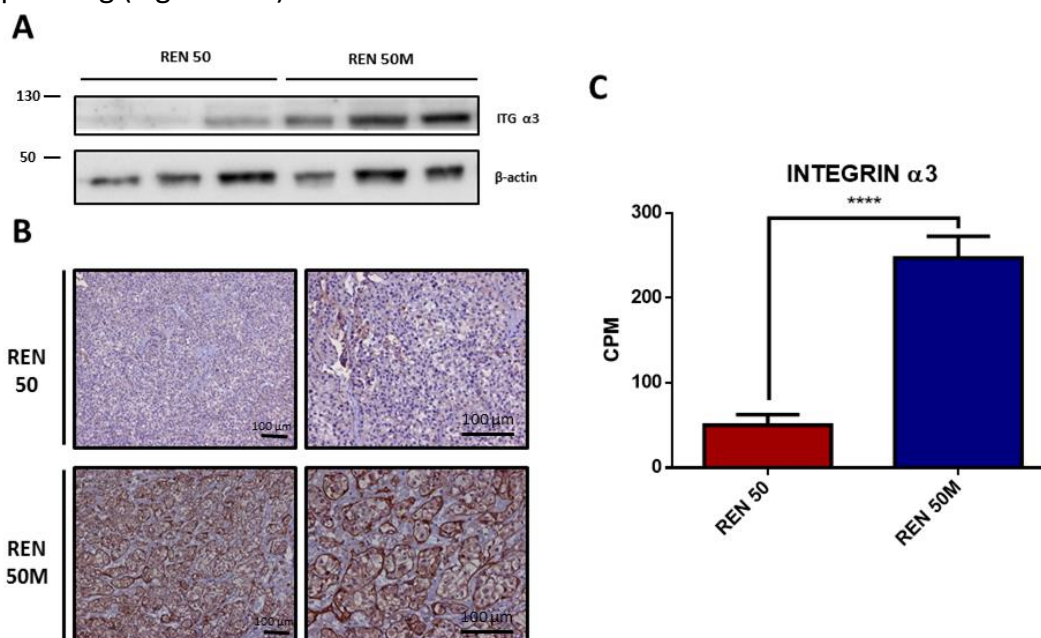
Figure 60. Integrin α3 analysis in PDOX models. A) Western blot of Integrin α3 protein levels in Ren 50 and Ren 50M tumors relativized by its β-actin. B) Inmunihistochemistry of Integrin α3 in Ren 50 and Ren 50M tumors. C) Results from RNA-seq analysis of Integrin α3. In Y-axis it is expressed as Counts per million (CPM). Error bars represent S.D, n=3. Mann Whitney test, p<0.001 ***)

Then, we moved to analyze Integrin α5 in our PDOX models. Results confirmed clear differences in expression levels of this integrin between Ren 50 and Ren 50M by WB (Figure 61A), IHC (Figure 61B), and RNA-sequencing (Figure 61C).
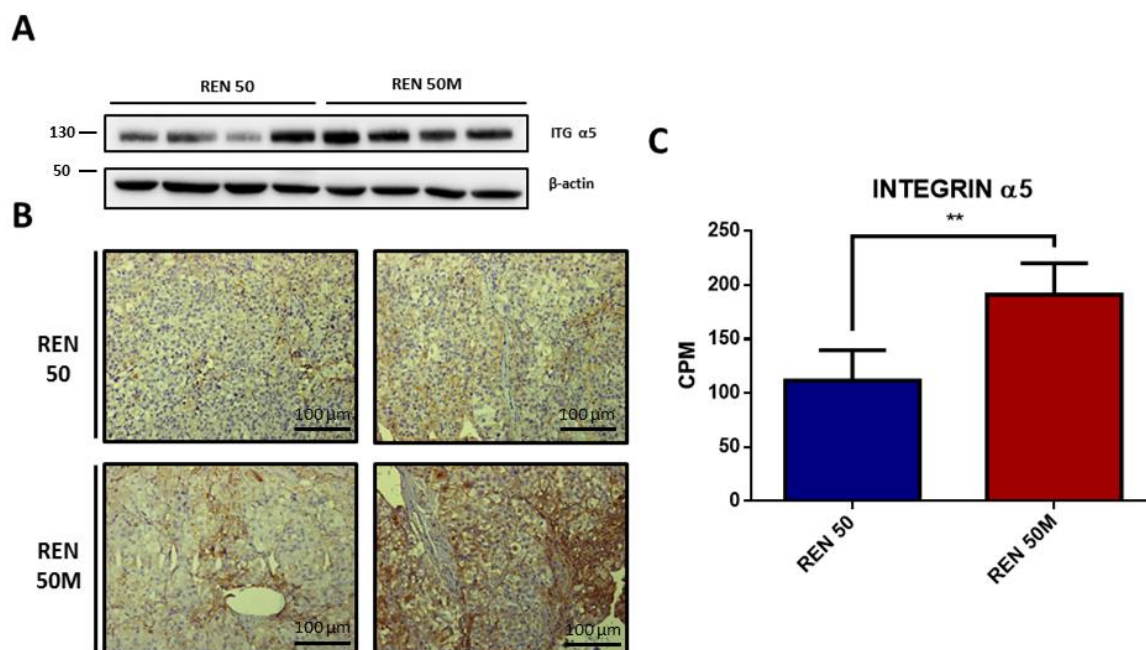
Figure 61. Integrin α5 analysis in PDOX models. A) Western blot of Integrin α5 protein levels in Ren 50 and Ren 50M tumors relativized by its β-actin. B) Inmunihistochemistry of Integrin α5 in Ren 50 and Ren 50M tumors. C) Results from RNA-seq analysis of Integrin α5. In Y-axis it is expressed as Counts per million (CPM). Error bars represent S.D, n=3. Mann Whitney test, p<0.001 ***)

As it has been described in the literature, the principal β-subunit integrin with which α3 and α5 dimerize is integrin β1. To confirm results from RNA-seq previously shown in Table 12B, we proceeded to analyze by WB total Integrin β1 but also the activated form from Integrin β1. Results showed that there are no higher differences comparing Ren 50 and Ren 50M by Western Blot (Figure 62A). However, clear differences were observed by IHC (Figure 62B) and by RNA-seq (Figure 62C).
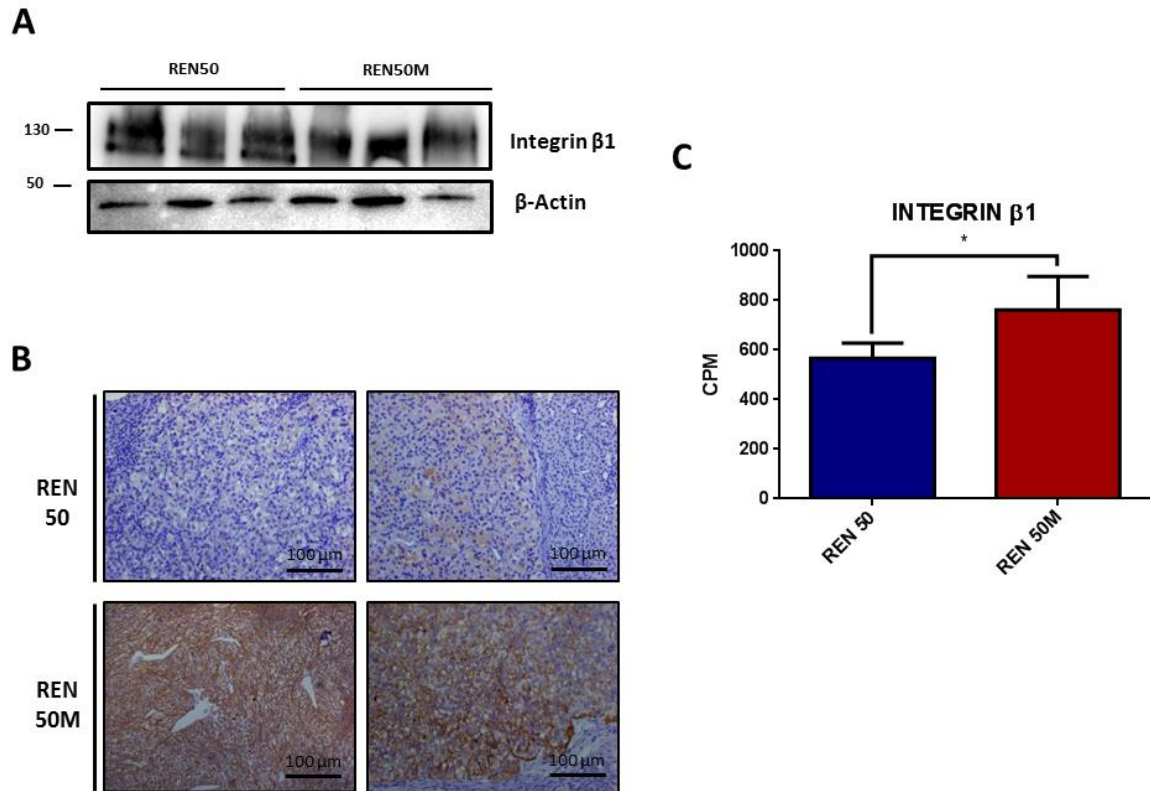
Figure 62. Integrin β1 analysis in PDOX models. A) Western blot of total Integrin β1 and activated protein levels in Ren 50 and Ren 50M tumors relativized by its β-actin. B) Inmunihistochemistry of Integrin β1 in Ren 50 and Ren 50M tumors. C) Results from RNA-seq analysis of Integrin β1. In Y-axis it is expressed as Counts per million (CPM). Error bars represent S.D, n=3. Mann Whitney test, $p<0.05$ *)

1.3.4   Fibronectin was overexpressed in Ren 50M tumors

Once we have analyzed integrins expression, we wanted to check if these tumors had the expression of the ligand from these integrins. As it has been described in the literature, there are many ligands that integrins α3β1 and α5β1 can be attached, but the most important one is Fibronectin.

For that reason, we moved to analyze its expression in our PDOX models. Results showed that there were clear differences in Fibronectin deposition in Ren50M tumors checked by WB (Figure 63A) and by IHC (Figure 63B).
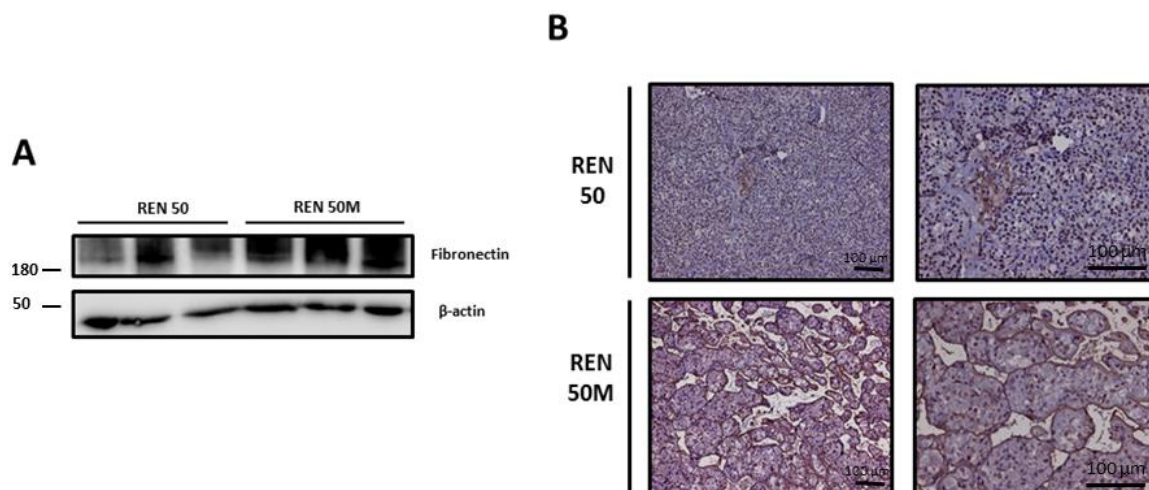
Figure 63. Fibronectin analysis in PDOX models. A) Western blot of fibronectin protein levels in Ren 50 and Ren 50M tumors relativized by its β-actin. B) Inmunihistochemistry of fibronectin in Ren 50 and Ren 50M tumors.

1.3.5   Integrin α3 was overexpressed in SN12C tumors

Once we validated the presence of these integrins and ligands in our PDOX model, we moved to analyze the same integrins in SN12C *in vivo* tumors to know if the higher aggressiveness of SN12C tumors is due to the same integrins and ligands as Ren50M tumors. For that reason, we checked the expression of Integrin α3 by IHC (Figure 64A), WB (Figure 64B), and by ICF (Figure 64C). Results showed a huge increase in these integrins if we compared them with human PDOX models. Also, thanks to ICF analysis we confirmed that integrin α3 is making dimer with integrin β1 as they are co-expressed in the cellular membrane.
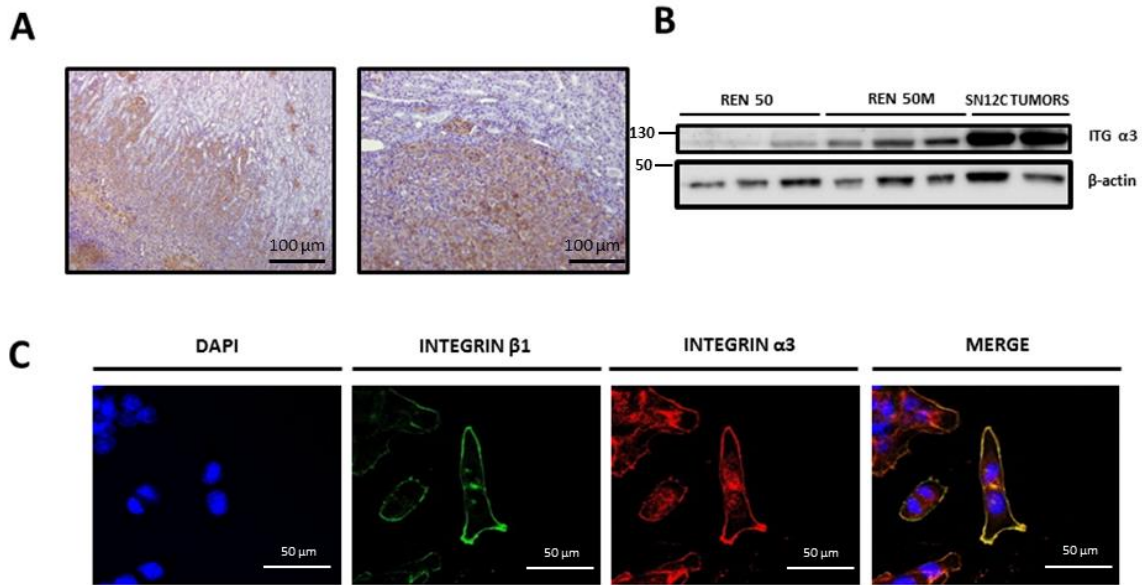
Figure 64. Integrin α3 analysis in SN12C tumors. A) Immunohistochemistry of Integrin α3 protein levels in SN12C tumors. B) Western blot of Integrin α3 protein levels in SN12C tumors relativized by its β-actin. C) Inmunocitofluorescence of Integrin α3 (red) and integrin β1 (green) and DAPI (blue).

1.3.6 Integrin α5 was slightly expressed in SN12C tumors

We next moved to analyze integrin α5 in SN12C tumors. Results showed that by IHC (Figure 65A) we have higher expression in the invasive front of the tumor but not much expression outside the invasive front. For that reason, by WB (Figure 65B) we did not see clear differences if we compare with PDOX models. And finally, thanks to ICF analysis (Figure 65C) we confirmed that integrin α3 is making dimer with integrin β1 as we saw co-expression of both integrins in the invasive front of *in vitro* cultured SN12C.
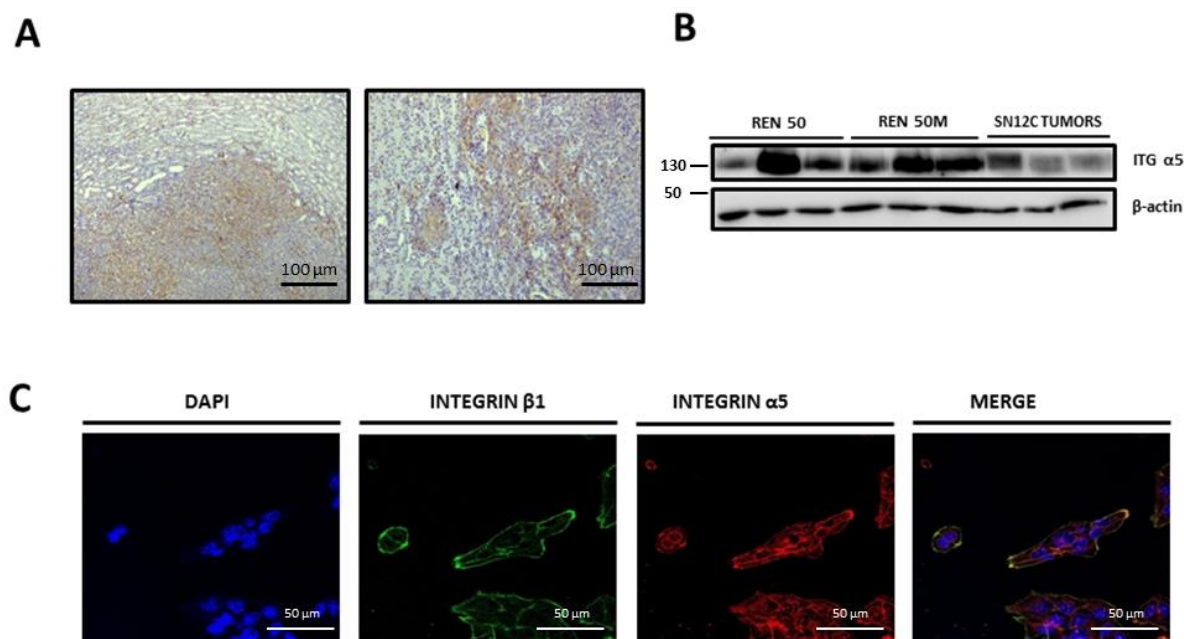
Figure 65. Integrin α5 analysis in SN12C tumors. A) Immunohistochemistry of Integrin α5 protein levels in SN12C tumors. B) Western blot of Integrin α5 protein levels in SN12C tumors relativized by its β-actin. C) Inmunocitofluorescence of Integrin α5 (red) and integrin β1 (green) and DAPI (blue).

1.3.7   Fibronectin was slightly expressed in SN12C tumors

Finally, we moved to study fibronectin expression of SN12C tumors. As similar occurred with integrin α5, we detected by IHC (Figure 66A) higher expression in the invasive front of tumors and slightly expression in the rest of tumor parenchyma. However, not much expression was identified by WB (Figure 66B).
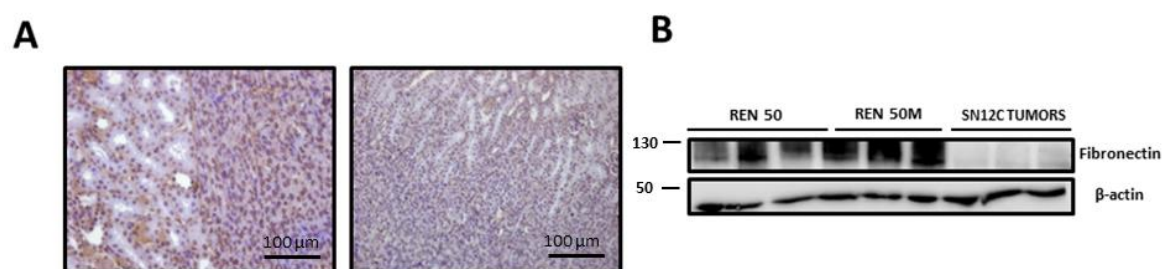
Figure 66. Fibronectin analysis in SN12C tumors. A) Immunohistochemistry of Fibronectin protein levels in SN12C tumors. B) Western blot of Fibronectin protein levels in SN12C tumors relativized by its β-actin.

Considering all these experiments, we confirmed the presence of the different integrins and their ligand in Ren 50M and SN12C tumors that could be responsible for the higher aggressive phenotypes of both tumor types.

2. ROLE OF F2R IN CIRCULATING TUMOR CELLS (CTC) AND DISSEMINATED TUMOR CELLS (DTC)

Many effects of F2R in tumor cells are known and how it is affecting the primary tumors. But once cells escape from the primary tumor and are inside blood vessels, the effects of this coagulative protein receptor in circulating and disseminated tumor cells are not well described. Due to this lack of information, we studied what is happening with this receptor in CTCs and DTCs.

2.1 Early F2R knockdown in SN12C circulating tumor cells (CTC)

To know if the presence of F2R is conferring new abilities to CTC to facilitate the colonization of distant organs, we decided to inoculate SN12C knocked down cells through the tail vein. Immediately, the next day after tumor cell inoculation, we administrate doxycycline to mice to decrease F2R expression.

2.1.1 Metastasis from shF2R inoculated SN12C cells presented a clear decrease in F2R expression

After 1 month of doxycycline administration, we decided to sacrifice the mice, and metastasis was analyzed to check the expression of F2R. Metastasis from shNS -DOX (Figure 67A), shNS +DOX (Figure 67B), shF2R -DOX (Figure 67C) presented higher levels of F2R expression, and metastasis from shF2R +DOX (Figure 67D) showed a clear decrease of F2R expression.
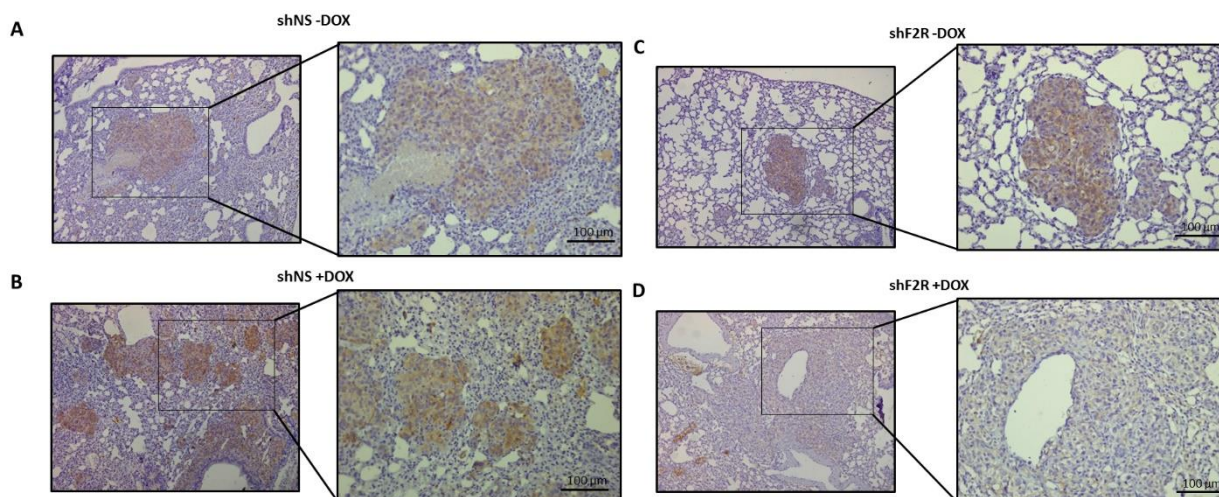
Figure 67. F2R expression analysis in metastasis from SN12C shF2R inoculated cells through the tail vein. Cells were inoculated through the tail vein and after 24 hours, doxycycline was administrated to mice for 1 month. Immunohistochemical analysis of F2R in metastasis from shNS -DOX (A), shNS +DOX (B), shF2R -DOX (C) and shF2R +DOX (D). n=5 mice were analyzed in shNS and n=10 mice were analyzed in shF2R mice.

Once it was confirmed the decrease of F2R expression when doxycycline was administered in SN12C shF2R inoculated mice, we moved on to analyze different parameters related to metastasis.

2.1.2 F2R knocked down SN12C cells presented less capacity to form metastatic lesions in the lung

Results showed that there were no differences in the affected lung lobes (Figure 68A). Moreover, there were significant differences in the number of foci lesions if we compare shNS +DOX with shF2R +DOX (Figure 68B). Unexpectedly, doxycycline treatment was increasing metastasis so for that reason we decided to compare those groups who received doxycycline treatment but differences in the F2R expression. We also analyzed the size of metastatic lesions by dividing the total metastatic area by the number of foci lesions and we did not find any difference comparing shNS +DOX with shF2R +DOX (Figure 68C). Furthermore, we categorize each lesion into small, medium, or large, and no differences appeared (Figure 68D).

Figure 68. SN12C shF2R mice administered with doxycycline presented less number of metastatic lesions but no differences in terms of size were presented. Different parameters related to metastasis were analyzed in shNS (n=5) and shF2R (n=10) inoculated mice. A) Number of lung lobes with lesions was quantified. B) Number of foci lesions quantified per mouse. C) The size of each lesion was quantified by dividing the total metastasis area by the number of foci lesions. D) Lesions were classified as Small, Medium, and Large depending on their size. Mann Whitney test, p<0,05*. Images from lungs were taken with Zeiss Axio Observer Z1+ Apotome inverted microscope at 4X and a mosaic was created with all pictures to quantify.

2.1.3 F2R knocked down SN12C cells metastatic lesions presented same proliferative rate as those with higher F2R expression

To confirm that there were no differences in the size of metastatic lesions, we decided to analyze the cell proliferation of different foci lesions. Results confirmed that there were no differences in the size of lesions (Figure 69)

Figure 69. Proliferation analysis of metastasis lesions from mice inoculated with SN12C shF2R through the tail vein. Proliferation was analyzed by Inmunohistrochemistry of the Ki67 proliferative marker. A) Representative images from each group of tumors at 10X. B) Quantification of total proliferative cells vs total cells. Results are represented in % of proliferative cells. Error bars represent S.D, n=5 different lesions and n=3 mice analyzed per group. Mann Whitney test, p>0.05 ns)

2.1.4   F2R knocked down SN12C cells presented less metastatic capacity

Finally, we analyzed the total metastasis area relativized by the total lung area analyzed and we clear confirmed that if we compare animals who received doxycycline treatment, in those who had F2R reduction, we had a clear decrease in total metastasis (Figure 70)
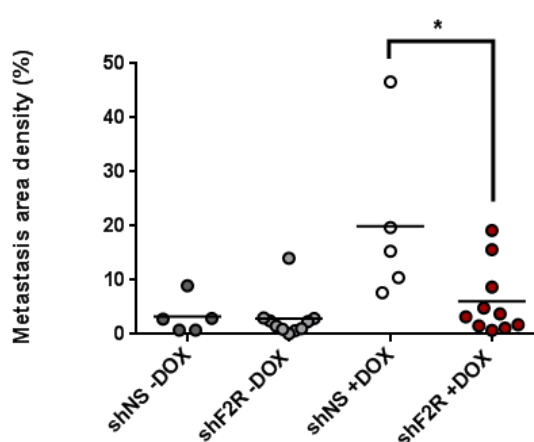
Figure 70. Metastasis area density quantification of metastatic lesions from mice inoculated with SN12C shF2R through the tail vein. Total metastasis area density was determined by quantifying the total metastatic area normalized by the total lung area of each lung. Images from lungs were taken with Zeiss Axio Observer Z1+ Apotome inverted microscope at 4X and a mosaic was created with all pictures to quantify. Mann Whitney test, p<0,05*.

2.1.5 F2R knocked down SN12C cells showed less activation of de PI3K/AKT signalling pathway

As it was described in the previous results section about the possible relation between F2R and PI3K/AKT signalling pathway and as we confirmed that knocked-down cells had clear inactivation of AKT, we wanted to evaluate the activation of the AKT signalling pathway by IHC in the metastatic lesions. Results confirmed that both groups of animals - shNS not administrated (Figure 71A) or administrated with doxycycline (Figure 71B)- and shF2R -DOX (Figure 71C) presented higher levels of p-AKT compared with shF2R mice administrated with doxycycline (Figure 71D) that no activation of AKT was detected.
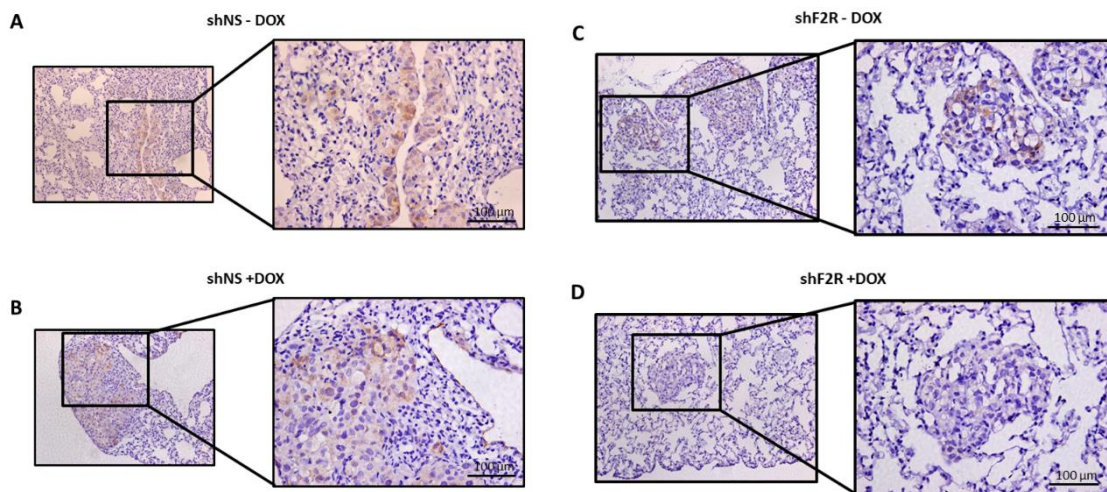
Figure 71. p-AKT expression analysis in metastasis from SN12C shF2R inoculated cells through the tail vein. Cells were inoculated through the tail vein and after 24 hours, doxycycline was administrated to mice for 1 month. Immunohistochemical analysis of p-AKT in metastasis from shNS -DOX (A), shNS +DOX (B), shF2R -DOX (C), and shF2R +DOX (D). n=5 mice were analyzed in shNS and n=10 mice were analyzed in shF2R mice.

Considering all these interesting results we can conclude the possible implication of F2R on metastasis. Concretely, F2R could be implicated in the latest steps of the metastatic cascade, when cells needed to extravasate from lug capillaries and colonize lung parenchyma. To acquire this objective, PI3K/AKT signaling pathway could be playing an interesting role in DTCs survival.

2.2 F2R previously knocked down SN12C cells as inoculated CTCs

Considering the previous results from the early F2R knockdown expression and the decrease in the number of metastatic lesions, we decided to inoculate SN12C cells previously treated with doxycycline to inject cells without F2R expression. Then, after 5 days we sacrificed mice to analyze if the absence of F2R was affecting the colonization of SN12C cells. This will help to establish the reason for the decrease in the number of foci lesions in SN12C shF2R +DOX group compared with SN12C shNS +DOX group.

2.2.1 F2R previously knocked down SN12C cells tend to present less capacity to form metastatic lesions in the lung

We decided to quantify the number of micrometastatic lesions in different groups of inoculated shRNA SN12C cells, and the results showed that we also had an increase of metastatic lesions in the shNS +DOX group. We found an unexpected effect of doxycycline that was inducing metastasis in our model. As we did previously, we compared the group of shNS +DOX with shF2R +DOX, and we found a decrease in the metastatic colonization of those cells that had less F2R expression (Figure 72).
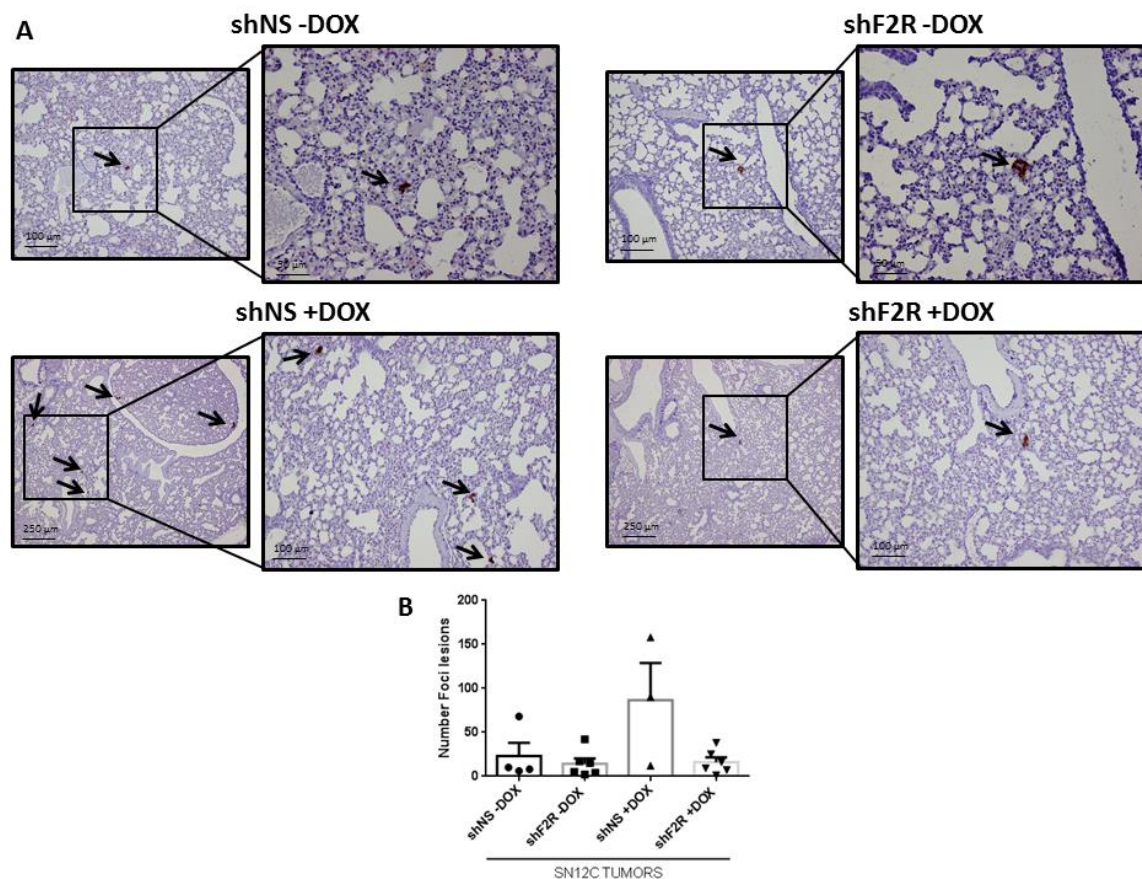
Figure 72. Lower levels of F2R tend to be associated with less metastatic colonization. Cells were inoculated through the tail vein previously pre-treated with doxycycline and were administrated to mice for 5 days. A) Inmunohistochemical analysis of human vimentin in metastasis from shNS -DOX, shNS +DOX, shF2R -DOX, and shF2R +DOX. n was as minimum 3 mice analyzed per each group.

2.3   Late F2R knockdown in SN12C circulating tumor cells

Having these interesting results into account that confirmed the possible relation between F2R and metastasis when cells are directly into the bloodstream, we wanted to evaluate if knocking down the receptor after 30 days of inoculation into mice had the same effect. As we were decreasing F2R expression after many days of cells injection, it is supposed that we were not affecting either survival in circulation or extravasation from the vasculature to secondary tissue; we supposed that we are affecting the process of colonization and stabilization of metastatic lesions at secondary sites.

2.3.1   F2R knocked down SN12C DTC had less capacity to grow in the lungs

After 2 months of the experiment, we euthanized animals, and many parameters related to metastasis were analyzed. Results showed analyzing lung affected lobes, that there were fewer affected lobes in those animals inoculated with SN12C shF2R administrated with doxycycline (Figure 73A). However, there were no significant differences in the number of foci lesions if we compare shF2R groups of animals administrated or not with doxycycline, but clear decrease tendencies are shown (Figure 73B). Moreover, we did not find statistical differences in the size of these lesions comparing shF2R -DOX with shF2R +DOX, but lesions tend to be smaller (Figure 73C). For that reason, after performing the categorical classification of lesions, we found that shF2R +DOX mice presented more small lesions than shF2R -DOX mice (Figure 73D).

Figure 73. SN12C shF2R mice administered with doxycycline presented a tendency to decrease the number and the size of lung lesions. Different parameters related to metastasis were analyzed in shNS (n=5) and shF2R (n=10) inoculated mice. A) Number of lung lobes with lesions was quantified. B) Number of foci lesions quantified per mouse. C) The size of each lesion was quantified by dividing the total metastasis area by the number of foci lesions. D) Lesions were classified as Small, Medium, and Large depending on their size.   Mann Whitney test, $p<0,05*$. Images from lungs were taken with Zeiss Axio Observer Z1+ Apotome inverted microscope at 4X and a mosaic was created with all pictures to quantify.

Then, we decided to analyze the proliferation of different metastatic lesions as we found differences in the size when we decrease F2R expression. Results confirmed that there was a decrease in the proliferation of those lesions with less F2R expression (Figure 74).
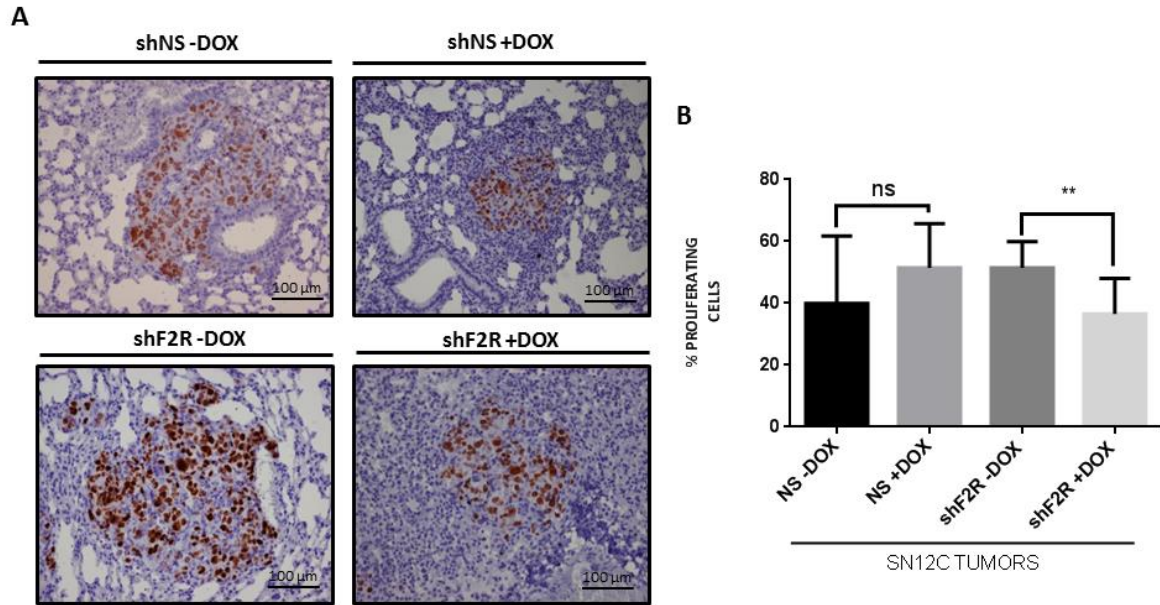
Figure 74. Proliferation analysis of metastatic lesions revealed a lower proliferative rate in knocked down F2R metastatic lesions. Proliferation was analyzed by Inmunohistrochemistry of Ki67 proliferative marker. A) Representative images from each group of tumors at 10X. B) Quantification of total proliferative cells vs total cells. Results are represented in % of proliferative cells. Error bars represent S.D, n=5 different lesions and n=5 mice analyzed per each group. Mann Whitney test, p<0.005 **)

Finally, we analyzed the total metastasis area relativized by the total lung area analyzed and we clearly confirmed that after decreasing F2R expression, we had a clear reduction of metastatic area density (Figure 75).
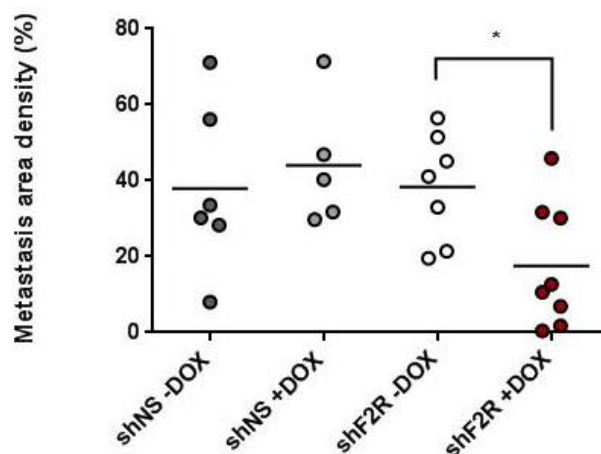
Figure 75. Metastasis area density was decreased in mice inoculated with SN12C shF2R (late doxycycline administration) through the tail vein. Total metastasis area density was determined by quantifying the total metastatic area normalized by the total lung area of each lung. Images from lungs were taken with Zeiss Axio Observer Z1+ Apotome inverted microscope at 4X and a mosaic was created with all pictures to quantify. Mann Whitney test, $p < 0,05*$.

Altogether, we confirmed that F2R is contributing to the metastatic process in the later steps of the metastatic process. F2R could be necessary for cancer cells to grow once they have colonized lung parenchyma.

2.4 Coagulation-related factors analysis

As it was described in the Hypothesis and Objectives section, the main purpose of this thesis is to evaluate what is happening with the coagulation factors and their pathway to metastasis. It has been described that cancer represents a highly prothrombotic state, and one of the main important factors in the regulation of blood hemostasis is platelets. When they become activated, many events occur to activate the regulation of hemostasis. For that reason, we wanted to analyze what was happening with platelets when we co-culture with RCC cell line trying to mimic what is happening with CTC and its interactions with platelets.

2.4.1   F2R was not inducing platelet activation and aggregation

Considering all this data, and the interesting results that we obtained in the different *in vivo* experiments performed, we tried to elaborate a possible hypothesis that could explain this decrease in metastasis after inhibiting or decreasing F2R expression. We hypothesize that SN12C or cells from Ren 50M tumors, as they have higher expression of F2R, once they are in the bloodstream, can secrete one or several factors that induce platelet activation and aggregation. Thus, platelets secrete thrombin and other factors that cleavage Fibrinogen into fibrin, facilitating the formation of a shield between platelets and cancer cells that prevents Natural Killer clearance causing an increase in CTC survival and facilitating its colonization (Figure 76).
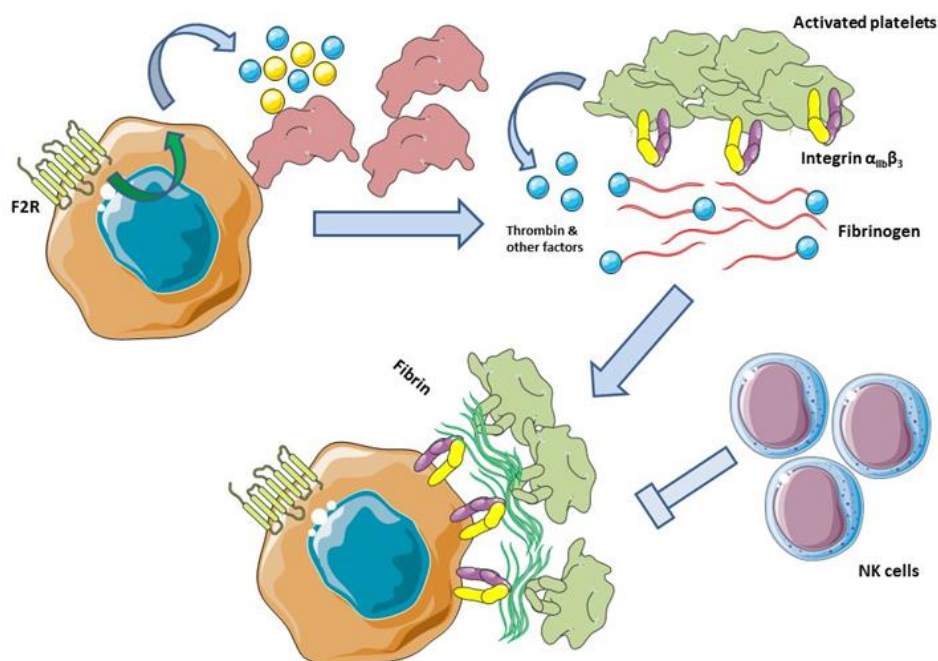
Figure 76. Hypothesis of the possible mechanism by which F2R is affecting CTC. CTC as they have higher expression of F2R, once they are in the bloodstream, they can secrete one or several factors that induce platelet activation and aggregation. Thus, platelets secrete thrombin and other factors that cleavage Fibrinogen into fibrin, facilitating the formation of a shield between platelets and cancer cells that prevents Natural Killer clearance.

To further develop this hypothesis, we performed an experimental approach between SN12C WT cells, SN12 shRNA cells, and platelets. All these experiments were performed in Multiplate Analyzer™ in collaboration with Dr. José Luis Ferreiro from Hospital Universitari de Bellvitge. We firstly analyzed if SN12C WT secreted media could induce platelet aggregation of human healthy platelets. Results confirmed that SN12C was not able to induce platelet aggregation (Figure 77A). Furthermore, we wanted to test in SN12C shF2R cells but also, no differences were observed despite decreasing F2R expression(Figure 77B). Besides, we tested the same experiments but incubated with SN12C WT cells to check if this platelet aggregation could be induced by the presence of cells. After testing with different numbers of cells, we concluded that no differences were observed (Figure 77B)
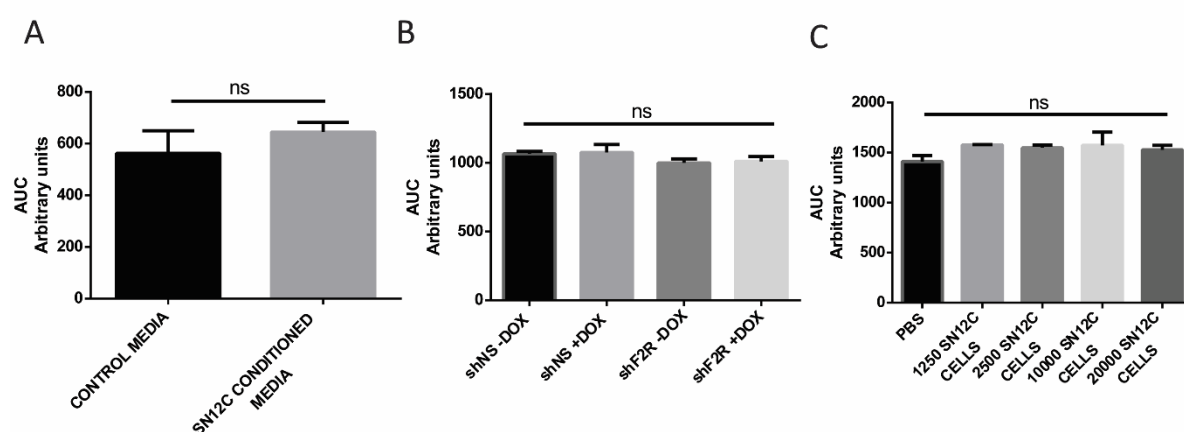
Figure 77. Platelet aggregation did not show alterations when we incubate with cells or supernatants. A) Platelet aggregation analysis of control media and SN12C supernatant media of SN12C cells. B) Platelet aggregation analysis of the different shNS and shF2R supernatants media after Doxyxycline administration. C) Platelet aggregation analysis of a different number of cells, 1250, 2500, 10000, and 20000. Results were represented showing Area Under the Curve parameters measured in arbitrary units of the Multiplate Analyzer™. Error bars represent S.D, Wells/condition n=minimum of 2. Mann Whitney test, p>0.05 ns

We can conclude with these results that the secreted factors of SN12C cells or the presence of that cells did not affect the platelet aggregation. For that reason, seemed that no effects of the blood hemostasis are happening due to the presence of CTC in contact with the blood.

Nevertheless, we wanted to evaluate different parameters related to blood clotting to see if blood hemostasis is affected due to the presence of Ren 50M tumors or SN12C tumors.

2.4.2   F2R higher expression was not affecting the formation of blood clots

As was described in Section 3 of the introduction, the coagulation pathway is composed of two paths: the intrinsic and the extrinsic pathway. There are different tests that measure alterations of each pathway. Concretely, Prothrombin time measures if there is any alteration of the coagulation factors of the intrinsic pathway. In contrast, Thromboplastin partial activated time measures alterations of the coagulation factors of the extrinsic pathway. We decided to measure both parameters in Ren 50M and SN12C tumors. Results showed that there were no differences in Prothrombin time (Figure 78A) nor thromboplastin partial activated time (Figure 78B).
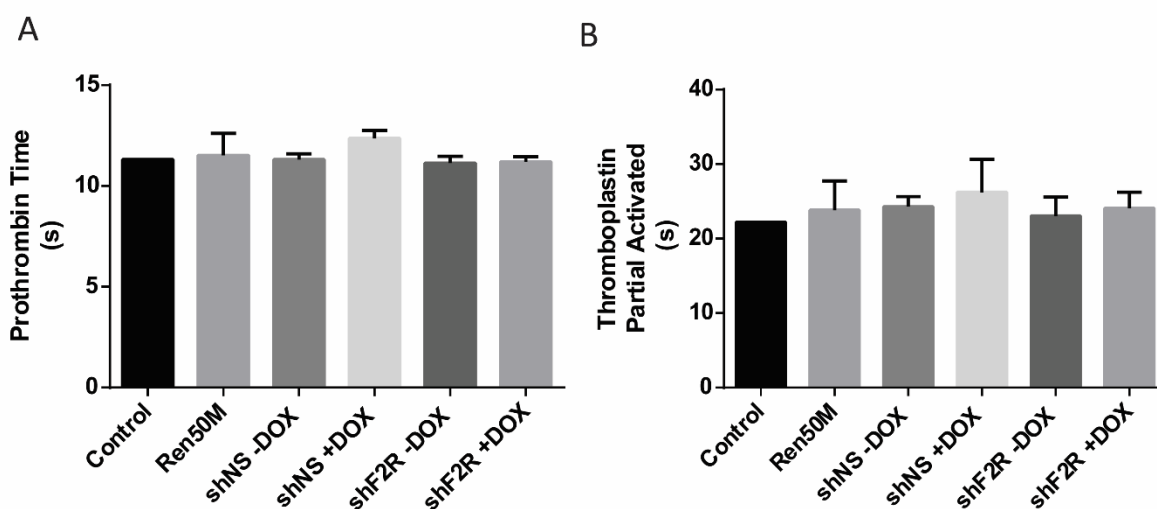
Figure 78. Blood coagulation alterations were not observed in Ren 50M and SN12C tumors. A) Prothrombin time analysis in Ren 50M tumors and different shNS and shF2R tumors compared with control mice. B) Thromboplastin Partial activated time in Ren 50M tumors and different shNS and shF2R tumors compared with control mice. These results were obtained in collaboration with Servei d'Hematologia Clinica Veterinaria from UAB. Error bars represent S.D, Wells/condition n=minimum of 3.

Considering all the coagulation-related analyses we concluded that no alterations in the blood coagulation were observed. However, trying to evaluate the hypothesis presented

in Figure 76, we wanted to analyze what is occurring with fibrin and fibrinogen due to its possible implication in metastasis.

It is known that fibrin and fibrinogen are the main players in the coagulation cascade. For that reason, we performed different experiments to detect the presence of these factors. As we had hypothesized that Fibrin/Fibrinogen could be playing an important role in favoring metastasis, we wanted to analyze its presence in the blood of PDOX models but also in the SN12C shF2R generated tumors.

2.4.3   Ren 50M and SN12C tumors presented higher levels of Fibrinogen

Fibrinogen levels analysis were obtained by analyzing plasma from a different group of mice that had Ren 50M tumors or SN12C shRNA tumors. This analysis was performed in Servei d'Hematologia Clinica Veterinaria from UAB. Results showed that Ren50M presented higher levels of fibrinogen compared with the atimic control group and other renal tumors. Besides, if we removed the tumor (nephrectomy, Ren 50M cure), levels of fibrinogen were recovered (Figure 79). Furthermore, analyzing SN12C shRNA tumors we obtained higher levels of fibrinogen.
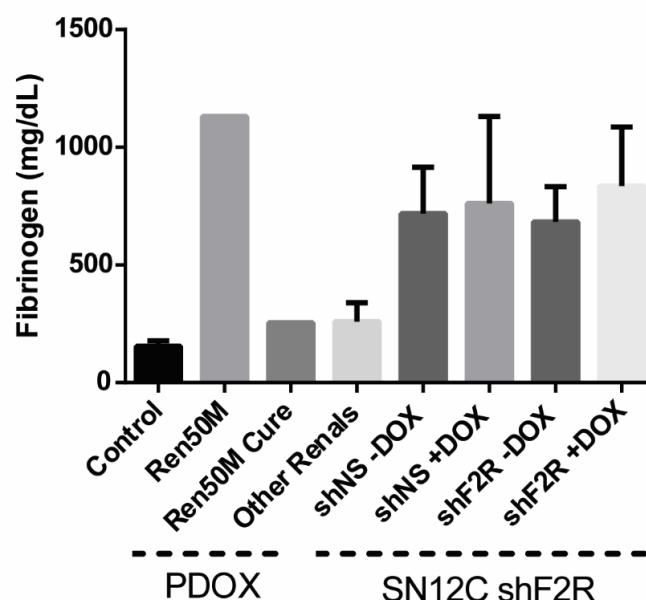
Figure 79. Fibrinogen levels in different PDOX models. Plasma from atimic mice (control), Ren 50M tumors, Ren 50M after tumor nephrectomy (Ren 50M cure), other PDOX renal models, and SN12C shRNA tumors were analyzed to check fibrinogen levels. Error bars represent S.D,

2.4.4   Fibrin expression was detected in Ren 50M metastatic lesions

Furthermore, to check the levels of fibrin in PDOX models, we performed Martius Scarlet Blue (MSB) staining technique that is used for fibrin visualization. Results showed that in normal tissue, Ren 50 presented higher levels of fibrin compared with Ren 50M (Figure 80A). However, more fibrin deposits in the tumor and metastasis (Figure 80B) from Ren 50M were found compared with Ren 50.
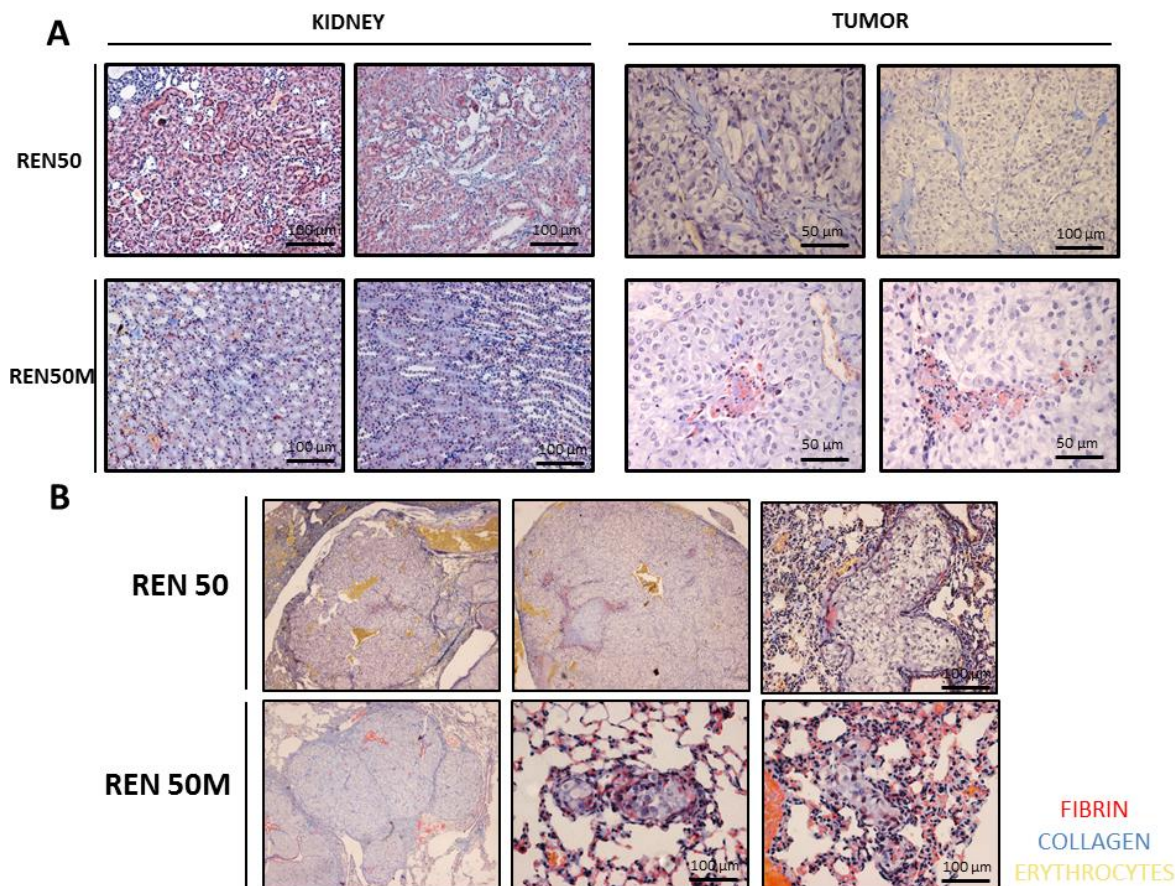
Figure 80. Fibrin detection in Ren50 and Ren50M tumors. MSB staining was performed to analyze fibrin (in red) levels in our PDOX renal models. Also, MSB stained collagen (blue) and erythrocytes (yellow). A) Representative images from normal Kidney (left) and tumors (right) in Ren 50 and Ren50M of MSB staining. B) Representative images from metastasis in lungs from MSB staining.

Altogether with these results, we can conclude that fibrinogen and fibrin could be contributing to cancer cells metastasize through different mechanisms, so further studies are needed to know more about their role in metastasis.

3. VALIDATION OF F2R AND ITS INTERACTORS IN PATIENTS

In collaboration with Carlota Rubio-Pérez, from Núria López-Bigas laboratory in the Institut de Recerca Biomèdica (IRB) and Roderic Espín from IDIBELL institute, we further studied the relationship between our main candidate F2R and its downstream interactors described and clinical data from The Cancer Genome Atlas (TCGA).

3.1 F2R is expressed in many cancer types being RCC the most overexpressed

We first wanted to analyze whether RNA expression of F2R could be associated with any RCC subtype. Analyzing data from TCGA, results showed that F2R presented higher expression in ccRCC (KIRC) compared to the other most common RCC histological subtypes, chromophobe (KICH) and papillary (KIRP) (Figure 81).
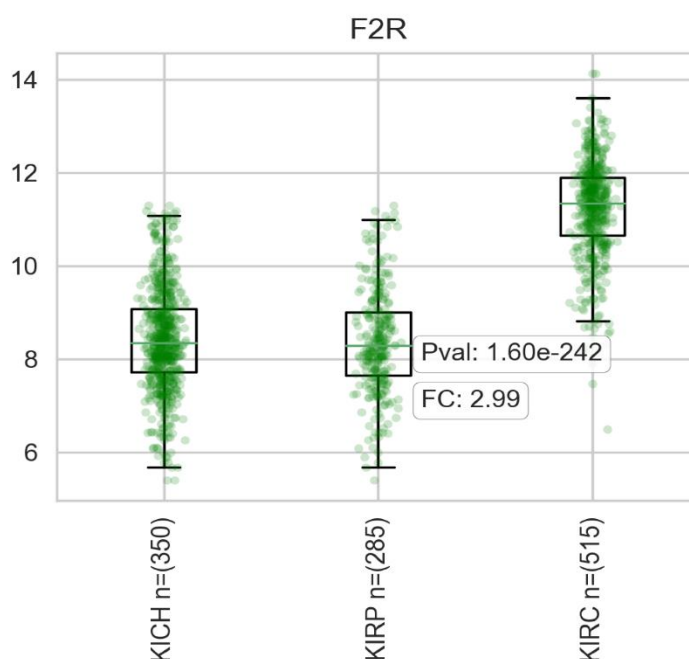
Figure 81. F2R expression is higher in ccRCC than in the other two main RCC subtypes. Boxplots represent the expression of F2R in different RCC subtypes: KICH, KIRP, and KIRC. Each green dot represents an individual patient. Expression values are expressed in log2 RSEM (a normalization measure of RNA seq counts) and statistically significant differences were found using the Mann-Whitney test when comparing KIRC expression to the other subtypes. P-value and FC are represented inside the plot.

Next, we decided to check whether the expression distribution of F2R is different across all 18 TCGA other cancer types, not only focusing on RCC. Results showed that patients with ccRCC (KIRC) are those who have the highest expression of F2R (Figure 82).
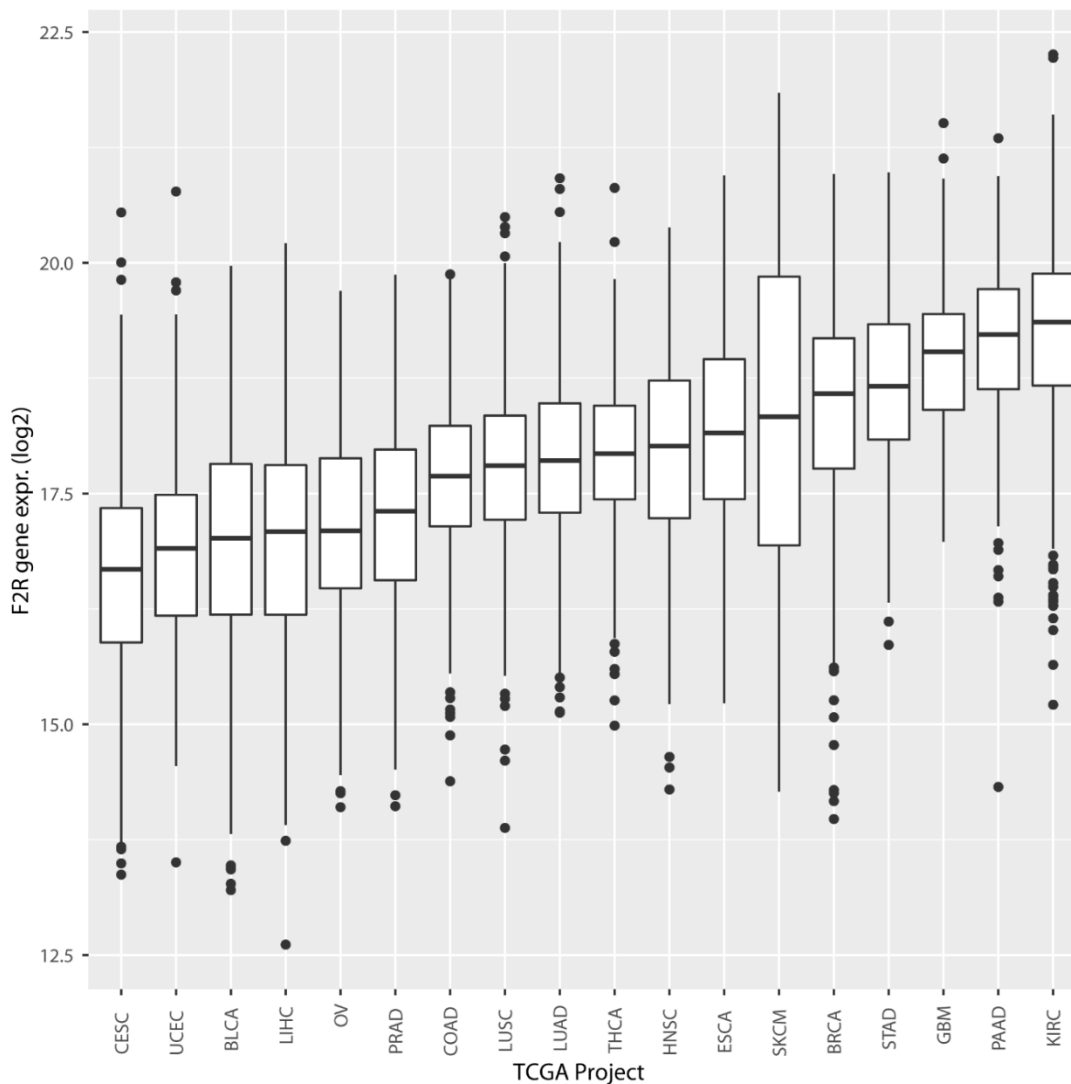
Figure 82. ccRCC is the highest cancer type with the highest expression of F2R. Boxplots represent the distribution of expression of F2R across 18 TCGA solid types of cancer. Expression values are expressed in log2 FPKM-UQ (RNA-Seq-based expression normalization method).

3.2 Different F2R interactors are overexpressed in RCC patients

Furthermore, it was analyzed the expression of the different F2R interactors previously described: Integrin α3 (Figure 83A), Integrin α5 (Figure 83B), Integrin β1 (Figure 83C), and Fibronectin (Figure 83D). In the case of Integrin α5, ccRCC was cancer with the

highest expression of these integrins. Besides, Integrin β1 was also clearly expressed in ccRCC being the 2nd tumor with the highest expression.
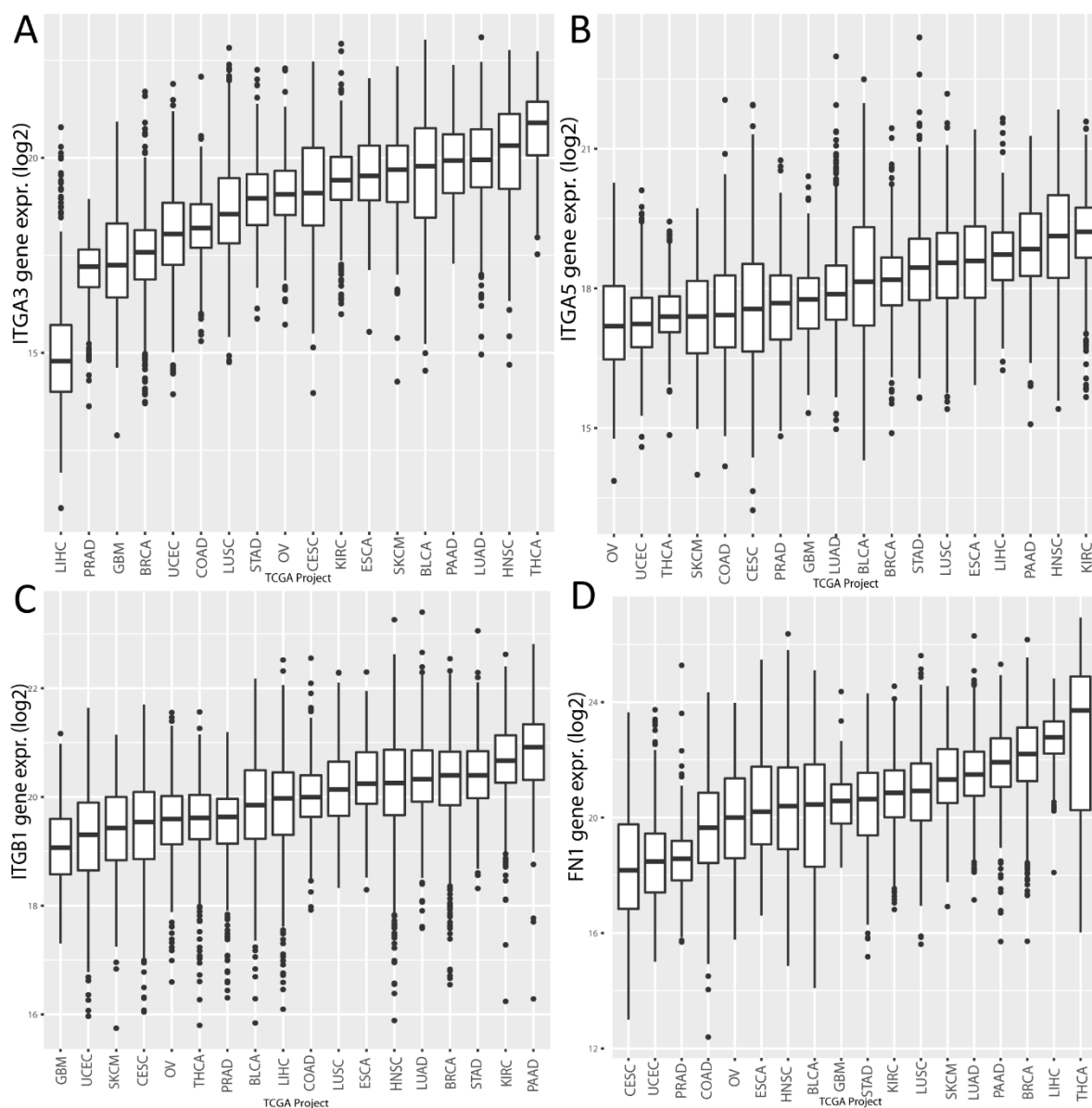
Figure 83. ccRCC is the highest cancer type with the highest expression of integrin α5 and integrin β1. Boxplots represent the distribution of expression of integrin α5 (B) and integrin β1 (C) across 18 TCGA solid types of cancer. It was also checked the expression of integrin α3 (A) and fibronectin (D). Expression values are expressed in log2 FPKM-UQ (RNA-Seq-based expression normalization method)

3.3   Overexpression of coagulation-related genes in patients tends to worse prognosis

Furthermore, we analyzed if the overexpression of F2R has an impact on the prognosis of ccRCC patients. To do so, we ranked the patients according to the expression of F2R

and we compared the prognosis of the percentage 85 patients to the rest. Results showed that the overexpression of F2R is not influencing on survival of ccRCC patients (Figure 84A).

Besides, we decided to further check this parameter when considering all genes obtained in GSEA analysis with a positive enrichment core directly involved in the coagulation pathway (TFPi, SERPINE 1, F2R, F13A1, and ITGB3). Results did not show statistically significant differences. Nevertheless, we could observe a tendency for worse survival in patients when tumors present an overexpression of coagulation-involved genes (Figure 84B).
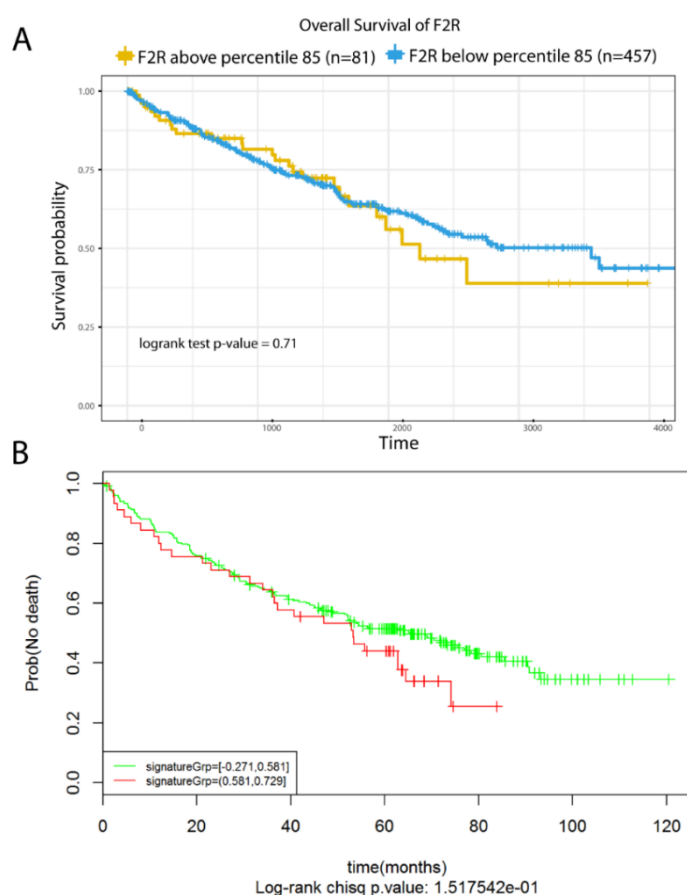
Figure 84. ccRCC patients with overexpression of F2R do not present worse survival rates. However, patients with overexpression of genes involved in the coagulation pathway tend to present worse survival. A) Kaplan-Meier plot of overall survival in 538 ccRCC patients (from TCGA). Patients were divided into two groups regarding their RNA expression levels. Blue line represents patients whose expression is below percentile 85. Orange line represents patients whose expression is above percentile 85. Data were analyzed by Log-rank test. B) Kaplan-Meier plot of overall survival in 498 ccRCC patients (from TCGA). Patients were divided into two groups regarding the gene set involved in coagulation (TFPi, SERPINE 1, F2R, F13A1, and ITGB3) RNA expression. Red line represents patients whose expression is above percentile 85. Green line represents patients whose expression is below percentile 85. Data were analyzed by Log-rank test.

3.4 F2R interactors are associated with a worse prognosis in RCC patients

Furthermore, seeking to obtain more insights on the consequences of overexpression of the different integrins analyzed during this thesis in the clinical setting, we wanted to investigate whether its overexpression has an impact on the prognosis of ccRCC patients. To do so, we ranked the patients according to the expression of integrin α3, integrin α5, and fibronectin and we compared the prognosis of the percentage 85 patients to the rest.

Results confirmed that ccRCC patients who have an overexpression of integrin α3 (Figure 85A), integrin α5 (Figure 85B), or fibronectin (Figure 85C) have a worse prognosis compared with those who have lower expression levels.
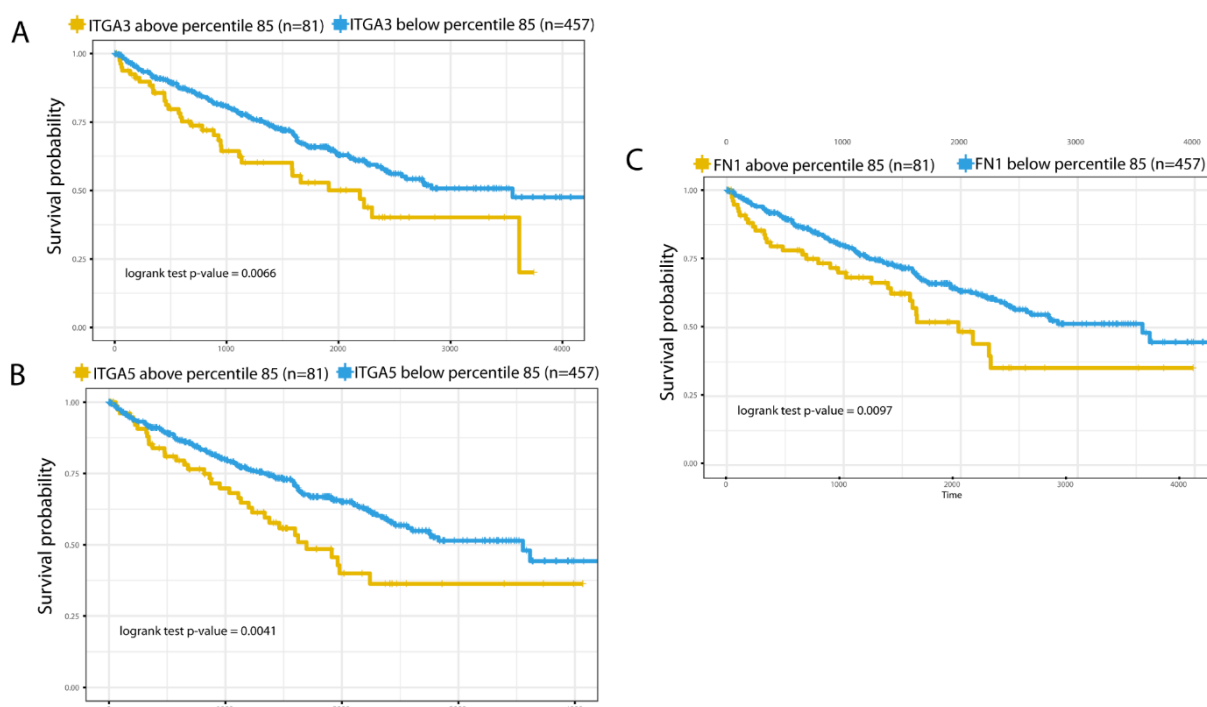
Figure 85. Integrin α3, Integrin α5, and Fibronectin are negative prognostic factors in patients with ccRCC. Kaplan-Meier plot of overall survival in 538 ccRCC patients (from TCGA). Patients were divided into two groups regarding their Integrin α3 (A), Integrin α5 (B), and Fibro RNA expression levels. Blue line represents patients whose expression is below percentile 85. Orange line represents patients whose expression is above percentile 85.

3.5   Correlation between F2R and its downstream effectors

It was also interesting to analyze the possible correlation between F2R with the different interactors in ccRCC patients. In the case of integrin α3 (Figure 86A) no correlation was observed, but in integrin α5 (Figure 86B), integrin β1 (Figure 86C), and fibronectin (Figure 86C) a strong correlation was observed.
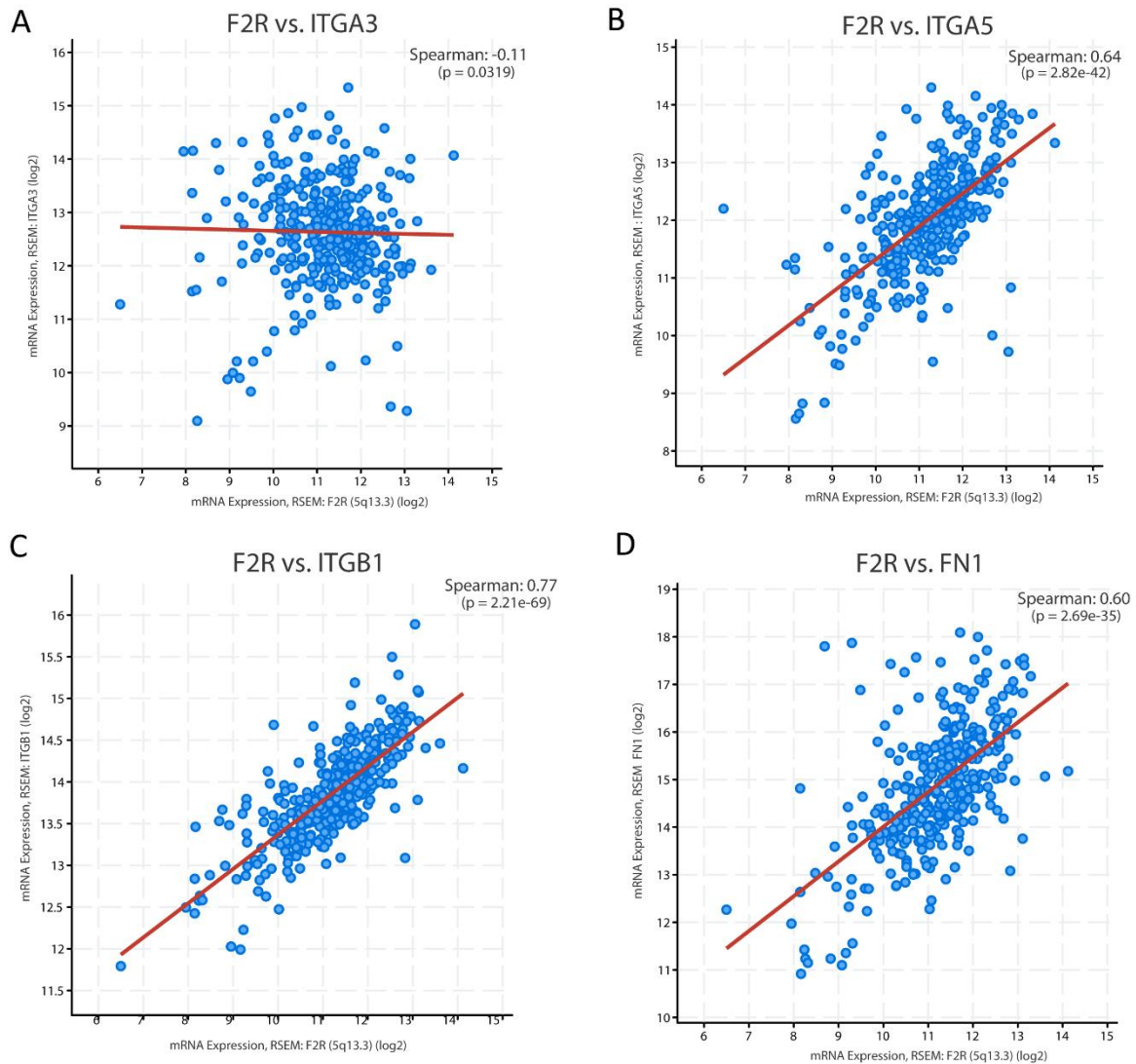
Figure 86. F2R expression positively correlates with integrin α5, integrin β1, and fibronectin in patients with ccRCC. Association studies between F2R and Integrin α3 (A), integrin α5 (B), integrin β1 (C), and fibronectin (D). Spearman's rank correlation coefficient is represented with the p-value.

Overall, these data from the clinics support that F2R and its interactors could be considered an interesting target for metastatic RCC, but also for other cancer types

DISCUSSION

1. METASTASIS IN REN 50 AND REN 50M

Metastasis is the hallmark of cancer that is responsible for the major part of cancer-related deaths worldwide. It accounts the 90% of cancer deaths in patients(Chaffer & Weinberg, 2011a). But nowadays, the mechanisms of the metastatic process remain poorly understood. For that reason, establishing the biological mechanisms of the metastatic process has become an attractive target for metastatic patients to improve patients overall survival (Fares et al., 2020). Approximately, one-third of patients with RCC present metastasis at the time of diagnosis, and the overall survival at five years of those patients is 8% (Gong et al., 2016). Considering this dramatic data, the principal objective of this thesis is to identify new biological mechanisms that could explain the metastatic process trying to detect new therapeutic target opportunities.

RCC has become one of the most cancer types that have higher intratumor heterogeneity and clonal evolution (Gerlinger et al., 2014; Saeed et al., 2019). This clonal heterogeneity helps cancer progression and malignization developing advantage traits to a group of cells conferring them the ability to generate metastasis. Moreover, this variability of different types of cancer cells could be associated with different drug responsiveness from one patient to another (Crusz et al., 2016).

Functional studies based on model systems that try to recapitulate genetic and phenotypic patterns of patients' profiles are useful for identifying new biomarkers and therapeutic targets. For that reason, patient-derived xenografts have become an effective model in the last years as they can reproduce the histology, the metastatacic capacity, and different treatment responses (Lum et al., 2012). The main problem of PDOX models is that researchers implant only a piece of the tumor, so we are "selecting" and discarting different clones present in the tumor (Alizadeh et al., 2015).

In our PDOX model of Ren 50 and Ren 50M occurs something similar. The Ren 50 patient had many clones in their RCC tumor, and when we implanted them into our orthotopic mouse, a selection of these clones was made. Through different passages of primary RCC growth on mice, we randomly selected different polyclonal cells with lower metastatic

capacity. However, in the orthotopic mouse a polyclonal group of cells having a higher expression of the coagulation factor genes scape and made the macrometastasis in the lung, which gave rise to the Ren 50M tumors.

During the exhaustive analysis of the two variants generated, we decided to stop the growth of both tumor lines for a while. Once we had analyzed both variants and confirmed the differences at the gene expression level, we were unable to re-grow the tumors when we descryopreserved this tumor. When we solved the cryopreservation problems and obtained tumor growth, we were unable to reproduce the levels of metastasis common to Ren 50M. Therefore, we decided to implant the tumors by disgregation and injecting the disgregated tumor cells directly into the kidney, instead of implanting pieces as we had previously done.

Having this new way of generating Ren 50M tumors, we managed to recapitulate the incidence of metastasis that we had at the origin of the project. It should be noted that this intrarenal injection facilitates greater dissemination of cells throughout the renal parenchyma and, therefore, a greater facility for generating metastasis. When analyzing the primary tumors generated in this way, the growth was not as homogeneous and localized as it was when the piece was implanted in the renal capsule.

By generating the primary tumors in this new way, we wanted to validate that we maintained the gene expression of our candidate. Indeed, there was no change in F2R expression or tumor histology. However, we could not reproduce the same metastasis inhibition results with vorapaxar that we obtained with SN12C tumors. It should also be noted that the number of mice in this experiment was low (n=5) and perhaps, we started treatment with the drug very late. As a reference to starting the vorapaxar treatment, we used the same times as the experiment of the SN12C tumors. However, as the growth was more disseminated and not so localized, the treatments were performed at a more advanced stage of cancer due to the problems of measuring the primary tumor by palpation. Further studies with vorapaxar in Ren 50M PDOX model are needed to confirm that F2R inhibition is affecting the metastatic capacity in these tumors.

2. ROLE OF F2R IN PRIMARY TUMORS

F2R has been described to regulate multiple processes such as survival, proliferation, cytokine/growth factor secretion, and motility (Wojtukiewicz et al., 2015a). This is why this receptor may be playing a fundamental role in the establishment of cancer having described in more than 30 reviews the possible interplay between F2R and tumorogenesis (Bar-Shavit, Maoz, Kancharla, Jaber, et al., 2016; Remiker & Palumbo, 2018; Ruf & Mueller, 2006; Sharma et al., 2019; Wojtukiewicz et al., 2015b)

The vast majority of authors suggest that F2R promotes tumor growth. However, others have argued that overexpression of the receptor limits tumor progression in different contexts (Adams et al., 2018; Queiroz et al., 2014). In our case, focusing specifically on RCC, with the results shown we conclude that F2R is favoring tumor malignancy, contributing to the metastatic process.

Previous results from the in vivo experiment from the tumor model generated from the SN12C cell line and the treatment with vorapaxar showed that pharmacological inhibition with this drug reduces metastasis in mice. One of the mechanisms that may explain the reduction of metastasis could be associated with the effect on primary tumor growth. However, we demonstrate that after vorapaxar treatment we did not see any effect on the tumor growth. It has been described that in Ovarian cancer, the inhibition with vorapaxar reduces cell proliferation, but no evidence in vivo experiments have been demonstrated (Chanakira et al., 2017).

Few studies have been conducted with vorapaxar to analyze its effects on cancer. However, other types of inhibitors have been used to inhibit F2R. In vitro, it has been validated that inhibition of F2R by an allosteric antagonist correlates with decreased cell growth in a model of cervical adenocarcinoma (Burns & Thevenin, 2015). The use of pepducins has been proposed to inhibit F2R due to their antagonistic power. In a breast cancer model, it has been described that after inhibition of F2R with pepducins, there is also no effect on the growth of the primary tumor, with a clear reduction in metastasis (E. Yang et al., 2009), as we have demonstrated with vorapaxar. These results, therefore,

suggest that we can link the decrease in metastasis to other mechanisms independent of tumor proliferation and growth.

As shown in results, we have validated an effect on the invasiveness of tumors when F2R has been inhibited. Although we are working in a mouse model when using vorapaxar, we know that the effects we are going to obtain are associated due to the inhibition of F2R mainly presented in tumor cells(C. Zhang et al., 2012). As it has been described the important role of platelets in metastasis, we confirmed that murine platelet F2R is not being affected by the inhibition of vorapaxar, as murine platelets lack this receptor and are activated by other receptors of the PAR family. (S. R. Coughlin, 2000; Heuberger & Schuepbach, 2019a).

To validate more specifically which is the mechanism by which vorapaxar is inhibiting this invasiveness, we wanted to validate it through in vitro studies. These studies showed that there was no effect on the migratory capacity of cells, but neither was it affecting the inhibition of the AKT signaling pathway. Considering these results and coupled with the limited in vitro data found in the literature, we were unable to establish the mechanism by which vorapaxar was affecting the invasiveness capacity of the SN12C in vivo tumors.

One of the possible explanations for the ineffectiveness of vorapaxar in vitro could be associated that it is a pro-drug that must be metabolized in the liver. However, studies have shown that vorapaxar is already able to inhibit F2R with high potency without needing to be metabolized or activated in the liver (Fala, 2015; Hawes et al., 2015). Further studies are needed to try to demonstrate why vorapaxar has no effect in vitro.

Despite this, vorapaxar is a new PAR1 antagonist recently approved in the US for the reduction of thrombotic cardiovascular events in patients with a history of myocardial infarction or peripheral arterial disease (brand name Zontivity)(Fala, 2015). Several clinical trials are ongoing with this drug, but none are focused on cancer and metastasis. (Flaumenhaft & de Ceunynck, 2017). Therefore, after validation of metastasis reduction in

other cancer models, this drug could be proposed for use in the clinic as a preventive treatment in patients with elevated F2R levels.

One of the negative aspects to use drug inhibitors is the possibility of affecting unknown off-targets that can be affecting our cell viability or unmasking real effects. This is what happened with the SCH 79797 inhibitor. This, despite showing very interesting results in terms of migration and invasion of cells and spheroids in vitro, as demonstrated in a melanoma model (Silini et al., 2010), had some drug-associated toxicity leading to cell death, as other groups have described. (di Serio et al., 2007).

For that reason, and after the surprising results of metastasis reduction with vorapaxar, we decided to perform genetic inhibition of F2R. As with vorapaxar, the growth of the primary tumor in the kidney was not affected after the decrease in F2R expression. However, in a glioma model, a decrease in primary tumor growth has been described in those tumors in which F2R was downregulated (Gao et al., 2020). Considering that, it seems that depending on the origin of the primary tumor, tumor growth may or may not be affected.

In addition, and corroborating with the data obtained in the vorapaxar in vivo experiment, the decrease of F2R expression in tumors also led to a clear decrease in the invasive capacity of tumors, which was also confirmed by migration and invasion studies performed in vitro and as other groups have shown (Cisowski et al., 2011; Gao et al., 2020; Silini et al., 2010). However, despite not having statistically significant differences in terms of lung metastatic area density reduction, a clear downward trend is seen after decreasing F2R expression. These differences could be bigger since, as we showed in vitro, the reduction in F2R expression is around 60%, but the remaining 40% may be masking a bigger reduction of metastasis.

One of the positive aspects of performing this reduction at the genetic level gives us specificity, as we are only acting at the level of F2R in the tumor cell. However, if we compare the study of inhibition with vorapaxar and that of the genetic reduction of F2R, despite tendencies going in the same direction, the effects of pharmacological inhibition

are greater. This can be explained by the remaining F2R expression, but also by the fact that with pharmacological inhibition we could be inhibiting F2R in other cells of the tumor stroma and not only in the tumor cell. This opens a new opportunity to study the involvement of F2R in tumor stromal cells and how it is affecting malignancy.

Considering the clear implication that F2R may have in tumor malignancy described in different studies in different tumor types, little has been described specifically about the relationship between F2R and tumor malignancy in RCC. That is why all the therapeutic approaches we have made through pharmacological inhibitions and decrease in gene expression of F2R open up a new horizon to what is the role of this receptor in a tumor that has not been described deeply.

Moving to the molecular mechanism of how F2R is contributing to metastasis, it is interesting to know more about the receptor and its mechanisms of activation. As it has been previously described, F2R is a seven-transmembrane G-protein–coupled receptor that belongs to a family of receptors whose defining feature is irreversible proteolytic activation. G proteins are composed of three subunits, Gα, Gβ, and Gγ which are located in the inner part of the plasma membrane. Upon ligand binding, the signal is transmitted through conformational changes, which consequently result in the activation of a specific signaling pathway (Bar-Shavit, Maoz, Kancharla, Nag, et al., 2016). Following proteolytic cleavage or induction of agonist peptides, a tethered ligand that interacts with a shallow binding site varies depending on the activator, so the engaged signaling pathways vary between tissues and cell lines. So, depending on the tethered ligand we have the activation of a specific signaling pathway will occur (Heuberger & Schuepbach, 2019b; Vu et al., 1991).

We have confirmed that in our model that the PI3K/AKT signalling pathway is inactivated when the downregulation of F2R expression takes place, consistent with other authors have shown in a breast cancer model (Kancharla et al., 2015; Zecchin et al., 2020). In addition, pharmacological inhibition by pepducins also showed a clear effect on the inactivation of this signalling pathway (E. Yang et al., 2009)

Another factor that leads us to suspect that this signaling pathway is playing an important role in the most aggressive tumors was obtained through exhaustive RNA-seq analysis where we compared expression levels of non-aggressive tumors (Ren 50) versus aggressive tumors (Ren 50M). In Ren 50M, one of the genes that is overexpressed more than 600-fold compared to Ren 50 tumors is G Protein Subunit Gamma 4. The gamma subunit of GPCRs has been described as one of the activators of the PI3K/AKT pathway (Steinhoff et al., 2005). Even though GPCRs emerge as oncogenes that regulate cancer-associated signaling networks, their role in tumor biology is not clearly understood. Furthermore, large-scale genome studies of multiple human tumors have uncovered overexpression of GPCRs in cancer (Feigin, 2013).

As we are working with the Thrombin receptor, it has been described that could be activated by different ligands. In our case, F2R is activated by different proteases, being Thrombin its main activator. Other potential activators described are Tissue Factor, Trypsin, and MMPs. (Heuberger & Schuepbach, 2019b; X. Liu et al., 2017). In our case, we have validated that thrombin is activating PI3K/AKT signaling pathways in our SN12C model, as described in breast cancer (E. Yang et al., 2009) In addition, we have validated how there is an increase in the invasive capacity of tumor cells in vitro, as published by other authors in other models of breast cancer and melanoma. (Boire et al., 2005; Shi et al., 2004c).

In addition, we have used and developed the activating peptide TFLLRN-NH2. This peptide contains the amino acids required for F2R activation following proteolytic activation by thrombin. This peptide is a specific F2R agonist that selectively activates F2R without activating other receptors of the F2R family (Hollenberg et al., 1997). As we have validated with thrombin, the activating peptide also activates the PI3K/AKT pathway as well as the invasive and migratory capacity of SN12C.

It was also validated that the activation by the TFLLRN peptide affected the migration of other RCC cell lines such as RCC4 that expressed similar levels of F2R like SN12C. Furthermore, we also validate this increase of the migration capacity in a very aggressive mouse renal adenocarcinoma cell line -called Renca- that expressed lower levels of F2R.

Despite that, a slight tendency of increasing cell migration was found. We could conclude that also in a mouse cell model, the activation of F2R is also having similar results of increasing cell migration.

Other activating peptides, such as SFLLRN, can induce activation of the PI3K/AKT pathway, but it has been discovered that this peptide could be affecting the activation of other receptors of F2R family (Hollenberg et al., 1997; E. Yang et al., 2009). In the last years, it has been described the PAR-PAR interactions in different cell types- Concretely, cooperative signaling between F2R (PAR1) and PAR2 was observed in carcinoma cells, suggesting a possible dimerization in carcinogenesis (Lin & Trejo, 2013; McEachron et al., 2010; Shi et al., 2004a). In addition, Shi et al describe that thrombin stimulates the motility of metastatic tumor cells by a mechanism that requires not only the activation of PAR1 but also the simultaneous activation of PAR2 (Shi et al., 2004a). Considering that, further studies of PAR family interactions and cooperations are needed to validate our models, as we also found that F2RL2 -also called PAR3- is also overexpressed in Ren 50M tumors.

One of the other important aspects to assess is what is happening upstream to F2R in tumors in vivo. As it is a receptor that is activated by multiple proteases, it would be interesting to determine if in both SN12C tumors and Ren50M tumors there are any factors that are potentially secreted by cancer cells acting at the tumor cell level to activate its malignancy. For that reason, it would be interesting to analyze the secretome of SN12C cells in vitro and analyze whether they can secrete proteases that can activate the F2R present in them. Furthermore, in our in vivo kidney tumor tissues we could analyze histologically the presence or absence of activators, as well as analyze whether the secretion is present in the blood.

Considering this last premise, we hypothesize that this mechanism could be important at the later stages of the metastatic cascade: colonization and growth in the metastatic organ. If tumors with high levels of F2R can secrete factors that activate their F2R, a higher activating survival pathway PI3K/AKT will be happening. Therefore, it will be an advantage for these cells to survive in a hostile environment such as the lung thanks to AKT activation.

Regarding the studies performed with integrins and their possible implication on the process of cellular migration and invasion, it has been described as a trait essential for metastasis. Enhanced migration is key across the metastatic cascade and is involved in the initial scattering of cells and migration from the primary tumor (W. G. Jiang et al., 2015). This process is helped by the presence of integrins, essential for the attachment of cancer cells to the different components of the ECM. Several integrins have been linked to metastatic likelihood and cancer. Here we described 3 integrins that could be implicated in the acquisition of malignancy of cancer cells: integrin α3, integrin α5, and integrin β1.

According to the data obtained from de RNA-seq, the most overexpressed integrin in our metastatic PDOX model Ren 50M was integrin α3. Besides, in SN12C tumors this expression is higher than Ren 50M. It has been described that integrin α3 is dimerizing with integrin β1. This pair of integrin is considered a promiscuous receptor, which appears to recognize a variety of ECM proteins including, laminin-1, laminin-5, collagen, and fibronectin among others. Expression of α3β1 integrin varies during tumor progression. For example, primary melanomas express low levels of α3β1, whereas metastatic melanomas express high levels of this integrin (Natali et al., 1993). Besides, it also has been described that Gliomas and glioblastomas are considered aggressive tumors, they are characterized by an overexpression of α3β1 playing a major role in both cell-matrix interactions and invasion (Fukushima et al., 1998).

The presence of this integrin not only has been related to the acquisition of malignancy. It has been described to promote prosurvival and proliferative signals required for the malignant growth of basal mammary epithelial cells, helping with the cancer initiation and progression (Cagnet et al., 2013). Considering that, we can conclude that this integrin is not also contributing to the scape of cancer cells from the primary tumor, it could be also necessary to be present in the moment of colonization and growth in the new metastatic organ. For that reason, targeting both pairs of integrins could be an interesting approach to blocking cancer progression, as other groups demonstrate (Melchiori et al., 1995; White et al., 2004).

In our case, very little is described in the literature about integrin α3β1 and RCC, and despite the fact of having described this higher expression in our models, more studies on inhibiting these integrins in vitro and in vivo are needed to further confirm the implication of this integrin in tumor malignization.

In the case of α5 integrin, there are more studies in the literature relating to its possible involvement in malignancy and metastasis. In colon carcinoma and basal-like breast cancer increased integrin α5 is associated with tumor progression and metastasis (Gong et al., 1997; McFarlane et al., 2015). Besides, Murillo et al. showed that colon cancer cells had a reduced cell attachment and an increase in apoptosis after inhibiting integrin α5(Murillo et al., 2004).

Surprisingly, in RCC there also seems to be a clear involvement of integrin α5 in tumor malignancy. Hase et al. have shown that the LOX-like protein (LOXL2) promotes tumor progression by regulating integrin α5 levels in ccRCC. Furthermore, it has been described the implication of integrin α5 in bone metastasis from RCC patients (Haber et al., 2015) Besides, in a recently published paper, Breuksch et al described that integrin α5 triggers the metastatic potential in RCC. They demonstrated that patients with RCC expressed a significantly higher level of integrin α5 in tumors than in normal tissue. But also this integrin expression correlated with tumor grade, the development of distant metastases, and the reduction of survival. Finally, they demonstrate that the use of blocking integrin α5 antibody is useful to decrease the migration and the adhesion of RCC cancer cells (Breuksch et al., 2017).

Moving to our results, we showed that integrin α5 was overexpressed in Ren 50M and not in Ren 50, but in SN12C tumors there was no higher expression. Despite this fact, the higher expression of this integrin was located in the invasion front of these tumors. For that reason, we conclude that despite having lower levels, it's the one that is pushing the tumor to invade normal tissue contributing to the malignization of SN12C tumors.

To further confirm the implication of this integrin in metastasis, further in vitro experiments with the blocking antibody of integrin α5 will need. Furthermore, it will be

interesting to test this treatment in our in vivo Ren 50M and SN12C tumors to see the possible effects on metastasis. Nowadays, in the clinic exists a specific blocking antibody integrin α5 called Volociximab that is under a clinical trial and showed promising results in cancer treatment in rabbits with Vx2 tumors (Bhaskar et al., 2007, 2008). Besides, more inhibitors of this integrin are appearing, for example, ATN-161, which showed a reduction in tumor progression in breast and colon cancer (Khalili et al., 2006; Stoeltzing et al., 2003). Furthermore, it was demonstrated in phase I of the study a stabilization of the disease in one-third of all patients with solid tumors treated with ATN-161 (Cianfrocca et al., 2006).

Two common things share the alpha subunits integrins analyzed: the beta integrin which is dimerizing, but also the ligand to which they are binding (Fibronectin).

On the one hand, the studies of integrin β1 revealed that there were higher levels in Ren 50M than in Ren 50, but changes were not as higher as with the other integrins despite having statistical differences. As it is an integrin that is binding through many different alpha subunits, this could be the reason for not having higher differences. Even though it has been described its implication in many cancers such as gastric, breast, and lung cancer (C. Hu et al., 2017; X. Li et al., 2013; Williams & Coppolino, 2014).

On the other hand, we have the ligand of both integrins: the Fibronectin. Integrin α3β1 can bind to many other ECM components, but integrin α5β1 only binds to fibrinogen. Fibrinogen has long been proposed to play an important role in the pathobiology of cancer. However, the role of FN in tumorigenesis and malignization has been highly controversial (Taylor et al., 1998; Topalovski & Brekken, 2016). Concretely, in RCC as it happens in colorectal cancer, higher levels of plasma, serum, or urine fibrinogen expression could be detected in later stages and metastatic renal cell carcinoma or colorectal cancer patients and may clinically serve as excellent non-invasive prognostic biomarkers(Hegele et al., 2004; Saito et al., 2008). In our Ren 50M tumors, we can observed higher expression compared with Ren 50 and could be useful as a prognostic biomarker analyzed in tumors, but we could check the presence of fibrinogen in plasma from Ren 50M tumors.

Considering all the data regarding the overexpression of F2R and the different integrins in the high aggressiveness in vivo tumors, we wondered to know a possible interplay between all these factors. For that reason, we started analyzing the way of activation of integrins. The integrin family of cell adhesion receptors mediates bi-directional signaling: 'inside-out' signaling activates the ligand-binding function of integrins and 'outside-in' signaling mediates cellular responses induced by ligand binding to integrins leading to cell spreading, retraction, migration, and proliferation (Shen et al., 2012).

Taking into account these two ways of integrins activation, we hypothesize possible crosstalk between F2R and integrins α3β1 and α5β1 could be happening in our in vivo Ren 50M and SN12C tumors. The activation of F2R leads to the activation of (PI3K)/AKT signaling pathways. This pathway has been described that can activate integrins to adopt a high-affinity conformation via the protein adaptors kindlin and talin. These protein adaptors and many others that bind to the cytoplasmatic tails of integrins, it is formed a complex called adhesome. All this complex is connected to the actomyosin cytoskeleton driving an adhesion strengthening and the migration of cells (Robertson et al., 2015; Spoerri et al., 2020; Sun et al., 2019).

All this hypothesis is supported by the in vitro experiments performed inhibiting at different levels of the (PI3K)/AKT signaling pathway. Gallein inhibitor (a Gβγ inhibitor) and Perifosine (an AKT inhibitor) showed the same inhibitory potential for cell migration. So, by affecting this pathway, we could be affecting the invasive capacity of cancer cells in tumors, but it depends on the tumor type because in some cases AKT inhibition pathway could promote breast cancer metastasis(W. Li et al., 2018). However, many AKT inhibitors are under different phases of clinical trials. Furthermore, and in the case of Gallein, it has been described that inhibits the metastatic spread of tumor cells in prostate cancer (Sanz et al., 2017). Considering all this information, further studies are needed to validate the hypothesis of the possible crosstalk between F2R and integrins.

However, we could not validate in Ren 50M tumors an increase of the activation of AKT as we were expected to have. In addition, AKT is considered an important HUB that is

implicated in many different processes in tumors (R. Liu et al., 2020), so for that reason, we could not have higher differences.

Another important signal that was a key point to analyze the possible implication of integrins in the aggressiveness of tumors was the upregulation of the Focal Adhesion Kinase (FAK) pathway that we found in Ren 50M tumors. Most integrins bind their ligands via the arginine-glycine-aspartic acid (RDG) sequence and consequently recruit different signaling kinases like the focal adhesion kinase (FAK) (Abbi & Guan, 2002).

3. ROLE OF F2R IN LATER STEPS OF THE METASTATIC CASCADE

One of the reasons why there are not many treatments to block metastasis is the lack of models that recapitulate the complicated process of metastasis. Thus, to mimic the metastatic process, current models consist of systemic injection of cancer cells. However, these models have been criticized because these models do not recapitulate the different stages of the metastatic cascade as they avoid the first steps such as the growth of the primary tumor, and the invasion and intravasation of the tumor cells (Hart2 & Fidler, 1980). However, the fact that we can dissect the metastatic cascade in different steps gives us the benefit of being able to know specifically in which part of the process our receptor is involved.

As it has been previously described in the introduction, it is known that metastasis is an extremely inefficient process because few cells scaping from the primary tumor successfully can form secondary tumors. It has been described that early steps in the metastatic cascade are completed very efficiently. By contrast, later steps in the process are inefficient (Chambers et al., 2002). Considering that we decided to perform the in vivo experiments avoiding the first steps of the metastatic cascade, we decided to inoculate cells directly into the bloodstream.

On the one hand, the first in vivo was performed decreasing the expression of F2R just the day after inoculating cells through the tail vein. If we consider that the decrease of F2R after doxycycline administration occurs 48 hours after the doxycycline induction, cells are inside the bloodstream with F2R for 72 hours, and after that, cells start to

decrease F2R expression. Authors described that with this model of generating metastasis cells are directly became trapped in the capillaries of the lungs shortly after injection due to size restrictions imposed by mouse capillaries (Rashid et al., 2013; S. Yang et al., 2009). Considering this information, with this in vivo experiment we were affecting the step of extravasation and colonization into the lung and the implication of F2R in that process.

Results from this experiment showed that there was an unexpected increase in metastasis in those mice who were administered doxycycline. Very little is known about the implication of doxycycline inducing metastasis. *Nanda et al* found a similar effect in the combination with an inductor of colon cancer, not in the group of doxycycline alone (Nanda et al., 2016). But the vast majority of studies published tend to produce the contrary effect: decreasing tumor burden of metastasis (Addison et al., 2016; Duivenvoorden et al., 2002).

Considering this increase in the doxycycline, we decided to compare the groups of doxycycline administration. So, we selected the group of shNS +DOX as the group that had higher levels of F2R, and the group shF2R +DOX as the group that had lower levels of F2R, trying to compare if there was any effect on the capacity of extravasation and colonization. We concluded that F2R is needed for SN12C to extravasate and colonize as we saw that in the group with higher F2R more lesions were formed compared with the group with less F2R expression.

Similar results were obtained when we performed the same experiment but instead of using a genetic decreasing of the receptor, it was used pharmacological inhibition with vorapaxar.

To validate that F2R could be implicated in CTC extravasation and colonization, we decided to perform the experiment of inoculating SN12C shRNA cells but previously treated with doxycycline to validate that F2R is implicated in that process. Then, we sacrificed mice 5 days after cell inoculation to see if there were differences in the formation of metastasis in the first days of metastasis formation. Results confirmed that

doxycycline is also affecting the initial steps of metastatic colonization. However, clear differences were observed if we compare those cells with decreased levels of F2R.

Considering all these in vivo experiments, we confirmed that F2R is playing an interesting role at later steps of the metastatic cascade, concretely in the extravasation and colonization step.

In addition and taking into account that the proliferation was not affected in the early stages of metastasis formation (as we also demonstrated) we had a clear decrease in the total metastasis area in knocked down F2R tumors. For that reason, we also hypothesize and demonstrate in vitro and in vivo that the decrease of F2R provokes a decrease in the activation of the survival-associated pathway PI3K-AKT. Thus, could be associated with the higher capacity of those SN12C cells with higher F2R that can survive in hostile tissue and growth to form metastatic lesions. This hypothesis is supported by many authors that described a PI3K/AKT inhibitors as a valid therapeutic target in the treatment of metastatic tumors (Hinz & Jücker, 2021; B. Li et al., 2017).
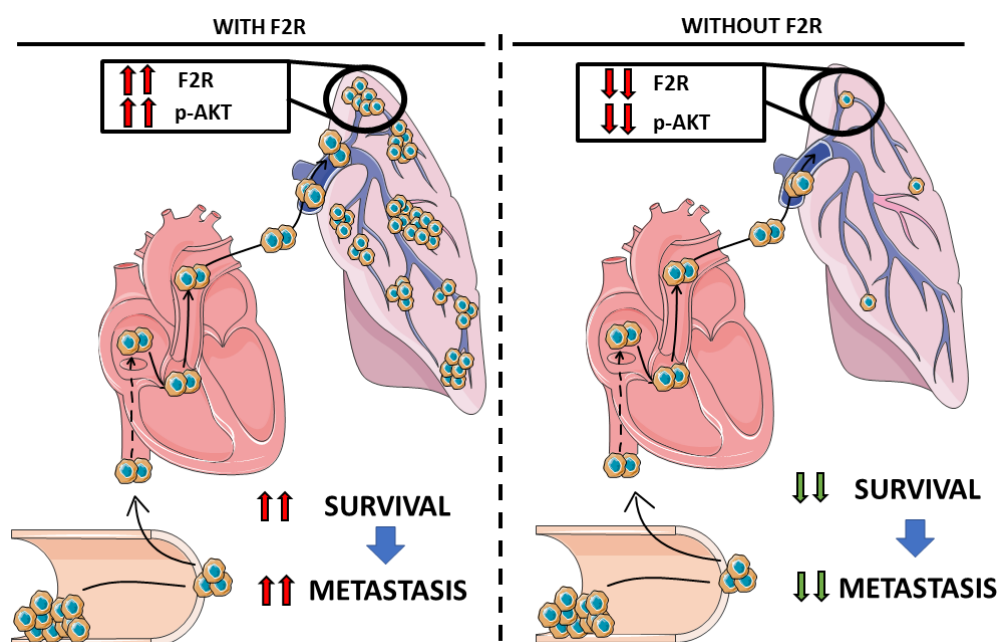
Figure 87. Schematic representation of the effects of F2R in micrometastasis formation. The presence of F2R is conferring pro-survival signals through AKT signaling pathway to DTC for growing in lung parenchyma.

Furthermore, to extravasate and colonize, CTC needs to activate the mechanisms of cell motility and invasion to colonize the new metastatic lung parenchyma. For that reason,

it has been hypothesized that integrins could also be playing an important role in this step of the metastatic cascade in addition to the implication of integrin in the primary tumor invasion.

Concretely, it has been described that tumor cell integrin α3β1 is important to bind to the deposits of laminin that are present in the pulmonary vasculature, helping CTC to arrest and colonize lungs (Wang et al., 2004). In addition, the blood clotting cascade is selectively involved in lung metastasis and associated with integrin activation. It has been described that those aggregates of platelets, fibrin, and carcinoma cells support local recruitment of plasma fibronectin, and Fibrin–fibronectin complexes induce αvβ3 integrin activation, triggering invasive protrusions and pro-invasive EMT signaling in the cancer cells (Knowles et al., 2013; Malik et al., 2010)

In our studies checking the presence of coagulation-related factors in our aggressive models, we saw the presence of fibrin in Ren 50M metastasis. Furthermore, fibrinogen levels in plasma in Ren 50M tumors were higher than in control mice. Besides, after nephrectomy, it was complete recovery of fibrinogen levels displaying a possible important role of fibrinogen in tumor aggressiveness, as other group described (Sahni et al., 2008; Simpson-Haidaris & Rybarczyk, 2001). We can conclude that having higher levels of these coagulation factors could be helping for CTC to extravasate and colonize metastatic organs (Knowles et al., 2013; Malik et al., 2010). So, we can describe these factors as prognostic factors of tumor aggressiveness.

It was also fascinating to know that SN12C tumors also overexpressed fibrinogen in plasma. SN12C tumors are independent tumors from Ren 50M. The only feature they share is the presence of higher levels of F2R. Furthermore, we also concluded that the overexpression of fibrinogen is not only related to the presence of F2R, as we saw no differences in fibrinogen in different SN12C shRNA-generated tumors.

On the other hand, we performed the experiment in which the F2R gene knockdown was performed one month after injection. This experiment was performed to assess whether

F2R is involved in the growth of the lesions once the metastatic lesions had formed and stabilized. The results show that there is no change in the number of lesions, as the lesions have been growing for one month with no change in F2R levels, unlike the experiment where the receptor expression was eliminated as soon as the cells were injected. However, we did observe that the size of the lesions was smaller in those animals with the decreased receptor. Having smaller lesions explained the decrease in the total metastatic area density. With that, an interesting paradigm is opened, because depending on the stage of the metastatic growth, we influence the growth of metastatic lesions or not after decreasing F2R.

From all the in vivo experiments we can conclude the possible involvement of F2R in the steps of extravasation and colonization, as well as once the lesions have been stabilized, F2R is one of the factors necessary for the subsequent growth of these lesions.

It is also interesting to note that in the experiment in which we have primary tumor growth, we are taking into account all the steps of the metastatic cascade. In that, the processes of extravasation and formation of new lesions -which we were forced with the tail-injected experiments- we also have. Therefore, with both experiments - the genetic knockdown of F2R and the pharmacological inhibition with vorapaxar - we are affecting the process of extravasation and colonization, but we could also are affecting the ability of these cells to survive in the blood. Considering that, many authors have described the important role that platelets and other factors present in the blood can play in protecting CTCs from being eliminated by the immune system (Gay & Felding-Habermann, 2011; Strilic & Offermanns, 2017).

Although it is a well-described mechanism, with the experiments of mixing the SN12C supernatant or directly contacting the platelets with the cells, no difference was observed in the ability of the tumor cells to induce platelet activation and/or aggregation. So, we cannot associate that the decrease in metastasis is due to a decrease in cell survival of CTC that escape from the primary tumor.

4. CLINICAL RELEVANCE OF F2R AND RELATED FACTORS IN THE CLINICS

The risk that we took when we started this project was the lack of reproducibility as we work with a biopsy from a patient. For that reason, putting our results in context with other patients should be necessary.

Results obtained from the analysis of patients revealed that RCC is one of the cancers with the highest expression of F2R, therefore, we can conclude that the patient's biopsy through which this project has been generated, was not a specific case of high expression of F2R.

One aspect to take into account is that despite being expressed in many cancer types, we did not find evidence that it is an unfavorable prognostic factor of the disease in patients with ccRCC. However, taking into consideration all RCC patients (regardless of the histopathological classification discussed above) it does appear to be an unfavorable prognostic factor for the disease (data not shown).

Due to the possible involvement of F2R in the different stages of the metastatic cascade and due to its involvement in tumor malignancy described by other groups, F2R could be an emerging anti-cancer drug target. However, its inhibitors are currently in clinical use to treat acute coronary syndromes. With our findings, we propose the use of the already FDA-approved drug vorapaxar as a novel anti-cancer drug for targeting metastasis. Currently, there are many ongoing clinical trials using vorapaxar, but none of them is focused on cancer metastasis (Flaumenhaft & de Ceunynck, 2017b).

However, very recently has been proposed the use of pepducins in breast, lung, and ovarian cancer has. This peptide has been described as a modulator of GPCR signaling, important for the downstream activating signaling pathways of F2R (Covic & Kuliopulos, 2018).

Besides, although during all the thesis we have focused on only one factor of the coagulation cascade, many others were abnormally increased. That is why we decided to perform the same survival study of the patients but separate those who had

overexpression of the different factors that were mostly altered in the coagulation cascade. These results showed that there was indeed a tendency for a worse prognosis if the coagulation cascade genes were overexpressed.

As we previously highlighted, cancer is a highly prothrombotic state. Cancer-associated thrombosis is associated with Venous Thromboembolism (VTE). Active cancer accounts for 20% of the overall incidence of VTE (Heit et al., 2016). Concretely, in RCC patients there is an increased risk of venous thromboembolism (VTE), with rates varying between 1.2% and 3.5% (Chew et al., 2006; Yokom et al., 2014). For that reason, was interesting to find that in Ren 50M we have an increase of factors of the coagulation pathway that could explain the higher risk of having this hipercoagulant state. The American College of Chest Physician guidelines recommends anticoagulant thromboprophylaxis for acutely ill hospitalized medical patients at increased risk of VTE (Yokom et al., 2014). For that reason, our proposal of the usage of vorapaxar in those patients with a higher risk of VTE could have a potential dual clinical benefit of attenuating cancer-associated thrombosis which represents the second leading cause of death for cancer patients but also decreasing the risk of generating metastasis.

However, in our model, there were no differences and no alteration in the formation of clots in the blood analyzed from Ren 50M tumors. Furthermore, if we had had problems with the blood coagulation of these animals, they would have died of thrombus and coagulation problems, but this was not the case. Many animals have been euthanized throughout the project, and the endpoint criteria were the welfare of the animal, which was compromised by tumor growth and not by clotting problems.

One of the possible explanations that we can find for the fact that there were no problems with the coagulation cascade despite the fact of having increased many different factors of this pathway is due to the lack of the activators of this pathway. It is worth remembering that the coagulation pathway is activated after a cascade of activation of different proteases.

Another possible explanation for not having this coagulation pathway activated is that of the 12 factors of the coagulation cascade that were found to be overexpressed in Ren 50M tumors, many of them were activators of the coagulation cascade such as F2R, FXIIIA, F2RL2, ITGB3... but many others were inhibitors of the coagulation cascade. This was the case for Tissue Factor Pathway Inhibitor (TFPI) and Serpin Peptidase 1 (SERPINE1). Therefore, a balance may be established between procoagulant factors and factors that inhibit the pathway.

Finally, it is worth remembering that these factors are increased in tumor cells, but not at the systemic level. It is certain that at the systemic level something is happening due to the presence of the tumor since as we have shown, phenotypically the mice with the Ren 50M tumors presented a reddish skin compared with mice with Ren 50 tumors, even though no differences were found in different blood-related factors (data not shown).

We can therefore conclude that the tumor cells are benefiting from the expression of the coagulation cascade factors to acquire more aggressive characteristics that favor metastasis, but without altering the blood coagulation of the mice, as other groups have been validated (L. Hu et al., 2009; X. Jiang et al., 2004; Kasthuri et al., 2009)

Besides, the results of patient survival associated with the overexpression of the different integrins are very interesting. Both α3 and α5 integrins and their ligand fibronectin are factors that, are overexpressed in patients with ccRCC, and are a negative prognostic factor of the disease. They could therefore be used as biomarkers of tumor malignancy.

In addition, the studies carried out on gene correlations were surprising as there is a correlation between the expression of our F2R receptor and integrin α5, integrin β1, and fibronectin. In other words, there is not only a correlation between F2R and the activation of integrins but there is also a regulation at the genetic level.

Considering all the results obtained from the integrins, it seems to indicate that the α5β1 integrin could have special relevance in the development of RCC and could be used as a possible biomarker of tumor aggressiveness. In addition, and as mentioned above, there

are different blocking antibodies that are in the clinical trial phase and inhibitor drugs that are in the process of being generated. Therefore, it might be interesting to test different inhibitors in patients with high expression of this integrin.

As a conclusion, we suggested that F2R is playing an important role in the very early stages of the metastatic cascade adding to the effects of the later steps of the cascade. For that reason, F2R inhibition could be an interesting target to inhibit preventively to avoid the escape of tumor cells from the primary tumor.
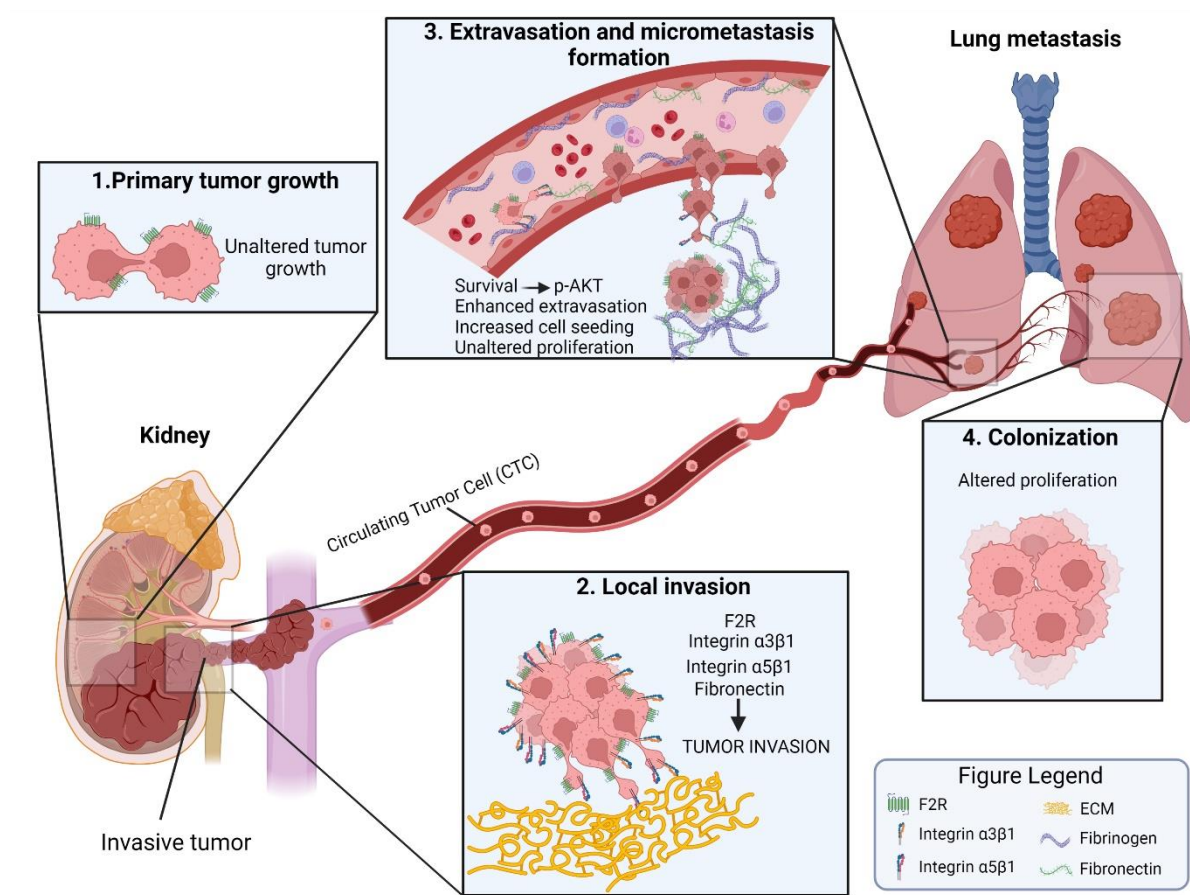
Figure 88. Schematic representation of the pleiotropic effects of F2R in the metastatic cascade. No alteration was founded in proliferation on primary tumor. However, a possible interplay between F2R and different integrins had been validated as potential inductors of tumor invasiveness. Furthermore, and thanks to these integrins, the process of extravasation and micometastasis formation could be enhanced together with the activation of the pro-survival AKT signaling pathway. Finally, an effect on colonization and macrometastasis formation was observed when we decreased F2R expression. Original figure created with BioRender.com

CONCLUSIONS

1. Coagulation factor II Thrombin Receptor (F2R) is playing pleiotropic effects in the metastatic cascade in Kidney tumors. Besides, the overexpression of different coagulation pathway candidates related to F2R could be also enhancing tumor malignization.

2. Loss of function studies directly implicates F2R in the invasive capacity of RCC tumors.

3. Gain-of-Function studies by F2R activation implicate this molecule in the invasive capacity of kidney cancer cells and tumors promoting their aggressiveness.

4. Integrin α3β1 and integrin α5β1 are plausible downstream effectors in RCC primary tumor invasiveness mediated by F2R.

5. Mechanistically, F2R activation seems to be activating integrins α3β1 and α5β1 via PI3K/AKT signaling pathway to promote cell migration and a higher metastatic capacity in kidney cancer cells.

6. F2R is also playing a promalignant important role in the extravasation and colonization steps of the metastatic cascade and not only affects the primary tumor.

7. Mechanistically, F2R produces an activation of PI3K/AKT signaling pathway that is a key mediator of DTC survival in the metastatic site.

8. Despite RCC tumor models studied have an overexpression of many genes from the coagulation pathway, no alteration on the blood hemostasis is observed, possibly because upstream triggers of coagulation might not be activated.

9. In patients, F2R expression alone is not associated with poor prognosis in ccRCC patients despite this is the cancer type with higher F2R expression. However, overexpression of a coagulation pathway geneset is associated with poor prognosis in ccRCC patients, which substantiates the clinical role of coagulation candidates in RCC malignization.

10. Clinically, F2R-associated integrins and their ligands are associated with poor prognosis in ccRCC patients suggesting a clinical confirmation of the malignization mechanism of F2R.

REFERENCES

Abbi, S., & Guan, J. L. (2002). Focal adhesion kinase: protein interactions and cellular functions. *Histology and Histopathology*, *17*(4), 1163–1171. https://doi.org/10.14670/HH-17.1163

Aceto, N., Bardia, A., Miyamoto, D. T., Donaldson, M. C., Wittner, B. S., Spencer, J. A., Yu, M., Pely, A., Engstrom, A., Zhu, H., Brannigan, B. W., Kapur, R., Stott, S. L., Shioda, T., Ramaswamy, S., Ting, D. T., Lin, C. P., Toner, M., Haber, D. A., & Maheswaran, S. (2014). Circulating tumor cell clusters are oligoclonal precursors of breast cancer metastasis. *Cell*, *158*(5), 1110–1122. https://doi.org/10.1016/J.CELL.2014.07.013

Adams, G. N., Rosenfeldt, L., Frederick, M., Miller, W., Waltz, D., Kombrinck, K., McElhinney, K. E., Flick, M. J., Monia, B. P., Revenko, A. S., & Palumbo, J. S. (2015). Colon Cancer Growth and Dissemination Relies upon Thrombin, Stromal PAR-1, and Fibrinogen. *Cancer Research*, *75*(19), 4235–4243. https://doi.org/10.1158/0008-5472.CAN-15-0964

Adams, G. N., Sharma, B. K., Rosenfeldt, L., Frederick, M., Flick, M. J., Witte, D. P., Mosnier, L. O., Harmel-Laws, E., Steinbrecher, K. A., & Palumbo, J. S. (2018). Protease-activated receptor-1 impedes prostate and intestinal tumor progression in mice. *Journal of Thrombosis and Haemostasis : JTH*, *16*(11), 2258–2269. https://doi.org/10.1111/JTH.14277

Alberelli, M., & de Candia, E. (2014). Functional role of protease activated receptors in vascular biology. *Vascular Pharmacology*, *62*(2), 72–81. https://doi.org/10.1016/j.vph.2014.06.001

Alizadeh, A. A., Aranda, V., Bardelli, A., Blanpain, C., Bock, C., Borowski, C., Caldas, C., Califano, A., Doherty, M., Elsner, M., Esteller, M., Fitzgerald, R., Korbel, J. O., Lichter, P., Mason, C. E., Navin, N., Pe'Er, D., Polyak, K., Roberts, C. W. M., … Zucman-Rossi, J. (2015). Toward understanding and exploiting tumor heterogeneity. *Nature Medicine*, *21*(8), 846. https://doi.org/10.1038/NM.3915

American Cancer Society. (2018). https://www.cancer.org/cancer/kidney-cancer/detection-diagnosis-staging/survival-rates.html

Amin, M. B., Edge, S. B., Greene, F. L., Schilsky, R. L., Brookland, R. K., Washington, M. K., Gershenwald, J. E., Compton, C. C., Hess, K. R., Sullivan, D. C., Jessup, M. J., Brierley, J. D., Gaspar, L. E., Balch, C. M., Winchester, D. P., Asare, E. A., Madera, M., Gress, D. M., & Meyer, L. R. (2017). American Joint Committee on Cancer (AJCC). AJCC Cancer Staging Manual. In *AJCC Cancer Staging Manual*. https://link.springer.com/book/9783319406176

Attieh, Y., & Vignjevic, D. M. (2016). The hallmarks of CAFs in cancer invasion. *European Journal of Cell Biology*, *95*(11), 493–502. https://doi.org/10.1016/J.EJCB.2016.07.004

Bar-Shavit, R., Maoz, M., Kancharla, A., Jaber, M., Agranovich, D., Grisaru-Granovsky, S., & Uziely, B. (2016). Protease-activated receptors (PARs) in cancer: Novel biased signaling and targets for therapy. *Methods in Cell Biology*, *132*, 341–358. https://doi.org/10.1016/BS.MCB.2015.11.006

Bar-Shavit, R., Maoz, M., Kancharla, A., Nag, J. K., Agranovich, D., Grisaru-Granovsky, S., & Uziely, B. (2016). G Protein-Coupled Receptors in Cancer. *International Journal of Molecular Sciences 2016, Vol. 17, Page 1320*, *17*(8), 1320. https://doi.org/10.3390/IJMS17081320

Beavon, I. R. G. (2000). The E-cadherin-catenin complex in tumour metastasis: structure, function and regulation. *European Journal of Cancer (Oxford, England : 1990)*, *36*(13 Spec No), 1607–1620. https://doi.org/10.1016/S0959-8049(00)00158-1

Bhaskar, V., Fox, M., Breinberg, D., Wong, M. H. L., Wales, P. E., Rhodes, S., DuBridge, R. B., & Ramakrishnan, V. (2008). Volociximab, a chimeric integrin alpha5beta1 antibody, inhibits the growth of VX2 tumors in rabbits. *Investigational New Drugs*, *26*(1), 7–12. https://doi.org/10.1007/S10637-007-9078-Z

Bhaskar, V., Zhang, D., Fox, M., Seto, P., Wong, M. H. L., Wales, P. E., Powers, D., Chao, D. T., DuBridge, R. B., & Ramakrishnan, V. (2007). A function blocking anti-mouse integrin alpha5beta1 antibody inhibits angiogenesis and impedes tumor growth in vivo. *Journal of Translational Medicine*, *5*. https://doi.org/10.1186/1479-5876-5-61

Bianchi, M., Sun, M., Jeldres, C., Shariat, S. F., Trinh, Q. D., Briganti, A., Tian, Z., Schmitges, J., Graefen, M., Perrotte, P., Menon, M., Montorsi, F., & Karakiewicz, P. I. (2012). Distribution of metastatic sites in renal cell carcinoma: a population-based analysis. *Annals of Oncology : Official Journal of the European Society for Medical Oncology*, *23*(4), 973–980. https://doi.org/10.1093/ANNONC/MDR362

Binnewies, M., Roberts, E. W., Kersten, K., Chan, V., Fearon, D. F., Merad, M., Coussens, L. M., Gabrilovich, D. I., Ostrand-Rosenberg, S., Hedrick, C. C., Vonderheide, R. H., Pittet, M. J., Jain, R. K., Zou, W., Howcroft, T. K., Woodhouse, E. C., Weinberg, R. A., & Krummel, M. F. (2018). Understanding the tumor immune microenvironment (TIME) for effective therapy. *Nature Medicine*, *24*(5), 541–550. https://doi.org/10.1038/S41591-018-0014-X

Boire, A., Covic, L., Agarwal, A., Jacques, S., Sherifi, S., & Kuliopulos, A. (2005). PAR1 is a matrix metalloprotease-1 receptor that promotes invasion and tumorigenesis of breast cancer cells. *Cell*, *120*(3), 303–313. https://doi.org/10.1016/J.CELL.2004.12.018

Brabletz, T. (2012). To differentiate or not--routes towards metastasis. *Nature Reviews. Cancer*, *12*(6), 425–436. https://doi.org/10.1038/NRC3265

Breuksch, I., Prosinger, F., Baehr, F., Engelhardt, F. P., Bauer, H. K., Thüroff, J. W., Heimes, A. S., Hasenburg, A., Prawitt, D., & Brenner, W. (2017). Integrin α5 triggers the metastatic potential in renal cell carcinoma. *Oncotarget*, *8*(64), 107530. https://doi.org/10.18632/ONCOTARGET.22501

Burns, K. E., & Thevenin, D. (2015). Down-regulation of PAR1 activity with a pHLIP-based allosteric antagonist induces cancer cell death. *Biochemical Journal*, *472*(3), 287–295. https://doi.org/10.1042/BJ20150876

Cagnet, S., Faraldo, M. M., Kreft, M., Sonnenberg, A., Raymond, K., & Glukhova, M. A. (2013). Signaling events mediated by α3β1 integrin are essential for mammary tumorigenesis. *Oncogene 2014 33:34*, *33*(34), 4286–4295. https://doi.org/10.1038/onc.2013.391

Cairns, P. (2011). Renal Cell Carcinoma. *Cancer Biomarkers*, *9*(1–6), 461. https://doi.org/10.3233/CBM-2011-0176

Cancer. (n.d.). Retrieved April 29, 2022, from https://www.who.int/health-topics/cancer#tab=tab_1

Carmeliet, P. (2005). VEGF as a key mediator of angiogenesis in cancer. *Oncology*, *69 Suppl 3*(SUPPL. 3), 4–10. https://doi.org/10.1159/000088478

Cerami, E., Gao, J., Dogrusoz, U., Gross, B. E., Sumer, S. O., Aksoy, B. A., Jacobsen, A., Byrne, C. J., Heuer, M. L., Larsson, E., Antipin, Y., Reva, B., Goldberg, A. P., Sander, C., & Schultz, N. (2012). The cBio cancer genomics portal: an open platform for exploring multidimensional cancer genomics data. *Cancer Discovery*, *2*(5), 401–404. https://doi.org/10.1158/2159-8290.CD-12-0095

Chackalamannil, S., Wang, Y., Greenlee, W., Hu, Z., Xia, Y., Ahn, H., Boykow, G., Hsieh, Y., Palamanda, J., Agans-fantuzzi, J., Kurowski, S., Graziano, M., & Chintala, M. (2008). Discovery of a Novel, Orally Active Himbacine-based Thrombin Receptor Antagonist (SCH 530348) with Potent Antiplatelet Activity. *Journal of Medicinal Chemistry*, *51*(11), 3061–3064.

Chaffer, C. L., & Weinberg, R. A. (2011a). A perspective on cancer cell metastasis. *Science*, *331*(6024), 1559–1564. https://doi.org/10.1126/science.1203543

Chaffer, C. L., & Weinberg, R. A. (2011b). A perspective on cancer cell metastasis. *Science (New York, N.Y.)*, *331*(6024), 1559–1564. https://doi.org/10.1126/SCIENCE.1203543

Chambers, A. F., Groom, A. C., & MacDonald, I. C. (2002a). Dissemination and growth of cancer cells in metastatic sites. *Nature Reviews. Cancer*, *2*(8), 563–572. https://doi.org/10.1038/NRC865

Chambers, A. F., Groom, A. C., & MacDonald, I. C. (2002b). Dissemination and growth of cancer cells in metastatic sites. *Nature Reviews. Cancer*, *2*(8), 563–572. https://doi.org/10.1038/NRC865

Chanakira, A., Westmark, P. R., Ong, I. M., & Sheehan, J. P. (2017). Tissue factor-factor VIIa complex triggers protease activated receptor 2-dependent growth factor release and migration in ovarian cancer. *Gynecologic Oncology*, *145*(1), 167–175. https://doi.org/10.1016/J.YGYNO.2017.01.022

Chaudhry, R., Usama, S. M., & Babiker, H. M. (2021). Physiology, Coagulation Pathways. *StatPearls*. https://www.ncbi.nlm.nih.gov/books/NBK482253/

Chew, H. K., Wun, T., Harvey, D., Zhou, H., & White, R. H. (2006). Incidence of venous thromboembolism and its effect on survival among patients with common cancers. *Archives of Internal Medicine*, *166*(4), 458–464. https://doi.org/10.1001/ARCHINTE.166.4.458

Chiang, S. P. H., Cabrera, R. M., & Segall, J. E. (2016). Tumor cell intravasation. *American Journal of Physiology. Cell Physiology*, *311*(1), C1–C14. https://doi.org/10.1152/AJPCELL.00238.2015

Cianfrocca, M. E., Kimmel, K. A., Gallo, J., Cardoso, T., Brown, M. M., Hudes, G., Lewis, N., Weiner, L., Lam, G. N., Brown, S. C., Shaw, D. E., Mazar, A. P., & Cohen, R. B. (2006). Phase 1 trial of the

antiangiogenic peptide ATN-161 (Ac-PHSCN-NH(2)), a beta integrin antagonist, in patients with solid tumours. *British Journal of Cancer*, *94*(11), 1621–1626. https://doi.org/10.1038/SJ.BJC.6603171

Cisowski, J., O'Callaghan, K., Kuliopulos, A., Yang, J., Nguyen, N., Deng, Q., Yang, E., Fogel, M., Tressel, S., Foley, C., Agarwal, A., Hunt, S. W., McMurry, T., Brinckerhoff, L., & Covic, L. (2011). Targeting protease-activated receptor-1 with cell-penetrating pepducins in lung cancer. *American Journal of Pathology*, *179*(1), 513–523. https://doi.org/10.1016/J.AJPATH.2011.03.025/ATTACHMENT/92355C17-478D-4E6E-9225-251A6810649C/MMC4.PDF

Cohen Even-Ram, S., Maoz, M., Pokroy, E., Reich, R., Katz, B., Gutweinţ, P., Altevogtţ, P., & Bar-Shavit, R. (2001). Tumor Cell Invasion Is Promoted by Activation of Protease Activated Receptor-1 in Cooperation with the αvβ5 Integrin. *The Journal of Biological Chemistry*, *276*(14), 10952–10962. https://doi.org/10.1074/jbc.M007027200

Coughlin, S. (2005). Protease-activated receptors in hemostasis, thrombosis and vascular biology. *Journal of Thrombosis and Haemostasis*, *3*(8), 1800–1814. https://doi.org/10.1111/j.1538-7836.2005.01377.x

Coughlin, S. R. (2000). Thrombin signalling and protease-activated receptors. *Nature 2000 407:6801*, *407*(6801), 258–264. https://doi.org/10.1038/35025229

Covic, L., & Kuliopulos, A. (2018). Protease-Activated Receptor 1 as Therapeutic Target in Breast, Lung, and Ovarian Cancer: Pepducin Approach. *International Journal of Molecular Sciences*, *19*(8). https://doi.org/10.3390/IJMS19082237

Crusz, S. M., Tang, Y. Z., Sarker, S. J., Prevoo, W., Kiyani, I., Beltran, L., Peters, J., Sahdev, A., Bex, A., Powles, T., & Gerlinger, M. (2016). Heterogeneous response and progression patterns reveal phenotypic heterogeneity of tyrosine kinase inhibitor response in metastatic renal cell carcinoma. *BMC Medicine*, *14*(1). https://doi.org/10.1186/S12916-016-0729-9

Darmoul, D., Rie Gratio, V., Lè Ne Devaud, H., Rè Se Lehy, T., & Laburthe, M. (2003). Aberrant Expression and Activation of the Thrombin Receptor Protease-Activated Receptor-1 Induces Cell Proliferation and Motility in Human Colon Cancer Cells. In *The American Journal of Pathology* (Vol. 162). https://doi.org/10.1016/S0002-9440(10)64283-6

de Falco, S. (2014). Antiangiogenesis therapy: an update after the first decade. *The Korean Journal of Internal Medicine*, *29*(1), 1. https://doi.org/10.3904/KJIM.2014.29.1.1

Degen, J. L., & Palumbo, J. S. (2012). Hemostatic factors, innate immunity and malignancy. *Thrombosis Research*, *129 Suppl 1*(SUPPL. 1), S1. https://doi.org/10.1016/S0049-3848(12)70143-3

di Serio, C., Pellerito, S., Duarte, M., Massi, D., Naldini, A., Cirino, G., Prudovsky, I., Santucci, M., Geppetti, P., Marchionni, N., Masotti, G., & Tarantini, F. (2007). Protease-activated receptor 1-selective antagonist SCH79797 inhibits cell proliferation and induces apoptosis by a

protease-activated receptor 1-independent mechanism. *Basic & Clinical Pharmacology & Toxicology*, *101*(1), 63–69. https://doi.org/10.1111/J.1742-7843.2007.00078.X

Dobin, A., Davis, C., Schlesinger, F., Drenkow, J., Zaleski, C., Jha, S., Batut, P., Chaisson, M., & Gingeras, T. (2013). STAR: ultrafast universal RNA-seq aligner. *Bioinformatics*, *29*(1), 15–21. https://doi.org/10.1093/bioinformatics/bts635

Dorsam, R. T., & Gutkind, J. S. (2007). G-protein-coupled receptors and cancer. *Nature Reviews Cancer 2007 7:2*, *7*(2), 79–94. https://doi.org/10.1038/NRC2069

Dudani, S., de Velasco, G., Wells, J. C., Gan, C. L., Donskov, F., Porta, C., Fraccon, A., Pasini, F., Lee, J. L., Hansen, A., Bjarnason, G. A., Beuselinck, B., Pal, S. K., Yuasa, T., Kroeger, N., Kanesvaran, R., Reaume, M. N., Canil, C., Choueiri, T. K., & Heng, D. Y. C. (2021). Evaluation of Clear Cell, Papillary, and Chromophobe Renal Cell Carcinoma Metastasis Sites and Association With Survival. *JAMA Network Open*, *4*(1). https://doi.org/10.1001/JAMANETWORKOPEN.2020.21869

Duivenvoorden, W. C. M., Vukmirovic´popovic´, S., Vukmirovic´popovicvukmirovic´popovic´, S ˇ A ´rka Lhoták, V., Seidlitz, E., Hirte, H. W., Tozer, R. G., & Singh, G. (n.d.). *Doxycycline Decreases Tumor Burden in a Bone Metastasis Model of Human Breast Cancer 1*. Retrieved May 20, 2022, from http://aacrjournals.org/cancerres/article-pdf/62/6/1588/2501259/1588.pdf

Erdogan, B., Ao, M., White, L. M., Means, A. L., Brewer, B. M., Yang, L., Washington, M. K., Shi, C., Franco, O. E., Weaver, A. M., Hayward, S. W., Li, D., & Webb, D. J. (2017). Cancer-associated fibroblasts promote directional cancer cell migration by aligning fibronectin. *The Journal of Cell Biology*, *216*(11), 3799–3816. https://doi.org/10.1083/JCB.201704053

Fala, L. (2015). Zontivity (Vorapaxar), First-in-Class PAR-1 Antagonist, Receives FDA Approval for Risk Reduction of Heart Attack, Stroke, and Cardiovascular Death. *American Health & Drug Benefits*, *8*(Spec Feature), 148. /pmc/articles/PMC4665045/

Fares, J., Fares, M. Y., Khachfe, H. H., Salhab, H. A., & Fares, Y. (2020). Molecular principles of metastasis: a hallmark of cancer revisited. *Signal Transduction and Targeted Therapy*, *5*(1). https://doi.org/10.1038/s41392-020-0134-x

Feigin, M. E. (2013). Harnessing the genome for characterization of G-protein coupled receptors in cancer pathogenesis. *The FEBS Journal*, *280*(19), 4729–4738. https://doi.org/10.1111/FEBS.12473

Flaumenhaft, R., & de Ceunynck, K. (2017). Targeting PAR1: Now What? *Trends in Pharmacological Sciences*, *38*(8), 701–716. https://doi.org/10.1016/J.TIPS.2017.05.001

Frisch, S. M., & Francis, H. (1994). Disruption of epithelial cell-matrix interactions induces apoptosis. *The Journal of Cell Biology*, *124*(4), 619–626. https://doi.org/10.1083/JCB.124.4.619

Fuhrman, S. A., Lasky, L. C., & Limas, C. (1982). Prognostic significance of morphologic parameters in renal cell carcinoma. *The American Journal of Surgical Pathology*, *6*(7), 655–663. https://doi.org/10.1097/00000478-198210000-00007

Fukushima, Y., Ohnishi, T., Arita, N., Hayakawa, T., & Sekiguchi, K. (1998). INTEGRIN 31-MEDIATED INTERACTION WITH LAMININ-5 STIMULATES ADHESION, MIGRATION AND INVASION OF MALIGNANT GLIOMA CELLS. *J. Cancer*, *76*, 63–72. https://doi.org/10.1002/(SICI)1097-0215(19980330)76:1

Ganesh, K., & Massagué, J. (2021). Targeting metastatic cancer. *Nature Medicine*, *27*(1), 34–44. https://doi.org/10.1038/S41591-020-01195-4

Gao, G., Yang, M., Wang, F., Dang, G., Zhang, X., Zhao, J., Wang, X., & Jin, B. (2020). Coagulation factor 2 thrombin receptor promotes malignancy in glioma under SOX2 regulation. *Aging (Albany NY)*, *12*(11), 10594. https://doi.org/10.18632/AGING.103281

Gay, L., & Felding-Habermann, B. (2011a). Contribution of platelets to tumour metastasis. *Nature Reviews Cancer*, *11*(2), 123–134. https://doi.org/10.1038/nrc3004

Gay, L., & Felding-Habermann, B. (2011b). Contribution of platelets to tumour metastasis. *Nature Reviews Cancer*, *11*(2), 123–134. https://doi.org/10.1038/nrc3004

Gay, L. J., & Felding-Habermann, B. (2011). Contribution of platelets to tumour metastasis. *Nature Reviews. Cancer*, *11*(2), 123–134. https://doi.org/10.1038/NRC3004

Gerlinger, M., Horswell, S., Larkin, J., Rowan, A. J., Salm, M. P., Varela, I., Fisher, R., Mcgranahan, N., Matthews, N., Santos, C. R., Martinez, P., Phillimore, B., Begum, S., Rabinowitz, A., Spencer-Dene, B., Gulati, S., Bates, P. A., Stamp, G., Pickering, L., … Swanton, C. (2014). Genomic architecture and evolution of clear cell renal cell carcinomas defined by multiregion sequencing. *Nature Genetics*, *46*(3), 225–233. https://doi.org/10.1038/NG.2891

Giancotti, F. G. (2000). Complexity and specificity of integrin signalling. *Nature Cell Biology 2000 2:1*, *2*(1), E13–E14. https://doi.org/10.1038/71397

Giancotti, F. G. (2013). Mechanisms governing metastatic dormancy and reactivation. *Cell*, *155*(4), 750. https://doi.org/10.1016/J.CELL.2013.10.029

Gieseler, F., Ungefroren, H., Settmacher, U., Hollenberg, M. D., & Kaufmann, R. (2013). Proteinase-activated receptors (PARs) - Focus on receptor-receptor- interactions and their physiological and pathophysiological impact. *Cell Communication and Signaling*, *11*(1), 1. https://doi.org/10.1186/1478-811X-11-86

Gomis, R. R., & Gawrzak, S. (2017). Tumor cell dormancy. *Molecular Oncology*, *11*(1), 62–78. https://doi.org/10.1016/J.MOLONC.2016.09.009

Gong, J., Maia, M. C., Dizman, N., Govindarajan, A., & Pal, S. K. (2016). Metastasis in renal cell carcinoma: Biology and implications for therapy. *Asian Journal of Urology*, *3*(4), 286. https://doi.org/10.1016/J.AJUR.2016.08.006

Gong, J., Wang, D. H., Sun, L. Z., Zborowska, E., Willson, J. K. V., & Brattain, M. G. (1997). Role of alpha 5 beta 1 integrin in determining malignant properties of colon carcinoma cells. *Cell Growth & Differentiation : The Molecular Biology Journal of the American Association for Cancer Research*, *8*(1), 83–90. https://europepmc.org/article/med/8993837

Griesmann, H., Drexel, C., Milosevic, N., Sipos, B., Rosendahl, J., Gress, T. M., & Michl, P. (2017). Pharmacological macrophage inhibition decreases metastasis formation in a genetic model of pancreatic cancer. *Gut*, *66*(7), 1278–1285. https://doi.org/10.1136/GUTJNL-2015-310049

Gupta, G. P., & Massagué, J. (2006). Cancer Metastasis: Building a Framework. In *Cell* (Vol. 127, Issue 4, pp. 679–695). https://doi.org/10.1016/j.cell.2006.11.001

Haber, T., Jöckel, E., Roos, F. C., Junker, K., Prawitt, D., Hampel, C., Thüroff, J. W., & Brenner, W. (2015). Bone Metastasis in Renal Cell Carcinoma is Preprogrammed in the Primary Tumor and Caused by AKT and Integrin α5 Signaling. *The Journal of Urology*, *194*(2), 539–546. https://doi.org/10.1016/J.JURO.2015.01.079

Hamidi, H., & Ivaska, J. (2018). Every step of the way: Integrins in cancer progression and metastasis. *Nature Reviews Cancer*, *18*(9), 533–548. https://doi.org/10.1038/s41568-018-0038-z

Han, N., Jin, K., He, K., Cao, J., & Teng, L. (2011). Protease-activated receptors in cancer: A systematic review. *Oncology Letters*, *2*(4), 599–608. https://doi.org/10.3892/ol.2011.291

Hanahan, D. (2022). Hallmarks of Cancer: New DimensionsHallmarks of Cancer: New Dimensions. *Cancer Discovery*, *12*(1), 31–46. https://doi.org/10.1158/2159-8290.CD-21-1059

Hanahan, D., & Weinberg, R. (2011a). Hallmarks of cancer: The next generation. *Cell*, *144*(5), 646–674. https://doi.org/10.1016/j.cell.2011.02.013

Hanahan, D., & Weinberg, R. A. (2000). The Hallmarks of Cancer. *Cell*, *100*(1), 57–70. https://doi.org/10.1016/S0092-8674(00)81683-9

Hanahan, D., & Weinberg, R. A. (2011b). Hallmarks of cancer: the next generation. *Cell*, *144*(5), 646–674. https://doi.org/10.1016/J.CELL.2011.02.013

Hart2, I. R., & Fidler, I. J. (1980). Role of Organ Selectivity in the Determination of Metastatic Patterns of B16 Melanoma1. *CANCER RESEARCH*, *40*, 2281–2287. http://aacrjournals.org/cancerres/article-pdf/40/7/2281/2408786/cr0400072281.pdf

Hawes, B. E., Zhai, Y., Hesk, D., Wirth, M., Wei, H., Chintala, M., & Seiffert, D. (2015). In vitro pharmacological characterization of vorapaxar, a novel platelet thrombin receptor antagonist. *European Journal of Pharmacology*, *762*(1), 221–228. https://doi.org/10.1016/J.EJPHAR.2015.05.046

Hegele, A., Heidenreich, A., Kropf, J., von Knobloch, R., Varga, Z., Hofmann, R., & Olbert, P. (2004). Plasma levels of cellular fibronectin in patients with localized and metastatic renal cell

carcinoma. *Tumour Biology : The Journal of the International Society for Oncodevelopmental Biology and Medicine*, *25*(3), 111–116. https://doi.org/10.1159/000079142

Heit, J. A., Spencer, F. A., & White, R. H. (2016). The epidemiology of venous thromboembolism. *Journal of Thrombosis and Thrombolysis*, *41*(1), 3. https://doi.org/10.1007/S11239-015-1311-6

Hernández, N., Correa, E., Avila, E., Vela, T., & Pérez, V. (2009). PAR1 is selectively over expressed in high grade breast cancer patients: a cohort study. *Journal of Translational Medicine*, *7*, 47. https://doi.org/10.1186/1479-5876-7-47

Heuberger, D. M., & Schuepbach, R. A. (2019a). Protease-activated receptors (PARs): Mechanisms of action and potential therapeutic modulators in PAR-driven inflammatory diseases. *Thrombosis Journal*, *17*(1), 1–24. https://doi.org/10.1186/S12959-019-0194-8/TABLES/7

Heuberger, D. M., & Schuepbach, R. A. (2019b). Protease-activated receptors (PARs): Mechanisms of action and potential therapeutic modulators in PAR-driven inflammatory diseases. *Thrombosis Journal*, *17*(1), 1–24. https://doi.org/10.1186/S12959-019-0194-8/TABLES/7

Hinz, N., & Jücker, M. (2021). AKT in Bone Metastasis of Solid Tumors: A Comprehensive Review. *Cancers*, *13*(10). https://doi.org/10.3390/CANCERS13102287

Hiratsuka, S., Watanabe, A., Aburatani, H., & Maru, Y. (2006). Tumour-mediated upregulation of chemoattractants and recruitment of myeloid cells predetermines lung metastasis. *Nature Cell Biology*, *8*(12), 1369–1375. https://doi.org/10.1038/NCB1507

Holash, J., Maisonpierre, P. C., Compton, D., Boland, P., Alexander, C. R., Zagzag, D., Yancopoulos, G. D., & Wiegand, S. J. (1999). Vessel cooption, regression, and growth in tumors mediated by angiopoietins and VEGF. *Science (New York, N.Y.)*, *284*(5422), 1994–1998. https://doi.org/10.1126/SCIENCE.284.5422.1994

Hollenberg, M. D., Saifeddine, M., Al-Ani, B., & Kawabata, A. (1997). Proteinase-activated receptors: Structural requirements for activity, receptor cross-reactivity, and receptor selectivity of receptor-activating peptides. *Canadian Journal of Physiology and Pharmacology*, *75*(7), 832–841. https://doi.org/10.1139/Y97-110/ASSET/Y97-110.FP.PNG_V03

Hsieh, J. J., Le, V., Cao, D., Cheng, E. H., & Creighton, C. J. (2018). Genomic classifications of renal cell carcinoma: a critical step towards the future application of personalized kidney cancer care with pan-omics precision. *The Journal of Pathology*, *244*(5), 525–537. https://doi.org/10.1002/PATH.5022

Hsieh, J. J., Purdue, M. P., Signoretti, S., Swanton, C., Albiges, L., Schmidinger, M., Heng, D. Y., Larkin, J., & Ficarra, V. (2017a). Renal cell carcinoma. *Nature Reviews Disease Primers*, *3*, 1–19. https://doi.org/10.1038/nrdp.2017.9

Hsieh, J. J., Purdue, M. P., Signoretti, S., Swanton, C., Albiges, L., Schmidinger, M., Heng, D. Y., Larkin, J., & Ficarra, V. (2017b). Renal cell carcinoma. *Nature Reviews. Disease Primers*, *3*. https://doi.org/10.1038/NRDP.2017.9

Hu, C., Ni, Z., Li, B. S., Yong, X., Yang, X., Zhang, J. W., Zhang, D., Qin, Y., Jie, M. M., Dong, H., Li, S., He, F., & Yang, S. M. (2017). hTERT promotes the invasion of gastric cancer cells by enhancing FOXO3a ubiquitination and subsequent ITGB1 upregulation. *Gut*, *66*(1), 31–42. https://doi.org/10.1136/GUTJNL-2015-309322

Hu, L., Ibrahim, S., Liu, C., Skaar, J., Pagano, M., & Karpatkin, S. (2009). Thrombin induces tumor cell cycle activation and spontaneous growth by down-regulation of p27Kip1, in association with the up-regulation of Skp2 and MiR-222. *Cancer Research*, *69*(8), 3374–3381. https://doi.org/10.1158/0008-5472.CAN-08-4290

Humphries, J. D., Byron, A., & Humphries, M. J. (2006). Integrin ligands at a glance. *Journal of Cell Science*, *119*(19), 3901–3903. https://doi.org/10.1242/JCS.03098

Iheanacho, K., & Vaishampayan, U. (2020). Perioperative approaches to kidney cancer. *Clinical Advances in Hematology & Oncology : H&O*, *18*(1), 56–65. https://pubmed.ncbi.nlm.nih.gov/32511222/

Isermann, B. (2017). Homeostatic effects of coagulation protease-dependent signaling and protease activated receptors. *Journal of Thrombosis and Haemostasis*, *15*(7), 1273–1284. https://doi.org/10.1111/jth.13721

Jenne, C. N., & Kubes, P. (2015). Platelets in inflammation and infection. *Platelets*, *26*(4), 286–292. https://doi.org/10.3109/09537104.2015.1010441

Jiang, W. G., Sanders, A. J., Katoh, M., Ungefroren, H., Gieseler, F., Prince, M., Thompson, S. K., Zollo, M., Spano, D., Dhawan, P., Sliva, D., Subbarayan, P. R., Sarkar, M., Honoki, K., Fujii, H., Georgakilas, A. G., Amedei, A., Niccolai, E., Amin, A., … Santini, D. (2015). Tissue invasion and metastasis: Molecular, biological and clinical perspectives. *Seminars in Cancer Biology*, *35*, S244–S275. https://doi.org/10.1016/J.SEMCANCER.2015.03.008

Jiang, X., Bailly, M. A., Panetti, T. S., Cappello, M., Konigsberg, W. H., & Bromberg, M. E. (2004). Formation of tissue factor-factor VIIa-factor Xa complex promotes cellular signaling and migration of human breast cancer cells. *Journal of Thrombosis and Haemostasis : JTH*, *2*(1), 93–101. https://doi.org/10.1111/J.1538-7836.2004.00545.X

Kancharla, A., Maoz, M., Jaber, M., Agranovich, D., Peretz, T., Grisaru-Granovsky, S., Uziely, B., & Bar-Shavit, R. (2015). PH motifs in PAR1&2 endow breast cancer growth. *Nature Communications*, *6*. https://doi.org/10.1038/NCOMMS9853

Kasthuri, R. S., Taubman, M. B., & Mackman, N. (2009). Role of Tissue Factor in Cancer. *Journal of Clinical Oncology*, *27*(29), 4834. https://doi.org/10.1200/JCO.2009.22.6324

Kaufmann, R., Rahn, S., Pollrich, K., Hertel, J., Dittmar, Y., Hommann, M., Henklein, P., Biskup, C., Westermann, M., Hollenberg, M., & Settmacher, U. (2007). Thrombin-mediated hepatocellular carcinoma cell migration: Cooperative action via proteinase-activated receptors 1 and 4. *Journal of Cellular Physiology*, *211*(3), 699–707. https://doi.org/10.1002/jcp.21027

Kessenbrock, K., Plaks, V., & Werb, Z. (2010). Matrix Metalloproteinases: Regulators of the Tumor Microenvironment. *Cell*, *141*(1), 52–67. https://doi.org/10.1016/J.CELL.2010.03.015

Key Statistics About Kidney Cancer. (n.d.). Retrieved April 26, 2022, from https://www.cancer.org/cancer/kidney-cancer/about/key-statistics.html

Khalili, P., Arakelian, A., Chen, G., Plunkett, M. L., Beck, I., Parry, G. C., Doñate, F., Shaw, D. E., Mazar, A. P., & Rabbani, S. A. (2006). A non-RGD-based integrin binding peptide (ATN-161) blocks breast cancer growth and metastasis in vivo. *Molecular Cancer Therapeutics*, *5*(9), 2271–2280. https://doi.org/10.1158/1535-7163.MCT-06-0100

Knowles, L. M., Gurski, L. A., Engel, C., Gnarra, J. R., Maranchie, J. K., & Pilch, J. (2013). Integrin αvβ3 and fibronectin upregulate Slug in cancer cells to promote clot invasion and metastasis. *Cancer Research*, *73*(20), 6175–6184. https://doi.org/10.1158/0008-5472.CAN-13-0602

Labelle, M., Begum, S., & Hynes, R. O. (2011). Direct signaling between platelets and cancer cells induces an epithelial-mesenchymal-like transition and promotes metastasis. *Cancer Cell*, *20*(5), 576–590. https://doi.org/10.1016/J.CCR.2011.09.009

Lambert, A. W., Pattabiraman, D. R., & Weinberg, R. A. (2017). Emerging Biological Principles of Metastasis. *Cell*, *168*(4), 670–691. https://doi.org/10.1016/J.CELL.2016.11.037

Leach, J., Morton, J. P., & Sansom, O. J. (2019). Neutrophils: Homing in on the myeloid mechanisms of metastasis. *Molecular Immunology*, *110*, 69–76. https://doi.org/10.1016/J.MOLIMM.2017.12.013

Li, B., Xu, W. W., Lam, A. K. Y., Wang, Y., Hu, H. F., Guan, X. Y., Qin, Y. R., Saremi, N., Tsao, S. W., He, Q. Y., & Cheung, A. L. M. (2017). Significance of PI3K/AKT signaling pathway in metastasis of esophageal squamous cell carcinoma and its potential as a target for anti-metastasis therapy. *Oncotarget*, *8*(24), 38755. https://doi.org/10.18632/ONCOTARGET.16333

Li, M., Wang, Y., Li, M., Wu, X., Setrerrahmane, S., & Xu, H. (2021). Integrins as attractive targets for cancer therapeutics. *Acta Pharmaceutica Sinica B*, *11*(9), 2726–2737. https://doi.org/10.1016/J.APSB.2021.01.004

Li, W., Hou, J. Z., Niu, J., Xi, Z. Q., Ma, C., Sun, H., Wang, C. J., Fang, D., Li, Q., & Xie, S. Q. (2018). Akt1 inhibition promotes breast cancer metastasis through EGFR-mediated β-catenin nuclear accumulation. *Cell Communication and Signaling*, *16*(1), 1–13. https://doi.org/10.1186/S12964-018-0295-1/FIGURES/6

Li, X., Ishihara, S., Yasuda, M., Nishioka, T., Mizutani, T., Ishikawa, M., Kawabata, K., Shirato, H., & Haga, H. (2013). Lung cancer cells that survive ionizing radiation show increased integrin α2β1- and EGFR-dependent invasiveness. *PloS One*, *8*(8). https://doi.org/10.1371/JOURNAL.PONE.0070905

Lima, L. G., & Monteiro, R. Q. (2013). Activation of blood coagulation in cancer: implications for tumour progression. *Bioscience Reports*, *33*(5), 701–710. https://doi.org/10.1042/BSR20130057

Lin, H., & Trejo, J. (2013). Transactivation of the PAR1-PAR2 heterodimer by thrombin elicits β-arrestin-mediated endosomal signaling. *The Journal of Biological Chemistry*, *288*(16), 11203–11215. https://doi.org/10.1074/JBC.M112.439950

Linehan, W. M., Srinivasan, R., & Schmidt, L. S. (2010). The genetic basis of kidney cancer: a metabolic disease. *Nature Reviews. Urology*, *7*(5), 277–285. https://doi.org/10.1038/NRUROL.2010.47

Liu, R., Chen, Y., Liu, G., Li, C., Song, Y., Cao, Z., Li, W., Hu, J., Lu, C., & Liu, Y. (2020). PI3K/AKT pathway as a key link modulates the multidrug resistance of cancers. *Cell Death & Disease*, *11*(9). https://doi.org/10.1038/S41419-020-02998-6

Liu, X., Yu, J., Song, S., Yue, X., & Li, Q. (2017). Protease-activated receptor-1 (PAR-1): a promising molecular target for cancer. *Oncotarget*, *8*(63), 107334. https://doi.org/10.18632/ONCOTARGET.21015

Loew, R., Heinz, N., Hampf, M., Bujard, H., & Gossen, M. (2010). Improved Tet-responsive promoters with minimized background expression. *BMC Biotechnology*, *10*, 1–13. https://doi.org/10.1186/1472-6750-10-81

Love, M., Huber, W., & Anders, S. (2014). Moderated estimation of fold change and dispersion for RNA-seq data with DESeq2. *Genome Biology*, *15*(12), 550. https://doi.org/10.1186/s13059-014-0550-8

Lu, X., Mu, E., Wei, Y., Riethdorf, S., Yang, Q., Yuan, M., Yan, J., Hua, Y., Tiede, B. J., Lu, X., Haffty, B. G., Pantel, K., Massagué, J., & Kang, Y. (2011). VCAM-1 promotes osteolytic expansion of indolent bone micrometastasis of breast cancer by engaging α4β1-positive osteoclast progenitors. *Cancer Cell*, *20*(6), 701–714. https://doi.org/10.1016/J.CCR.2011.11.002

Lum, D. H., Matsen, C., Welm, A. L., & Welm, B. E. (2012). Human Primary Tumorgraft Models: Comparisons with Traditional Oncology Pre-Clinical Models and The Clinical Relevance and Utility of Primary Tumorgrafts in Basic and Translational Oncology Research. *Current Protocols in Pharmacology / Editorial Board, S.J. Enna (Editor-in-Chief) ... [et Al.]*, *CHAPTER*(SUPPL.59), Unit14.22. https://doi.org/10.1002/0471141755.PH1422S59

Luzzi, K. J., MacDonald, I. C., Schmidt, E. E., Kerkvliet, N., Morris, V. L., Chambers, A. F., & Groom, A. C. (1998). Multistep nature of metastatic inefficiency: dormancy of solitary cells after successful extravasation and limited survival of early micrometastases. *The American Journal of Pathology*, *153*(3), 865–873. https://doi.org/10.1016/S0002-9440(10)65628-3

Ma, X., Liu, Y., Liu, Y., Alexandrov, L. B., Edmonson, M. N., Gawad, C., Zhou, X., Li, Y., Rusch, M. C., John, E., Huether, R., Gonzalez-Pena, V., Wilkinson, M. R., Hermida, L. C., Davis, S., Sioson, E., Pounds, S., Cao, X., Ries, R. E., … Zhang, J. (2018). Pan-cancer genome and transcriptome analyses of 1,699 paediatric leukaemias and solid tumours. *Nature 2018 555:7696*, *555*(7696), 371–376. https://doi.org/10.1038/nature25795

Malik, G., Knowles, L. M., Dhir, R., Xu, S., Yang, S., Ruoslahti, E., & Pilch, J. (2010). Plasma fibronectin promotes lung metastasis by contributions to fibrin clots and tumor cell invasion. *Cancer Research*, *70*(11), 4327–4334. https://doi.org/10.1158/0008-5472.CAN-09-3312

Massagué, J., & Obenauf, A. C. (2016). Metastatic colonization by circulating tumour cells. *Nature*, *529*(7586), 298–306. https://doi.org/10.1038/NATURE17038

McEachron, T. A., Pawlinski, R., Richards, K. L., Church, F. C., & Mackman, N. (2010). Protease-activated receptors mediate crosstalk between coagulation and fibrinolysis. *Blood*, *116*(23), 5037–5044. https://doi.org/10.1182/BLOOD-2010-06-293126

McFarlane, S., McFarlane, C., Montgomery, N., Hill, A., & Waugh, D. J. J. (2015). CD44-mediated activation of α5β1-integrin, cortactin and paxillin signaling underpins adhesion of basal-like breast cancer cells to endothelium and fibronectin-enriched matrices. *Oncotarget*, *6*(34), 36762–36773. https://doi.org/10.18632/ONCOTARGET.5461

Melchiori, A., Mortarini, R., Carlone, S., Marchisio, P. C., Anichini, A., Noonan, D. M., & Albini, A. (1995). The alpha 3 beta 1 integrin is involved in melanoma cell migration and invasion. *Experimental Cell Research*, *219*(1), 233–242. https://doi.org/10.1006/EXCR.1995.1223

Moch, H., Cubilla, A. L., Humphrey, P. A., Reuter, V. E., & Ulbright, T. M. (2016). The 2016 WHO Classification of Tumours of the Urinary System and Male Genital Organs—Part A: Renal, Penile, and Testicular Tumours. *European Urology*, *70*(1), 93–105. https://doi.org/10.1016/J.EURURO.2016.02.029

Moserle, L., & Casanovas, O. (2013). Anti-angiogenesis and metastasis: a tumour and stromal cell alliance. *Journal of Internal Medicine*, *273*(2), 128–137. https://doi.org/10.1111/JOIM.12018

Munshi, H. G., & Stack, M. S. (2006). Reciprocal interactions between adhesion receptor signaling and MMP regulation. *Cancer Metastasis Reviews*, *25*(1), 45–56. https://doi.org/10.1007/S10555-006-7888-7

Murillo, C. A., Rychahou, P. G., & Evers, B. M. (2004). Inhibition of alpha5 integrin decreases PI3K activation and cell adhesion of human colon cancers. *Surgery*, *136*(2), 143–149. https://doi.org/10.1016/J.SURG.2004.04.006

Muszbek, L., Bereczky, Z., Bagoly, Z., Komáromi, I., & Katona, É. (2011). Factor XIII: a coagulation factor with multiple plasmatic and cellular functions. *Physiological Reviews*, *91*(3), 931–972. https://doi.org/10.1152/PHYSREV.00016.2010

Nanda, N., Dhawan, D. K., Bhatia, A., Mahmood, A., & Mahmood, S. (2016). Doxycycline Promotes Carcinogenesis & Metastasis via Chronic Inflammatory Pathway: An In Vivo Approach. *PLoS ONE*, *11*(3). https://doi.org/10.1371/JOURNAL.PONE.0151539

Natali, P. G., Bartolazzi, A., Cavaliere, R., Bigotti, A., & Nicotra, M. R. (1993). Integrin expression in cutaneous malignant melanoma: association of the alpha 3/beta 1 heterodimer with tumor progression. *International Journal of Cancer*, *54*(1), 68–72. https://doi.org/10.1002/IJC.2910540112

National Cancer Institute. (n.d.). Retrieved March 24, 2020, from
   https://seer.cancer.gov/statfacts/html/kidrp.html%0D

Obenauf, A. C., & Massagué, J. (2015). Surviving at a Distance: Organ-Specific Metastasis. *Trends in Cancer*, *1*(1), 76–91. https://doi.org/10.1016/j.trecan.2015.07.009

Palumbo, J. (2008). *Mechanisms Linking Tumor Cell – Associated Procoagulant Function to Tumor Dissemination*. *1*(212), 154–160. https://doi.org/10.1055/s-2008-1079255.

Peinado, H., Alečković, M., Lavotshkin, S., Matei, I., Costa-Silva, B., Moreno-Bueno, G., Hergueta-Redondo, M., Williams, C., García-Santos, G., Ghajar, C. M., Nitadori-Hoshino, A., Hoffman, C., Badal, K., Garcia, B. A., Callahan, M. K., Yuan, J., Martins, V. R., Skog, J., Kaplan, R. N., … Lyden, D. (2012). Melanoma exosomes educate bone marrow progenitor cells toward a pro-metastatic phenotype through MET. *Nature Medicine*, *18*(6), 883–891. https://doi.org/10.1038/NM.2753

Peinado, H., Lavotshkin, S., & Lyden, D. (2011). The secreted factors responsible for pre-metastatic niche formation: Old sayings and new thoughts. *Seminars in Cancer Biology*, *21*(2), 139–146. https://doi.org/10.1016/J.SEMCANCER.2011.01.002

Peinado, H., Zhang, H., Matei, I. R., Costa-Silva, B., Hoshino, A., Rodrigues, G., Psaila, B., Kaplan, R. N., Bromberg, J. F., Kang, Y., Bissell, M. J., Cox, T. R., Giaccia, A. J., Erler, J. T., Hiratsuka, S., Ghajar, C. M., & Lyden, D. (2017). Pre-metastatic niches: organ-specific homes for metastases. *Nature Reviews. Cancer*, *17*(5), 302–317. https://doi.org/10.1038/NRC.2017.6

Pontes, O., Oliveira-Pinto, S., Baltazar, F., & Costa, M. (2022). Renal cell carcinoma therapy: Current and new drug candidates. *Drug Discovery Today*, *27*(1), 304–314. https://doi.org/10.1016/J.DRUDIS.2021.07.009

Quail, D. F., & Joyce, J. A. (2013). Microenvironmental regulation of tumor progression and metastasis. *Nature Medicine*, *19*(11), 1423–1437. https://doi.org/10.1038/NM.3394

Queiroz, K. C. S., Shi, K., Duitman, J. W., Aberson, H. L., Wilmink, J. W., van Noesel, C. J. M., Richel, D. J., & Spek, C. A. (2014). Protease-activated receptor-1 drives pancreatic cancer progression and chemoresistance. *International Journal of Cancer*, *135*(10), 2294–2304. https://doi.org/10.1002/IJC.28726

Rashid, O. M., Nagahashi, M., Ramachandran, S., Dumur, C. I., Schaum, J. C., Yamada, A., Aoyagi, T., Milstien, S., Spiegel, S., & Takabe, K. (2013). Is tail vein injection a relevant breast cancer lung metastasis model? *Journal of Thoracic Disease*, *5*(4), 385. https://doi.org/10.3978/J.ISSN.2072-1439.2013.06.17

Raucher, D., & Sheetz, M. P. (2000). Cell Spreading and Lamellipodial Extension Rate Is Regulated by Membrane Tension. *The Journal of Cell Biology*, *148*(1), 127. https://doi.org/10.1083/JCB.148.1.127

Remiker, A. S., & Palumbo, J. S. (2018). Mechanisms coupling thrombin to metastasis and tumorigenesis. *Thrombosis Research*, *164 Suppl 1*, S29–S33. https://doi.org/10.1016/J.THROMRES.2017.12.020

Renal Cell Carcinoma Staging and Life Expectancy | New Health Advisor. (n.d.). Retrieved April 27, 2022, from https://www.newhealthadvisor.org/Renal-Cell-Carcinoma-Staging.html

Rini, B. I. (2007). Vascular Endothelial Growth Factor–Targeted Therapy in Renal Cell Carcinoma: Current Status and Future Directions. *Clinical Cancer Research*, *13*(4), 1098–1106. https://doi.org/10.1158/1078-0432.CCR-06-1989

Robertson, J., Jacquemet, G., Byron, A., Jones, M. C., Warwood, S., Selley, J. N., Knight, D., Humphries, J. D., & Humphries, M. J. (2015). Defining the phospho-adhesome through the phosphoproteomic analysis of integrin signalling. *Nature Communications 2015 6:1*, *6*(1), 1–13. https://doi.org/10.1038/ncomms7265

Ronca, R., Benkheil, M., Mitola, S., Struyf, S., & Liekens, S. (2017). Tumor angiogenesis revisited: Regulators and clinical implications. *Medicinal Research Reviews*, *37*(6), 1231–1274. https://doi.org/10.1002/MED.21452

Ruf, W., & Mueller, B. M. (2006). Thrombin generation and the pathogenesis of cancer. *Seminars in Thrombosis and Hemostasis*, *32 Suppl 1*(SUPPL. 1), 61–68. https://doi.org/10.1055/S-2006-939555

Saeed, K., Ojamies, P., Pellinen, T., Eldfors, S., Turkki, R., Lundin, J., Järvinen, P., Nisen, H., Taari, K., af Hällström, T. M., Rannikko, A., Mirtti, T., Kallioniemi, O., & Östling, P. (2019). Clonal heterogeneity influences drug responsiveness in renal cancer assessed by ex vivo drug testing of multiple patient-derived cancer cells. *International Journal of Cancer*, *144*(6), 1356–1366. https://doi.org/10.1002/IJC.31815

Sahni, A., Simpson-haidaris, P. J., Sahni, S. K., Vaday, G. G., & Francis, C. W. (2008). Fibrinogen synthesized by cancer cells augments the proliferative effect of fibroblast growth factor-2 (FGF-2). *Journal of Thrombosis and Haemostasis : JTH*, *6*(1), 176–183. https://doi.org/10.1111/J.1538-7836.2007.02808.X

Saito, N., Nishimura, H., & Kameoka, S. (2008). Clinical significance of fibronectin expression in colorectal cancer. *Molecular Medicine Reports*, *1*(1), 77–81. https://doi.org/10.3892/MMR.1.1.77

Sanz, G., Leray, I., Muscat, A., Acquistapace, A., Cui, T., Rivière, J., Vincent-Naulleau, S., Giandomenico, V., & Mir, L. M. (2017). Gallein, a Gβγ subunit signalling inhibitor, inhibits metastatic spread of tumour cells expressing OR51E2 and exposed to its odorant ligand. *BMC Research Notes*, *10*(1), 541. https://doi.org/10.1186/S13104-017-2879-Z

Sharma, B. K., Flick, M. J., & Palumbo, J. S. (2019). Cancer-Associated Thrombosis: A Two-Way Street. *Seminars in Thrombosis and Hemostasis*, *45*(6), 559–568. https://doi.org/10.1055/S-0039-1693472

Shen, B., Delaney, M. K., & Du, X. (2012). Inside-out, outside-in, and inside-outside-in: G protein signaling in integrin-mediated cell adhesion, spreading, and retraction. *Current Opinion in Cell Biology*, *24*(5), 600–606. https://doi.org/10.1016/J.CEB.2012.08.011

Sherwood, L. M., Parris, E. E., & Folkman, J. (1971). Tumor angiogenesis: therapeutic implications. *The New England Journal of Medicine*, *285*(21), 1182–1186. https://doi.org/10.1056/NEJM197111182852108

Sherwood, L. M., Parris, E. E., & Folkman, J. (2010). Tumor Angiogenesis: Therapeutic Implications. *Http://Dx.Doi.Org/10.1056/NEJM197111182852108*, *285*(21), 1182–1186. https://doi.org/10.1056/NEJM197111182852108

Shi, X., Gangadharan, B., Brass, L. F., Ruf, W., & Mueller, B. M. (2004a). Protease-Activated Receptors (PAR1 and PAR2) Contribute to Tumor Cell Motility and Metastasis. *Mol Cancer Res*, *2*(7), 395–402. http://aacrjournals.org/mcr/article-pdf/2/7/395/3138255/395-402.pdf

Shi, X., Gangadharan, B., Brass, L. F., Ruf, W., & Mueller, B. M. (2004b). Protease-Activated Receptors (PAR1 and PAR2) Contribute to Tumor Cell Motility and Metastasis. *Molecular Cancer Research*, *2*(7), 395–402. https://doi.org/10.1158/1541-7786.395.2.7

Shi, X., Gangadharan, B., Brass, L. F., Ruf, W., & Mueller, B. M. (2004c). Protease-Activated Receptors (PAR1 and PAR2) Contribute to Tumor Cell Motility and Metastasis. *Molecular Cancer Research*, *2*(7), 395–402. https://doi.org/10.1158/1541-7786.395.2.7

Silini, A., Ghilardi, C., Ardinghi, C., Bernasconi, S., Oliva, P., Carraro, F., Naldini, A., Bani, M. R., & Giavazzi, R. (2010). Protease-activated receptor-1 (PAR-1) promotes the motility of human melanomas and is associated to their metastatic phenotype. *Clinical and Experimental Metastasis*, *27*(1), 43–53. https://doi.org/10.1007/S10585-009-9301-8/FIGURES/5

Simpson-Haidaris, P. J., & Rybarczyk, B. (2001). Tumors and Fibrinogen. *Annals of the New York Academy of Sciences*, *936*(1), 406–425. https://doi.org/10.1111/J.1749-6632.2001.TB03525.X

Soto, A., Smith, T., Chen, B., Bhattacharya, S., Cordova, I., Kenakin, T., Vaidehi, N., & Trejo, J. (2015). N-linked glycosylation of protease-activated receptor-1 at extracellular loop 2 regulates G-protein signaling bias. *Proceedings of the National Academy of Sciences of the United States of America*, *112*(27), E3600-8. https://doi.org/10.1073/pnas.1508838112

Soto, A., & Trejo, J. (2010). N-Linked Glycosylation of Protease-activated Receptor-1 Second Extracellular Loop: a critical determinant for ligand-induced receptor activation and internalization. *The Journal of Biological Chemistry*, *285*(24), 18781–18793. https://doi.org/10.1074/jbc.M110.111088

Spiegel, A., Brooks, M. W., Houshyar, S., Reinhardt, F., Ardolino, M., Fessler, E., Chen, M. B., Krall, J. A., Decock, J., Zervantonakis, I. K., Iannello, A., Iwamoto, Y., Cortez-Retamozo, V., Kamm, R. D., Pittet, M. J., Raulet, D. H., & Weinberg, R. A. (2016). Neutrophils Suppress Intraluminal NK Cell-Mediated Tumor Cell Clearance and Enhance Extravasation of Disseminated Carcinoma Cells. *Cancer Discovery*, *6*(6), 630–649. https://doi.org/10.1158/2159-8290.CD-15-1157

Spoerri, P. M., Strohmeyer, N., Sun, Z., Fässler, R., & Müller, D. J. (2020). Protease-activated receptor signalling initiates α5β1-integrin-mediated adhesion in non-haematopoietic cells. *Nature Materials 2020 19:2*, *19*(2), 218–226. https://doi.org/10.1038/S41563-019-0580-4

Steinhoff, M., Buddenkotte, J., Shpacovitch, V., Rattenholl, A., Moormann, C., Vergnolle, N., Luger, T. A., & Hollenberg, M. D. (2005). Proteinase-Activated Receptors: Transducers of Proteinase-Mediated Signaling in Inflammation and Immune Response. *Endocrine Reviews*, *26*(1), 1–43. https://doi.org/10.1210/ER.2003-0025

Stoeltzing, O., Liu, W., Reinmuth, N., Fan, F., Parry, G. C., Parikh, A. A., McCarty, M. F., Bucana, C. D., Mazar, A. P., & Ellis, L. M. (2003). Inhibition of integrin alpha5beta1 function with a small peptide (ATN-161) plus continuous 5-FU infusion reduces colorectal liver metastases and improves survival in mice. *International Journal of Cancer*, *104*(4), 496–503. https://doi.org/10.1002/IJC.10958

Strilic, B., & Offermanns, S. (2017). Intravascular Survival and Extravasation of Tumor Cells. *Cancer Cell*, *32*(3), 282–293. https://doi.org/10.1016/J.CCELL.2017.07.001

Subramanian, A., Tamayo, P., Mootha, V. K., Mukherjee, S., Ebert, B. L., Gillette, M. A., Paulovich, A., Pomeroy, S. L., Golub, T. R., Lander, E. S., & Mesirov, J. P. (2005). Gene set enrichment analysis: A knowledge-based approach for interpreting genome-wide expression profiles. *Proceedings of the National Academy of Sciences of the United States of America*, *102*(43), 15545–15550. https://doi.org/10.1073/PNAS.0506580102/SUPPL_FILE/06580FIG7.JPG

Sun, L., Li, P. B., Yao, Y. F., Xiu, A. Y., Peng, Z., Bai, Y. H., & Gao, Y. J. (2018). Proteinase-activated receptor 2 promotes tumor cell proliferation and metastasis by inducing epithelial-mesenchymal transition and predicts poor prognosis in hepatocellular carcinoma. *World Journal of Gastroenterology*, *24*(10), 1120. https://doi.org/10.3748/WJG.V24.I10.1120

Sun, Z., Costell, M., & Fässler, R. (2019). Integrin activation by talin, kindlin and mechanical forces. *Nature Cell Biology 2019 21:1*, *21*(1), 25–31. https://doi.org/10.1038/s41556-018-0234-9

Taylor, G. A., Jeffers, M., Webb, C. P., Koo, H. M., Anver, M., Sekiguchi, K., & vande Woude, G. F. (1998). Decreased fibronectin expression in Met/HGF-mediated tumorigenesis. *Oncogene*, *17*(9), 1179–1183. https://doi.org/10.1038/SJ.ONC.1202004

Tellez, C., & Bar-Eli, M. (2003). Role and regulation of the thrombin receptor (PAR-1) in human melanoma. *Oncogene 2003 22:20*, *22*(20), 3130–3137. https://doi.org/10.1038/sj.onc.1206453

Topalovski, M., & Brekken, R. A. (2016). Matrix control of pancreatic cancer: New insights into fibronectin signaling. *Cancer Letters*, *381*(1), 252–258. https://doi.org/10.1016/J.CANLET.2015.12.027

Tun, H. W., Marlow, L. A., von Roemeling, C. A., Cooper, S. J., Kreinest, P., Wu, K., Luxon, B. A., Sinha, M., Anastasiadis, P. Z., & Copland, J. A. (2010). Pathway Signature and Cellular Differentiation in Clear Cell Renal Cell Carcinoma. *PLOS ONE*, *5*(5), e10696. https://doi.org/10.1371/JOURNAL.PONE.0010696

van den Berg, Y. W., van den Hengel, L. G., Myers, H. R., Ayachi, O., Jordanova, E., Ruf, W., Spek, C. A., Reitsma, P. H., Bogdanov, V. Y., & Versteeg, H. H. (2009). Alternatively spliced tissue factor induces angiogenesis through integrin ligation. *Proceedings of the National Academy of Sciences of the United States of America*, *106*(46), 19497–19502. https://doi.org/10.1073/PNAS.0905325106/SUPPL_FILE/0905325106SI.PDF

Vanharanta, S., Shu, W., Brenet, F., Ari Hakimi, A., Heguy, A., Viale, A., Reuter, V. E., Hsieh, J. J. D., Scandura, J. M., & Massagué, J. (2012). Epigenetic expansion of VHL-HIF signal output drives multiorgan metastasis in renal cancer. *Nature Medicine 2012 19:1*, *19*(1), 50–56. https://doi.org/10.1038/nm.3029

Voss, M. H., Molina, A. M., & Motzer, R. J. (2011). mTOR Inhibitors in Advanced Renal Cell Carcinoma. *Hematology/Oncology Clinics of North America*, *25*(4), 835–852. https://doi.org/10.1016/J.HOC.2011.04.008

Vu, T. K. H., Hung, D. T., Wheaton, V. I., & Coughlin, S. R. (1991). Molecular cloning of a functional thrombin receptor reveals a novel proteolytic mechanism of receptor activation. *Cell*, *64*(6), 1057–1068. https://doi.org/10.1016/0092-8674(91)90261-V

Wang, H., Fu, W., Im, J. H., Zhou, Z., Santoro, S. A., Iyer, V., DiPersio, C. M., Yu, Q. C., Quaranta, V., Al-Mehdi, A., & Muschel, R. J. (2004). Tumor cell alpha3beta1 integrin and vascular laminin-5 mediate pulmonary arrest and metastasis. *The Journal of Cell Biology*, *164*(6), 935–941. https://doi.org/10.1083/JCB.200309112

White, D. E., Kurpios, N. A., Zuo, D., Hassell, J. A., Blaess, S., Mueller, U., & Muller, W. J. (2004). Targeted disruption of beta1-integrin in a transgenic mouse model of human breast cancer reveals an essential role in mammary tumor induction. *Cancer Cell*, *6*(2), 159–170. https://doi.org/10.1016/J.CCR.2004.06.025

Williams, K. C., & Coppolino, M. G. (2014). SNARE-dependent interaction of Src, EGFR and β1 integrin regulates invadopodia formation and tumor cell invasion. *Journal of Cell Science*, *127*(Pt 8), 1712–1725. https://doi.org/10.1242/JCS.134734

Wojtukiewicz, M. Z., Hempel, D., Sierko, E., Tucker, S. C., & Honn, K. v. (2015a). Protease-activated receptors (PARs)—biology and role in cancer invasion and metastasis. *Cancer Metastasis Reviews*, *34*(4), 775. https://doi.org/10.1007/S10555-015-9599-4

Wojtukiewicz, M. Z., Hempel, D., Sierko, E., Tucker, S. C., & Honn, K. v. (2015b). Protease-activated receptors (PARs)--biology and role in cancer invasion and metastasis. *Cancer Metastasis Reviews*, *34*(4), 775–796. https://doi.org/10.1007/S10555-015-9599-4

Yang, E., Boire, A., Agarwal, A., Nguyen, N., O'Callaghan, K., Tu, P., Kuliopulos, A., & Covic, L. (2009). Blockade of PAR1 signaling with cell-penetrating pepducins inhibits Akt survival pathways in breast cancer cells and suppresses tumor survival and metastasis. *Cancer Research*, *69*(15), 6223–6231. https://doi.org/10.1158/0008-5472.CAN-09-0187

Yang, S., Zhang, J. J., & Huang, X. Y. (2009). Orai1 and STIM1 Are Critical for Breast Tumor Cell Migration and Metastasis. *Cancer Cell*, *15*(2), 124–134.

https://doi.org/10.1016/J.CCR.2008.12.019/ATTACHMENT/CDDE0812-350C-4308-B690-E7E4E7A1E599/MMC2.AVI

Yokom, D. W., Ihaddadene, R., Moretto, P., Canil, C. M., Reaume, N., le Gal, G., & Carrier, M. (2014). Increased risk of preoperative venous thromboembolism in patients with renal cell carcinoma and tumor thrombus. *Journal of Thrombosis and Haemostasis*, *12*(2), 169–171. https://doi.org/10.1111/JTH.12459

Yu, J. L., May, L., Klement, P., Weitz, J. I., & Rak, J. (2004). Oncogenes as regulators of tissue factor expression in cancer: implications for tumor angiogenesis and anti-cancer therapy. *Seminars in Thrombosis and Hemostasis*, *30*(1), 21–30. https://doi.org/10.1055/S-2004-822968

Yu, M., Bardia, A., Wittner, B. S., Stott, S. L., Smas, M. E., Ting, D. T., Isakoff, S. J., Ciciliano, J. C., Wells, M. N., Shah, A. M., Concannon, K. F., Donaldson, M. C., Sequist, L. v., Brachtel, E., Sgroi, D., Baselga, J., Ramaswamy, S., Toner, M., Haber, D. A., & Maheswaran, S. (2013). Circulating breast tumor cells exhibit dynamic changes in epithelial and mesenchymal composition. *Science (New York, N.Y.)*, *339*(6119), 580–584. https://doi.org/10.1126/SCIENCE.1228522

Zavyalova, M. v., Denisov, E. v., Tashireva, L. A., Savelieva, O. E., Kaigorodova, E. v., Krakhmal, N. v., & Perelmuter, V. M. (2019). Intravasation as a Key Step in Cancer Metastasis. *Biochemistry. Biokhimiia*, *84*(7), 762–772. https://doi.org/10.1134/S0006297919070071

Zecchin, D., Moore, C., Michailidis, F., Horswell, S., Rana, S., Howell, M., & Downward, J. (2020). Combined targeting of G protein-coupled receptor and EGF receptor signaling overcomes resistance to PI3K pathway inhibitors in PTEN-null triple negative breast cancer. *EMBO Molecular Medicine*, *12*(8), e11987. https://doi.org/10.15252/EMMM.202011987

Zhang, C., Srinivasan, Y., Arlow, D. H., Fung, J. J., Palmer, D., Zheng, Y., Green, H. F., Pandey, A., Dror, R. O., Shaw, D. E., Weis, W. I., Coughlin, S. R., & Kobilka, B. K. (2012). High-resolution crystal structure of human protease-activated receptor 1. *Nature*, *492*(7429), 387–392. https://doi.org/10.1038/NATURE11701

Zhang, X. H. F., Wang, Q., Gerald, W., Hudis, C. A., Norton, L., Smid, M., Foekens, J. A., & Massagué, J. (2009). Latent bone metastasis in breast cancer tied to Src-dependent survival signals. *Cancer Cell*, *16*(1), 67–78. https://doi.org/10.1016/J.CCR.2009.05.017

Zhao, X., & Guan, J. L. (2011). Focal adhesion kinase and its signaling pathways in cell migration and angiogenesis. *Advanced Drug Delivery Reviews*, *63*(8), 610–615. https://doi.org/10.1016/j.addr.2010.11.001